PREPARATION AND CHARACTERISATION OF PALLADIUM/SILVER/CARBON NANOTUBES COMPOSITES FOR THE TREATMENT OF INDUSTRIAL ANIMAL FEEDS PROCESSING WASTEWATER

BY

USMAN, Nurudeen Ayodeji
MTech/SPS/2017/7288

DEPARTMENT OF CHEMISTRY
FEDERAL UNIVERSITY OF TECHNOLOGY, MINNA

AUGUST, 2021

ABSTRACT

This study focused on the development of Pd-Ag-CNTs nanocomposites for the removal of selected heavy metals and other water quality indicators in industrial animal feed processing wastewater. Silver and palladium nanoparticles were produced using green synthesis method. While Carbon nanotubes (CNTs) were produced via catalytic chemical vapour deposition (CCVD) method and then purified by acid treatment by mixture of H_2SO_4 and HNO_3. The solution of 2-mercaptpoethylamine in N, N'-dicyclohexylcarbondiimide (DCC) was used as a coupling and dehydrating agent for the formation of amide group on the purified CNTs. Pd-CNTs and Ag-CNTs were produced along with Pd-Ag-CNTs through a combination of ultrasonic-assisted wet impregnation method. Different analytical tools such as HRSEM, HRTEM, EDS, SAED, XRD and BET were used to characterise the prepared nanostructured materials. The HRSEM results revealed that PdNPs and AgNPs were well dispersed on the CNTs matrix. The EDS confirmed that Pd and Ag were successfully deposited on CNTs. XRD pattern confirmed a graphitic, face-centred cubic structure upon modifications with Ag and Pd nanoparticles with an average crystallite sizes of 26.10 nm (Pd-Ag-CNTs) > 18.74 nm (Pd-CNTs) > 13.6 nm (Ag-CNTs) > 13.00 nm (P-CNTs). The BET results showed increased in surface area of Pd-Ag-CNTs compared to CNTs and the order ofthe increment were: 392.5 m^2/g (Pd-Ag-CNTs) >356.3 m^2/g (Pd-CNTs) > 352.5 m^2/g (Ag-CNTs) >227.63 m^2/g (P-CNTs). Pd-Ag-CNTs nanocomposites were used as an adsorbent for the treatment of industrial animal feed processing wastewater. The effect of the nano-adsorbent removal on wastewater indicator parameters and selected heavy metals such as copper (Cu), iron (Fe), manganese (Mn) and nickel (Ni) were investigated. Effect of contact time, adsorbent dosage and temperature on the adsorption potentials of Pd/Ag/CNTs were assessed via a batch mode process. Linear and nonlinear regression methods were used for determination of the optimum adsorption isotherms and kinetics using the experimental adsorption equilibrium data. The coefficient of determination (R^2), the sum of the squares errors (SSE) and Chi-square (χ^2) were used in the nonlinear regression. The optimum condition based on each parameters was 90 min of contact time, 60 mg of adsorbent dosage and 80 °C of temperature, where the adsorption of Ni ions (99.84 %) was higher in removal efficiency than other analyzed metal ions: Fe (88.36 %), Cu (77.86 %) and Mn (77.64 %). The isotherm data best fitted Florry-Huggins isotherm model based on the χ^2, SSE and regression co-efficient values of 0.9947 (Cu), 0.9787 (Fe), 0.9924 (Mn) and 0.7098 (Ni), while the kinetic data suited pseudo-second order and thus predicted best the experimental data.The thermodynamic study was found to be non-spontaneous and endothermic in nature due to positive values of standard Gibb's free energy and enthalpy change respectively. This study demonstrated that Pd/Ag/CNTs exhibits exceptional adsorptive properties for the removal of selected metal ions from industrial animal feed processing wastewater.

TABLE OF CONTENTS

Content	**Page**
Title page	i
Declaration	ii
Certification	iii
Dedication	iv
Acknowledgments	v
Abstract	vii
Table of Contents	viii
List of Tables	xvi
List of Figures	xviii
List of Plates	xx
List of Appendices	xxii
List of Abbreviations, Glossary and Symbols	xxiii

CHAPTER ONE

1.0	**INTRODUCTION**	**1**
1.1	Background to the Study	1
1.2	Statement of the Research Problem	4
1.3	Justification of the Study	6
1.4	Aim and Objectives of the Study	6

CHAPTER TWO

2.0	**LITERATURE REVIEW**	**8**
2.1	Animal Feeds Wastewater	8
2.2	Effects of Animal Feed Wastewater on the Environment	9

2.3 Quality Parameters for Characterisation of Animal Feed Processing Wastewater 10
2.3.1 Dissolved oxygen 11
2.3.2 Biochemical oxygen demand 11
2.3.3 Chemical oxygen demand 12
2.3.4 Total suspended solids 12
2.3.5 pH 12
2.3.6 Total phosphorus 13
2.3.7 Total nitrogen 14
2.3.8 Sulphate 14
2.3.9 Heavy metals 14
2.3.9.1 Copper 15
2.3.9.2 Iron 15
2.3.9.3 Manganese 16
2.3.9.4 Nickel 16
2.4 Wastewater Treatment Technologies 17
2.4.1 Adsorption technology 19
2.4.2 Types of adsorption 22
2.4.3 Factors influencing adsorption from aqueous solution 24
2.4.3.1 Nature of adsorbent and adsorbate 24
2.4.3.2 Surface area and porosity of the adsorbent 25
2.4.3.3 Influence of temperature 25
2.4.3.4 Effect of adsorbent dosage 26
2.4.3.5 Effect of solution and adsorbent pH 26
2.4.3.6 Effect of contact time 27

2.4.4 Modelling and mechanism of adsorption 27

2.4.5 Adsorption equilibrium 28

2.4.5.1 Langmuir isotherm model 29

2.4.5.2 Freundlich isotherm model 30

2.4.5.3 Dubinin-Radushkevich isotherm model 31

2.4.5.4 Temkin isotherm model 32

2.4.5.5 Halsey isotherm model 33

2.4.5.6 Flory-Huggins isotherm model 33

2.4.6 Adsorption kinetics 34

2.4.6.1 Pseudo-first-order kinetic model 34

2.4.6.2 Pseudo-second-order kinetic model 35

2.4.6.3 Intra-particle diffusion model 35

2.4.6.4 Thermodynamic studies 36

2.5 Nano-adsorbents in Wastewater Treatment 37

2.5.1 Silver and palladium nanoparticle 37

2.5.2 Synthesis method of nanoparticles 40

2.5.2.1 Physical synthesis approach 40

2.5.2.2 Chemical synthesis approach 40

2.5.2.3 Green chemistry approach 41

2.5.3 Phytochemical constituents of plant extract 42

2.5.4 Carbon Nanotubes 44

2.5.5 Synthesis Method of Carbon Nanotubes 45

2.5.5.1 Chemical Vapour Deposition (CVD) 46

2.5.6 Nanocomposites 48

2.5.7 Functionalization/Preparation of metal matrix nanocomposites 50

2.6 Characterisation Techniques 53
2.6.1 UV–visible spectroscopy 53
2.6.2 X-ray Diffraction 54
2.6.3 High resolution 54
2.6.4 High resolution transmission electron microscopy 55
2.6.5 Energy Dispersive Spectroscopy 56
2.6.6 Brunauer-Emmett-Teller 56

CHAPTER THREE

3.0 MATERIALS AND METHODS 58
3.1 Materials, Reagents and Equipments `` 58
3.1.1 Equipments/Apparatus 58
3.1.2 Collection of Plant materials, Kaolin and Industrial animal feed processing wastewater 58
3.2 Methodology 61
3.2.1 Preparation of plants extract 61
3.2.2 Phytochemical screening 61
3.2.2.1 Determination of phenols 61
3.2.2.2 Determination of flavonoids 62
3.2.2.3 Determination of alkaloids 62
3.2.2.4 Determination of tannins 62
3.2.2.5 Determination of saponins 63
3.2.3 Synthesis of silver nanoparticles 63
3.2.4 Synthesis of palladium nanoparticles 64
3.2.5 Preparation and optimization of Fe-Ni/Kaolin catalyst 64

3.2.6 Synthesis of carbon nanotubes 65

3.2.7 Purification/Functionalisation of as-synthesized carbon nanotubes 66

3.2.8 Synthesis of Ag-CNTs nanocomposites 66

3.2.9 Synthesis of Pd-CNTs nanocomposites 66

3.2.10 Synthesis of Pd-Ag-CNTs nanocomposites 67

3.2.11 Impregnation of the prepared palladium and silver nanoparticles onto carbon nanotubes 68

3.3 Characterisation techniques of the synthesized nanomaterials 69

3.3.1 UV-Visible spectroscopy 69

3.3.2 HRTEM and SAED 69

3.3.3 HRSEM and EDS 70

3.3.4 XRD 70

3.3.5 BET 70

3.4 Characterisation of WastewaterBefore and After Treatment with Nano-adsorbent 71

3.4.1 Physicochemical characterisation 71

3.4.1.1 Temperature 71

3.4.1.2 pH 71

3.4.1.3 Turbidity 72

3.4.1.4 Conductivity, total suspended solid and total dissolve solid 72

3.4.1.5 Dissolved Oxygen 72

3.4.1.6 Biochemical oxygen demand 72

3.4.1.7 Chemical oxygen demand 72

3.4.1.8 Metal analysis 73

3.5 Batch Adsorption Study 74

3.5.1 Effect of contact time 74
3.5.2 Effect of adsorbent dosage 74
3.5.3 Effect of temperature 74

3.6 Data Analysis of Batch Adsorption on Industrial Animal Feed Processing Wastewater 75
3.6.1 Data analysis using adsorption isotherm, kinetics and themodynamic models 76
3.6.2 Stastical error validity of adsorption model 78

3.7 Review summary and Identified Knowledge gaps 78

CHAPTER FOUR

4.0 RESULTS AND DISCUSSION 80
4.1 Phytochemical Analysis of the Extract 80
4.2. Characterisation of Palladium and Silver Nanoparticles 82
4.2.1 Uv-Vis Spectroscopy analysis of silver and palladium nanoparticles 82
4.2.2 HRSEM and EDS analysis of silver and palladium nanoparticles 84
4.2.3 HRTEM analysis and SAED patterns of palladium and silver nanoparticles 86
4.2.4 XRD Analysis of the prepared silver and palladium nanoparticles 88
4.3 Synthesis and Characterisation of Carbon Nanotubes 91
4.3.1 Preparation of bi-metallic (Fe-Ni) kaolin catalyst 91
4.3.2 Synthesis and purification of carbon nanotubes 92

onto carbon nanotubes
4.3.4 Characterisation of carbon nanotubes and impregnated carbon nanocomposites 93
4.3.4.1 HRSEM and EDS analysis of purified carbon nanotubes and nanocomposites 93
4.3.4.2. HRTEM and SAED patterns of the synthesized carbon nanotubes and nanocomposites 97
4.3.4.3 XRD pattern of the purified carbon nanotubes and impregnated carbon nanotubes 102
4.3.4.4 Brunauer-Emmett-Teller (BET) analysis of purified carbon nanotubes and impregnated nanocomposites 108
4.4 Treatment of industrial animal feed processing wastewater 110
4.4.1 Physicochemical Analysis of Industrial Animal Feed Processing Wastewater 110
4.4.2 Heavy metal analysis of Industrial animal feed processing wastewater 116
4.4.3 Batch Adsorption of heavy metals in animal feed processing industry wastewater 119
4.4.4 Adsorption Isotherm Model 126
4.4.5 Adsorption Kinetic Study 138
4.4.6 Adsorption Thermodynamics Study 141

CHAPTER FIVE

5.0 CONCLUSION AND RECOMMENDATIONS 149
5.1 Conclusion 149
5.2 Recommendations 151

5.3 Contribution to knowledge 151

REFERENCES **152**

APPENDICES **183**

LIST OF TABLES

Tables **Page**

2.1: Summary of Conventional Methods used for the Treatment of Polluted Industrial Wastewater with their Shortcomings 18

2.2: Wastewater Treatment using CNTs 51

3.1: List of Equipment/Apparatus 59

3.2: List of Chemicals/Reagents used 60

4.1: Phytochemical Constituents of Banana peels, Plantain peel and *Agerantum conyzoides* (goat weed) Leave Extracts 80

4.2: Yield of Fe-Ni/Kaolin Catalyst at Pre- and Post-calcination 91

4.3: Elemental Composition (EDS) of the Synthesized CNTs-based Nanocomposites 95

4.4: Crystalline size of CNTs, Ag-CNTs, Pd-CNTs and Pd-Ag-CNTs Nanocomposites 107

4.5: Brunauer-Emmett-Teller (BET) Analysis of the Functionalized Carbon Nanotubes 108

4.6: Physicochemical Characterization of Animal Feed Processing Industry Wastewater (before and after adsorption study) and WHO Guideline Limits 111

4.7: Mean Concentration of Selected Heavy Metals of Industrial Animal Feed Processing Wastewater (before and after adsorption study) and Standard Limit 116

4.8a: Isotherm Constants for the Adsorption of Metal Ions on Pd-Ag-CNTs Nanocomposites 131

4.8a: Isotherm Constants for the Adsorption of Metal Ions on Pd-Ag-CNTs Nanocomposites 132

4.9: Removal Efficiency of Various Adsorbents and Present Study 137

4.10: Kinetic Model Parameters for the Adsorption of Selected Metal Ion by Pd-Ag-CNTs Nanocomposites 140

4.11: Constants of Thermodynamics Model through Adsorption of Selected Metal Ions (Cu, Fe, Mn and Ni) by Pd-Ag-CNTs 143

4.12a: Comparison of Maximum Adsorption Capacity of Pd-Ag-CNTs with other Adsorbents Reported in Literature 146

4.12b: Comparison of Maximum Adsorption Capacity of Pd-Ag-CNTs with other Adsorbents Reported in Literature 147

LIST OF FIGURES

Figure **Page**

2.1: Classification of Technologies Available for Pollutant Removal and examples of techniques 17

2.2: Schematic Demonstration of CVD Method (a) Horizontal Furnace (b) Vertical Furnace 47

3.1: Multi-step Mechanistic Pathway for Wet Impregnation of PdNPs, AgNPs and Pd/AgNPs onto MWCNTs 68

4.1: UV-Vis Spectograph of Synthesized Silver Nanoparticles (AgNPs) 83

4.2: UV-Vis Spectrograph of Synthesized Palladium Nanoparticles (PdNPs) 84

4.3: EDS Spectra of Synthesized (a) AgNPs and (b) PdNPs using *Agerantum conyzoides* 85

4.4: X-ray Diffraction Patterns of Silver Nanoparticles (AgNPs) 88

4.5: X-ray Diffraction Patterns of Palladium Nanoparticles (PdNPs) 89

4.6: X-ray Diffraction Pattern of Purified-CNTs 103

4.7: X-ray Diffraction Pattern of Synthesized Ag-CNTs Composites 104

4.8: X-ray Diffraction Pattern of Synthesized Pd-CNTs Composites 105

4.9: X-ray Diffraction pattern of Synthesized Pd-Ag-CNTs Composites 106

4.10: Percentage Removal of Metal ion Adsorption on Pd-Ag-CNTs Nanocomposites [dosage (10 mg/50 cm^3), Stirring Speed (200 rpm), andTemperature(30 °C)] 121

4.11: Effect of Adsorbent dosage on Heavy Metals Adsorption onto Pd-Ag-CNTs Nanocomposites (Time of contact (60 min.), Stirring speed (200 rpm), and temperature (30 °C)] 123

4.12: Effect of Temperature on Metal ion Adsorption onto Pd-Ag-CNTs Nanocomposites [Adsorbent dosage (10 mg/50 cm^3), Stirring speed (200 rpm), and Time of contact (60 min.) 125

LIST OF PLATES

Plate		Page
I:	(a) Various Equipment used in Blending Raw Materials to Produce Feeds (b) Wastewater coming out of the Processing Industry Through Cleaningof Machines, Containers or Flushing the Working Floor (c)UntreatedWastewater Discharged into the Water Body	8
II:	(a) Effect of Industrial Animal Feed Processing Wastewater on Aquatic species (b) Effect of Industrial Animal Feed Processing Wastewater on Plant Vegetation.	10
III:	Procedure of Biochemical Synthesized AgNPs (a) Aqueous Solution of Silver Nitrate salt (b) *Agerantum conyzoides* Leaves Extract (c) Mixtureof Silver Nitrate Solution and Leaves Extract at 0 min (d) Mixture of $AgNO_3$ Solution and Leave Extract after 30 min.	81
IV:	Procedure of Biochemical Synthesized PdNPs (a) Aqueous solution of 1 mM of Palladium Chloride Salts (b) Plant Extract of *Agerantum Conyzoides* (c) Aqueous Solution of Palladium Chloride Salt with *Agerantum conyzoides* Leave Extract at 0 min, and (d) Aqueous Solutionof Palladium Chloride Salt with Leave Extract after 30 min ofStirring.	81
V:	High Resolution Scanning Electron Microscope Image of (a) AgNPs (b) PdNPs	85
VI:	High Resolution Transmission Electron Microscope Image of AgNPs and PdNPs (c & d) Selected Area Electron Diffraction (SAED) Patterns of AgNPs and PdNPs	87

VII: High Resolution Scanning Electron Microscopy Images of (a) P-CNTs (b) Ag-CNTs (c) Pd-CNTs (d) Pd-Ag-CNTs 94
VIII: (a) & (b) High Resolution Transmission Electron Microscopy Images of P- MWCNTs at Different Magnification (c) SAED Pattern of P-MWCNTs 98
IX: (a) & (b) High Resolution Transmission Electron Microscopy Images of Ag-CNTsNanocomposite at Different Magnification (c) SAED Pattern of Ag-CNTs Nanocomposites 99
X: (a) & (b) High Resolution Transmission Electron Microscopy Images of Pd-CNTs Nanocomposite at Different Magnification (c) SAED Pattern of Pd-CNTs Nanocomposites 100
XI: (a) & (b) High Resolution Transmission Electron Microscopy Images of Pd-Ag-CNTsNanocomposite at Different magnification (c) SAED Pattern of Pd-Ag-CNTs Nanocomposites 101

LIST OF APPENDICES

Appendix **Page**

A: Percentage Removal of Selected Heavy Metal Ions onto Pd-Ag-CNTs with Respect to Contact Time 183

B: Percentage Removal of Selected Heavy Metal Ions onto Pd-Ag-CNTs with Respect to Adsorbent Dosage 183

C: Percentage Removal of Selected Heavy Metal Ions onto Pd-Ag-CNTs with Respect to Effect of Temperature 184

D: Experimental Batch Adsorption Data of Cu using Pd-Ag-CNTs 184

E: Experimental Batch Adsorption Data of Fe using Pd-Ag-CNTs 185

F: Experimental Batch Adsorption Data of Mn using Pd-Ag-CNTs 185

G: Experimental Batch Adsorption Data of Ni using Pd-Ag-CNTs 186

H: (I-IV): Linear Plot of Langmuir Isotherm Model 187

I: (I-IV): Linear Plot of Freundlich Isotherm Model 188

J: (I-IV): Linear Plot of Freundlich Isotherm Model 189

K: (I-IV): Linear Plot of Temkin Isotherm Model 190

L: (I-IV): Linear Plots of Halsey Isotherm Model 191

M: (I-IV): Linear Plots of Florry-Huggin’s Isotherm Model 192

N: (I-IV): Linear Plots of Pseudo-First-Order kinetic Model 193

O: (I-IV): Linear Plots of Pseudo-Second-Order Kinetic Model 194

P: (I-IV): Linear Plots of Intraparticles Diffusion MODEL 195

Q: Linear Plots of Thermodynamics 196

LIST OF ABBREVIATIONS

AAS	Atomic absorption spectrophotometer
AFPIWW	Animal Feed Processsing Industry Wastewater
APHA	American Public Health Association
ASTDR	Agency for Toxic Substances and Disease Registry
BDH	British Drug House
BET	Brunauer-Emmett-Teller
BOD	Biological oxygen demand
CCVD	Catalytic Chemical Vapour Deposition
COD	Chemical oxygen demand
CVD	Chemical Vapour Deposition
DO	Dissolved oxygen
D-R	Dubinin-Radushkevich
EDS	Energy dispersive X-ray spectroscopy
EPA	Environmental Protection Agency
HRSEM	High resolution scanning electron microscope
HRTEM	High resolution transmission electron microscope
IUPAC	International Union of Pure and Applied Chemistry
NIS	National Industrial Standard
NTU	Nephelometric turbidity units
MWCNTs	Multi walled carbon nanotubes
MWNTs	Multi walled nanotubes
PAC	Powdered activated carbon
SEM	Scanning electron microscope
SWCNTs	Single walled carbon nanotubes

SWNTs	Single walled nanotubes
TDS	Total dissolved solids
TEM	Transmission electron microscopy
UN	United nation
USEPA	United State Environmental Protection Agency
USA	United State of America
UV	Ultraviolet
WHO	World Health Organization
XRD	X-ray diffraction

CHAPTER ONE

1.0 INTRODUCTION

1.1 Background to the Study

The discharge of untreated liquid wastewater generated via natural and anthropogenic activities in developing countries has continued to create more environmental and ecological imbalances (Nguyen *et al*., 2020). One of such anthropogenic activitiesis is the process of manufacturing animal feeds.This involves the use of raw agricultural ingredients such as corn, wheat, sorghum, forage, vitamins, additives and minerals to formulate nutritious feeds tailored for specific dietary needs of animals (Blair, 2018). According to the statistics released by the International Feed Industry Federation (Lombard *et al*., 2020), not fewer than thirty-eight thousand feed mills manufacture 80 percent of the global industrial feed. Despite the trends in production rate within the industry, the world's ten largest feed manufacturers produces less than 65 million tons annually (Lombard *et al*., 2020). This account for less than 11 percent of global feed output, implying that the global feed industry still remains broadly based with many local and regional commercial feed companies as well as specialized firms.

Nigeria is one of the major manufacturers of animal feed in the sub-Saharan Africa and produce about 5.3 metric tons of feeds annually (Osabohien *et al*., 2020). Alhough, the demand for animal feed has increased the economic output of this nation (Nigeria) and the world at large, the liquid waste generated from the industries remain a source of concern to the environmentalist. This is because the industries utilizes large volume of water during their operation, and as a consequence, unknown volume of wastewater containing different toxic organic, inorganic and microbial constituents are released untreated into the water bodies (Hu *et al*., 2017). The animal feed processing industry wastewater is characterized with colour, offensive odour and high turbidity (Bankole *et al.*, 2019b). Thus, direct discharge of untreated animal feed processing wastewater into the water bodies cause different pollution problems (Taman *et al.*, 2015).

For instance, the bio-accumulation of toxic pollutants in human diets have been linked to the discharged of untreated wastewater into ecosystem. Effect of chronic and acute exposure of human to inorganic arsenic in the wastewater includes diarrhea, vomiting, salivation and abdominal pains (Yang and Massey, 2019). Other mineral supplements such as selenium, chromium, copper and nickel is of great concern since they are used as additives in feeds and can be found in water bodies through washing of the equipments. Organic pollutants and emerging chemicals (dioxins and chlorinated compounds) have been shown to be present at low levels in industrial animal feed processing wastewater (Cheng *et al.*, 2021), however, there is insufficient information on the subject of their toxicity and transfer to edible tissue or milk, to assess whether those contaminants are hazardous to irrigated crops or farm animals. High level of chemical oxygen demand, biochemical oxygen demand and low level of dissolved oxygen can affect lakes and reservoirs, thereby causing death of plants and aquatic animals (Inyinbor *et al.*, 2018).

In view of the effects of exposure to industrial animal feed processing wastewater, it is imperative to reduce the concentration of these pollutants in wastewater before discharge into waterbodies (Long *et al.*, 2018). Different techniques have been used for the treatment of industrial wastewater. However, most traditional or conventional techniques such as filtration, precipitation, sedimentation, floatation, membrane separation and ion exchange among others are ineffective and very expensive due to increase energy consumption (Aziz *et al.*, 2018; Crini *et al.*, 2018). Over the years, chemical methods such as coagulation and precipitation technology involving addition of coagulant has been widely used because of its increased capacity in biodegradation and economic reliability (Yuan *et al*., 2018). But, this process has a low removal rate of dissolved substances and generates a large amount of chemical sludge (Li and Yang, 2018). Physical methods such as filtration, sedimentation and floatation, are also becoming less effective since they are suitable only for elimination of inorganic metals or dissolve compounds which are only part of the pollutants present in wastewater (Crini *et al*., 2018). Biological methods of treatment such as bioreactors, biological activated sludge (BAS) and enzymatic decomposition involve the use of microorganisms for the biodegradation of organic contaminants. However, the process is very slow and inefficient to remove non-degradable compounds in water bodies (Crini *et al* ., 2018).

On the contrary, adsorption technology has become the major technique for wastewater treatment due to its high efficiency and simplicity in design (Ji *et al*., 2019). This method utilizes porous solids (activated carbon, silica gel, artificial pumice and others) to hold up contaminants present in wastewater and also has a wide variety of target contaminant (Li and Yang, 2018). One of the commonest adsorbent is activated carbon which has been widely used to treat wastewater. However, production cost of commercial activated carbon is high and the regeneration efficiency of the adsorbent is very low (Li and Yang, 2018). Thus, it is essential to find more efficient adsorbents, hitherto, nanotechnology approach based on the utilization of nanomaterial as nano-adsorbent to remove different contaminants from polluted wastewater (Huang *et al*., 2019).

Among the nanomaterials, carbon-based nanomaterial such as carbon nanotubes (CNTs) and metallic nanomaterial including silver nanoparticles (AgNPs) and palladium nanoparticles (PdNPs) have been extensively investigated as effective nanoadsorbent to purify industrial wastewater (Gusain *et al*., 2020; Aboelfetoh *et al*., 2021; Hagarová and Nemček, 2021). Carbon nanotubes is widely studied due to its large specific surface areas, hollow and layered structures make it an ideal nanoadsorbent. Silver nanoparticle is considered a very effective adsorbent materials for various types of water pollutions due to its specific surface area and bactericidal properties (Aboelfetoh *et al*., 2021). Furthermore, palladium particles stand out as effective nanoadsorbent owing to its increased activity and stability for wastewater remediation. Nevertheless, information regarding inclusive removal of organic, inorganic and/or microbial pollutants from industrial animal feed processing wastewater has not been reported for the effectiveness of the three material combined as composite. Thus, the present study focused on the synthesis, characterization and application of Pd-CNTs, Ag-CNTs and Pd-Ag-CNTs ternary nanocomposite for the treatment of industrial animal feed processing wastewater.

1.2 Statement of the Research Problems

The quantity of wastewater generated from animal feed processing industries has not been documented throughout the developed and developing countries (Nigeria inclusive). Although the only available literature revealed that industrial animal feed processing wastewater are discharged indiscriminately due to non-functional or inefficient treatment technology (Bankole *et al*., 2019b). Industrial animal feed processing wastewater is often characterized with high concentration of water indicator parameters such as chemical oxygen demand (COD), biochemical oxygen demand (BOD), heavy metals, suspended solid amongst others. The haphazard discharge of untreated animal feed processing wastewater into the water bodies affect the receiving soil and vegetation, causing oxygen depletion in water which result to reduction of fish population and other aquatic species. Effect of acute exposure of human to nickel metals in animal feed processing industry wastewater includes inhibition of oxidative enzymes activity, diarrhea, nausea, shortness of breath and vomiting. Chronic exposure of nickel ions leads to lung cancer, renal edema, pulmonary fibrosis and skin dermatitis (Hussain *et al*., 2017). The presence ofcopper in its toxic nature causes other adverse effects on receiving waters in the aquatic system. Furthermore, high level of chemical oxygen demand (COD), biochemical oxygen demand (BOD) and low level of dissolved oxygen can affect lakes and reservoir, thereby causing death of plants and aquatic animals.

Several conventional wastewater treatment methods have clearly proven inefficient to remove such pollutants effectively, especially removal of heavy metal concentration in the range of 1-100 mg/L (Bora and Dutta, 2014). The application of one metallic nanoparticles such as silver or palladium nanoparticle in wastewater treatment plants accumulate as sludges and are deployed as agricultural fertilizers (Zuykov *et al*., 2011). This in turn complicate the growth of plants as majority of the silver or palladium in sludge remain in the upper soil layer (through run off of surface water) to form complexes as $AgSO_4$ or $PdSO_4$ (Stensberg *et al*., 2011). The synthesis procedures of palladium and silver nanoparticles using chemical and physical methods are complex, not eco-friendly and generate toxic substances. CNTs synthesis using arc discharge and laser ablation produces impure CNTs with low quality, less structural and chemical imperfections (Bankole *et al*., 2018).

1.3 Justification of the Study

Adsorption techniques when combine with nanotechnology is considered a rational route to improve the conventional treatment technologies. Application of nanoadsorbent offer significant advantages such as flexibility in design and operations, reversibility of the process and reduction of the complex treatment time. Application of Pd-CNTs, Ag-CNTs and Pd-Ag-CNTs as a nanoadsorbent for the treatment of animal feed wastewater is expected to remove colour, suspended solids and reduce the level of COD, BOD and other physicochemical indicators prior to the release of the wastewater into water bodies. Green synthesis methods of producing Pd and Ag nanoparticles is simple, cost effective and environmentally friendly compared with other physical and chemical methods. Also, the use of catalytic chemical vapour deposition provide a simple, economical and versatile method of producing high quality CNTs, high yield of bulk product and less quantity of unpurified nanotubes. The incorporation of palladium nanoparticles is expected to act as a catalyst to improve the surface area and surface functionality of CNTs. Silver nanoparticles with smaller size are most valuable due to their higher surface area to volume ratio (Butt, 2020). The intercalation of the composite with silver nanoparticles will provide a superior antibacterial properties, and by extension, enhance the adsorption properties of the material to be able to remove both chemical and biological pollutant in animal feed processing wastewater.

1.4 Aim and Objectives of the Study

The aim of this research work is to prepare and characterize palladium/silver/carbon nanotube composites for the treatment of industrial animal feeds processing wastewater. While the aim of the study will be achieved through the following objectives:

i. Production of carbon nanotubes from Fe-Ni/Kaolin catalyst via chemical vapour deposition method.
ii. Green synthesis of palladium and silver nanoparticles using aqueous extracts of *Agerantum conyzoides*.
iii. Wet impregnation of the synthesized Pd and Ag nanoparticles onto the produced carbon nanotubes.
iv. Characterization of synthesized nanoparticles and nanocomposites using High Resolution Scanning Electron Microscopy (HRSEM), High Resolution Transmission Electron Microscopy (HRTEM), X-ray Diffraction (XRD), Energy Dispersive X-ray spectroscopy (EDS), Brunauer-Emmett-Teller (BET) and Selected Area Electron Diffraction.
v. Analysis of industrial animal feed processing wastewater by determining some physicochemical parameters (such as pH, temperature, turbidity, conductivity, TDS, TSS, DO, COD, and BOD) and heavy metals (such as Fe, Mn, Cu and Ni) before and after the batch adsorption treatment.
vi. Investigation of the adsorption behaviour of the prepared Pd/Ag/CNTs nanocomposite on industrial animal feed processing wastewater via batch adsorption process involving variation of the contact time, mass of nanoadsorbent and temperature.

CHAPTER TWO

2.0 LITERATURE REVIEW

2.1 Animal Feeds Wastewater

Feeds are naturally occurring ingredient or materials given to animals for healthy living and sustenance (Wilkinson and Lee, 2018). They are often termed animal feed (Food grown or developed for livestock). Manufacturing animal feed is a process of converting raw materials of different physical, chemical and nutritional composition into homogenous mixture of desired nutritional response in the animal (Abbas *et al*., 2009; Thomas, 2017). The process is more of a physical than chemical and the production process could be achieved using different equipment shown in Plate I (a).

Plate I: (a) Various Equipment used in Blending Raw Materials to Produce Feeds (b) Wastewater coming out of the Processing Industry Through Cleaning of Machines, Containers or Flushing the Working Floor (c) Untreated Wastewater Discharged into the Water Body.

Some of the raw materials used in manufacturing animal feed have undergone extensive processing prior to inclusion into a mixed feed. For instance, denaturing of soya beans through extraction and heat treatment help to remove anti-nutritional constituents. All these processes generate wastewater that can no longer be used for other operational purposes and hence, discharged directly or indirectly from the facilities displayed in Plate I (b and c) (Zero Discharge of Hazardous Chemical (ZDHC), 2016).

2.2 Effects of Animal Feed Wastewater on the Environment

Industries are often considered as an "engine" of economic growth of any nation (Dadi *et al*., 2016). Nevertheless, studies have shown that the negative impact of industrial growth have outweigh its advantages, as in most cases, toxic wastewater are generated and discharged untreated into the environment (Malik and Khan, 2014). Most animal feed processing industries operating in Nigeria do not have wastewater treatment technology, and where such exist, they are non-functional or inefficient, leading to serious environmental pollution and health problems (Emodi, 2015).

The environmental concerns is related to the volume of water used during the operational processes such as washing of raw materials and products, cleaning of machines, containers or flushing the working floor. As a consequence, generating large amount of wastewater that contains high concentration of pollutant indicators such as chemical oxygen demand, biochemical oxygen demand, suspended solids and toxic metals. It may also be excessively acidic or alkaline (Abdallh *et al*., 2016). For instance, high BOD increase the demands of dissolved oxygen (DO). This signify the depletion of the oxygen (O_2) required by other aquatic organisms to survive (Al Badaii *et al*., 2013).

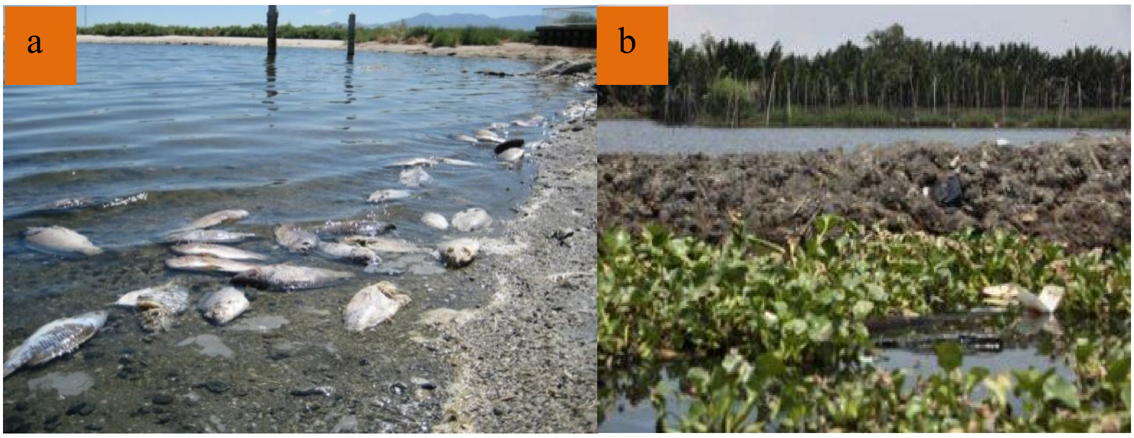

Plate IIa: Effect of industrial animal feed processing wastewater on aquatic species
Plate IIb: Effect of Industrial animal feed processing wastewater on plant vegetation.

From the perspective of human health, some pollutants suppress the immune system, which may have major or even deadly health effects on animals as seen in Plate II (a) (Minnesota Pollution Control Agency, (MPCA), 2009). Also, wastewater with organic loads that contains large quantities of suspended solids can reduce the amount of light available to photosynthetic organisms and on discharge, alter the characteristic of the receiving soil, rendering it an unsuitable substance for many ecological activities as shown in Plate II (b) (Rashed, 2013).

2.3 Quality Parameters for Characterization of Animal Feed Processing Wastewater

Wastewater is characterized in terms of its physical, chemical and biological constituents. As such, the concentration of pollutants and pollutants indicators in the animal feed processing wastewater is usually determined using precise and accurate analytical tools. However, the most common parameters used in characterizing wastewater leaving a processing plants and other processing operations includes, pH, dissolved oxygen (DO), biochemical oxygen demand (BOD), chemical oxygen demand

(COD), total suspended solids, total phosphorus (TP), and total nitrogen (TN) amongst others (Bankole *et al*., 2019b).

2.3.1 Dissolved oxygen (DO)

Dissolved oxygen refers to the level of free oxygen molecule present in water (Wei *et al*., 2019). Dissolved oxygen is necessary to existence of many lifes in water and the amount needed varies from creature to creature (Sunar *et al*., 2018). Dissolved oxygen requirement ranges from 0 to 14 mg/l. Increased stress on aquatic life require adequate dissolved oxygen levels, which is very essential for all aquatic habitats. A concentration of 5 mg/l DO is recommended for optimum fish health (Niwa *et al*., 2016). Sensitivity to low levels of DO is species specific, however most species of fish are distressed when DO falls between 2 and 4 mg/l and death usually occur below 2 mg/L. Dissolved oxygen levels can be reduced by process such as respiration process in aquatic organism.

2.3.2 Biochemical oxygen demand

Biochemical oxygen demand (BOD) is the quantity of oxygen used by microbes while consuming organic matter in wastewater, thereby causing degradation of biological material under aerobic conditions (American Public Health Association (APHA), 2017). The amount of organic matter in the water determines the quantity of oxygen organisms required to decay the biological matter, resulting to increasing demand of dissolved oxygen and consequently, increase in BOD level. It is possible to assess the performance of wastewater treatment techniques by measuring the BOD of the animal feed processing wastewater. Factors such as temperature, dilution rate, toxic substance and presence of anaerobic organism can influence this test (Environmental Protection Agency (EPA), 1997). According to Nigeria International Standard (NIS), 6 mg/L is the standard limits for safe water (NIS, 2015) and EPA reported permissible limit of 5-7 mg/l (USEPA, 2018).

2.3.3 Chemical oxygen demand

Chemical oxygen demand (COD) is an essential indicator parameter for estimating the organic content in water. COD gives estimation on how much oxygen would be depleted from a body of receiving water and is expressed in unit of milligrams per liter (mg/l) (Akpor and Muchie, 2019). Sources of organic matter in the water bodies maybe from the raw material used during the processing operation. This can be present either in dissolved form or as particulate organic matter (APHA, 2017). The COD test uses oxidizing agent such as potassium dichromate to oxidize organic matter in the wastewater. The test is extensively used because it takes less time (about 3 h) than other tests such as the BOD which takes 5 days (Geerdink *et al.*, 2017). Standard limit discharge allows a concentration of 40 mg/L in industrial wastewater

2.3.4 Total suspended solids (TSS)

Total suspended solids are solids in water that can be trapped by a filter (Giardino *et al.*, 2017; Zafisah *et al.*, 2018). Total suspended solid include a wide variety of material, such as silt, decaying plant and animal matter, and most importantly industrial wastes. Increase concentration of suspended solids can result to health risk for aquatic life. In addition, TSS can be divided into suspended solids, organic solids, inorganic solids and colloidal suspended solids (70% organic and 30% of inorganic). According to Nigeria International Standards (2015), TSS limit of wastewater is 0.75mg/l.

2.3.5 pH

pH is the concentration of hydrogen ions in water and shows the level of acidity or basicity of an aqueous solution (Dirisu *et al.*, 2016). pH of the environment has a profound effect on the microbial growth rate and also affect the function of metabolic enzymes (Kennedy *et al.*, 2019). Low or high pH alter the structure of the enzymes and stop growth. Nevertheless, most microorganisms can survive within a pH range of 6.5 to 8.5. If the pH of the wastewater is outside the range 5.5-8.5, there may be considerable interference with biological processes. The range 0-6.99 denotes the level of decreasing acidity, pH number 7 is neutral, while the range 7.1-14 denotes increasing basicity (EPA, 2007). However, irregular pH in treatment processes can result in a significant decrease in the rate of removal of pollutants from the wastewater (Nidheesh and Gandhimathi, 2014).

2.3.6 Total phosphorus

Total phosphorus (TP) is any compound that gives rise to phosphate ions (National Pollutant Inventory (NPI), 2019). These includes orthophosphate (dissolved inorganic phosphate) polyphosphate (complex compounds derived from detergents and organically bound phosphate, dissolved and suspended organic phosphates). Total phosphate is naturally limited in most fresh water systems because it is not as abundant as carbon and nitrogen (Swedish EPA, 2006). Phosphorus been an essential nutrient for plants, animals and humans can lead to pollution effect if present in large quantity in the water bodies. This can promote excessive algae bloom, accelerated plant growth and low dissolved oxygen from the decomposition of additional vegetation (Minnesota Pollution Control Agency (MPCA), 2009). According to environmental protection agency, acceptable range for total phosphorus is 10 µg/L to 40 µg/L (Swedish EPA, 2006)

2.3.7 Total nitrogen

Total Nitrogen (TN) is an essential nutrient for plants and animals (EPA, 2013). Total nitrogen in wastewater is usually in the form of organic nitrogen, ammonia or ammonium, nitrate and nitrite. Excess nitrogen in water bodies can harm aquatic life and even cause over stimulation of growth in aquatic plants and algae. This can use up dissolved oxygen as they decompose and block light of deeper waters. This parameter is a growth limiting nutrient in aquatic environments and limit is specified in the wastewater treatment techniques regulations for discharges to sensitive water bodies (EPA, 1997). Acceptable range of total nitrogen is recommended to be 2 mg/L to 6 mg/L by environmental protection agency (EPA, 2013).

2.3.8 Sulphate

Sulphate is an important nutrient for tissue development in plants and animals (Aniyikaiye *et al*., 2019). It is sometimes present in high concentration in many wastewater and natural water bodies (Silva *et al*., 2012). The presence of sulphate ion (SO_4^{2-}) in wastewater maybe as a result of anthropogenic emission from different industries. Certain industry may contain different concentrations depending on the level of usage of sulphate-containing compound in their constituent material. Although, the damage caused by sulphate emissions is not direct since it is a non-toxic compound. Nevertheless, increase level of sulphate concentrations can unbalance the natural sulphur cycle (Lens *et al*., 1998)

2.3.9 Heavy metals

Heavy metals are naturally occurring compounds found in the earth crust, but anthropogenic acivities can increase their availability in different environmental compartments (El-Kady and Abdel-Wahhab, 2018). They are known to be highly soluble in aquatic environments, and as such, can be easily absorbed by living organisms (Mishra *et al*., 2019). Several studies have repoeted heavy metals in the liver, gills, and muscles tissues of various species of fish in contaminated water bodies (Mehmood *et al*., 2019). Once (heavy metals) enter the food chain, they may end up accumulating in the human body. Since heavy metals containing materials are used in industries, toxicity is likely to occur. Thus, this section highlights the heavy metals mostly identify in animal feed processing industry wastewater.

2.3.9.1 Copper

Copper is an essential trace mineral that occurs in all body tissues (Olukosi *et al*., 2018). It is vital for a range of body functions including the production of red blood (Anderson *et al*., 2017). An adult human needs around 1.2 milligrams of copper a day, to help enzymes transfer energy in cells. As human need copper in their diets, animal does because of its antimicrobial activity and growth-promoting effects. Copper has been added to feed mixtures for growing animals at rather high concentrations for several decades (Hassan *et al*., 2018). However, the Cu supplementation of animal diets is regulated by the EU Council Directive 70/524/EEC (EFSA, 2004). This directive limits the total Cu content to 175 mg/kg dry matter (DM) in piglets up to the age of 16 weeks, to100 mg/kg DM in pigs up to the age of 6 months, and to 35mg/kg DM in older pigs. Excess copper in feed formulations may affect aniimal health. This can be detrimental to aquatic species in water and consequently affect human through their food chain.

2.3.9.2 Iron

Iron (Fe) is an indispensable element for the functioning of organs and tissues of higher animals, including fish, because of its vital role in physiological processes such as oxygen transport, cellular respiration and lipid oxidation reactions (Singh and Onuegbu, 2021; Behera *et al*., 2014). Iron is also one of the most essential micronutrients in terms of its effect on the functioning of the immune system and defense against various infections (Maggini *et al*., 2018). Iron deficiency causes immune suppression, growth depression, changes in hematological parameters, susceptibility to diseases, poor food conversion and microcyticanemia in common carp (Ebrahimi *et al*., 2020). Iron is thus essential as feed supplement but its inclusion in excess quantity can be toxic. Its presence in natural water could adversely affect marine animal as a results of bio-accumulation. Hence, it is necessary to determine the occurrence level of Fe in wastewater coming from animal feeds manufacturing plants.

2.3.9.3 Manganese

Manganese is an essential trace mineral that is found in several foods including nuts, legumes, seeds, tea, whole grains, leafy green vegetables and animal feeds (Gharibzahedi *et al*., 2017). It is an essential nutrient because the body requires it to function properly. Manganese is an essential nutrient in humans and animals that plays a role in bone mineralisation, regulation of protein and energy metabolism, cellular protection from damaging free radical species and formation of glycosaminoglycans (Brokesh *et al*., 2020). The total body content is 15 mg and the daily requirement is between 4-10 mg. It is excreted in the bile and the pancreatic juice. Its deficiency causes a defective bone formation and leads to glucose intolerance, alopecia, reddening of hair and dermatitis. Toxicity symptoms include functional abnormalities of the central nervous system (Pallauf *et al*., 2012).

2.3.9.4 Nickel

Ni is considered both an essential and toxic element for humans, animals, plants and microorganisms (Kumar *et al*., 2021). Different forms of Ni occur naturally in the environment, and the element is widely applied in metallurgical, chemical and food-processing industries mainly as a catalyst (Genchi *et al.*, 2020). The essential function of Ni has been established in rats, poultry, swine, goats and sheep. Ni plays a role either as a structural component in specific metalloenzymes (urease, hydrogenase) or as a co-factor in facilitating intestinal absorption of ferric ions (Živkov *et al.*, 2017). The essentiality of nickel metal as feed supplement highlight the possible source of Ni in animal feed processing industry wastewater. This metal can get to the waterway through different operational activities carried out in the industry.

2.4 Wastewater Treatment Technologies

When water is polluted, de-contamination becomes necessary and the best purification approach to consider should be simple, easy and cost effective (Crini *et al.*, 2018).

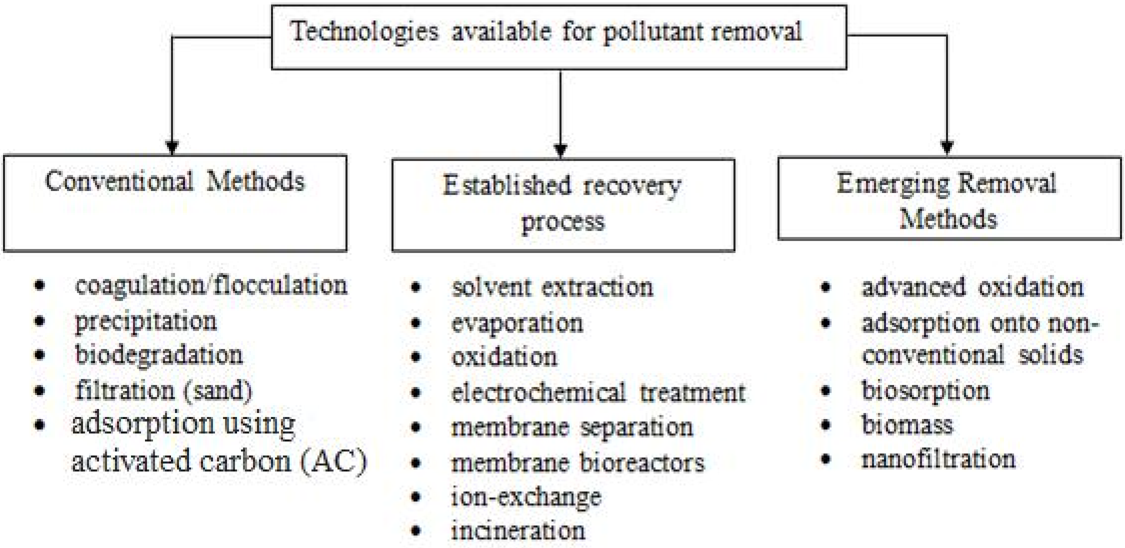

Figure 2.1: Classification of technologies available for pollutant removal and examples of techniques (Rathoure and Dhatwalia, 2016).

In general, conventional wastewater treatment technology shown in figure 2.1, consists of a combination of physical, chemical and/or biological processes. These processes are often employed to remove solids including colloids, organic matter and nutrients soluble contaminants (metals, organics) from wastewater. However, multitude of the techniques classified as conventional methods, including recovery processes and emerging removal methods can be used to treat industrial wastewater (Rathouse and Dhatwalia, 2016). Hence, selection of the method depend on the wastewater characteristics (Sharma and Sanghi, 2012). Each treatment has its own constraints not only in terms of cost, but also in terms of feasibility, efficiency, practicability, reliability, environmental impact, sludge production, operation difficulty, pre-treatment requirements and the formation of potentially toxic by-products (Crini *et al.*, 2018). Thus, technologies for wastewater treatment are reviewed, aiming to offer a brief introduction of treatment of animal feed processing industry wastewater.

Table 2.1: Summary of conventional methods used for the treatment of polluted industrial wastewater with their shortcomings

Conventional Methods for Wastewater Treatment	Shortcomings
Coagulation/flocculation	Requires adjunction of non-reusable chemicals (coagulants, flocculants, aid chemicals) Physicochemical monitoring of the effluent (pH) Increased sludge volume generation (management, treatment, cost).
Chemical precipitation	Chemical consumption (lime, oxidants, H_2S, etc.) Physicochemical monitoring of the effluent (pH) Ineffective in removal of the metal ions at low

	concentration
Filtration	Bubble sizes filtration process for flocs Formation of chemical sludge (filtering problems)
Membrane separation	Investment costs are often too high for small and medium industries High pollution load in the concentrates Expensive and prone to fouling
Floatation	Ineffective for removal of smaller particles High initial capital cost, energy costs, maintenance and operation costs no negligible
Ion exchange	Economic constraints (initial cost of the selective resin, maintenance costs, regeneration time-consuming, etc.) Large volume requires large columns Rapid saturation and clogging of the reactors

Source: Crini *et al.* (2018).

2.4.1 Adsorption technology

Adsorption technology is recognized as an effective and economic method of pollutant removal from wastewaters. The process is characterized by the concentration of molecules onto the surface of a sorbent (Owlad *et al*., 2009; Zinicovscaia, 2016). This process is considered better than other methods because of its convenience, simplicity of design and operation, and the reversibility of the process. Furthermore, this process can remove or minimize different types of pollutants and thus have wider applicability in wastewater pollution control (Zinicovscaia, 2016). A fundamentally important characteristic of good adsorbents is their high porosity and consequent larger surface area with more specific adsorption sites (Bhatnagar and Minocha, 2014). Some adsorbents such as silica gel, commercial zeolites, porous pellets of NaF, iron oxide, pulverized lime stone or dolomite, alkalized alumina, bauxite, xanthate, chitosan, activated carbon, peat moss, bone gelatin beads, bentonite and lignin amongst others have been extensively used for adsorption (Gupta and Balomajumder, 2015; Zare *et al.*, 2015). However, the specific and selective nature of particular adsorbents renders it effective only for few certain applications.For instance, activated carbon (AC) is one of the most widely used sorbents, and usually applied for the removal of organic pollutants from wastewater due to large micropore and mesopore volumes and high surface area (Wong *et al.*, 2018). Nevertheless, the adsorption efficiency of these adsorbentswere considered very low compared to nanosized carbon materials (especially carbon nanotubes), and cannot be applied for complex wastewater treatment processes (Sadegh *et al.*, 2016).

Since the discovery of carbon nanotubes (CNTs) (Iijima, 1991), it has become the favourite adsorbent among carbon based materials because of the unique physical and chemical properties (Ouyang *et al.*, 2002 and Sadegh *et al.*, 2015). Both types of CNTs; single-walled (SWCNTs) and multi-walled (MWCNTs) have been explored as high performance adsorbents for pre-concentration of heavy metal ions (Ravelo-Pérez *et al.*, 2010), organic pollutants (Rastkari *et al.*, 2009) and biological impurities (Upadhyayula *et al.*, 2009) due to their large specific surface area (Perez-Lopez and Merkoçi, 2012; Herrero-Latorre *et al.*, 2018). A comparison of the adsorptive capacity between the carbon nanotubes (CNTs) and commercial powder-activated carbon (PAC) was carried out on Zn^{2+}, with the initial Zn^{2+} concentration range of 10-80 mg/l. The maximum adsorption of Zn^{2+} evaluated by the Langmuir isotherm model for the SWCNTs, MWCNTs and PAC were 43.66, 32.68 and 13.04 mg/g respectively. The time taken to reach equilibrium was minimal and the authors suggested that SWCNTs and MWCNTs were preferably used for removal of Zn^{2+} from aqueous solution. In another study, Gul and Nasreen reported that the concentration of Zn^{2+} sorbed onto the CNTs increased with increasing temperatures. Based on the same condition, the Zn^{2+} sorption capacity of the CNTs was greater compared to that of the commercially available PAC, replicating the fact that the SWCNTs and MWCNTs are better effective sorbents than PAC (Gul and Nasreen, 2018).

Other reports showed that some trace elements including Pb, Ni, Cu, Cr and Cd can be removed by CNTs. Kandah and Meunier (2007) highlighted their achievement in adsorption of some heavy metals using functionalized CNTs and found that the prepared CNTs had high adsorptive capacity. They reported Langmuir model as the most suitable with adsorptive capacity of 18.08 and 49.26 mg/g respectively, with maximum adsorption uptake of Ni^{2+}. The authors found CNTs as the most effective nickel ion sorbent based on the high adsorptive capacity and the short adsorption time (Chen *et al.*, 2009; Sadegh *et al.*, 2016). In addition, Atieh (2011) used CNTs supported by activated carbon for removal of Cr^{6+} from wastewater. The maximum adsorption capacity obtained from batch adsorption experiments using AC-CNTs coated adsorbent was 9.0 mg/g. It was concluded that AC coated with CNTs was most effective for the adsorption of chromium ions.

Huang *et al*. (2008) modified MWCNTs for preconcentration of Pb (II) ion. The MWCNTs were immobilized by the tri-(2-aminoethyl) amine (TAA), which has been demonstrated as a good chelating reagent for metal ions. The MWCNTs-TAA composites were investigated for its adsorptive capacity on Pb (II) through solid phase extraction (SPE), a process using a micro-column packed with MWCNTs-TAA. The result indicated that the dispersibility of pristine-MWCNTs is obviously not as effective as MWCNTs-TAA. Although, both pristine-MWCNTs and MWCNTS-TAA showed good selectivity for adsorption of Pb (II) ions.

A critical in-depth reviewof literature revealed that the structural features, morphology, curvature of sidewalls, π-conjugative structures and active sites are some of the physical properties possessed by CNTs that have facilitated their adsorptive properties (Sadegh *et al*., 2016). Furthermore, the length and size of material which ranged from nanometers to millimetres (length) with diameters upto 100 nm has been seen to exhibit a larger specific surface area, high porosity hollow and layered structures. These unique properties are the cause of strong interactions between CNTs and other molecules or atoms through π-π electronic transition and hydrophobic interactions, consequently, making them promising adsorbent material (Gusain *et al*., 2020). For this reason, efforts have been made to develop more effective CNT-based adsorbents for the removal of heavy metals, traces of organic pollutants and inorganic substances from aqueous solution such as industrial animal feed processing wastewater.

2.4.2 Types of adsorption

Fundamentally, there are two forms of adsorption process namely: physical adsorption and chemical adsorption and may be distinguished based on the nature of interaction or bonding involved (Ahmed and Jhung, 2017). The third, which required an appropriate amount of energy to activate and conduct the transfer of molecules onto a solid surface is simply refers to as “activated adsorption”. It is said to be a surface phenomenon that is catalytically active when part of molecule is taken up and remains attached to the surface. Adsorption phenomenon occurs at interfaces between solid-gas, liquid-gas, solid-liquid, solid-solid and liquid-liquid and only solid-liquid interface has found better applications in water and wastewater treatment (Shen *et al*., 2018).

In physical adsorption process (Physisorption), there exist weak intermolecular forces including Vander Waals, hydrogen bond and dipole-dipole interactions between the adsorbate and the solid surface (adsorbent) (Ammendola *et al*., 2017). There is no transfer or sharing of electron and yet, new equilibrium adjustment takes place without losing the original association of electron with their respective interacting species (Ammendola *et al*., 2017). These weak forces are characterized by low heats of adsorption typically below 10 Kcal/mole, no violent or disruptive structural changes. This type of adsorption process is substantial only at temperature lower than the boiling point of adsorbate. Therefore, increase temperatures tend to hinder physical adsorption process. Nonetheless, better adsorption equilibrium is achieved more quickly since no activation energy is required and it can involve multiple layers of adsorbate as its allowed for pore measurements. Physisorption is reversible in nature and non-specific with respect to the adsorbent, thus allowing adsorbate to fully adsorb and desorb. In this process, surface area and porosity are important properties that influence the quality and character of an adsorbent (Condon, 2019).

Chemical adsorption simply occur when strong electrostatic forces such as electrovalent and covalent chemical bonds exist between the solid phase material (adsorbent) and the molecules which adhered on the surface of the material through exchange of electrons (Li *et al*., 2017). This process is characterized by large interaction potentials which lead to increase heat of adsorption usually within 50-200 Kcal/mole and can occur at high temperatures (Ammendola *et al*., 2017). As in the case of most chemical reactions, chemisorption is usually associated with an activation energy, which implies that molecular species attracted to a surface active site must pass through an energy barrier before they are strongly bonded to the surface. Generally, the reaction is irreversible in nature and nonspecific with both adsorbate and adsorbent (Karunadasa and Solis-Ibarra, 2019). Chemical adsorption process measures the amount of surface active sites which ensured promotion of a specific catalytic reaction. Critical parameters for chemisorption measurement include the area of the active element, metal dispersion, surface acidity and exposed proportion of the active element (Ammendola *et al.*, 2017).

2.4.3 Factors influencing adsorption from aqueous solution

A good number of materials including synthetic, natural and semi-synthetic adsorbent have been investigated for pollutant removal from aqueous solution (Abazari *et al.*, 2019). The amount of species usually adsorbed from the solution on to a solid phase depends on different operating conditions such as nature of adsorbent and adsorbate, surface area and porosity of the adsorbent, effect of temperature, adsorbent dosage, solution pH and contact time (Iftekhar *et al.*, 2018). In order to see the effects of various parameters. It is necessary to have a substantial knowledge on different operating conditions to achieve efficient adsorption process. In this section, the factors influencing adsorption from aqueous solutions are highlighted as follow.

2.4.3.1 Nature of adsorbent and adsorbate

The physicochemical nature of an adsorbent determines its effect on both rate of adsorption and adsorption capacity (Ipek *et al.*, 2017). Thus, an adsorbent type basically depends on the chemical composition of the solid material. But, the surface upon which the adsorption process takes place is influenced by the presence of pores, edges, corners, cracks and pre-treatment (activation) (Angin, 2014). As in the case of adsorbate, adsorption can be attributed to several factors including its solubility in the experimental solvent, its chemical constituents and physical state in solution among others. Solubility of the solute (adsorbate) is a controlling factor in the study of adsorption equilibrium. Large increase in adsorption could lead to decrease in solubility of the solute (Cunningham *et al*., 2018). That is, the greater the solubility, the stronger the bond between the solute-solvent interaction and the lesser the extent of adsorption (Mananghaya *et al*., 2019).

2.4.3.2 Surface area and porosity of the adsorbent

The extent of accumulation of molecular species on to a solid phase is directly proportional to the specific surface area of an adsorbent (Tandon and Sai, 2020). Specific surface area can be described as the active portion of the total surface that is available for adsorption. Therefore, the level of adsorption achieved per unit weight of the adsorbent material is greater when the material is more porous and finely divided. Studies have shown that porous materials like modified carbon; break up bigger particles into smaller ones, which can open up some tiny, sealed pores in the material and may become available for adsorption (Huang *et al*., 2008) and thus, leading to dependence of adsorption capacity on particular size of a material (Yu *et al*., 2019)

2.4.3.3 Influence of temperature

Temperature is one of the important variables that are unlikely to change in natural water bodies (Ali *et al*., 2016). Largely, the temperature of solution influences the extensive nature of the adsorbent (Ali *et al*., 2016; Iftekhar *et al*., 2018), which plays a crucial role in an adsorption studies. Lower temperature range usually from 20-30 °C is favorable to larger adsorption, but decreases with temperature increase above a critical value. Only in few cases, elevated temperature improves the adsorption of contaminants on to solid surface (Iftekhar *et al*., 2018). Studies have demonstrated that the binding of metallic particles to the active sites of a solid material at lower temperature is more rapid, easy and reversible due to low energy requirement (Bernal *et al*., 2018). But in reality, temperature variation depends on the nature of adsorbate-adsorbent interaction (Bernal *et al*., 2018).

2.4.3.4 Effect of adsorbent dosage

The concentration of an adsorbent is one of the most important factors affecting adsorption process (Le-Minh *et al*., 2018). In general, the degree of adsorption of a solute increases with increase in the dose of an adsorbent due to increase in exchangeable adsorption site (Uddin, 2017; Rao *et al*., 2019). Hence, the total solute adsorption per unit weight of an adsorbent can decrease upon the increase in adsorbent dosage interference caused by the interaction of an active sites of an adsorbent material with the adsorbeate (Xie *et al*., 2015; Iftekhar *et al*., 2018). Studies have shown that increase in concentration of an adsorbent lead to an increase in accumulation of pollutant (Adeyemo *et al*., 2017). Torab-Mostaedi *et al*. (2015) found that after certain increase in concentration of the adsorbent, the removal rate decreases due to exhausiveness of the binding sites. Thus, it is important to optimize the dose of an adsorbent for better and efficient pollutant removal.

2.4.3.5 Effect of solution and adsorbent pH

Adsorption process is very much dependent on pH of the solution. pH remains an important process variable that can directly influence the uptake of molecular species from aqueous solution because it can affect surface characteristics of an adsorbent (Crini *et al*., 2019). In order to understand the effect of hydrogen ion concentration on pollutant removal from aqueous solution, the majority of colored materials encountered in industrial wastewater explain the whole concept. Therein, most of the materials are negatively charged and ordinary carbon will give better decolorization with changes in pH of the solution. Thus, the pH of the adsorbent itself is a basic factor, as this may greatly influence the acidic or basic level of the liquid. Recently, studies revealed that adsorption of metal ions on adsorbent is due to ionic force existing between them and at lower pH values; the metals are in competition with the H^+ in the solution (Zhang *et al.*, 2019).

2.4.3.6 Effect of contact time

To a significant level, contact time influences the economic efficiency of adsorption process as well as adsorption kinetics. Hence, representing one of the performance governing factor affecting adsorption process (Srivastava *et al.*, 2015). Numerous studies have shown that adsorption efficiency of pollutant, especially metal ions increases with increase in contact time of the adsorbent (Patel, 2019). On the contrary, Haldorai *et al.* (2015) observed that there is always a reduction in adsorption efficiency of metal ion when there is an increase in contact time from 60 to 150 min. Generally, metal adsorptions occur in two steps and equilibrium is always achieved after which any further adjustment in time do not show any increase in adsorption. Therefore, adsorption rate is usually faster and the accumulations of pollutants normally occur at the initial contact time (Banerjee and Chattopadhyaya, 2017).

2.4.4 Modeling and mechanism of adsorption

Batch adsorption is characterized by the adsorption equilibrium (adsorption capacity), adsorption kinetics and the thermodynamics of the process (Romero *et al.*, 2016; Bai *et al.*, 2020). The experimental set up of this process is simple and easily reproducible (Fan *et al.*, 2020). The batch process is often used to adsorb solutes from liquid solution to be treated when adsorbent are mixed and agitated in a contacting reactor under a period of time to enable the system reach an equilibrium. Following the resulting solution, the mixture (slurry) would be filtered to separate the adsorbent and adsorbate from the solution. In a solid-liquid system, batch adsorption studies employ the fact that adsorption process leads to variation in the concentration of the solution. Thus, adsorption isotherms are constructed in order to evaluate the concentration of adsorbate in the medium prior and after adsorption at a fixed temperature (Naushad *et al.*, 2019).

As with many other process, data including adsorption equilibrium and adsorption kinetic studies are performed using different operational parameters, which usually involve mixing of fixed volume of contaminant solution in a closed flask, with a known quantity of the adsorbent in controlled conditions of contact time, a known degree of agitation, temperature range and pH of the solution. Then, the residual concentration of the adsorbate can be determined quantitatively by using a linear regression equation presented in Equation 2.1

$$q_e = \frac{v(C_o - C_t)}{m} \qquad 2.1$$

Where q_e (mg/g) is the concentration of the adsorbate per unit mass of an adsorbent at time t, C_o and C_t (mg/L) are the initial feed concentration and final equilibrium concentration respectively. V is the volume of the feed solution in cm^3, and m, is the amount of the adsorbent in milligrams (mg). In view of the fact that adsorption process can be more complex. Several adsorption equilibriums were proposed.

2.4.5 Adsorption equilibrium

Adsorption equilibrium data is the most essential piece of information required for better understanding of an adsorption process. Therefore, adequate knowledge and interpretation of isotherm models are needed in optimizing the use of adsorbent, total improvement of adsorption mechanism pathway and effective design of the process operation (Ayawei *et al.*, 2017). In decades, linear regression analysis has been one of the utilized tools for describing the best fitting models because it estimates the distributions of adsorbates, evaluates the adsorption system and verifies the consistency of theoretical hypothesis of adsorption isotherm model (Sandoval *et al.*, 2018). The commonest isotherms used to describe the adsorption process in industrial wastewater include Langmuir, Freundlich, Temkin, Halsey, Flory-Huggins and Dubinin-Radushkevich isotherm models.

2.4.5.1 Langmuir isotherm model

The Langmuir isotherm which was primarily designed to describes monolayer adsorption process on to a surface containing a finite number of adsorption sites, is used to quantify and contrast the adsorptive capacity of different adsorbate (Elmorsi, 2011). Langmuir model account for the surface coverage by balancing the rate of adsorption and desorption (dynamic equilibrium). That is, once a site is filled up with adsorbate, no further sorption can take place at that site. This indicates that the surfaces have reached a saturation point where the maximum adsorption of the surface will be achieved. The isotherm is then expressed in linear form as represented in Equation 2.2 (Da'browski, 2001).

$$\frac{C_e}{q_e} = \frac{1}{K_L q_{max}} + \frac{C_e}{q_{max}} \qquad 2.2$$

By rearranging Equation 2.2,

$$\frac{1}{q_e} = \frac{1}{C_e} \cdot \frac{1}{q_{max}} + \frac{K_L}{q_{max}} \qquad 2.3$$

$$Q_{mmc} = \frac{q_{max}}{K_L} \qquad 2.4$$

Where q_e is the amount (mg/g) of adsorbate per unit mass of an adsorbent at equilibrium time, C_e is the equilibrium concentration of liquid after adsorption (mg/L), q_{max} and K_L are empirical constant from Langmuir isotherm model, related to maximum adsorption capacity (mg/g) and the heat of adsorption (dm^3/g), and Q_{mmc} is the maximum monolayer coverage capacities (mg/g). A plot of $1/q_e$ versus $1/C_e$ will give a straight line graph when Langmuir isotherm fits the adsorption process with the slope $1/q_{max}$ and intercept K_L/q_{max}. Inverse of the intercept will give the value of Q_{mmc}. Langmuir isotherm is however characterized by a dimensionless constant which is expressed as a separation factor R_L as shown in equation 2.5 (Ayawei *et al.*, 2015)

$$R_L = \frac{1}{1 + K_L C_o} \qquad 2.5$$

Where K_L is Langmuir constant (mg/g) and C_o is initial concentration of adsorbate (mg/g), R_L values indicates the adsorption type of Langmuir isotherm to be unfavourable when greater than 1, irreversible when $R_L = 0$, linear when$R_L = 1$ and it is said to be favourable when $0 < R_L < 1$.

2.4.5.2 Freundlich isotherm model

The Freundlich model was developed basically for adsorption process that take place on an energetically heterogeneous surface with different adsorption sites (Ayawei *et al.*, 2015). This isotherm also gives an expression which describes surface heterogeneity and experimental distribution of active sites and their energies. The linear form of freundlich model is given in Equation 2.6

$$q_e = K_f C^{1/n} \qquad 2.6$$

By rearrangement, Equation 2.7 is obtained

$$Log q_e = Log K_f + {}^{1}/_{n} Log C_e \qquad 2.7$$

Where K_f is freundlich adsorption capacity (L/mg) and $1/n$ is adsorption intensity; it also indicates the relative distribution of the energy and heterogeneity of the adsorbate site. By plotting the graph of $Log\ C_e$, a straight line graph will be obtained such that $1/n$ and Log$K$, represent the slope and intercept, respectively.

2.4.5.3 Dubinin-Radushkevich isotherm model

Dubinin Radushkevich (D-R) isotherm model is an experimental adsorption model that is commonly used in expressing adsorption mechanism with Gaussian energy distribution onto heterogenous surfaces (Saeidi and Parvini, 2016). This model is only fitted for intermediate range of solute concentrations data well because it reveals unlikely asymptotic properties and constraint of not being able to predict Henry's law at low pressure (Ayawei *et al.*, 2017).

The isotherm model is a semi-emperical equation in which adsorption of gases onto micro-porous solid material follows a pore filling mechanism (Wang and Guo, 2020). This model assumes a multi-layer character involving a weak Van Der Waal's forces, and it is generally applied to distinguish between chemical and physical adsorption of metal ions. A unique property of the D-R isotherm model is that it is temperature dependent. Thus, when a well of adsorption data are plotted at different temperatures "as a function of logarithms" of total solute adsorbed versus the square of potential energy, all suitable data will be fitted along the same curve, called the characteristic curve. The (D-R) isotherm equation is expressed as follow

$$q_e = q_m(- K_{(D-R)}\epsilon^2) \quad 2.8$$

$$\ln q_e = lnq_m - K_{(D-R)}\epsilon^2 \quad 2.9$$

Where q_m (mg/g) is the saturation theoretical capacity, $K_{(D\text{-}R)}$ is Dubinin-Radushkevich constant, representing the mean free energy of adsorption ($mol^{-2}KJ^{-2}$). Value of q_m and $K_{(D\text{-}R)}$ can be extrapolated from a graph of $\ln q_e$ versus ϵ^2. ϵ is polanyi potential which can be calculated as represented in Equation 2.10

$$\epsilon = RT\ln\left(1 + \frac{1}{C_e}\right) \qquad 2.10$$

$$E = \frac{1}{\sqrt{2K_{(D-R)}}} \qquad 2.11$$

Where, R is gas constant (8.314 $Jmol^{-1}K^{-1}$), T is absolute temperature and E as represented in equation 2.11, is the mean adsorption energy. If E < 8 $KJmol^{-1}$, the process is said to be physisorption, while if $8 \leq E \leq 16$ $KJmol^{-1}$, the results indicates that the process is chemisorption or the adsorption process is taken by ion exchange mechanism.

2.4.5.4 Temkin isotherm model

Temkin isotherm model is an adsorption model that explained the effect of indirect adsorbent-adsorbate interactions. This model presumes that the change in heat of adsorption (ΔH_{ads}) of all molecules in the layer is likely to decrease linearly rather than the logarithms coverage that will disregard the higher and lower concentration value. The Temkin model is valid for an intermediate range of ion concentration (Shahbeig *et al.*, 2013; Al-Ghouti and Da'ana, 2020). The isotherm is expressed as

$$q_e = \frac{RT}{b} lnK_T C_e \qquad 2.12$$

And, the linear form of Temkin isotherm model is represented in equation 2.13

$$q_e = AlnK_T + A\ln C_e \qquad 2.13$$

Where $A = \frac{RT}{b}$,

Where, b is Temkin constant which is related to the heat of adsorption (Jmol^{-1}) and K_T is Temkin isotherm constant (Lg^{-1}), representing the equilibrium binding constant or maximum binding energy. T is the absolute temperature and R is the universal gas constant (8.314 JMol^{-1}K^{-1}). A graph of q_e versus $ln\,C_e$ gives a line with slope, A, and intercept, A $ln\,K_T$

2.4.5.5 Halsey isotherm model

The Halsey Isotherm model is used generally to evaluate multi-layer adsorption of a solute onto adsorbent material at a relatively large distance from the surface (Ayawei *et al.*, 2015). The adsorption isotherm can be expressed as followed in equation 2.14

$$q_e = \frac{1}{n_H} ln \frac{K_H}{C_e} \qquad 2.14$$

and, the linear form is given by equation 2.15

$$q_e = \frac{1}{n_H} lnK_H - \frac{1}{n_H} lnC_e \qquad 2.15$$

Where, K_H and n_H are Halsey isotherm constant and they can be obtained from the slope and intercept of the plot of ln q_e against $ln\,C_e$

2.4.5.6 Flory-Huggins isotherm model

Flory-Huggins isotherm model is an empirical model that describes the degree of surface coverage properties of adsorbate on adsorbent. This model can also express the feasibility of an adsorption process as well as the spontaneity of the surface coverage. The linear form of the Flory-Huggins equation is expressed as follow in Equation 2.16

$$ln \frac{\theta}{C_o} = lnK_{FH} + nln\,(1 - \theta) \qquad 2.16$$

Where, $\theta = (1 - C_e/C_o)$ is the degree of surface coverage, n is number of adsorbates occupying adsorption sites, K_{FH} is Flory-Huggins equilibrium constant ($Lmol^{-1}$) and it is used to calculate spontaneity Gibb's free energy as shown in Equation 2.17

$$\Delta G^{\circ} = RTlnK_{FH} \tag{2.17}$$

Where, ΔG° is standard free energy change, T is absolute temperature, and R is universal gas constant (8.314 $Jmol^{-1}K^{-1}$).

2.4.6 Adsorption kinetics

For accurate measures of adsorption mechanism and the rate limiting steps, the knowledge about kinetic models is of utmost importance to select optimum parameters for the design of full scale batch process (Zhang *et al.*, 2018). In past few years, several models have been used by researchers to determine the models best fitted for experimental data obtained (Largitte and Pasquier, 2016). It is well known that there are steps in a solid-liquid interface adsorption viz-a-viz: migration of molecular species or ions from the bulk of solution to the material surface (Bulk diffusion), the molecule diffuses through the outer layer to the surface of the material (film diffusion); the ion then diffuses from the surface to the interior of the particle (pore diffusion, interparticle diffusion); and lastly, the molecules make contact with the active sites on the surface of the material (physical and chemical adsorption).

In essence, adsorption kinetics measure the rate of uptake caused during accumulation of adsorbate material with respect to time at a constant concentration and it is used to estimate the difussion of adsorbate in the pores of adsorbent (Banerjee and Chattopaadhyaya, 2017). Kinetic models explain the rate at which an adsorbate is retained or release from aqueous media to solid-phase interphase at a particular dosage, temperature, pH and contact time (Al-Saidi *et al.*, 2016). Among these kinetic models, three most widely used models including pseudo-first-order model, pseudo-second-order model and intra-particle diffusion model are summarized below.

2.4.6.1 Pseudo-first-order kinetic model

This model is represented in the linear form described by Equation 2.18

$$Ln\ (C_t) = Ln\ (C_e) - Kt \qquad 2.18$$

Where: C_t is the concentration of adsorbate adsorbed per unit mass of adsorbent (mg/g) at a particular time, while C_e is the concentration of adsorbate adsorbed per unit mass of adsorbent at equilibrium. $K$is the rate constant of first order sorption (min^{-1}). The plot of $ln\ (C_t)$ against t gives $Ln\ (C_e)$ and K as intercept and slope respectively.

2.4.6.2 Pseudo-second-order kinetic model

This kinetic model is given in Equation 2.19, where q_t (mg/g) and q_e (mg/g) are the amount of contaminants adsorbed at time t and equilibrium, respectively; K_2 is the equilibrium rate constant of pseudo-second-order adsorption (g/mg.min). The parameters K_2 and q_e can be obtained directly from the slope and intercept of the linear plot of $t/_{q_t}$versus t.

$$\frac{t}{q_t} = \frac{1}{K_2 q_e{}^2} + \frac{1}{q_e} t \qquad 2.19$$

2.4.6.3 Intra-particle diffusion model

This kinetic model explains the diffusion mechanism of adsorption process. In a batch system involving rapid stirring, there is a prospect that the migration of adsorbate from aqueous solution into the bulk of the adsorbent is the rate controlling step. This prospect was verified in terms of a graphical relationship between the amount of contaminant adsorbed and the square root of time. According to the intra-particle diffusion model proposed by Weber and Moris (1963), the initial rate of diffusion model is represented in Equation 2.20.

$$q_t = K_t t^{1/2} + C \qquad 2.20$$

Where q_t is the amount of contaminant on the surface of the adsorbent at time t (mg/g); C is the intercept (mg/g), K_t is the intra-particle diffusion rate constant (mg/g min$^{1/2}$) and t is the time (min). However, a plot of q_t against $t^{1/2}$ should be in a straight line when adsorption mechanism obeys the intra-particle diffusion process. But, if otherwise, it implies that intra-particle diffusion along with other models may control the adsorption rate.

2.4.7 Thermodynamic studies

The study on the effect of temperature provides additional information as regards the thermodynamic parameters such as change in standard Gibb's free enegy (ΔG^o), enthalpy (ΔH^o) and entropy (ΔS^o). The ΔG^o was determined by the relation in Equation 2.21 as recommended by Liu and Liu. (2008).

$$\Delta G^o = - RTLnK_c \qquad 2.21$$

R, denotes the gas constant (KJ/mol), T is the absolute temperature, and K_c represents the apparent equilibrium constant of the adsorption process, which was calculated at temperature interval using the relationship in equation (2.22)

$$K_c = q_e/C_e \qquad 2.22$$

Where, q_e (mg/g) is the equilibrium concentrations of metal ions on adsorbents (adsorption amount), and C_e is equilibrium of metal ion concentration (mg/g) in solution. Van't Hoff equation was used to evaluate the change in enthalpy (ΔH^o) and entropy (ΔS^o) from the slope and intercept of the plot of LnK_c against $1/T$ as represented in Equation 2.23

$$\Delta G^o = \Delta H^o - T\Delta S^o \qquad 2.23$$

On substituting Equation (2.23) into Equation (2.21), the Equation is given as

$$\mathrm{LnK}_c = -\frac{\Delta G^o}{RT} = \frac{\Delta S^o}{R} - \frac{\Delta H^o}{R}\left[\frac{1}{T}\right] \qquad 2.24$$

The plot of LnK_c as a function of $1/T$ yields a straight line graph, from which thermodynamic parameters (ΔH° and ΔS°) were calculated by the slope and intercept, respectively.

2.5 Nano-adsorbents in wastewater treatment

Several physicochemical techniques including adsorption technology have been used for the treatment of wastewater and different results have been reported (Agboola *et al*., 2020). However, nano-adsorbents are fast emerging as effective candidates for wastewater treatment in place of conventional technologies which, notwithstanding their efficacy are time consuming (Amin and Chetpattananondh, 2019).

The removal of pollutants from wastewater using nanomaterial has received considerable attention due to the large surface area and availability of active sites (Madima *et al*., 2020). The limitation of using nanomaterial for water treatment is in the aggregation of nanomaterial and toxicity issue. This can be overcomed by incorporating different nanomaterials with less toxic properties to form a composite with an improved adsorptive capacity. The immobilized nanocomposites with fascinating properties are usually stable and effective when used as an adsorbent in wastewater treatment technology. Thus, these adsorbent materials (nano-adsorbents) can be substituted for conventional materials that require more raw materials and is more energy demanding (Bhattacharya *et al*., 2013). Therefore, employing green chemistry principle in fabrication or manipulation of these nano-adsorbents can leads to a great reduction in the use of hazardous chemical for their synthesis.

2.5.1 Silver and palladium nanoparticle (AgNPs and PdNPs)

Earlier before now, silver ion and silver based compounds are among the recognized antimicrobial agent in 1000 BCE because of their medicinal importance and they have been applied successfully as an efficient health additive in Chinese and Indian Ayurveda medicine (Deshmukh *et al*., 2019). The choice of silver in this study is due to its multi-functional properties as a potent disinfectant (Deshmukh *et al*., 2019). Its nitrate form has been used for antimicrobial actions long time ago, but recently, nano-based silver (as in silver nanoparticles) has proven to be more efficient in antimicrobial action.

Silver nanoparticles (AgNPs) are highly toxic to microorganisms with strong antibacterial activity against a wide range of microorganisms, including viruses (Borrego *et al*., 2016), bacteria (Kalhapure *et al*., 2015, Suryawanshi *et al*., 2018) and fungi (Krishnaraj *et al*., 2012). This is because of its physicochemical properties in which larger surface area to volume ratio bring about higher surface exposure to the microbes which resulted to a better antimicrobial activity. Furthermore, the exceptional features such as size, shape, phases play an important role in bacterial inactivation or killing of bacteria. These properties of AgNPs justify its foremost application as an effective environmental disinfectant. Hitherto, AgNPs also play a fundamental role in water and wastewater purification, but its direct application might cause some problems such as their tendency to aggregate in aqueous media that gradually reduce their efficacy during long term usage (Li and Lenhart, 2012).

Wolska and Grudniak (2020). examined the bactericide effects of AgNPs on *Staphylococcus aureus, Pseudomona aeruginosa, Escherichia coli, Bacillus cereus, Listeria innocua* and *Salmonella choleraesuis* bacteria due to its higher toxic effect to their cells. The mechanisms of its action (AgNPs) are not clearly known and still remain under debate (Lu *et al*., 2016). Several theories have been put forward to explain the mechanistic action of AgNPs in combating microorganisms and literature search revealed that AgNPs possess broad scope to improve efficiently by optimizing its physicochemical parameters, which could results to greater binding capacity or capability to adhere to bacterial cell wall, and subsequently penetrate the wall. These penetrations can therefore leads to structural changes of the cell membrane and thus increase the permeability of the AgNPs (Ahmed *et al.*, 2018). As soon as the AgNPs are in contact with the bacteria cell, free radicals can be generated and these could lead to killing of the cells or possess the ability to damage the cells (Pandey *et al.*, 2014). In addition, the effect of AgNPs incorporated onto polyethersulfone (PES) microfiltration membrane had also been investigated by Ferreira *et al.* (2015). They highlighted that microorganisms near the membrane were suppressed remarkably. Thus, their findings revealed that PES-AgNPs membrane exhibited strong antibacterial properties and can be applicable for water purification.

Palladium nanoparticles (PdNPs) are also effective in catalysing a variety of reactions, such as denitrification and azo dye reduction (Johnson *et al.*, 2013). Palladium nanoparticle have been reported to improve the degradation ability of anaerobic granular sludge towards the iodinated contrast media "iohexol" (these compound are metabolically stable in wastewater body), that can hardly be degraded in conventional biologically wastewater treatment technology.

Commonly, metallic nanoparticles are often fabricated using chemical methods with lots of chemicals under harsh conditions. However, preparation through green synthesis route is regarded as a primary and environmentally friendly method as it uses non toxic chemicals as reducing and stabilizing agents. Unlike nanoparticle prepared using chemical methods, which are usually not stable, easily aggregate with activated sludge and influences toxic chemical sludge (Gurunathan and Kim, 2016; Zhou *et al.*, 2015).

The metallic nanoparticles formed by green route are in good dispersion and more stable (Hennebel *et al*., 2011).

2.5.2 Synthesis method of nanoparticles

Metallic nanoparticle is basically synthesized using three different approaches, such as physical, chemical and biochemical (Green Chemistry) methods (Zhang *et al*., 2016).

2.5.2.1 Physical synthesis approach

In physical processes, nanoparticles are usually synthesized by evaporation-condensation, which could be carried out using a furnace at atmospheric pressure (Kruis *et al*., 2000; Zhang *et al*., 2016). Conventional physical methods including spark discharging and pyrolysis were used for the preparation of AgNPs (Tien *et al*., 2008). Nanoparticles of various materials, such as Ag, Au, PbS and fullerence, have previously been synthesized using the evaporation-condensation methods (Natsuki *et al*., 2015). Jung *et al*., (2006) reported the synthesis of Ag nanoparticles via cube-furnace evaporation-condensation method using a small ceramic heater with a local heating area. The Ag nanoparticles formed are spherical and well dispersed. The advantage of physical methods are speed, radiation used as reducing agents, and no hazardous chemical involved, but has several drawbacks such as low yields and high energy consumption needed to raise the environmental temperature around the source material, solvent contamination, and lack of uniform distribution (Shameli *et al*., 2010; Elsupikhe *et al*., 2015). However, this process requires significant time to establish thermal stability.

2.5.2.2 Chemical synthesis approach

In chemical synthesis approach, chemical reduction methods (inorganic or organic solvents) are generally used for the preparation of silver nanoparticles. This synthesis method includes a hydrothermal method (Zou *et al*., 2007), sonochemical method (Liu *et al*., 2004), electrochemical method (Rodrigues-Sanchez *et al*., 2000), microwave assisted method (Yin *et al*., 2004), sol-gel method (Zhang *et al*., 2014) and wet chemical method (Panigrahi *et al*., 2006). The most common approach for synthesis of metallic nanoparticle is the wet chemical method, using organic and inorganic reducing agents for the reduction of metallic salt, forming a nucleus and the growth of the nucleus to a particle is usually controlled by capping agents which also prevents aggregation by steric hindrance or electrostatic repulsion.

In the course of preparing silver and palladium nanoparticles with controlled size and shapes, the precursor salts mixed with suitable solvents and capping agent is used to control the morphology to form well dispersed nanoparticle. This often prevents agglomeration and lead to the subsequent formation of the nanoparticles (Bhosale and Bhanage, 2015). Many researchers have reported the synthesis of silver nanoparticles with various size and morphology using different capping agents and reducing agents. Capping agent such as polyvinyl alcohol (Zielinska *et al*., 2009) and cetyl trimethyl ammonium bromide (CTAB) (Lee *et al*., 2004) are usually employed to bind the surface of nanoparticles and avoid their agglomeration. Various reducing agents used include sodium citrate, sodium borohydride, hydrazine hydrate, formaldehyde, elemental hydrogen, and dextrose among others.

2.5.2.3 Green chemistry approach

To overcome the shortcomings of chemical methods, biochemical methods have emerged as a viable option. In recent years, biochemical mediated synthesis of nanoparticles have been shown to be simple, cost effective, dependable and environmentally friendly. Thus, much attention has been given to the high yield of production of metallic nanoparticle of defined size. Using various biological systems including bacteria, fungi, plant extracts and biomolecules like vitamins and amino acids is an alternative method to chemical synthesis methods (Gurunathan *et al*., 2014; Gurunathan and Kim., 2016).

The metallic salt, reducing agent and capping agent are important components in chemical approach for synthesis of nanoparticles. However, the reducing, capping or stabilizing agents can be obtained from natural sources such as plant extracts and subsequently used in the synthesis of metallic nanoparticles of desired size and shape (Abdelghany *et al.,* 2018). More recently, several plant extracts have been emerged as novel resources for their ability to produce safe and non-toxic nanoparticles (Saminathan, 2015; Divya *et al*., 2016). For instance, Francis *et al*. (2017) reported the synthesis of silver nanoparticle via micro-wave assisted method. Leaf extract of *Elephantopus scaber* was employed for the fabrication of spherical silver nanoparticle in their study.

2.5.3 Phytochemical constituents of plant extract

Chemical substances mainly produced by plants are generally refers to phytochemicals and these substances possess biological activity. In the field of nanotechnology, plants remain the potential source to obtain various secondary active metabolites (Mohamad *et al*., 2013). Using their extracts in biochemical synthesis of various nanomaterials, they exhibit important functional groups such as hydroxyl and carboxylic groups containing compounds, which could perform the role of reducing agent as well as stabilizing agent. Basically, most plant contains secondary metabolites (such as phenolic compounds, vitamins, nitrogen compound, terpenoids, reducing sugar) that are rich in free radical scavenging molecules and some others that are very rich in antioxidants activity (Salam *et al*., 2014). However, in attempt to synthesize metallic nanoparticle that is free of toxic by-product, the synthesis procedures need to be carried out under appropriate temperature in an aqueous medium and thus, its worthy to be considered as a green process.

Recently, researchers have centered on plant-oriented nanoparticle synthesis due to its numerous advantages over conventional synthesis methods (Zohra *et al*., 2019). Amin *et al*. (2012) revealed that plant reduction mechanism is a factor in controlling the size of nanomaterial as well as its stability. With respect to that, aqueous extract of plant material are usually analysed quantitatively for their chemical constituents and phenolic compounds have been reported to be the most common metabolites present in all plants (Mohamad *et al*., 2013). Plant extract is considered as a cost effective approach since its preparation involved the use of agro-waste such as leave, roots, fruit peels and flowers. These natural resources can be employed either as a fresh or dried materials. However, it has been reported by Naithani *et al*. (2006) that phytochemicals and antioxidant content of plant material reduces when dried either directly under sunlight (Gopinath *et al*., 2012) or at room temperature (Mittal *et al*., 2013). Both methods reduce cost, but they require days or hours to dry the plant materials completely. On the contrary, Mohd *et al*. (2009) evidenced that samples dried with freeze-dryer was the pre-eminent method so as to preserve the content of reducing agents concurrently.

All the same, the types of solvent used during extraction significantly determine the quantity of reducing agents extracted. The extraction process generally involves dispersing the plant material in water under constant agitation. Other possible extraction can involve the use of organic solvent mainly ethanol or methanol, but, extraction done by aqua media is more favorable due to its simplicity since the aqueous extraction would be free of contamination from solvent. Also, Yu *et al.* (2012) shows that the concentration of the extract increase as the temperature increases from 60 to 80 ℃, and when the temperature is elevated to 90 ℃, there is no significant increase in the antioxidants content. Thus, it implies that antioxidants degraded as the temperature increased. This trend is confirmed by Michiels *et al.* (2012) who reported that too much heat destroyed the cell wall which helps in the release of antioxidants. Hence, it is necessary to control the degree of hotness to a moderate temperature during the preparation of plant extracts so as to achieve optimum yield.

2.5.4 Carbon nanotubes

In 1991, the Japanese researcher S. Iijima discovered carbon nanotubes (Iijima, 1991). They are allotropes of carbon that are composed of cylindrical graphite sheets rolled up in a tube-like structure (Mojica *et al.*, 2013). Carbon Nanotubes **(**CNTs) have attracted great interest as an emerging adsorbent due to their unique properties. With an extremely large specific surface area and abundant porous structures, CNTs possess exceptional adsorption capabilities and high adsorption efficiencies for numerous kinds of contaminants, such as dichlorobenzene, ethyl benzene (Peng *et al.*, 2003), Zn^{2+}, (Cho *et al.*, 2010), Pb^{2+}, Cu^{2+}, and Cd^{2+} (Li *et al.*, 2003), and dyes (Madrakian *et al.*, 2011). Carbon nanotubes may vary in length, diameter, chirality (symmetry of the rolled graphite sheet), and the number of layers (Mohamed and Shawky, 2018). They may be classified into two main groups according to their structure: single-walled nanotubes (SWCNTs) and multi-walled nanotubes (MWCNTs). CNTs that are composed of a single graphene sheet are termed as single-walled carbon nanotubes (SWCNTs).

Conversely, multilayers of graphene sheets are known as multi-walled carbon nanotubes (Liu *et al*., 2019).

Over the years, both MWCNTs (Madrakian *et al*., 2011) and SWCNTs (Yang *et al*., 2005) have been applied for the removal of contaminants in water. However, researchers have attributed the antimicrobial effects of CNTs to their unique physical, cytotoxic, and surface functionalizing properties (Upadhyayula *et al*., 2009), their fibrous shape (Kang *et al*., 2008), the size and length of the tubes, and number of layers (Li., 2008). The mechanisms of killing bacteria by CNTs are also due to the production of oxidative stress, disturbances to cell membrane, and so forth (Vecitis *et al*., 2010). Although single-walled CNTs are more detrimental against microorganisms than multiwalled CNTs (Kang *et al*., 2008) and dispersivity of CNTs is a more important parameter than length (Arias and Yang, 2009). In addition to their high sorption capacities (Amin *et al*., 2014), many researchers observed an extremely high adsorption rate of bacteria by single-walled CNTs,

To improve the adsorption, mechanical, optical, and electrical properties of carbon nanotubes, they are often combined with other metallic nanoparticles (Ray and Shipley, 2015). The functionalization increases the number of hydroxyl, carbonyl, amine or other groups on the surface of CNTs, enhancing their dispersibility, and thus improves specific surface area (Adeleye *et al*., 2016). For example, a study using CNTs as a support for magnetic iron oxide has been reported by Gupta *et al*. (2016), who combine the adsorption properties of CNTs with the magnetic properties of iron oxide. A "composite" adsorbent was prepared to remove chromium from water. Apart from owning excellent adsorption properties, the "composite" adsorbent can be easily separated from water via an external magnetic field (Song *et al*., 2019).

2.5.5 Synthesis method of carbon nanotubes

For the synthesis of CNTs, various methods can be utilized to fabricate CNTs of desired properties that are required for a specific application (Rahman *et al.*, 2019). Generally, those preferred methods for the synthesis of CNTs with less structural and chemical imperfection includes, arc discharge, laser ablation, and chemical vapour deposition (CVD) (Rahman *et al.*, 2019). Laser ablation process is technically similar to the arc discharge method (both using high temperature preparation techniques). The difference between these two methods is in the quality and purity of the obtained products. However, the arc discharge and the different types of CVD are the most promising techniques in the large scale production of carbon nanotubes and related nanomaterial (Rajaura *et al.*, 2019). Nonetheless, the CVD been the most utilized methods have replaced high temperature preparation techniques (arc discharge method) since the orientation, alignment, nanotube length, diameter, purity and density of CNTs can be precisely controlled in the former (low temperature preparation method by CVD) (Xu *et al.*, 2017)

2.5.5.1 Chemical vapour deposition (CVD)

While the arc discharge method is capable of producing large quantity of unpurified nanotubes, significant efforts is being directed towards production processes that offer more controllable routes to the production of carbon nanotubes. A class of processes that seems to offer the best chance to obtain a controllable process for the selective production of nanotubes with predefined properties is a chemical vapour deposition (CVD) (Herrera-

Ramirez *et al.*, 2019). CNTs can be grown on a variety of materials by the CVD approach and this make it viable to participate in ongoing processes for manufacturing materials that can be useful in wastewater treatment technologies (Rahman *et al*., 2019). This method can be further classified into various types including catalytic chemical vapour deposition (CCVD) (either thermal or plasma enhanced (PE)) which is now the standard method for the CNTs production (Rahman *et al*., 2019). Other CVD techniques are microwaves plasma-enhanced CVD, (MPECVD) (Brown *et al*., 2011). Hot filament (HFCVD) (Prasek *et al*., 2011) or oxygen-assisted CVD (Byon *et al*., 2007; Prasek *et al*., 2011) and radio-frequency CVD.

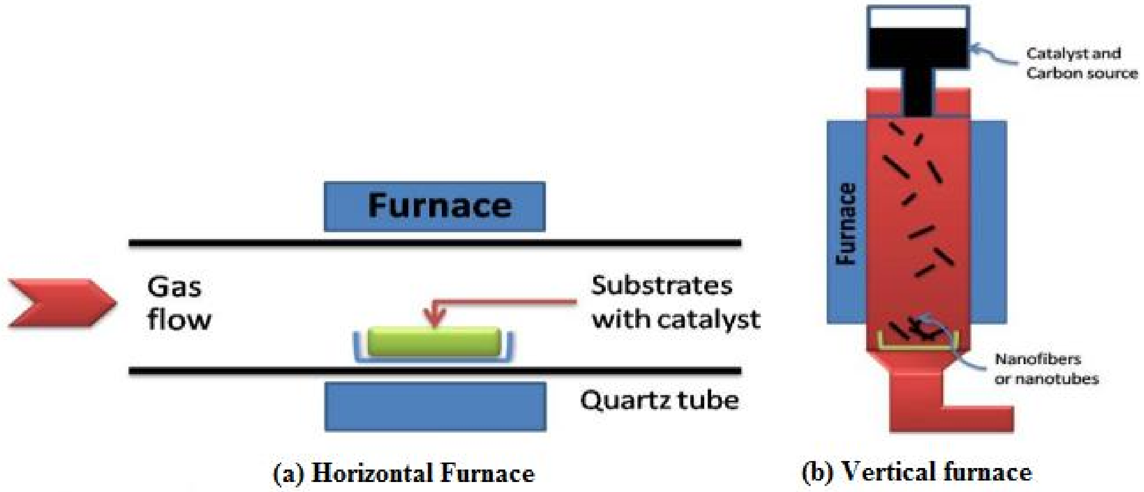

(a) Horizontal Furnace (b) Vertical furnace

Figure 2.2: Schematic Demonstration of CVD Method (a) Horizontal Furnace. (b) Vertical Furnace.

Catalytic chemical vapour deposition (CCVD) is considered to be a low cost viable process for large scale and high quality CNTs production and integration compared with other synthesis methods. The main advantages of CVD are easy control of the reaction course and high purity of the obtained material (Zhu *et al*., 2007). In general, chemical vapour deposition is the catalytic decomposition of hydrocarbon gas or carbon monoxide feedstock with the aid of support transition metal catalyst (Szabó *et al*., 2010). The experiment is basically performed at atmospheric pressure in a flow furnace. There are two types of furnace modality, one in which there is horizontal configuration and in another, there is vertical configuration. Figure 2.2 represent the schematic demonstration of CVD method.

On application, the horizontal configuration is the most popular and the catalyst is usually placed in the ceramics or quartz boat which is put into a quartz tube. The reaction mixture consists of an inert hydrocarbon and a source of hydrocarbon is passed over the catalyst bed at temperature range of 500 to 1000 °C. The system temperature is cooled to room temperature afterwards. Nonetheless, the vertical configuration is usually implemented in the sustained mass production of carbon nanotubes or carbon fibres. The catalyst and carbon source are both introduced at the top of the furnace and the resultant filaments build up during the flight, thereby accumulated at the lower portion of the chamber (Szabó *et al*., 2010; Rahman *et al*., 2019).

The characteristics of CNTs produced by the CVD techniques is dependent on the working parameters namely, the temperature and the operation pressure, the type, volume and concentration of hydrocarbon source, the nature, size and the reaction time (Puett *et al*., 2019). By varying the active particles on the surface of the catalyst, the diameter of the nanotubes can be controlled. Commonly used metal catalysts include Ni, Co, Fe or their combination, as Ni-Y, Fe-Ni, Co-Ni and others (Eatemadi *et al*., 2014). While regarding carbon source, the most favoured in CVD are hydrocarbon like CH_4 acetylene, ethane, ethylene, Xylene, or eventually their mixture, ethanol, or isobutene. The length of the nanotube synthesized via CCVD depend on reaction time and are generally longer than those obtained by other methods and even up to 60mm long tubes can be produced (Szabó *et al*., 2010).

2.5.6 Nanocomposites

A composite is defined as a combination of two or more materials with different physical and chemical properties and distinguishable interface (Mishra, 2014). In view of this, combining two or more different nanomaterials resulted to hybrid nanocomposites (Tepeli and Anik, 2016). However, the preparation methods of nanocomposites is challenging due to the control of elemental composition and stoichiometry in the nanophase. As such, the development of an efficient method to produce multi-functional nanocomposites with an appropriate structure is highly required in nanotechnology in order to investigate the full potential of their structural properties and composition of the synthesized products. Also, production of nanocomposites is vital to be able to examine and evaluate their possible technological usage in various field of study.

Nevertheless, nanocomposites have attracted many researchers and industry because of their potential multi-functional properties from both the nanomaterials and the host materials matrix (Uma *et al*., 2020). Their unique properties are not depicted by any of the constituent materials (Khan *et al*., 2016). Typically, the constituent that is present in greater amount is known as the matrix, while the material that is embedded into the matrix in order to improve the mechanical properties of the composites is called reinforcement (or nanomaterials). In general, nanocomposites possess anisotropy properties (properties are directionally dependent) which indicates the distinct property of constituents and inhomogenous distribution of the re-inforcement (Celik *et al*., 2016). These properties touted many researchers to develop interest in nanocomposite material because of its expectation of intense improvements in properties in such areas like sciences, drug delivery, fuel cell reactors, energy storage and wastewater remediation. Nanocomposites are classified based on the types of reinforcement materials (nanomaterials) and the matrix material used in their modification (Khan *et al*., 2016). Based on the types of matrix material, they are grouped into three different classes, Viz; polymer matrix nanocomposites, ceramic matrix nanocomposites and metal matrix nanocomposites.

2.5.7 Functionalization/Preparation of metal matrix nanocomposites

Metal matrix nanocomposite are materials reinforced by metallic nanoparticles (Moghadam *et al*., 2015). These composites can be made up of metal or alloy matrix filled with nanoparticles, and display physico-chemical and mechanical properties that is totally different from those of matrix and/or constituent material (Malaki *et al*., 2019). The nanoparticles are generally implanted to improve wear resistance, mechanical properties as well as damping characteristics and give superior properties to the newly produced composite material. In addition to this, nanoparticles act as a barrier in dislocation movement and thus improve in the mechanical properties. Owing to their improved properties due to nanoparticle embedment, researchers have made many attempts to uniformly and homogeneously dispersed carbon based nanomaterial into metal matrix by different methods (Hu *et al*., 2016).

On the basis of numerous studies, much progress has been made throughout the world on different synthesis methods of these nanocomposites. For instance, earlier reports by Lingamdinne (2019) stated that nanocomposite can be synthesized through 3 routes which includes hydrothermal method, ultrasonic-sonochemical method or the microwave method (Lingamdinne, 2019). This section briefly introduce and explain the ultrasonic-sonochemical method used in this study. Basically, the method is employed to prevent agglomeration, improve the dispersion and reduce the size of material. The framework of this method is the generation of ultrasounds using a titanium horn that can serve to reduce the van-der-waals forces in the prepared nanoparticle by ultra-sound irradiation (Peng *et al*., 2015). In respect to this method, Granbohm *et al*. (2017) have successfully prepared graphene oxide-Titanium-dioxide-silver nanocomposites (GO-TiO_2-Ag) by sonication of a mixture of graphene oxide solution (GO), Titanium oxide nanorod (TiO_2) and silver nanoparticles.The result obtained from this study showed that a novel nanocomposites (GO-TiO_2-Ag) were produced and this was used for high performance water purification and decontamination under solar irradiation.

In recent studies, the ultrasonic sonochemical method was also used for the preparation of nanocomposites such as Pd/Pt/carbon nanotubes nanocomposite (Yang *et al*., 2016), unzipped MWCNTs/TiO_2nanocomposites (Krishnaveni *et al*., 2020), starch/MWCNTs-glucose nanocomposite (Mallakpour, 2018) and poly(methylmethacrylate)/magnetite nanocomposites (Poddar *et al*., 2018). Hence, further research need to be conducted in order to explore the full potential of nanocomposites in wastewater treatment technology. The treatment technology therefore calls for a non-toxic, long term stable and effective nanocomposite materials for its applicability.

Table 2.2: Wastewater treatment using CNTs

Author (s)	Title	Knowledge Gap
Daoush and Hong. (2013)	Synthesis of Multi-walled carbon nanotubes/silver nanoparticle powders by chemiacal reduction in aqueous solution	The limitation of the study showed that green synthesis method was not employed in the preparation of Ag nanoparticle, CCVD was not used in the synthesis of CNT and co-doping of

		bi-metallic substrate onto CNTs was not done. The performance evaluation of the developed nano-adsorbents on real environmental wastewater was not done.
Larrude *et al.* (2014)	Synthesis and Characterization of Silver nanoparticle-Multiwalled Carbon Nanotubes Composites.	CNTs were not produced via CCVD methods, green method was not used for the synthesis of AgNPs and Co-doping of metallic nanoparticle on CNTs was not done
Babaei *et al.* (2015)	Nitrate removal from aqueous solution using CNTs magnetized by zerovalent iron.	The limitation of the research revealed that co-doping of bi-metallic substrate onto CNTs was not done, green synthesis method was not used for the preparation of AgNPs and performance evaluation of the developed nano-adsorbent on the real environmental wastewater was not done.
Dinh *et al.* (2015)	Water-dispersible silver nanoparticles-decorated carbon nanomaterials: Synthesis and enhanced antimicrobial activity.	The limitation of the study showed that green synthesis method was not employed in the preparation of Ag nanoparticle, CCVD was not used in the synthesis of CNT and co-doping of

		bi-metallic substrate onto CNTs was not done. Also, the performance evaluation of the developed nano-adsorbents on real environmental wastewater was not done.
Sahebian *et al*., (2016)	The decoration of multi-walled carbon nanotubes with nickel oxide nanoparticles using chemical method	The limitation of the study showed that green method was not employed in nanoparticle synthesis, CCVD was not used in the synthesis of CNT and co-doping of bi-metallic substrate onto CNTs was not done. The performance evaluation of the developed nano-adsorbents on real environmental wastewater was not done.
Aliyu *et al*., (2017)	Synthesize multi-walled carbon nanotubes via catalytic chemical vapour deposition method on Fe-Ni bimetallic catalyst supported on kaolin.	The research failed to incorporate metallic substrate onto CNTs. Not only that, the Pd/Ag/CNTs was not capped with polymer

2.6 Characterization Techniques

2.6.1 UV–visible spectroscopy

UV-Vis spectroscopy is the most important technique and simplest way to confirm the formation of nanoparticles. It is based on the absorption of ultrioviolet light or visible light by chemical compounds, which results in the production of distinct spectra. When the sample absorbs light, the electron present in it undergoes excitation thus enabling the electron to jump from ground state to excited state. The difference in the energies of the ground state and the excited state of the electron is always equal to the amount of ultraviolet radiation absorbed by it. Many reviewed literature reported characterization of various nanomaterial using UV-Visible spectroscopy. Singh *et al*. (2015) reported that biosynthesis of silver nanoparticles by plant crude extracts of *Emblica officinalis, Terminalia catappa* and *Eucalyptus hybrida* was observed upon addition of the extract into the flask containing the aqueous silver nitrate solution. The colour of the medium changed to brown within 2 minutes which indicate the formation of silver nanoparticles.

2.6.2 X-ray diffraction

X-ray diffraction (XRD) is a primary tool for probing structure of nanomaterial (Sharma *et al*., 2012). It offers unparalleled accuracy in the measurement of atomic spacing and it is the techniques of choice for determining strain stress in the films (Mohan and Renjanadevi, 2016). X-ray diffraction of nanomaterials provide a wealth of information, that is, from phase composition to crystal in size, from lattice strain to crystallographic orientation.

2.6.3 High resolution scanning electron microscopy

Recently, the field of nanoscience and nanotechnology has provided a driving force in the development of various high-resolution microscopy techniques in order to learn more about nanomaterials using a beam of highly energetic electrons to probe objects on a very fine scale (Zhao *et al*., 2015). Among various electron microscopy techniques, SEM is a surface imaging method, fully capable of resolving different particle sizes, size distributions, nanomaterial shapes, and the surface morphology of the synthesized particles at the micro and nanoscales (Lin *et al*., 2014). Using SEM, it is possible to probe the morphology of particles and derive a histogram from the images either by measuring and counting the particles manually, or by using specific software (Fissan *et al.*, 2014). The combination of SEM with energy-dispersive X-ray spectroscopy (EDX) can be used to examine silver powder morphology and also conduct chemical composition analysis. The limitation of SEM is that it is not able to resolve the internal structure, but it can provide valuable information regarding the purity and the degree of particle aggregation (Zhang *et al.*, 2016). The modern high-resolution SEM is able to identify the morphology of nanoparticles below the level of 10 nm.

2.6.4 High resolution transmission electron microscopy

The transmission electron microscope (TEM) operates on the same basic principles as the light microscope but uses electrons instead of light (Emam-Ismail *et al.*, 2019). TEM use electron as "light source" and their much lower wavelength make it possible to get a resolution a thousand times better than that with a light microscope. With the help of TEM, object can be seen in the order of a few angstroms (10^{-10} m). It can be used to obtain quantitative measures of particle and/or grain size, size distribution, and morphology (Cater and Williams, 2016). The magnification of TEM is mainly determined by the ratio of the distance between the objective lens and the specimen and the distance between objective lens and its image plane (Carter and Williams, 2016). TEM has two advantages over SEM: it can provide better spatial resolution and the capability for additional analytical measurements (Fissan *et al.*, 2014). The disadvantages include a required high vacuum, thin sample section (Zhang *et al.*, 2016) and the vital aspect of TEM is that sample preparation is time consuming. Therefore, sample preparation is extremely important in order to obtain the highest-quality images possible.

High resolution transmission electron microscopy is an imaging mode of the transmission electron microscope that allows the imaging of the crystallographic structure of a sample at an atomic scale. HRTEM has been widely and effectively used for analysis of crystal structures and lattice imperfections to study nanoscale properties of crystalline material such as semiconductors and metals (Pathak *et al*., 2013).

2.6.5 Energy dispersive spectroscopy

Energy dispersive spectroscopy is a techniques used to study the elemental composition in a reaction mixture (Zhang *et al*., 2016). EDS system are typically integrated into scanning electron microscopy. Kaviya *et al.* (2011) reported EDX spectrum reveals strong signals in the silver region and confirm the formation of AgNPs. Metallic silver nanocrystals generally show typical optical absorption peak appropriately at 3kev due to surface plasmon resonance. It was shown that silver (Ag 55.08%) was the major constituent element compared to chloride (44.92%). The energy dispersive spectroscopy (EDX) data showed very strong silver and weak signals of chlorides and carbon peaks, which indicate the reduction of silver ions to elemental silver possibly originated from the molecules attached to the surface of the AgNPs. The dense peak of silver strongly confirmed the reduction of silver nitrate to silver nanoparticles.

2.6.6 Brunauer-Emmett-Teller

The Brunauer-Emmett-Teller (BET) method has been employed extensively to characterize the specific surface areas of porous materials (Tian and Wu, 2018). The fundamental theory is associated with the adsorption of a gas on the material’s surface. This phenomenon is caused by van der Waals forces that are created by a film of the adsorbate, which consists of atoms, ions, or molecules on the surface of a substance that adsorbs these particles (Ambroz *et al*., 2018). The process of adsorption can be physical or chemical (Bardestani *et al*., 2019). While the physical process is related to van der Waals forces, the chemical adsorption process is due to the reaction between the solid and the adsorbate (gas). The amount of the adsorbed gas on the adsorbent material can be correlated with its surface area. However, the BET method works best for adsorbents with large pores because it assumes uniform adsorption of gas molecules on a flat surface without lateral interactions (Bardestani *et al*., 2019). For microporous materials (pore size less than 2 nm), recent experimental and computational investigations indicated that the BET analysis describes only an apparent "surface area" instead of the true geometrically accessible area.

CHAPTER THREE

3.0 MATERIALS AND METHODS

3.1 Materials, Reagents and Equipments

This section provides detailed description of the experimental procedures used to generate the data needed to achieve the outlined aim and objectives of the study. It also sets out the materials, as well as the analytical characterization techniques that were employed in this study.

3.1.1 Equipments/apparatus

The lists of equipment and apparatus used in this study are provided in Table 3.1, while the lists of chemicals/reagents used in this study are shown in Table 3.2 with their percentage purity and suppliers.

3.1.2 Collection of plant materials, Kaolin and industrial animal feed processing wastewater

Fresh plant sample of *Ageratum conyzoides* (Goat weed) were collected from Offa Local Government of Kwara State, North-central part of Nigeria. The leaves were separated from the stalks. Banana and plantain peels were obtained from Kure market Minna, Niger State. The plant materials were washed with distilled water and air-dried to remove residual debris. Portion of the plant materials were placed in a freeze dryer for about 72 h until all moisture was removed. The samples were freeze dried to preserve the phytochemicals and prevents the growth of microbes. Kaolin was collected from Gbako Local Government of Niger State, Nigeria. It was ensured that there were no further pretreatment before usage.

Table 3.1: List of equipment/apparatus

Instruments	Model	Manufacturer	Location/Source
Thermostat Oven	Gallenkamp	Gallenkamp, UK	Chemistry Lab, FUT MINNA
Magnetic Stirrer	78HW-1	Gallenkamp, UK	STEP B, FUT MINNA
Sieves (150 μm)	ASTM No. 100	Interlabs, Seithi	Geology Lab, FUT MINNA
Centrifuge	-	Gallenkamp, England	STEP B FUT, MINNA
Conductivity Meter	Kent EIL 5013	England	Niger State River Basin
Turbidity Meter	WT3020	Wagtech, Singapore	Niger State River Basin
Dissolved Oxygen Meter	Multi 3420	SET G, Germany	Niger State River Basin
Catalytic vapour depositor	XD 1200NT	VACUTEC, South Africa	STEP B FUT, MINNA
Ultrasonicator	SB25-12DT	Scientz, China	Mechatronic Lab, FUT MINNA
UV-Vis spectrophotometer	Shimadzu UV-1800	England	STEP B FUT, MINNA
High resolution scanning electron microscope	Zeiss Auriga	England	University of Western cape, South-Africa
High resolution Transmission electron	Zeiss Auriga	FEI, Netherland	University of Western cape, South-Africa

microscope			
XRD (X-ray Diffraction)	BrukerAxS D8 Cu-k radiation	Shimadzu Scientific Instrument	Themba Laboratory Cape Town, South-Africa
BET (Brunauer Emmett Teller)	NOVA 4200e	Quantachrome, UK	STEP B FUT, MINNA
AAS (Atomic absorption spectrophotometer)	Varian AAn240 FS	PG Instruments Ltd, UK	Multi-Users Research Laboratory, Zaria

Table 3.2: List of chemicals/reagents used

Reagent/Chemical Name	**Molecular Formular**	**% Purity**	**Supplier**
Silver nitrate	$AgNO_3$	99.0	Sigma-Aldrich
Palladium (ii) chloride	$PdCl_2$	99.0	Sigma-Aldrich
Tetraoxosulphate (vi) acid	H_2SO_4	99.9	BDH
Trioxo nitrate (v) acid	HNO_3	99.9	BDH
Nickel (ii) nitrate hexahydrate	$Ni\ (NO_3)_2.6H_2O$	99.99	Sigma-Aldrich
Iron (iii) nitrate nonahydrate	$Fe\ (NO_3)_2\ 9H_2O$	99.95	Sigma-Aldrich
Acetylene gas	C_2H_2	99.9	British Oxygen Company, Nigeria
Nitrogen gas	N_2	99.6	British Oxygen Company, Nigeria
N,N’-Dicyclohexylcarbodiimide	$C_{13}H_{22}N_2$	99.0	Sigma-Aldrich
2-Mercaptoethylamine	$NH_2CH_2CH_2SH$	95.0	Sigma-Aldrich

3.2 Methodology

A detailed description of the experimental procedure is given in this section: that is, preparation of the plant extracts, preparation of catalyst for CNTs synthesis, production and functionalization of CNTs, incorporation of the produced CNTs with palladium and silver nanoparticles.

3.2.1 Preparation of plant extracts

The extracts were prepared as reported by Sharma and Sanghi (2012) with slight modifications using a ratio of 1:10 (w/v), (10 g of plants materials and 50 cm^3 of distilled deionized water). The mixtures were homogenized thoroughly and adjusted to 100 cm^3 with de-ionized water. Afterwards, the resulting homogenate were transfer to Erlenmeyer flask and heated for 1 h. To obtain the aqueous extract, the homogenate were subjected to vacuum filtration using Whatman number 1 filter paper. The filtrates were kept at 4°C for the synthesis of palladium and silver nanoparticles and portion of the extracts were used for phytochemical screening.

3.2.2 Phytochemical screening

Extract from the plant materials were assessed for the presence of naturally occurring biologically active compounds (phytochemicals) like alkaloids, tannins, saponins, flavonoids, and phenols by using different standards as described by Adetunji *et al.* (2013).

3.2.2.1 Determination of phenols

The extract of the plant materials (0.01 cm^3) were dissolved in 10 cm^3 of distilled water, and 0.5 cm^3 was oxidized by 2.5 cm^3 of 10 % Folin-Ciocalteu's reagent which was then neutralized by 2 cm^3 of 7.5 % of sodium carbonate. The reaction mixture was incubated at 45 °C for 40 min. Gallic acid was used as a standard (Kolawole *et al*., 2007).

3.2.2.2 Determination of flavonoids

The flavonoid contents were determined using the method of Chang *et al*. (2002). 0.5 g of the extracts were added to a test tube containing 1.5 cm^3 of absolute methanol, 0.1 cm^3 of 10 % aluminum chloride, 0.1 cm^3 of 1M sodium acetate and 2.8 cm^3 of distilled water and incubated at ambient temperature for 30 min. Standard quercetin was used to prepare the calibration curve.

3.2.2.3 Determination of alkaloids

This was carried out according to the method employed by Oloyede (2005). 0.5 g of the extract was weighed and dissolved in 5 cm^3 of mixture of 96 % ethanol, 20 % sulphuric acid (1:1). The entire solution was filtered through Whatmann filter paper. 1 cm^3 of the filtrate was added to a test tube containing 5 cm^3 of 60 % H_2SO_4 and allow to age for 5 min. Thereafter, 5 cm^3 of 0.5 % formaldehyde was added and allowed to stand at room temperature for 3 h. Vincristine extinction co-efficient (E296, ethanol {ETOH}=15136 $m^{-1}cm^{-1}$) was used as standard alkaloids.

3.2.2.4 Determination of tannins

The method of American Organization of Analytical Chemist (AOAC, 1984) adopted by Rashmi *et al*. (2019) was employed for the determination of tannins content in the plant extracts. 200 mg of the extracts were weighed into a 100 cm^3 beaker and 20 cm^3 of 50 % methanol was added to it and covered with foil paper and heated in water bath shaker at 80 °C for 60 min. This was then filtered into a 100 cm^3 volumetric flask and 20 cm^3 of distilled water, 2.5 cm^3 of Follin-Denis reagent, and 10 cm^3 of sodium carbonate (0.5 M) were added and shaken vigorously. The reaction mixture were allowed to age for 20 min at room temperature for the formation of bluish-green colouration. Standard tannic acid was used to prepare the calibration curve. The absorbance was measured at 760 nm.

3.2.2.5 Determination of saponins

A known weight (500 mg) of the extract was weighed and dissolved in 20 cm^3 of 1 M HCl and heated over a water bath with continuous stirring at 80 °C for 4 h. The mixture was allowed to stand for 20 min at room temperature and filtered using Whatmann filtere paper. 50 cm^3 of petroleum ether was added and the other layer was collected and evaporated to dryeness. Thereafter, 5 cm^3 of acetone-ethanol (1:1), 6 cm^3 of ferrous sulphate and 2 cm^3 of concentrated sulphuric acid were added and allowed to stand for 10 min. Standard saponins was used to prepare the reference curve (Oloyede, 2005).

3.2.3 Synthesis of silver nanoparticle

An aliquot (5 cm^3) of aqueous plant extract sample was added to 50 cm^3 of 1mM of aqueous $AgNO_3$ solution at a ratio of 1:10 (v/v). The resulting mixture was stirred for 30 min at 200 rpm and heated on a magnetic stirrer hot plate at 60 °C. The formation of silver nanoparticles was determined by a change in colour of the reaction mixture (usually indicated by a dark-brown colouration). Once the colour of the solution intensifies, the solutions were kept in the dark room to prevent agglomeration of the nanoparticle. Confirmation of silver nanoparticle formation by the reduction of Ag^+ from $AgNO_3$ to Ag° was monitored using UV-Visible spectrophotometer (Abdelghany *et al.*, 2018).

3.2.4 Synthesis of palladium nanoparticles

In order to synthesize palladium nanoparticle, 10 cm^3 of aqueous plant extract were added to 200 cm^3 of (0.1 x 10^{-3} M) aqueous palladium chloride salt solution. The reaction mixture was placed on a magnetic stirrer with hot plate and heated at 60 °C with constant stirring speed of 200 rpm, under 30 min. The change in colour of the reaction mixture from light orange to dark brown indicates the formation of palladium nanoparticle. The bioreduction of Pd^{2+} into Pd° was monitored by UV-Visible spectrophotometer (Suryawanshi *et al*., 2018)

3.2.5 Preparation and optimization of Fe-Ni/Kaolin catalyst

Wet impregnation method was employed for the production of bimetallic catalyst (Fe-Ni) supported on kaolin substrate as described by Aliyu *et al*. (2017). In this method, a known weight of nickel nitrate hexahydrate and iron nitrate nonahydrate salts (10 wt% of the catalyst mixture which contain equal proportion by weight), 5 wt% each was dissolved in 50 cm^3 of distilled water. Thereafter, the mixture was added dropwise to 10 g of Kaolin support. The reaction mixture (slurry) was allowed to interact for 60 min under constant stirring. And later dried in an oven at 120 °C for 6 h followed by calcination at 550 °C in a furnace for 12 h until a brownish colouration was obtained. Then, the dried supported catalyst was ground and screened through a 15 µm sieve and further calcined at 500°C for another 12 h in the furnace in order to decompose the nitrates or render them friable.

The catalyst yield after calcination was determined using equation (3.1).

$$\% \text{ Yield } (Y\,\%) = \frac{Wt_A - Wt_B}{Wt_A} \times 100 \qquad 3.1$$

Where Y = Catalyst % yield, Wt_A and Wt_B, is the weight of sample before and after calcination in grams

3.2.6 Synthesis of carbon nanotubes

The synthesis of carbon nanotubes was carried out using catalytic chemical vapour deposition method. In this method, 1 g of the synthesized Fe-Ni/Kaolin catalyst was weighed and spread uniformly in a quartz boat placed at the centre of a tubular quartz reactor horizontally in an electrical tube furnace. Thereafter, the furnace was heated from room temperature to 700 °C at 10^0C/min while a carrier gas (N_2) was flown over the catalyst at 30cm^3/min until the desired temperature was reached. The flow rate of the carrier gas was raised to 350 cm^3/min and the carbon source (acetylene gas) was introduced at flow rate of 100 cm^3/min to produce CNTs under the continuous flow of nitrogen gas. The deposition of CNT growth over (Fe-Ni/kaolin) catalyst was examined for 90 minutes. Thereafter, the acetylene flow was stopped and nitrogen flow continuously to fill the reaction chamber till the furnace cooled to room temperature. The boat was removed from the quartz tube and weighed to determine the CNTs yield using Equation 3.2 (Taleshi, 2012).

$$\text{Yield } \% = \frac{\text{Wt}_2 - \text{Wt}_1}{\text{Wt}_1} \times 100 \qquad 3.2$$

Where Wt_1 = Initial weight of the catalyst before reaction,

Wt_2 = the weight of catalyst and carbon deposited after synthesis

The rate of CNT deposited was evaluated by Equation 3.3

$$\text{R } (\%/\text{min}) = \left(\frac{\text{Y}(\%)}{\text{t(min)}}\right) \qquad 3.3$$

Where R = the rate of carbon deposition (%/min),

Y = the carbon yield (%) and

t = the residence time of the reaction (min)

3.2.7 Purification/Functionalization of as-synthesized carbon nanotubes

A known weight of prepared CNTs were oxidized in a mixture of concentrated sulphuric acid and nitric acid (3:1) under the influence of ultrasonicator for 30min, to introduce OH, COOH functional groups on to CNTs and also act as a linker to attach other metallic nanoparticles. At the end of the acid treatment, the reaction mixture was diluted with distilled water and followed by filtration and further washed with distilled water until the pH of the filtrate was neutral. The obtained product was dried overnight in an oven at 120°C for subsequent analysis.

3.2.8 Synthesis of Ag-CNTs nanocomposites

A known weight of purified multi-walled carbon nanotubes (P-MWCNTs) (0.5 g) was dispersed in 20, 40, 60, 80 and 100 cm^3 of aqueous solution of synthesized silver nanoparticles respectively, by simple wet impregnation method. 10% V/V of N, N'-dicyclohexyl carbodiimide (DCC) and 2-Mercaptoethylamine (5 cm^3 of 0.1M) were added in to the mixture. The suspension was mixed and kept under stirring with magnetic stirrer hot plate for 30 min at 60 °C, and later ultrasonicated for 45 min. The resulting suspension, (CNTs doped AgNPs) were collected by centrifugation and washed with distilled-deionized water. The obtained products were dried in the oven at 120 °C for 8 h and different yield of the product were obtained for different ratio of the reaction mixture. The product that gives the best yield was slected for further analysis.

3.2.9 Synthesis of Pd-CNTs nanocomposites

Similarly, the same procedure highlighted in section 3.2.7.1 was employed in the preparation of CNTs doped palladium nanoparticles (Pd-CNTs nanocomposite).

3.2.10 Synthesis of Pd-Ag-CNTs nanocomposites

A known weight (1 g) of P-MWCNTs were dissolved in 80 cm^3 of equal volume of aqueous solution of silver nanoparticles and palladium nanoparticles respectively through wet impregnation method. The mixture were dispersed in 20 % v/v of DCC and 10 cm^3 of 0.1M 2-Mercaptoethylamine. The resulting suspensions were stirred for 30 min at 60 °C, under magnetic stirrer hot plate. The resultant mixture were then sonicated for 1 h, at 60 °C. The prepared materials were washed until the filtrate become neutral. Thereafter, the solid products were obtained by centrifugation and oven dried at 120 °C for 8 h. The produced nanocomposites was then calcined at 450 °C for 2 h in a furnace to dispersed Pd/AgNPs onto the MWCNTs. The multi-step mechanistic pathway for wet impregnation of PdNPs and AgNPs (differently and combined impregnation) onto MWCNTs were represented in Figure 3.1

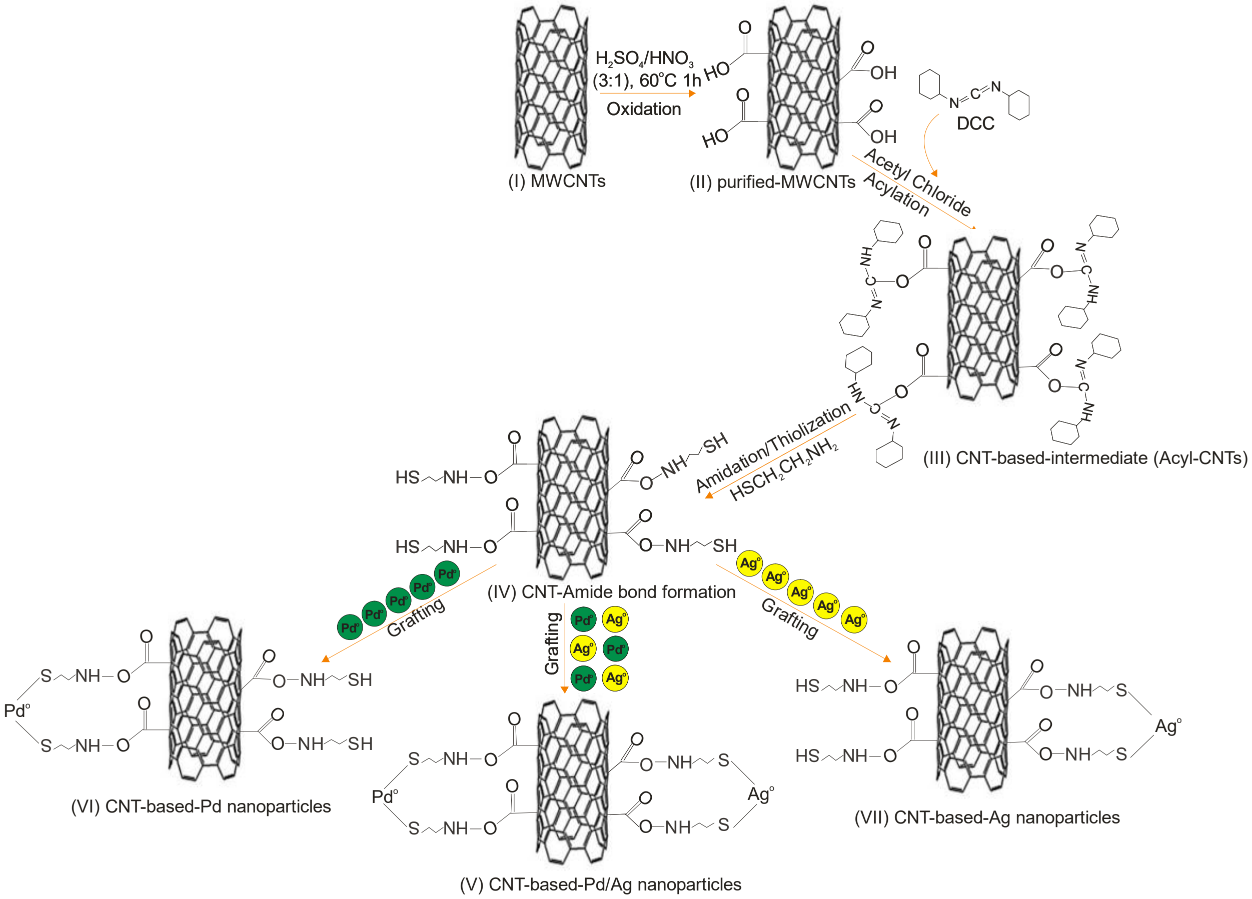

Figure 3.1(I-VII): Multi-step Mechanistic Pathway for wet Impregnation of PdNPs, AgNPs and Pd/AgNPs onto MWCNTs

3.2.11 Impregnation of the prepared palladium and silver nanoparticles onto carbon nanotubes

In this study, addition of 0.5 g of synthesized CNTs to the prepared palladium and silver nanoparticles were examined in different ratio, under stirring for 30 min. Different yield of the products were obtained and recorded in decreasing order: 0.5 g of CNTs to 40 cm^3 of AgNPs (1.05 g) > 0.5 g of CNTs to 20 cm^3 of AgNPs (0.93 g) > 0.5 g of CNTs to 60 cm^3 of AgNPs (0.54 g) > 0.5 g of CNTs to 80 cm^3 of AgNPs (0.45 g). The same trend was observed for the dispersion of CNTs in different ratio of the prepared PdNPs. Furthermore, Pd/Ag/CNTs composites were synthesized by mixing CNTs with AgNPs and PdNPs using wet impregnation method. The formation of the ternary Pd/Ag/CNTs composites were illustrated in Section 3.2.7 and Figure 3.1.

3.3 Characterization Techniques of the Synthesized Nanomaterials

The synthesized nanoparticles (palladium and silver nanoparticles) and carbon nanotubes (Pd-CNTs, Ag-CNTs and Pd-Ag-CNTs) nanocomposites were characterized using UV-Visible spectrophotometer, HRSEM, HRTEM, XRD, BET and EDS for their morphology and structure, mineralogical phase, specific surface area and elemental composition.

3.3.1 UV-Visible spectroscopy

The nanoparticles were analysed using Shimadzu UV-Visible spectrophometer 1800, working with a wavelength range of 200-800 nm using quartz cuvettes. A known volume (2 cm^3) of each of the prepared nanoparticles was poured into a quartz cuvette. The cuvette containing the sample was placed into the cuvette holder for measurement. Prior to sample measurements, background measurements was carried out using two empty pre-cleaned quartz cuvettes to subtract the interferences.

3.3.2 HRTEM and SAED

The morphological information and internal structure of the produced nanoparticles and nanocomposites were characterized using HRTEM coupled with SAED. 20 mg of the samples were dispersed in 10 cm^3 of methanol and the mixture was ultrasonicated for 40 min. About one or two drop of the nanoparticle suspension or slurry was/were dropped onto the carbon coated copper grid (400 mesh), with the aid of micropipette and dried at room temperature. After drying, the grid was loaded on the single-tilt sample holder and subsequently mounted onto the shaft of the electron microscope, and the internal structure of the image was determined.

3.3.3 HRSEM and EDS

The surface morphology and elemental composition of the synthesized Pd and Ag nanoparticles, carbon nanotubes and the prepared nanocomposites were examined using High Resolution Scanning Electron Microscopy coupled with Energy Dispersive X-ray spectroscopy. 0.05 g of the samples were sprinkled on a sample holder (carbon adhesive tapes) which was coated with metallic disc (Au-Pt disc) for the purpose of conductivity using Quorum T15OT for 5 min prior to analysis. The microscope operated at 5 keV was used for imaging at different areas and magnification. While 20 keV detector was used for the EDS analysis.

3.3.4 XRD

The XRD instrument (Bruker AXS D8 Advance) was used to determine the phase composition of the produced nanomaterial. About 1 g of each of the powdered nanoparticles and nanocomposites were pulverized separately and dispersed into a rectangular aluminium sample holder and clipped. Scan were run with a diffractometer operating at 45 keV and 40 mA, with a step size of 0.02 °/s in the 2θ range of 10^{o} to $90^{o.}$ and the phase identification was recorded from the XRD data.

3.3.5 BET

The surface area, pore volume and pore size of Pd-CNTs, Ag-CNTs and Pd-Ag-CNTs nanocomposites were determines using N_2 adsorption-desorption isotherm (Brunauer-Emmett-Teller analyzer; Model; NOVA 2400e). 120 mg of each sample was degassed at 250 °C (desired temperature) for 3 h under continuous flow of N_2. The specific surface area was obtained from the plots of adsorption data through Brunauer-Emmett-Teller equation showing multiple points at P/P_o between 0.05 and 0.20.

3.4 Charactrization of Wastewater Before and After Treatment with Nano-adsorbent

3.4.1 Physicochemical characterization

In this study, the American Public Health Association (APHA, 2017) methods were employed for the determination of different physicochemical parameters examined (before and after treatment) and the procedures employed for the determination are described as follow.

3.4.1.1 Temperature

The determination of temperature was carried out by digital thermometer (Mercury filled celcius thermometer). The probe of the thermometer was dipped in to the water sample and it was ensured that the entire thermometer was not totally submerged and held for about 1 min before the values were recorded. The reading was done in triplicate for each of the sample to ensure accuracy and the temperature of the raw wastewater was done on site directly in the water samples.

3.4.1.2 pH

The pH determination was done by electrometric method. A known volume (20 cm^3) of the water samples were measured into 50 cm^3 beaker. Buffer solutions (Acetate buffer pH = 4; Ammonium buffer pH = 10) were used to standardize the pH meter and the pH meter probe was rinsed with de-ionized water to be free of any contamination and inserted into thee sample. The reading was taken from the meter reader after stabilization of the results

3.4.1.3 Turbidity

The turbidity of raw and treated wastewater was determined through the use of turbidity meter. The meter was first calibrated before the sample cell was filled with the samples, and the turbidity values were read directly from the digital reader. The Nephelometric method (NTU) was employed in this study.

3.4.1.4 Conductivity, total suspended solid and total dissolve solid

Electrometric method was used for the determination of conductivity in the raw and treated wastewater. The conductivity probe was dipped into the water sample and the value measured (in μS/cm) from the meter. The total dissolved solid (TDS) as well as the total suspended solid (TSS) was also recorded from the conductivity measurement using APHA 2510B.

3.4.1.5 Dissolved oxygen

The determination of dissolved oxygen was also done using dissolve oxygen meter probe (DO_2 meter). The probe of the DO_2 meter was removed from the protective cover and immersed into the raw wastewater samples and the values was recorded in mg/L. The procedures were repeated for the treated wastewater samples.

3.4.1.6 Biochemical oxygen demand

The biochemical oxygen demand (BOD) for the raw and treated wastewater samples was determined after the measurement of dissolved oxygen (initial DO) through DO meter. Eight 300 cm^3 BOD bottles were filled with treated and untreated water samples (100 cm^3) and filled to the brim with dilution water. Four blank samples were prepared by filling the BOD bottles only with dilution water. Each of the bottles was incubated in the dark at 20 °C for five days to obtain the final DO through DO meter. The BOD concentrations were calculated using equation 3.4

$$BOD(\text{mg/L}) = [(DO_{initial} - DO_{final}) - (blankcorrection)] \times P \qquad 3.4$$

Where, $DO_{initial}$ is the DO of diluted samples after preparation, DO_{final} is the DO of the diluted samples after incubation for five days at 20 °C, and P is the decimal volumetric fraction of the total volume of the BOD bottles (300 cm^3) divided by the volume of the used samples (100 cm^3). Blank correction is the dissolved oxygen of the blank samples immediately after preparation minus the dissolved oxygen of the blank samples after five days incubation.

3.4.1.7 Chemical oxygen demand

The COD concentration was determined by employing COD reactor. The reactor was preheated to 150 °C prior to its usage. The blank solution was prepared by adding the mixture of 2 cm^3 of deionized water and 2 cm^3 of a standard solution (potassium hydrogen phthalate) into corresponding vials. Similarly, the same procedure was repeated for the wastewater samples. Both the blank and wastewater samples were added into the vial, mixed well and placed into the reactor at 150 °C for 2 h. Thereafter, the vials were allowed to cool to room temperature subsequent to removal from the reactor. Finally, the COD concentration were measured through photometer and converted to mg/L.

3.4.1.8 Metal analysis

The Atomic Absorption Spectrophotometry (AAS) method (model: Varian, AAn240 FS) was used to determine the concentration of selected heavy metal ions (copper, iron, manganese and nickel) present in animal feed processing industry wastewater. Prior to the analysis, 100 cm^3 of each water sample was digested with mixture of concentrated nitric and hydrochloric acid in 3:1. The samples were digested in a fume cupboard using a hot plate. The remaining solution (about 15 cm^3) was diluted with distilled-deionized water and filtered using Whatmann no. 1 filter paper. Afterwards, the resultant filtrate were made up to 50 cm^3 with deionized water and ready for AAS analysis

3.5 Batch adsorption study

The present study investigated the adsorptive capacity of Pd-Ag-CNTs, Pd-CNTs and Ag-CNTs using batch adsorption process for the treatment of animal feed processing industry wastewater. Batch adsorption was performed on the wastewater in order to see the effect of different operational parameters such as contact time, adsorbent dosage and temperature. The procedure for each parameter is elucidated as follows

3.5.1 Effect of contact time

The effect of contact time was investigated by adding 10 mg of Pd/Ag/CNTs nanoadsorbents into 250 cm^3 glass stoppered conical flask on a rotary shaker at 200 rpm, containing 50 cm^3 of the industrial animal feed processing wastewater. The pH of the industrial animal feed processing wastewater was 6.28. The effect of contact time was conducted by shaking the mixture at different contact time (15, 30, 45, 60, 75 and 90 min) under room temperature. The solution was filtered using Whatmann filter paper and the filtrate was packaged for AAS analysis to determine the residual concentration of copper, iron, manganese and nickel ions.

3.5.2 Effect of adsorbent dosage

The effect of adsorbent dosage on the removal efficiency of the toxic metals from wastewater was carried out by adding different amount of Pd/Ag/CNTs nanoadsorbents (10, 20, 30, 40, 50 and 60 mg) into 50 cm^3 of industrial animal feed processing wastewater, in a 250 cm^3 glass stoppered conical flasks. The recorded pH for the raw wastewater was 6.28. The mixture was agitated at 200 rpm on a rotary shaker at a temperature of 30 °C, for 60 min. Thereafter, the resultant mixture was filtered and the concentrations of the residual metals (Cu, Fe, Mn and Ni) were determined using AAS.

3.5.3 Effect of temperature

To evaluate the effect of temperature, 10 mg of the Pd/Ag/CNTs nano-adsorbent was added to 250 cm^3 glass stoppered conical flask containing 50 cm^3 of industrial animal feed processing wastewater. The mixture was shaken for 60 min (equilibrium time) in a thermostatic water bath shaker, and the temperature was varied from 30, 40, 50, 60, 70 to 80 °C. The solution was filtered using Whatmann filter paper, and the concentrations of the selected metal ions were determined using Atomic Absorption Spectrophotometer (AAS).

3.6 Data Analysis of Batch Adsorption on Industrial Animal Feed Processing Wastewater

All experimental work was done in triplicates and the mean values of result were recorded. One way analysis of variance (ANOVA) was employed for the data analysis using IBM SPSS statistics version 20. The percentage removal of adsorption of selected metals (% Removal) as well as the adsorption capacity (qe) were calculated based on Equation (3.5) and (3.6), respectively.

$$\% \, Removal = \frac{C_o - C_e}{C_o} \times 100 \qquad 3.5$$

$$q_e = \frac{(C_o - C_e)V}{W} \qquad 3.6$$

Where, C_o is the adsorbate initial concentration in mg/l, C_e is the equilibrium concentration (mg/l), q_e is the amount of adsorbate adsorbed per unit mass of the nanoadsorbebts (mg/g), V is the used volume of the solution containing the adsorbate (cm^3) and W is the mass of the adsorbent used (mg) during the adsorption process.

3.6.1 Data analysis using adsorption isotherm, kinetics and themodynamic models

To best describe the adsorption mechanism of selected metals namely copper, iron, manganese and nickel, Pd-Ag-CNTs nanoadsorbent was preferred based on the characterization results.The isotherm models; Langmuir, Freundlich, Dubini-Radushkevich (D-R), Temkin, Halsey and Flory-Huggins were employed in this work to examine the adsorption pattern.

Langmuir model was used to study the sorption capacity produced from unimolecular nature of adsorbents surface. The linear form of the Langmuir equation is given as follow: (See also Section 2.4.4.2; Equation 2.2)

$$\frac{C_e}{q_e} = \frac{1}{K_L q_{max}} + \frac{C_e}{q_{max}}$$

The Langmuir constant (K_L) related to the adsorption energy, and (q_{max} mg/g), the maximum adsorption capacity are respectively calculatedfrom the slope and intercept of the linear plot of C_e/q_e versusC_e. The separation factor R_L was calculated using the Equation 5 presented in Section 2.4.4.2. The R_L values were determined to indicates whether the adsorption process is favourable or not (El-Sayed *et al.*, 2014).

Freundlich Isotherm model describes systems where the adsorption process can take place on either homogeneous or heterogeneous surfaces (Multi-layer adsorption) with interactions between the adsorbed molecules. The linearized form of Freundlich equation is given as (See Equation 2.7):

$$Log q_e = Log K_f + {}^{1}\!/_{n}\, Log C_e$$

Where K_f is Freundlich adsorption capacity (L/mg) and $1/_n$ is adsorption intensity; it also indicates the relative distribution of the energy and heterogeneity of the adsorbate site. By plotting the graph of $Log\ C_e$, a straight line graph will be obtained such that $1/_n$ and Log K, represent the slope and intercept, respectively.

The Dubinin-Radushkevich (D-R) model is basically applied to distinguish physical process of adsorption of metal ions from chemical processes. The linear form of D-R equation is expressed in Equation 2.9.

$$\ln q_e = lnq_m - K_{(D-R)}E^2$$

Temkin model is based on a uniform distribution of the binding energies which takes into account the indirect interaction between adsorbate and molecules. The Temkin isotherm is represented in linear form as shown in equation 2.13, Section 2.4.4.2.

$$q_e = AlnK_T + A\ln C_e$$

The linearized form of Halsey and Flory-Huggins equations were presented in Equation 2.15 and 2.16 (See also Section 2.4.4.2)

$$q_e = \frac{1}{n_H} lnK_H - \frac{1}{n_H} lnC_e$$

$$ln\frac{\theta}{C_o} = lnK_{FH} + nln\,(1 - \theta)$$

The kinetic data of adsorption of selected metal ion under various contact times were treated using Lagergren's pseudo-first-order, pseudo-second-order and intra-particle diffusion rate equation as shown in Equation 2.18, 2.19 and 2.20, respectively (2.4.4.3).

The thermodynamic study was undertaken for the determination of the parameters (ΔG°, ΔH° and ΔS°) (Bouberka *et al*., 2005). The parameters were obtained from the plot of Van't Hoff equation (Qu *et al*., 2020) as given in Equation 2.24 (Section 2.4.4.4).

3.6.2 Stastical error validity of adsorption model

Sum of square error and Chi square error expressed by equation 3.7 and 3.8 was used to validate the isotherm and kinetic models

$$SSE = \sum_{i=1}^{n} (q_{cal} - q_{exp})^2 \qquad 3.7$$

$$\chi^2 = \sum_{i=1}^{n} \frac{(q_{exp} - q_{cal})}{q_{cal}} \qquad 3.8$$

3.7 Review summary and Identified Knowledge gaps

In this section, pollutants present in animal feed processing industry wastewater, its harmful effects on human and ecological system, as well as different wastewater treatment technology were reviewed. Synthesis method of carbon nanotubes, metallic nanoparticles (Pd and AgNPs) and their composites have been thoroughly reviewed. The review further identified source of the characterization techniques and application of composite materials as an adsorbent in wastewater treatment technology.

Based on literature search, it was observed that adsorption techniques combined with nanotechnology have been widely recognized and employed in the treatment of different industrial wastewater. But there is still little or no information on the study of synergistic effect of Pd and Ag on CNTs nanocomposites as nanoadsorbent for the treatment of animal feed processing industry wastewater. Clear insight to the review done on this study indicates that some gaps were identified and this study intends to fill the gaps. In the course of this work, the produced carbon nanotubes were doped with each of the PdNPs and AgNPs, the carbon nanotubes were also co-doped with the binary metallic nanoparticles. In addition, the adsorptive efficiency of the prepared nanocomposites was investigated on animal feed processing industry wastewater. The detailed experimental protocol and analytical techniques used in achieving the aim and various outline objectives of the research are provided in the next chapter.

CHAPTER FOUR

4.0 RESULTS AND DISCUSSION

4.1 Phytochemical Analysis of the Extract

The phytochemical screenings of banana peel extract (BPE), pineapple peel extract (PPE) and *Agerantum conyzoides* leave extract (ACE) revealed the presence of major secondary metabolites such as phenols, flavonoids, alkaloids, tannins and saponins as shown in Table 4.1. The total flavonoids content for BPE, PPE and ACE were determined to be 44.02±7.34, 30.53±6.22 and 30.03±6.24 mg/100 g. Quantitative estimation of alkaloids in BPE, PPE and ACE were found to be 6.51±1.89, 7.96±2.08 and 13.92±2.99 mg/100 g.

Table 4.1: Phytochemical constituents of banana peels, plantain peel and agerantum conyzoides (goat weed) leave extracts

Phytochemical constituents	**Sample Concentration (mg/100g)**		
	BPE	**PPE**	**ACE**
Phenols	265.06±23.05	269.54±25.56	311.95±34.21
Flavonoids	44.02±7.34	30.53±6.22	30.03±6.24
Alkaloids	6.51±1.89	7.96±2.08	13.92±2.99
Tannins	32.60±5.80	41.43±7.30	34.32±5.89
Saponins	340.13±29.78	215.99±23.11	391.49±36.67

Pineapple peel extracts contained the highest contents of tannins (41.43±7.30 mg/100 g) and phenol (269.54±25.56 mg/100 g)while the banana peel extract contained the lowest yield of tannins (32.60±5.80 mg/100 g). Saponins content were found to be highest acrossthe tested constituents.

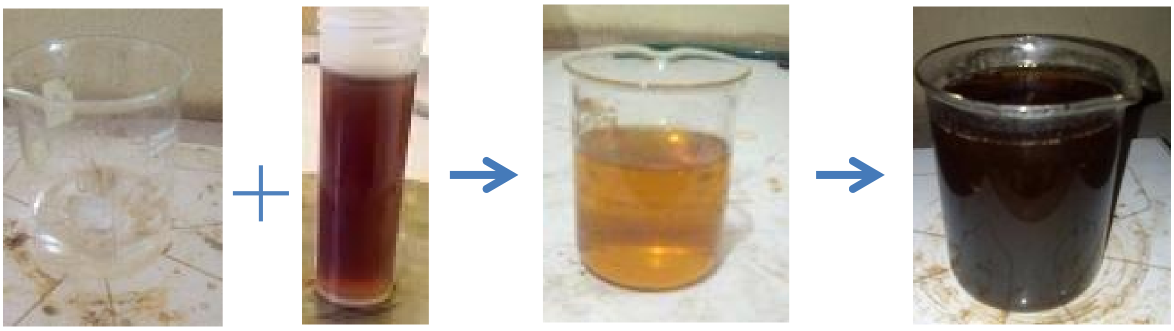
(a) $AgNO_3$ (b) Plants extracts (c) Extract + $AgNO_3$ (d) Synthesized AgNPs

Plate III: Procedure of Biochemical Synthesized AgNPs (a) Aqueous Solution of silver Nitrate Salt (b) *Agerantum conyzoides.* Leaves Extract (c) Mixture of Silver Nitrate Solution and Leaves Extract at 0 min (d) Mixture of $AgNO_3$ Solution and Leave Extract After 30 min of Stirring.


(a) $PdCl_2$ (b) Plant extract (c) Extract + $PdCl_2$ (d) Synthesized PdNPs

Plate IV (a-d): Procedure of Biochemical Synthesized PdNPs (a) Aqueous Solution of 1 mM of Palladium Chloride salts (b) Plant Extract of *Agerantum conyzoides* (c) Aqueous Solution of Palladium Chloride salt with *Agerantum conyzoides* Leave Extract at 0 min, and (d) Aqueous Solution of Palladium Chloride salt with Leave Extract after 30 min of Stirring.

As it can be observed, phenols were also present in other extracts with maximum of 311.95 mg/100 g and minimum of 265.05 mg/100 g concentration for ACE and BPE, respectively. This result implies that *Agerantum conyzoides* leave extract is very rich in phenols, flavonoids, tannins, alkaloids and saponins than other plant etracts. Several studies reported that these phytoconstituents play a leading role in the biochemical reduction of silver and palladium ions to silver and palladium in zero valent state (Ovais *et al*., 2018), as well as acting as stabilizing and capping the synthesized nanoparticles (Geethalakshmi and Sarada, 2012). This was noticeable in the formation of dark brown and dirty brown colouration, as indicated in Plate III and IV, after interaction with silver and palladium precursor salts.

4.2. Characterization of Palladium and Silver Nanoparticles

4.2.1 Uv-Vis spectroscopy analysis of silver and palladium nanoparticles

Uv-vis spectroscopy is one of the techniques used to monitor the formation of metal nanoparticles in aqueous solution. The formation of silver and palladium nanoparticles in aqueous solution was confirmed by measuring the absorption spectra in the wavelength range of 200-800 nm. A prominent, strong and broad absorbance peak was observed at 413.50 nm for AgNPs as shown in 4.1. The observed colour change during the reduction process of Ag^+ to Ag^o is an indication of formation of silver nanoparticles. The unique colour (optical properties) which was visually observed in the reaction mixture (plate III) and the appearance of the absorbance peaks (Figure 4.1) may be ascribed to surface plasmonic resonance of silver (John *et al*., 2018; Anandalakshmi *et al*., 2016). This occurs due to mutual oscillation of the conduction electrons on the surface of the Ag nanoparticles when aligned in resonance with the irradiated light of the wave. The combined oscillation of free electrons within the Ag nanoparticles and the surface resonance permit the scattering and absorption of light at a particular frequency, and thus, provide the characteristic colour of each nanoparticles (Aroca *et al*., 2006).

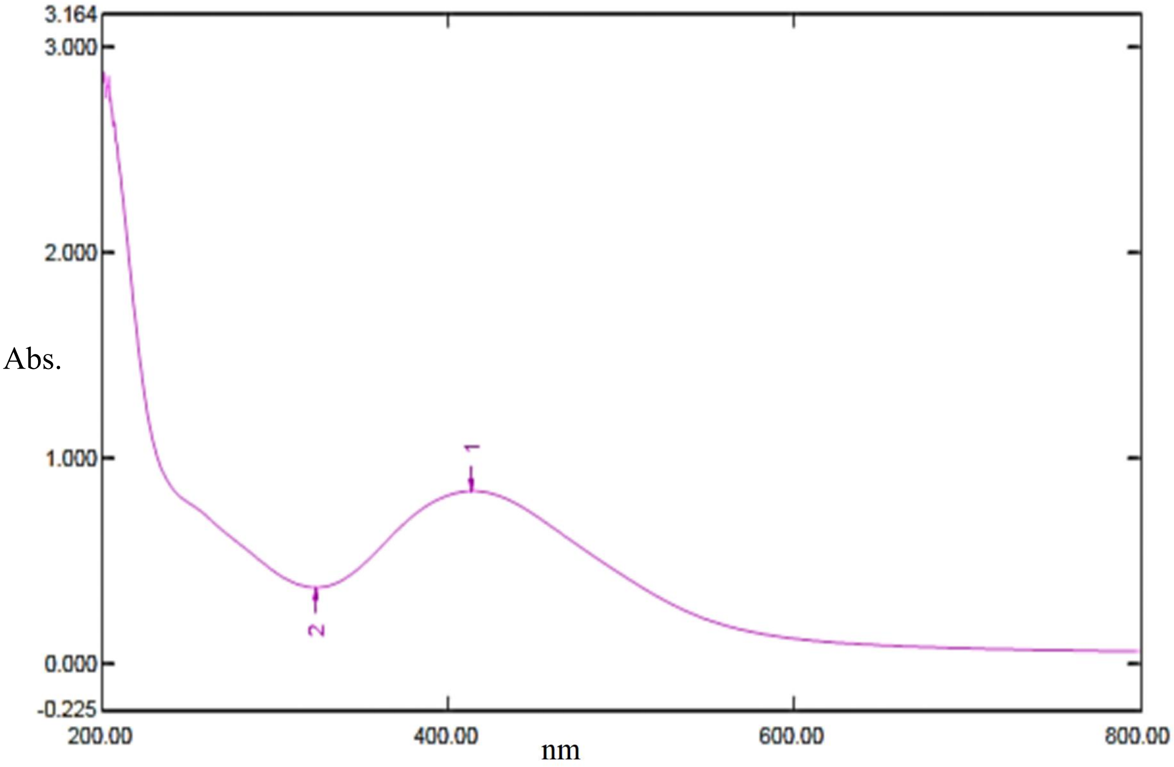

Figure 4.1: UV-Vis Spectograph of Synthesized Silver Nanoparticles (AgNPs)

Figure 4.1 displayed the Uv-vis spectrum of the synthesised AgNPs which fall within the maximum range of absorption spectra of 400-500 nm. Hence, the finding is consistent with the results described by other researchers thatprepared Ag nanoparticles using plant extract (Ali *et al.*, 2017; Ansari and Alzoairy, 2018). Similarly, Figure 4.2 demonstrated the Uv-vis spectrograph of the synthesized palladium nanoparticles (PdNPs) and the absorbance peak was noticed at 208.50 nm. An intense peak observed in the spectra indicated a higher concentration of the leave extracts, which has a strong correlation with particle size of the prepared nanoparticles (Kadam *et al.*, 2020).

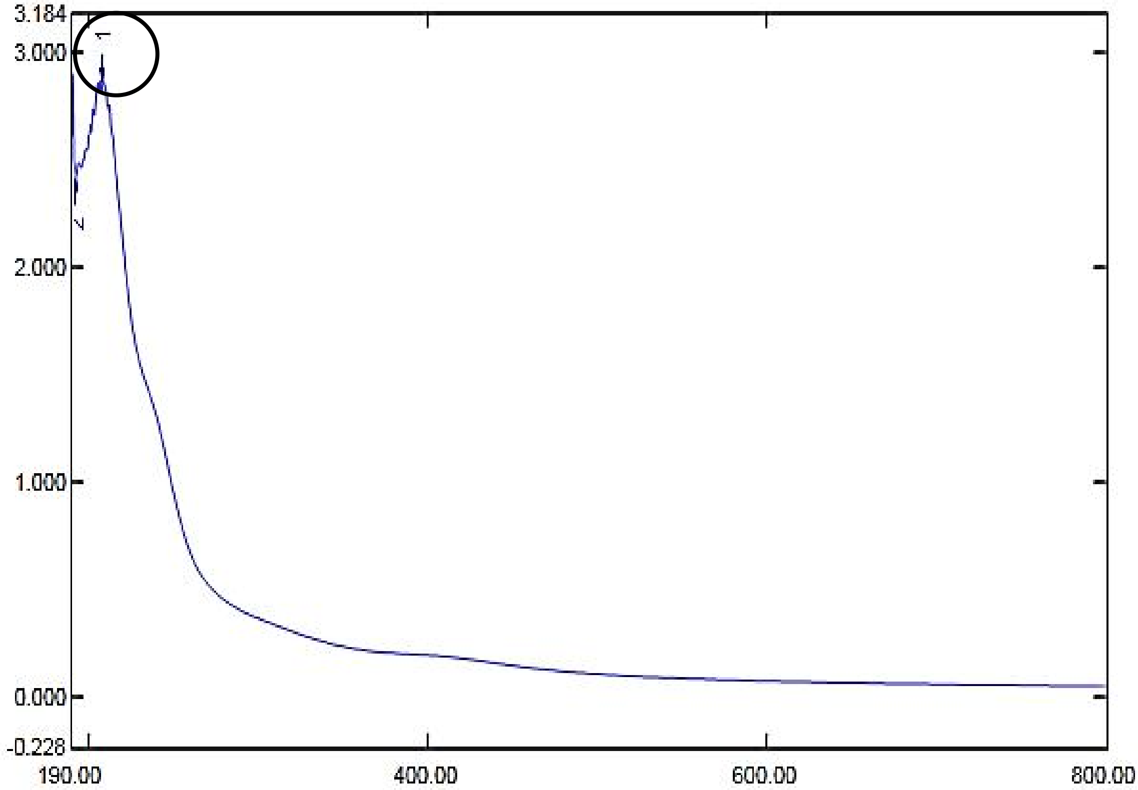

Figure 4.2:UV-Vis Spectograph of Synthesized Palladium Nanoparticles (PdNPs)

The result obtained does not correlate well with the reports stated by Arsiya *et al.* (2017) due to different range of absorbance peaks observed. Arsiya and colleagues identified PdNPs in the wavelength range 370-440 nm.The observed differences maybe linked to different plant material (which were grown under different environmental factors) used for the synthesis procedure including different reaction time (Borase *et al.*, 2014).

4.2.2 HRSEM and EDS analysis results of silver and palladium nanoparticles

The HRSEM micrographs of palladium nanoparticles (PdNPs) and silver nanoparticles (AgNPs) shown in plates V (a and b) revealed the shape of the synthesized nanoparticles. The structure of biochemical synthesized AgNPs were not clearly observed as depicted in Plate V (a), although the image showed a spherical agglomerated particles.

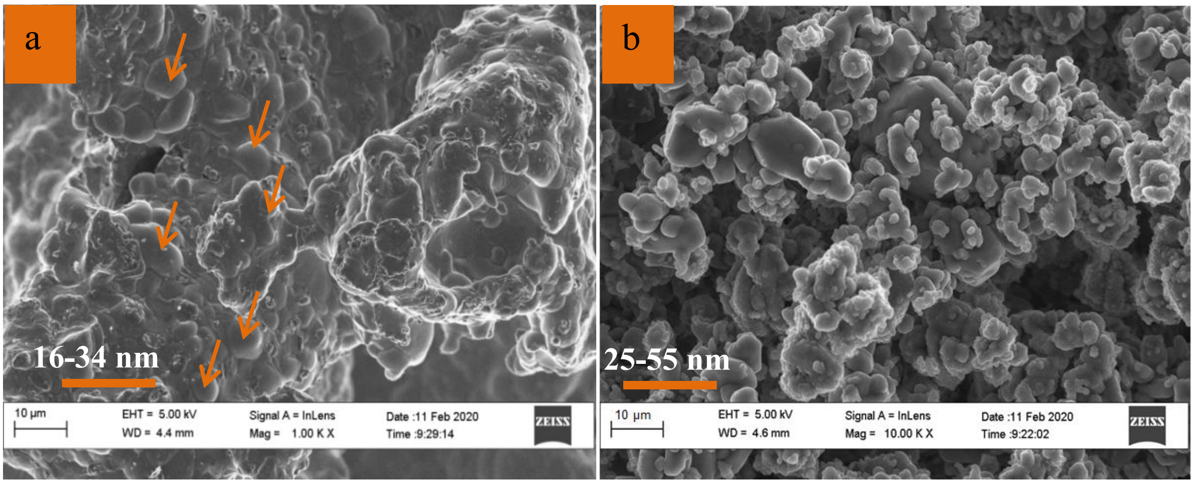

Plate V: High Resolution Scanning Electron Microscope image of (a) AgNPs (b) PdNPs

Ankanna *et al*. (2010) reported a relatively spherical shape nanoparticle with average particle size of 30-40 nm. Plate V (b) revealed both the formation of spherical and non-spherical (trigonal pyramidal, tetrahedral and hexagonal) nature of the nanoparticle with less aggregated surface.This is evidencethat *Agerantum conyzoides* leave extract act as reducing and capping agent in the reduction of palladium chloride to palladium nanoparticles compared to $AgNO_3$ to Ag°.

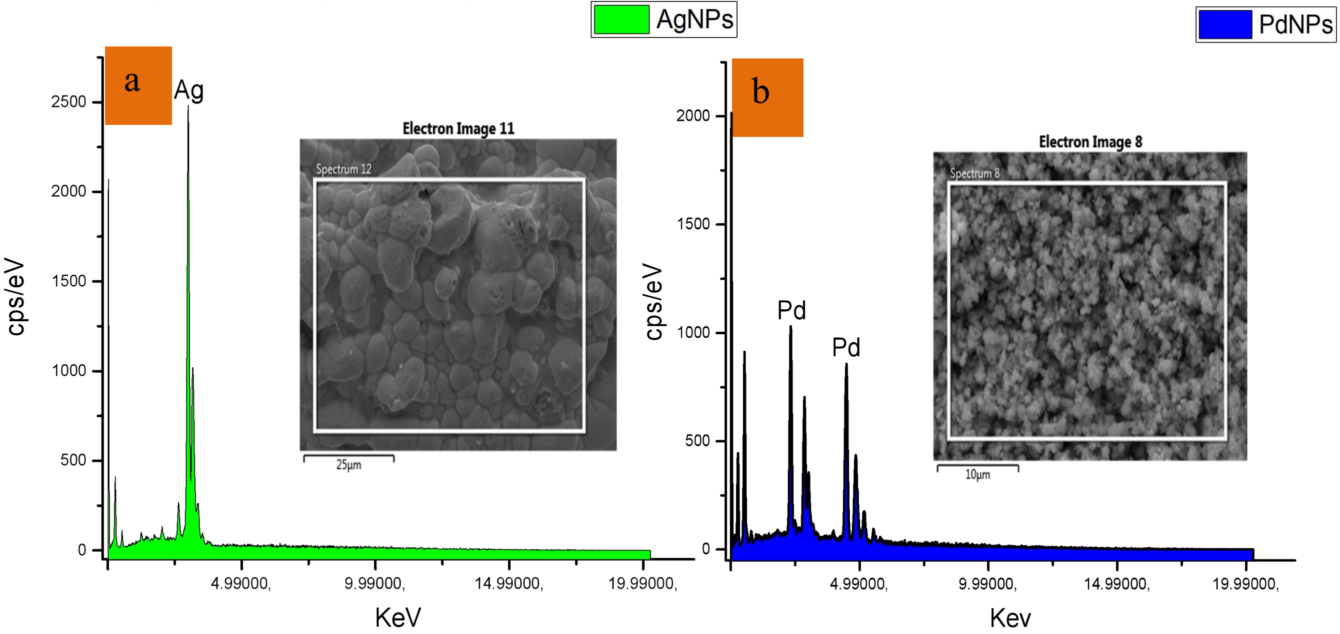

Figure 4.3: EDS Spectra of Synthesized (a) AgNPs and (b) PdNPs using *Agerantum conyzoides*

Figure 4.3 (a) and (b) show the energy dispersive X-ray spectroscopy of the produced nanoparticles. It was noticed from the spectrum figure 4.3 (a) that silver is present as major element with a strong signal of 89.70 % at 2.6 KeV, which was attributed to the surface plasmon resonance. Also, there exists 10.30 % of elemental oxygen which make up the quantitative information of biochemical synthesized AgNPs. The oxygen peak could be from the presence of surface hydroxyl group of secondary metabolites found in the leaves extract. Vijaykumar *et al*. (2013) reported the presence of silver nanoparticles in the range of 2-4 KeV. Similarly, silver nanoparticle was observed within the range of 2.5-4 KeV by Anandalakshmi *et al*. (2016). The differences in binding energy may be attributed to the size of the particles, that is, a decrease in size of nanoparticles leads to an increase in binding energy (Shin *et al*., 2004). In the case of figure 4.3 (b), two prominent peaks were observed at 2.2 and 4.2 KeV, and both corresponds to the absorbance peak of synthesized palladium nanoparticles. The spectrum indicates that the biochemical synthesized material primarily composed of Pd and O. This result is not in order with earlier reports described by Bankar *et al*. (2010) who also reported the presence of silica, and potassium in the EDS spectra of synthesized palladium nanoparticles. The observed differences could be due to differences in method used in the preparation of nanoparticles.

4.2.3 HRTEM analysis and SAED patterns of palladium and silver nanoparticles

The HRTEM analysis was carried out to examine the internal structure of the resultant nanoparticles. The HRTEM image of the synthesized silver nanoparticles displayed a clearspherical shape particles with an average particle size of 28.5nm. Additionally, the HRTEM-SAED pattern revealed a clear, diffraction ring patterns, which is an indicatives of the existence of multi-crystallites that corresponds to a face centered cubic (fcc) of crystal plane (111), (200), (220) and (311) of AgNPs. Similarly, the image (Plate (VI) b) of palladium nanoparticles indicated that the synthesized particles were fairly spherical in shape with mean size of 18.5 nm.

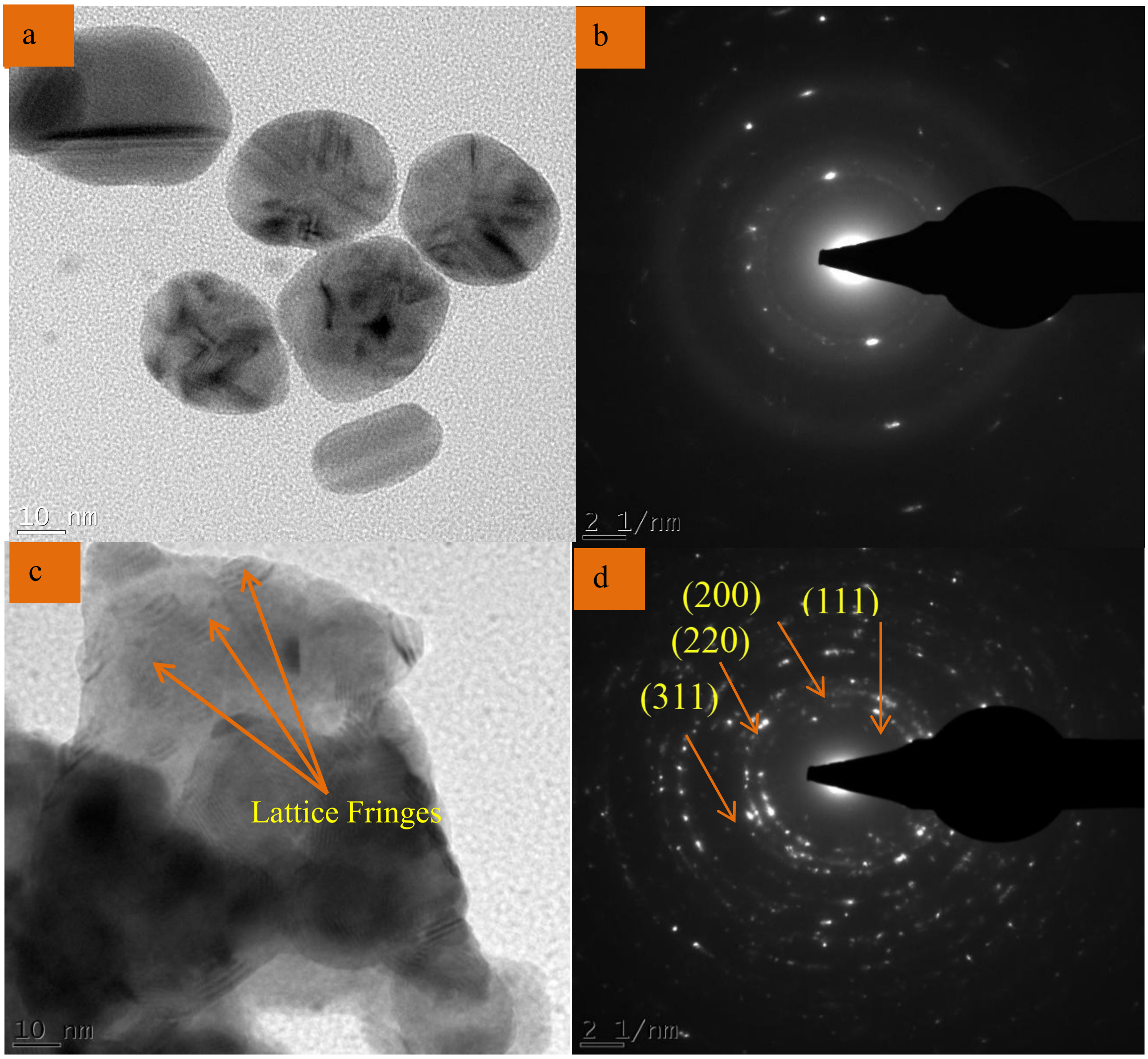

Plate VI: (a & b) High Resolution Transmission Electron Microscope Image of AgNPs and PdNPs (c& d) Selected Area Electron Diffraction (SAED) Patterns of AgNPs and PdNPs

The variation in particle size of PdNPs compared to the HRTEM results of AgNPs could be linked to the differences in reduction ability of the precursor salts (Nagar and Devra., 2018). The HRTEM image further showed the crystalline natures of the produce nanoparticles with different atomic resolution, and an interlayer spacing (lattice fringes) between the particles (Islam *et al*., 2018). The SAED pattern (plate (VI) d) reveals a well define bright circular rings which is an indication of formation of Ag and Pd nanoparticles. The results of SAED pattern were in agreement with the XRD, as each of the diffraction rings was found to be consistent with the face centered cubic structure of Pd (111), (200), (220) and (311) crystalline fringes.

4.2.4 XRD analysis of the prepared silver and palladium nanoparticles

The synthesized Ag and Pd nanoparticles were characterized using X-ray diffraction techniques to confirm the mineralogical phase of the synthesized materials.

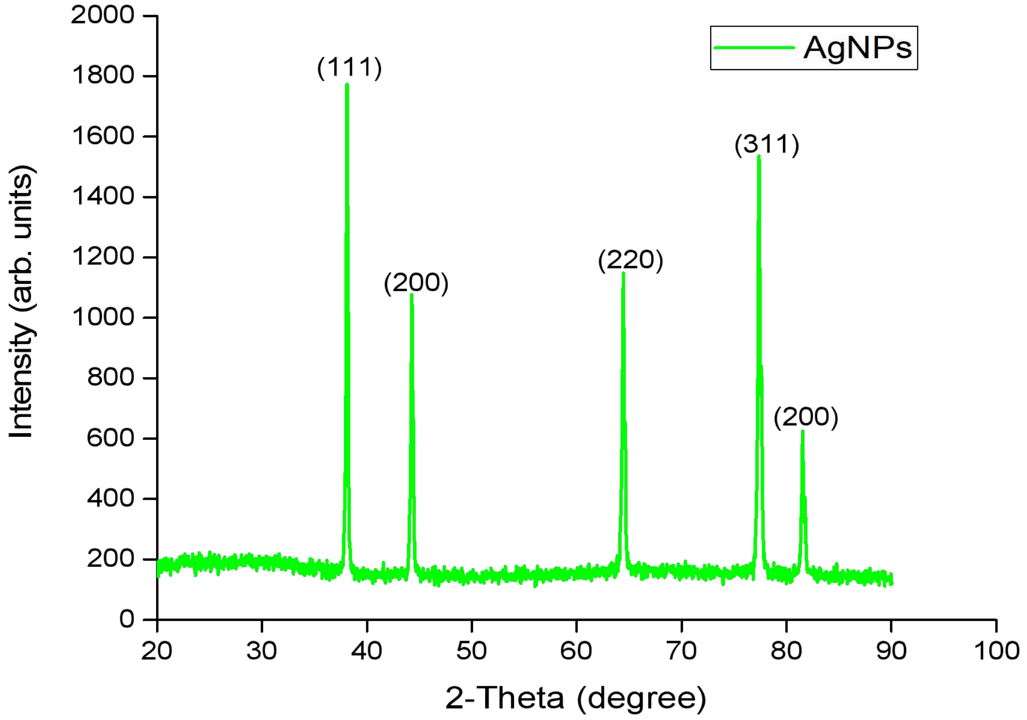

Figure 4.4: X-ray Diffraction Patterns of Silver Nanoparticles (AgNPs)

As revealed in figure 4.4, five (5) diffraction peaks of different intensities of AgNPs were observed between 20 to 90 °C at 2θ angles. The XRD patterns clearly reveals the important characteristic peaks at 2-theta values of 38.1^{o}, 44.3^{o}, 64.5^{o}, 77.4^{o} and 81.2^{o}, which corresponds to the planes (111), (200), (220), (311) and (222), respectively. All the peaks in the X-ray diffraction pattern were indexed with the planes of the face centered cubic structure of silver as per Joint Committee on Powder Diffraction Standards (JCPDS: No 04-0783). The average crystallite sizes of Ag nanoparticles were estimated using Debye-Scherrer's equation (Ajitha *et al.*, 2015) and estimated to be 37.21 nm.

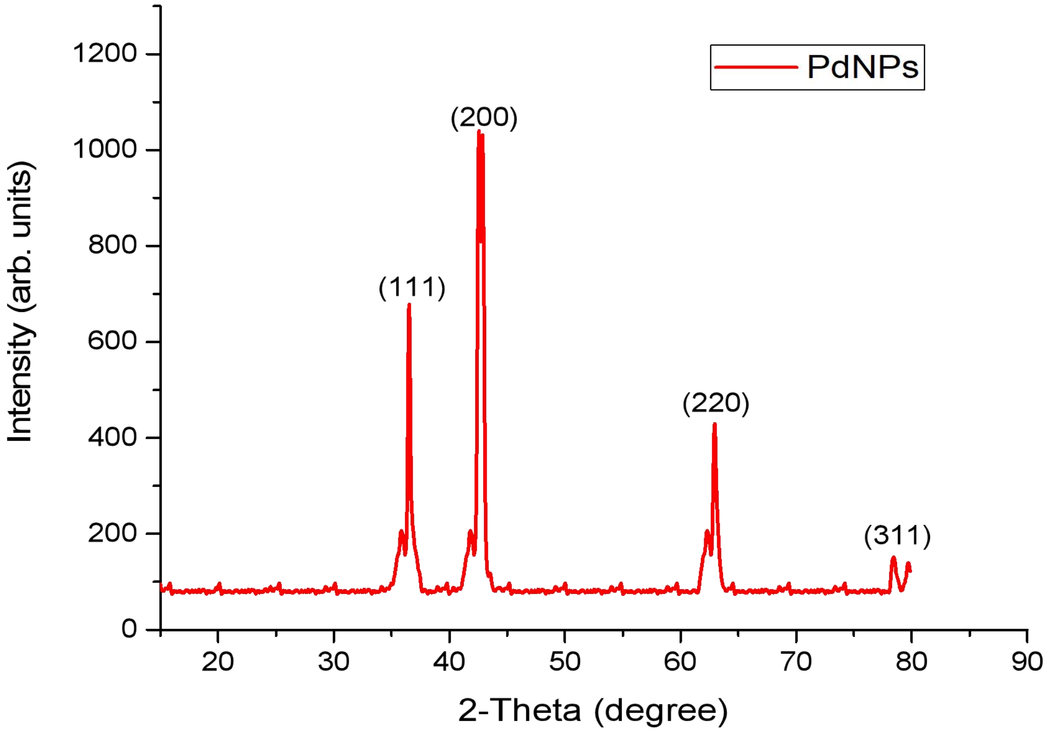

Figure 4.5: X-ray Diffraction Patterns of Palladium Nanoparticles (PdNPs)

A similar result was reported by previous researchers who also observed a number of Bragg's reflection plane at 2θ values of 38.09°, 44.27°, 64.46°, 77.46° and 81.63° (Khatami *et al.*, 2016; Turunc *et al.*, 2017). Kyaw *et al.* (2018) reported two distinct average crystallite sizes of 57.65 nm and 49.82 nm, which were found higher than the value recoreded in the present study. Similarly, Jebril *et al.* (2020) reported lower crystallite size of 21 nm. The observed differences in the average crystallite sizes of Ag nanoparticles may be ascribed to the orderliness of nanoparticles during the sample preparation. This may directly affect the intensities of the XRD patterns and consequently affect the crystallite size of the prepared nanoparticles.

As depicted in figure 4.5, the characteristic diffraction peaks observed at 2θ values of 36.5°, 42.7°, 62.9° and 78.5° represents the reflection planes (111), (200), (220) and (311). This is assigned to the face centered cubic structure of palladium nanoparticles in accordance to the JCPDS file 87-0639. The estimated crystallites size in different plane of palladium was calculated as 30.8, 15.9, 21.8, and 28.1 nm, with an average value of 24.2 nm. The intense peaks observed in the XRD pattern of PdNPs clearly indicated that the material is highly crystalline in nature and the observed phenomenon support the SAED pattern shown in plate VI (d). In a research conducted by Petla *et al*. (2012), average crystallite size of 13 nmwas reported for thepalladium nanoparticles prepared using soybean leaf etract. However, the reported crystallite is lower compared to the value recorded in the present study. The descripancy may be connected to different biomolecules present in the leaf extract used for the synthesis method (Kambale *et al*., 2020).

It is worth mentioning that, the average crystallite size estimated from the XRD pattern of multi-facet shapes of PdNPs is smaller compared to that of spherical Ag nanoparticles. The differences may be attributed to the similar deviation among the texture coefficient of various facets observed for the HRSEM analysis of both Ag and PdNPs. This means that even though the morphology is the same, the texture coefficient differs between polycrystalline bulk samples and nanoparticles (Navaladian *et al*., 2009). This variation is not surprising because of the effect of particle size in X-ray scattering. Similar phenomenon is observed in the work of Turunc *et al*. (2017), where different crystal orientation was recorded for both Pd and Ag nanoparticles, respectively.

4.3 Synthesis and Characterization of Carbon Nanotubes

4.3.1 Preparation of bi-metallic (Fe-Ni) kaolin catalyst

The yields of the Fe-Ni/Kaolin catalyst prepared based on the variation of the mass of catalyst support between (10 g and 8 g), stirring speed (2400 and 1200 rpm), drying time (12 and 10 h) and pre-calcination temperature (140 and 120 °C) for upper and lower level, respectively is shown in Table 4.2.

Table 4.2: Yield of Fe-Ni/Kaolin Catalyst at Pre-calcination

Level	Mass of support (g)	Stirring speed (rpm)	Drying time (h)	Pre-calcination temperature (°C)	Percentage yield (%)	Percentage yield after calcination (%)
Upper level (+)	10	2000	12	140	86.54	84.18
Lower level (-)	8	1000	10	120	85.24	82.92

Prior to calcination, the colour of the prepared catalyst was yellowish in nature and later changed to reddish brown after calcination. The initial colour originated from the mixture of brown and green colouration of Fe^{3+} and Ni^{2+}catalyst, as well as the cream colour of kaolin support. At calcination stage, the catalyst were subjected to high temperature to decompose volatile substances like nitrate and other inorganic ions, under a controlled environment. The heat treatment of the catalyst also involves oxidizing a weight portion of the sample and removal of the total moisture content present in the sample. The most essential part of calcination is the reduction of particle size of a material to a crystal form which was achieved at temperature above 400 °C.

Further heating above 400 °C, specifically calcination temperature (550°C) was employed in this work.

Calcination at 500 °C increase the specific surface area of the catalyst and consequently the yield of the catalyst. As depicted in Table 4.3, post calcination of the catalyst sample at 550 °C for 16 h, indicates noticeable effects on the catalyst yield. It was observed that the catalyst yield after calcination was found to be 84.18 and 82.92 % for upper and lower levels, respectively. The high catalyst yield was obtained at 12 h calcination time. This was linked to proper dispersion of metallic particles onto the kaolin substrate as well as increased the evaporation of water from mixture at drying time of 12 h compared to 10 h. The rise in drying time undoubtedly increased the concentration of the precursor material, and opening up of the pores of the materials until its saturated. As a consequence, increase the performance activity of the catalyst. This result agreed well with the work of Aliyu *et al*. (2017) who demonstrated variations in catalyst yield with two different pre-calcination time of 8 h and 10 h.

4.3.2 Synthesis and purification of carbon nanotubes

The multi-walled carbon nanotubes (MWCNTs) were produced via the deposition of acetylene gas on a kaolin supported catalyst. The yield of CNTs was evaluated through the deposition of acetylene gas in an electrical furnace, under continuous flow of a carrier gas at reaction temperature of 700 °C. The as-synthesized CNTs were treated with oxidative functional group (HNO_3 and H_2SO_4) to obtain purified carbon nanotubes (P-CNTs).

4.3.4 Characterization of carbon nanotubes and impregnated carbon nano composites

The purified carbon nanotubes and impregnated carbon nanocomposites were characterized in order to determine the morphology, particle size, mineralogical phase, and surface area of the developed adsorbents. These parameters unquestionably affect the adsorption performance of the adsorbents and thus, highlighted in the section 4.3.4.1 to 4.3.4.3, as follows.

4.3.4.1 HRSEM and EDS Analysis of purified carbon nanotubes and nanocomposites

The HRSEM images of purified carbon nanotubes (P-CNTs), as well as impregnated nanocomposites (palladium-carbon nanotubes (Pd-CNTs), silver-carbon nanotubes (Ag-CNTs/) and palladium-silver-carbon nanotubes (Pd-Ag-CNTs) is shown in Plate VII (a-d). Plate VII (a) revealed, as expected, that the P-CNTs are filaments with curve and interwoven web-like structures with shiny tips. The images also indicate a typical tube-like structure with diameters ranging from 16 to 38 nm (Plate VII a), which is a characteristic properties of the MWCNTs produced by this techniques (Madian *et al.*, 2017).

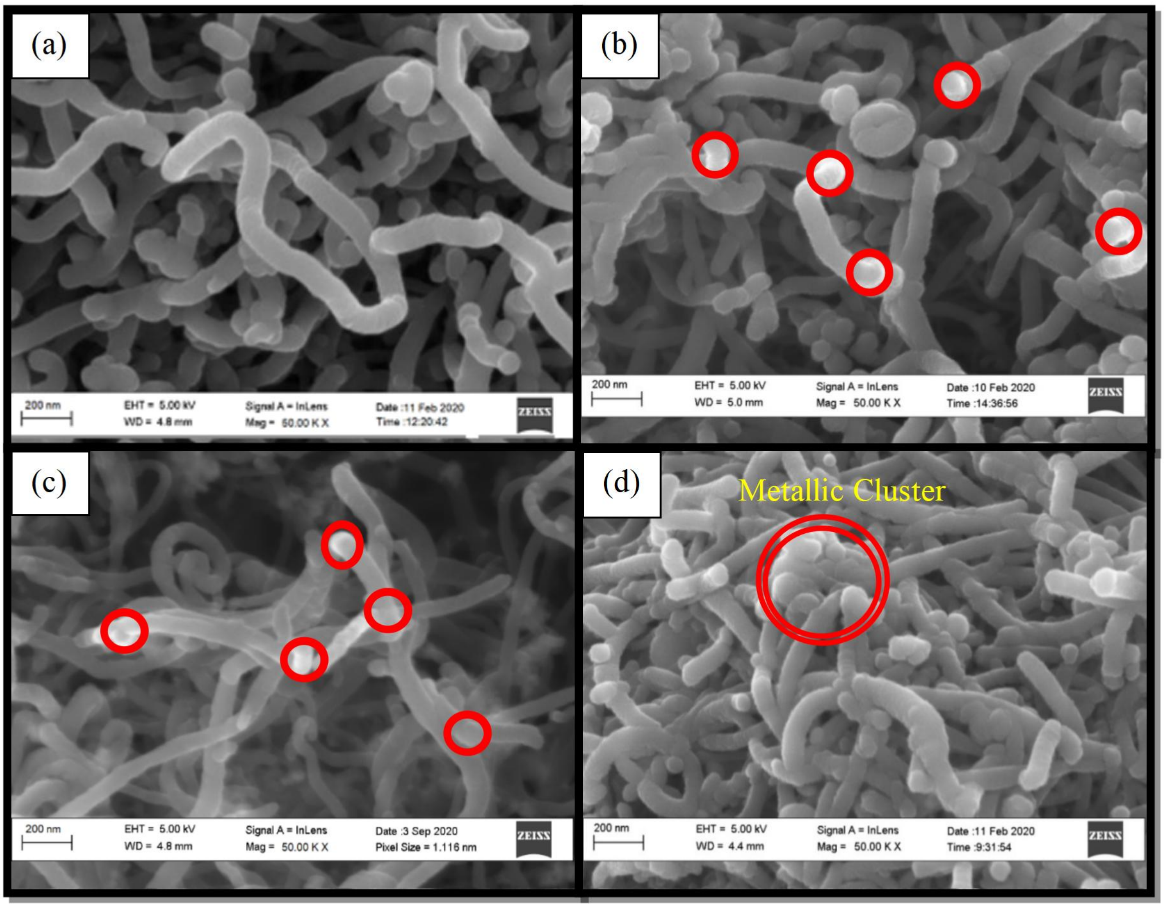

Plate VII: High Resolution Scanning Electron Microscopy Images of (a) P-CNTs (b) Ag-CNTs (c) Pd-CNTs (d) Pd-Ag-CNTs

The purification process of CNTs with oxidative acid treatment provided carboxilic acid groups at the defect sites of the CNTs, with negligible presence of metallic impurities. This process also led to cutting of the CNTs along the edges and basically around the openings, which enables the CNTs to be modified chemically. The EDS analysis result confirmed the elemental constituents present in the P-CNTs. As depicted in Table 4.5, the results reveal high content of carbon atom which signify high amount of the CNTs. However, less content of metallic impurities were present in the samples. The presence of metallic impurities observed in EDS results could be attributed to the calcination process employed during the preparation of the samples.

Table 4.3: Elemental composition (EDS) of the synthesized CNTs-based nanocomposites

	Elemental Composition (Atomic %)										
Composite Samples	C	Ag	Pd	O	Al	Si	K	Ca	Cl	Fe	Ni
P-CNTs	94.02	-	-	2.11	0.92	1.17	0.04	0.13	-	0.89	0.71
Ag-CNTs	87.82	7.98	-	1.78	0.9	0.87	0.07	0.04	-	0.3	0.24
Pd-CNTs	87.07	-	6.72	1.56	1.83	1.96	-	-	0.23	0.33	0.31
Pd-Ag-CNTs	67.76	9.4	4.4	4.29	3.33	2.57	0.91	1.21	1.71	2.97	1.45

As revealed in Plate VII (c-d), the HRSEM image of Ag-CNTs, Pd-CNTs, and Pd-Ag-CNTs were done to confirm the presence of Pd and Ag nanoparticles on CNTs surface. The results confirm the deposition of silver on CNTs (Plate VIIb) with indication of white crystals of AgNPs on the tips of the CNTs wall. This observation can be ascribed to high dense properties of the attached AgNPs, which makes the nanocrystals (AgNPs) attached freely on the surface of the nanotubes. However, the image demonstrated that upon the incorporation of silver nanoparticles, the multi-walled carbon nanotubes (MWCNT) remarkably shrunk in size when compared to that of P-CNTs, though equally its tube-like structure were still maintain as depicted in Plate VII (b). The diameter of the tubular structure reduced to a range of 9.8-36 nm, with average size of 15.16 nm. The tube probably shrunk due to higher ionic radii of silver (1.60 Å) atom compared to carbon atom (0.70Å), thereby, preventing the passage of AgNPs through the internal layer of the CNTs. According to EDS results shown in Table 4.4, the atomic weight (relative %) of metallic silver deposited on CNTs surface was 7.98 %. Other elemental compositions of silver doped CNTs reveal the presence of C, O, Fe, and Ni with other few impurities. The white crystal of different sizes shown in Plate VII (a) support the HRTEM results presented in Plate IX (a)

The HRSEM micrograph of palladium doped CNTs (Pd-CNTs) nanocompositesas shown in Plate VII (c) indicates a long clusters, curved tube-like structures forming bundles of filaments with length exceeding 10 nm. The image indicates that Pd nanoparticles were uniformly distributed all over the tubes and thus embedded in the CNTs bundles. This result implies that the presence of palladium nanoparticles restrains the graphitic nature of the MWCNTs which is an indication of improved mechanical properties of the composites (Pd-CNTs). The quantitative analysis of the composite (Pd-CNTs) were investigated using Energy Dispersive X-ray spectroscopy (EDS) and the result indicates the presence of C, O, Pd, Fe, and Ni with other insignificant amount of impurities. As shown in plate VII (d), it can be seen that the nanocomposite has spaghetti-like structure, thus indicating the existence of CNTs in the structure. The Pd/AgNPs grafted onto the outer surface of the CNTs have a thin clusters and agglomerated morphologies. This suggests the combined or antagonistic effects of the two metallic nanoparticles deposited on the CNTs wall. These effects can be linked to the fact that the Pd metal is less dense than carbon atom, while metallic silver is denser. This inference can be related to the high molecular weight of the combined nanoparticles which subsequently leads to the suppression and interference of the CNTs surface morphologies (Črešnar *et al*., 2021). The HRSEM result of Pd-Ag-CNTs reveals that the outer diameter of the CNTs gradually decreases upon dispersion of binary metallic nanoparticles, with size range of 12.5-35 nm. In order to confirm the elemental composition of the sample, EDS analysis was carried out on Pd-Ag-CNTs composite and the result reveals the presence of C, Ag, Pd, and other lower percentile weight of metallic impurities. The oxygen in the prepared nanocomposites originated from the oxygen containing compounds utilized for the purification process or the presence of phytoconstituents in plants extracts that was employed for nanoparticle synthesis (Ahsani *et al.*, 2020). However, the elemental composition of the ternary nanocomposites is in accordance with the observed morphology from the HRSEM analysis results. Despite the difficulties in distinguishing between the surface morphology of the composites, it should be clearly stated that the HRSEM micrograph of Pd-CNTs and Ag-CNTs are similar due to the fact that the pores on the surfaces were largely opened (Plate VII (b & c), but were more compacted in Pd-Ag-CNT composites (Plate VIId). This results is so because co-doped metallic nanoparticles is expected to boost the performance activity of the material in capturing some pollutants, and thus closing up the distances between the pores of the CNTs to give desired pore-size which can simply perform the role of adsorbent material.

4.3.4.2. HRTEM and SAED patterns of the synthesized carbon nanotubes and nanocomposites

The HRTEM results depicted in plate VIII, IX, X and XI indicated that the purified and impregnated CNTs predominantly consist of multiple layers. Plate VIII (a and b) indicates the HRTEM micrograph of the P-CNTs shows a tubular network. The inner pore diameter of the P-CNTs is 16.7 nm, while the external diameter of the P-CNTs wall is 38 nm. The entrapped impurities and the amorphous region noticed in the HRTEM results might be due to the period when the as-synthesized CNTs were removed from the electrical furnace. Also, the loss of temperature could lead to non-uniformity in the growth of CNTs (Qiu *et al.*, 2017).

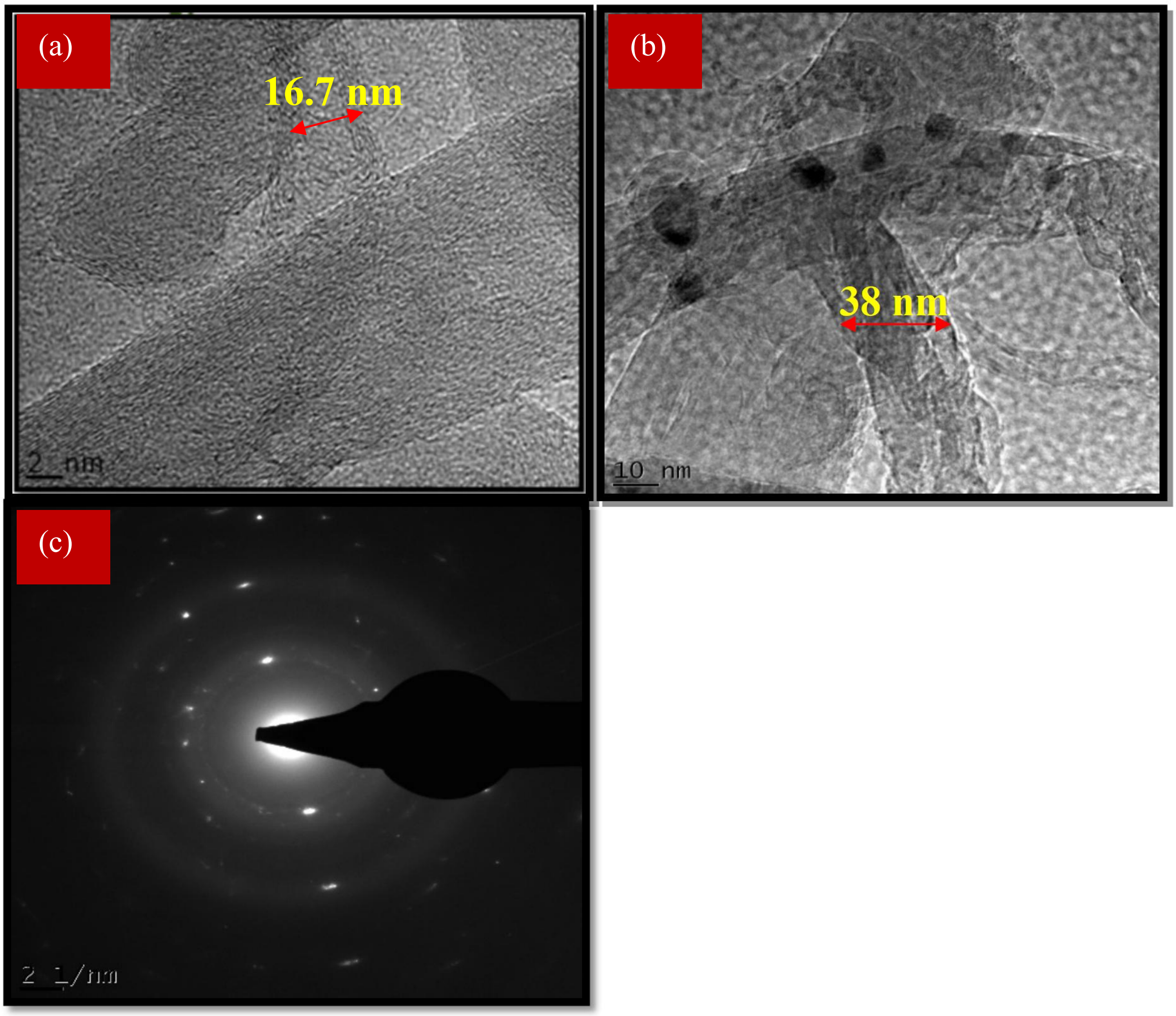

Plate VIII (a) & (b): High Resolution Transmission Electron Microscopy Images of P-MWCNTs at Different Magnifications (c) SAED Pattern of P-MWCNTs

Presented in Plate IX (a-c) is the HRTEM result and SAED pattern of Ag doped CNTs nanocomposites. It is clear that the Ag-CNTs nanocomposites had a narrow pore diameter distribution with internal cavity ranges from 12 to 17 nm with an average diameter of 13.5 nm.

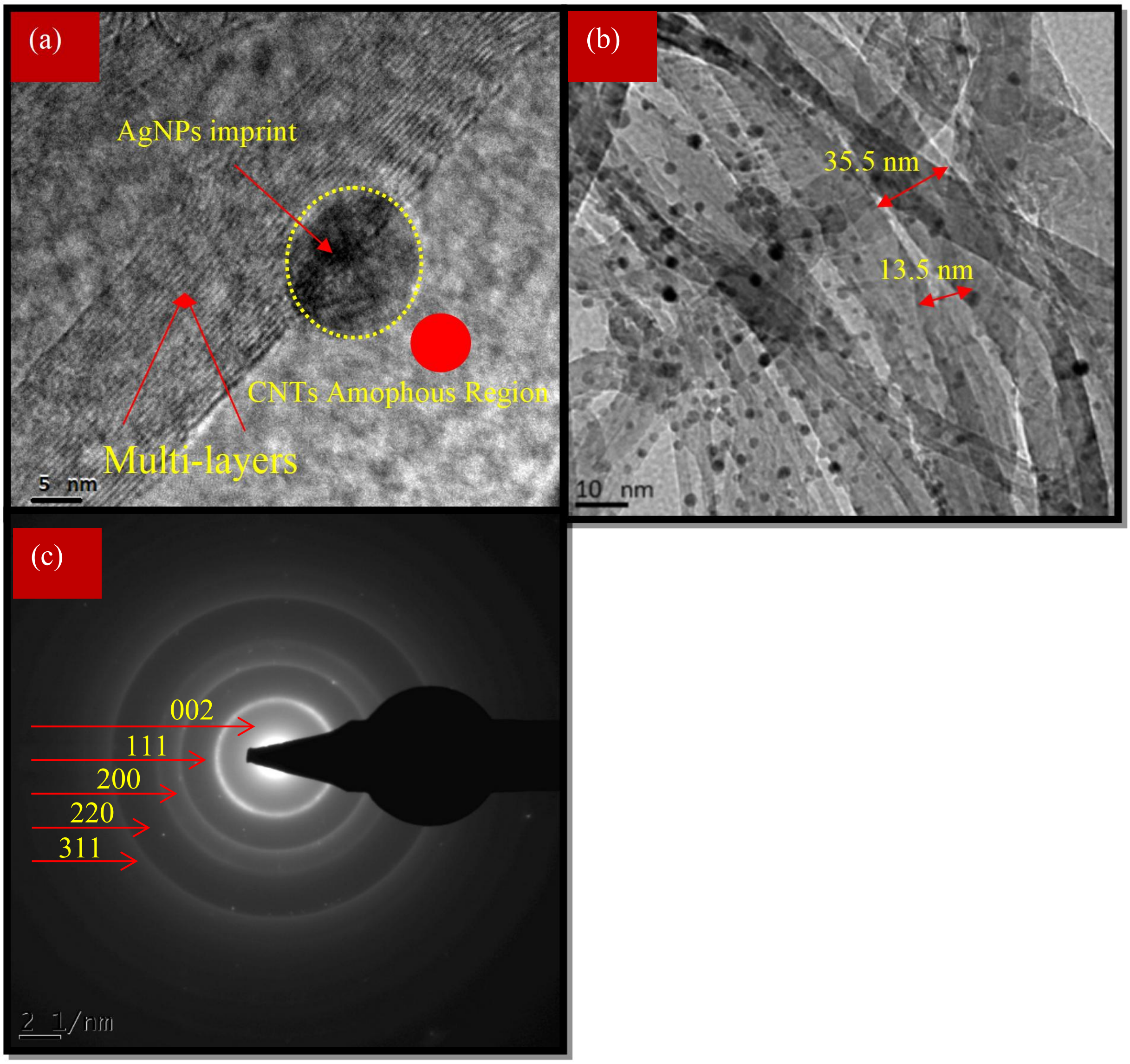

Plate IX (a) & (b): High Resolution Transmission Electron Microscopy Images of Ag-CNTs Nanocomposite at Different Magnification (c) SAED Pattern of Ag-CNTs Nanocomposites

The outer edges diameter was estimated to be 35.5 nm and an imprint at the edges of the Ag-CNTs external wall were observed. Unquestionably, it should be mentioned that it was AgNPs that were condensed within the lattice fringes of the CNT multi-layers, which was further confirmed by EDS spectrum presented in Table 4.5.

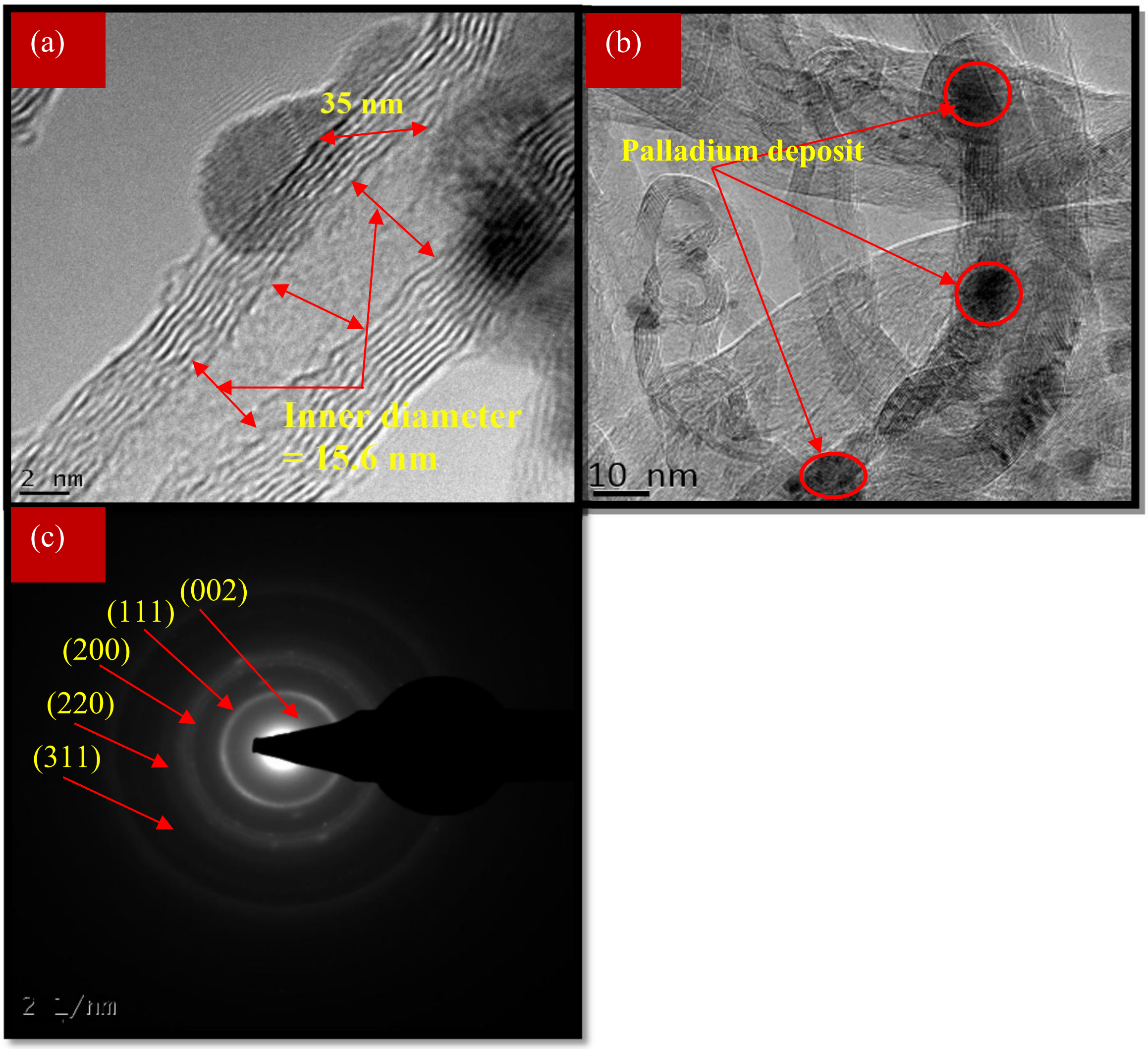

Plate X (a) & (b): High Resolution Transmission Electron Microscopy Images of Pd-CNTs Nanocomposite at Different Magnification (c) SAED Pattern of Pd-CNTs Nanocomposites

As shown in plate IX (c), the multiple graphitic layer revealed an estimated values of 0.334 nm for the distance between two graphene layer of Ag-CNTs nanocomposites (SAED pattern of Ag-CNTs). This obtained value is closely related to the figure reported by Chen *et al*. (2006) who employed CVD method for the synthesis of CNTs.

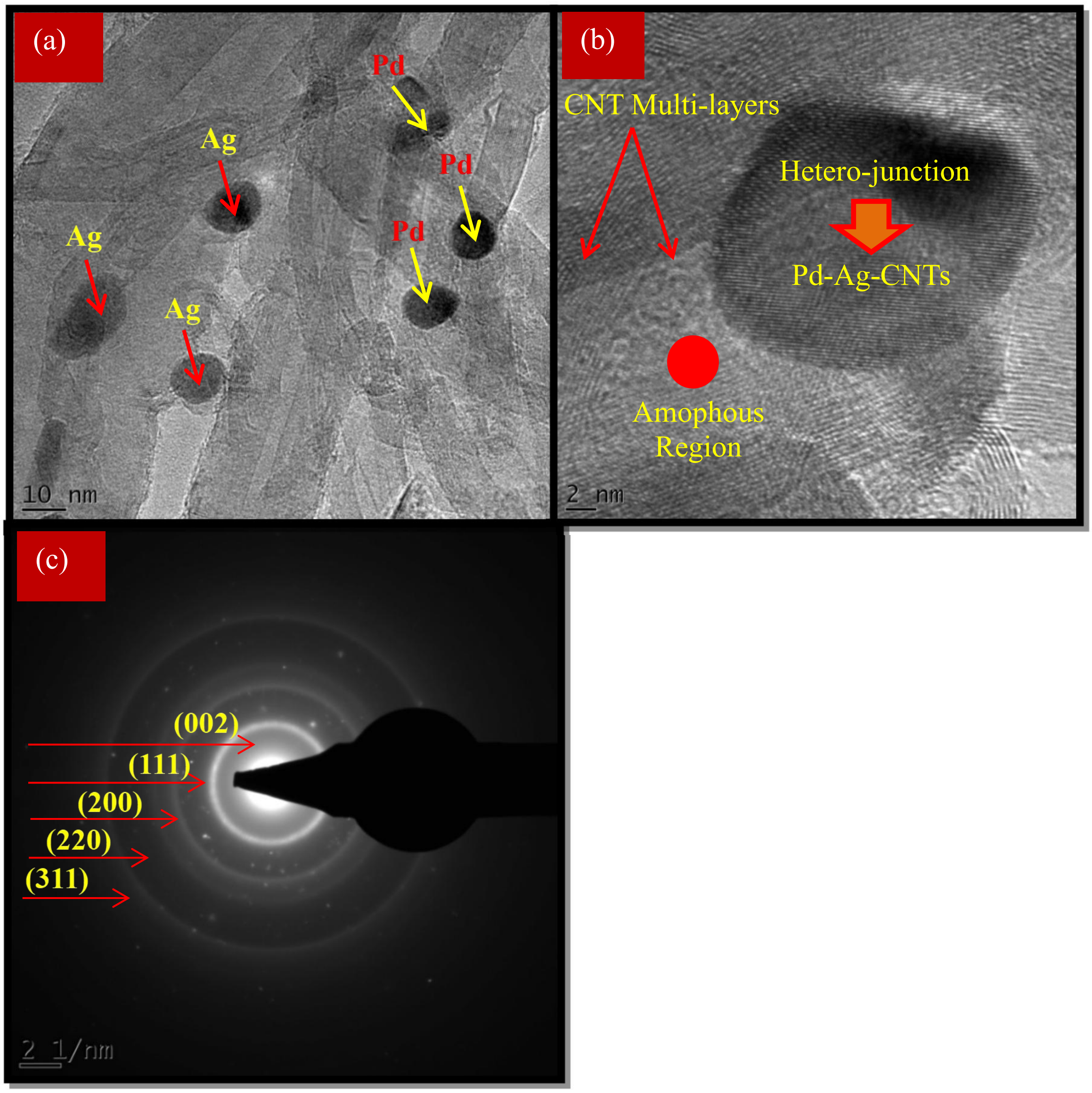

Plate XI (a) & (b): High Resolution Transmission Electron Microscopy Images of Pd-Ag-CNTs Nanocomposite at Different Magnification (c) SAED pattern of Pd-Ag-CNTs Nanocomposites

To investigate the presence of the synthesised Pd and Ag nanoparticles in the purified carbon nanotubes, HRTEM analysis was carried out on the prepared nanocomposite (Pd-Ag-CNTs). The result revealed that different etching of spherical shapes were locked up within the internal cavity of the hollow tubes and the pore diameter varied from 12 nm (internal diameter) to 32.5 nm (outer diameter). A plausible explanation for the decreased inner-outer diameter after modification may be due to a decrease in the layer on the outer wall of the tubes caused by bi-metallic Pd°/Ag° embedment. Furthermore, the dark bright spot observed when the HRTEM image was examined at higher magnification indicates the region where both metallic nanoparticles were concentrated (Hetero-junction) on the outer shell of the CNTs surface. The SAED pattern represented in plate XI (c) showed different concentric ring which further confirmed the graphitic nature of the P-MWCNT and the major improvement in the order of crystallinity of the Pd-Ag-CNTs nanocomposites. Thus, implying that the produced nanocomposites is polycrytalline in nature after immobilization with metallic nanoparticles.

4.3.4.3 XRD Analysis of the purified carbon nanotubes and impregnated carbon nanotubes

The synthesized carbon nanotubes and Pd-Ag/CNTs composites were further characterized using powdered X-ray diffraction techniques to verify the crystalline nature of the materials. As shown in figure 4.6, the XRD patterns of the purified-CNTs samples showed only two prominent diffraction angles at 2-theta value of 26.00° and 44.69°, which corresponds to the miller indices (002) and (100) of CNTs.

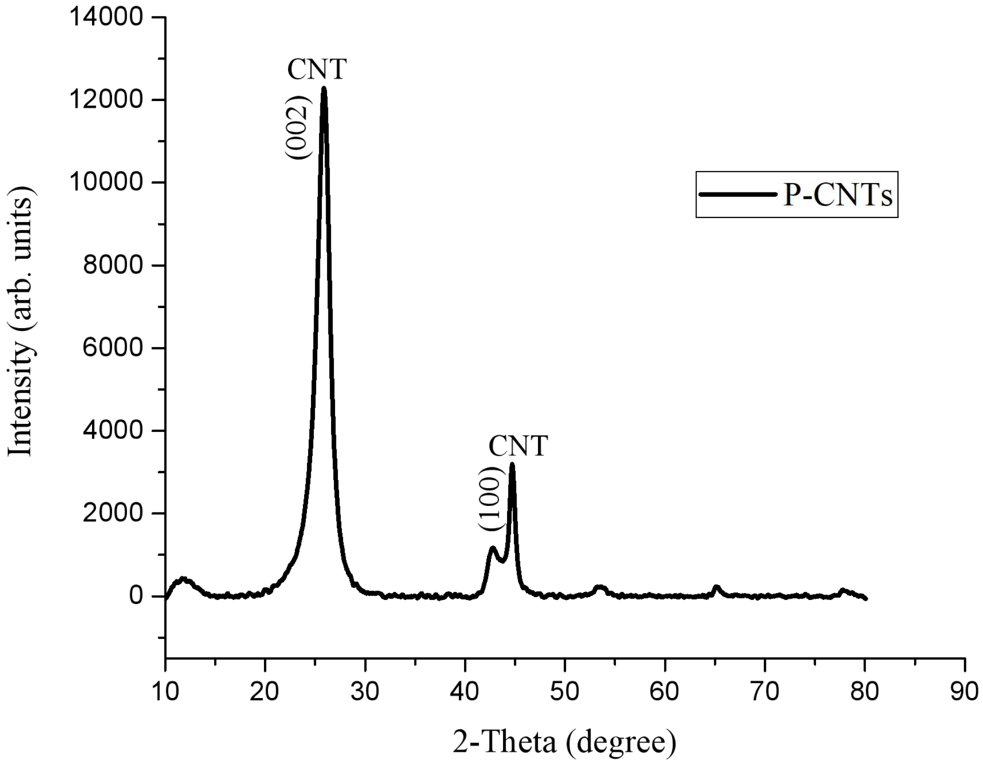

Figure 4.6:X-ray Diffraction Pattern of Purified-CNTs

This XRD result of purified carbon nanotubes is in accordance with the findings reported by Jatoi *et al.* (2020). In addition to the confirmation of the graphitic structure, the mineralogical phases of the prepared adsorbents, the XRD patterns of the Pd/Ag/CNTs, Ag/CNTs and Pd/CNTs were presented in Figure 4.7-4.9. In Figure 4.7, the intense peak observed at 2θ value of 26.13° with a characteristic plane of (002) correspond to graphite structure of CNTs, which corroborated the sharp bright spot noticed in the SAED pattern of plate IX (c) (Ag-CNTs). The other diffraction angles observed at 38.11°, 44.29°, 64.45° and 77.41° with crystal plane of (111), (200), (220) and (311) correspond with the face-centered cubic structure of silver nanoparticles.

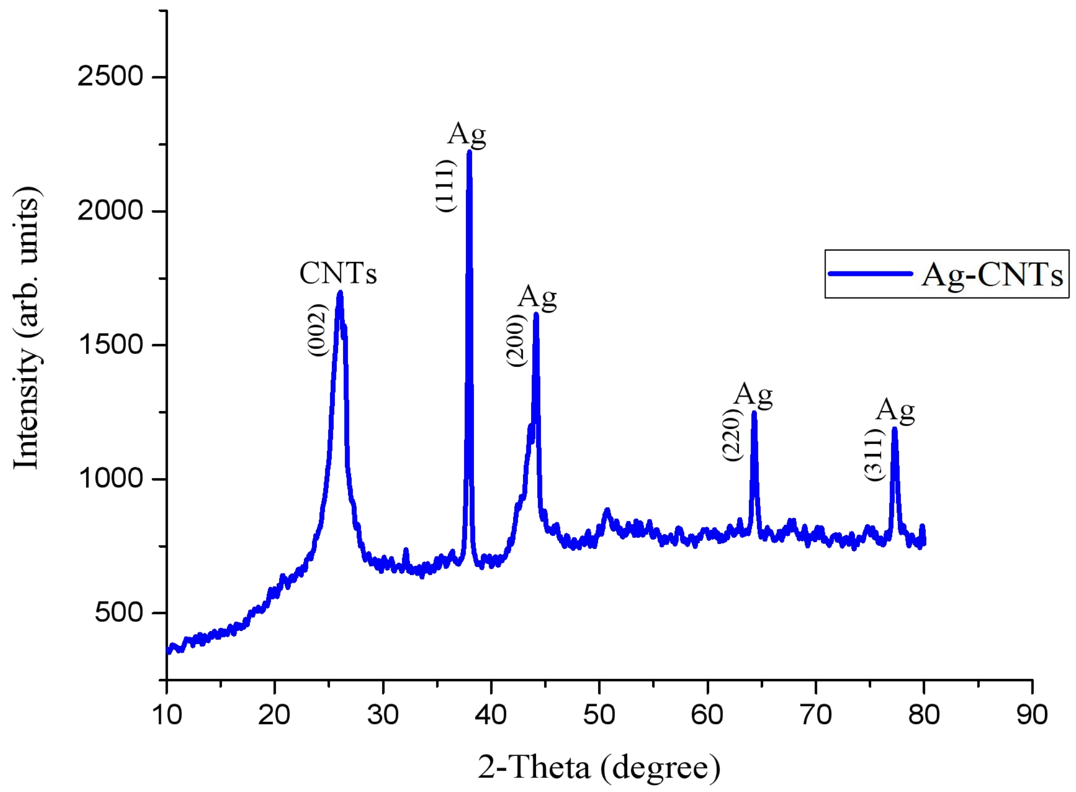

Figure 4.7:X-ray Diffraction Pattern of Synthesized Ag-CNTs Composites

The findings of the present study is in line with the reports described by Castle *et al.* (2011) and Jatoi *et al.* (2020). From their survey, the two authors observed a characteristic peak of CNTs at 26° (002) and other diffraction peaks which correspond to crystal plane of silver nanoparticle at 2-theta angle of 38.21° (111), 44.32° (200), 64.64° (220) and 77.42° (311).

The powder XRD results of the Pd-CNTs are shown in figure 4.8. Only one characteristic peak was noticed at 2-theta value of 26.30°, which is attributed to the (002) plane of CNTs. Other Bragg's reflection angles were found (2θ) at 38.25°, 43.71°, 62.95° and 78.46°which were indexed to (111), (200), (220) and (311) planes of palladium nanoparticles respectively.

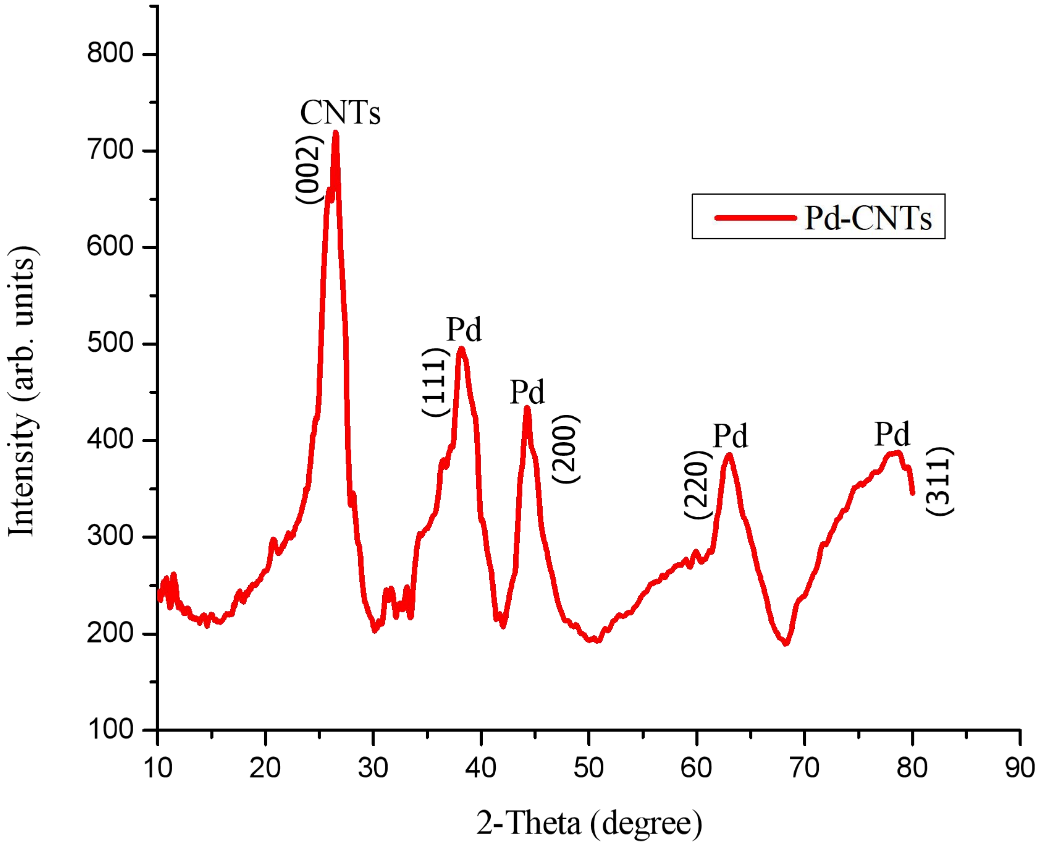

Figure 4.8: X-ray Diffraction Pattern of Synthesized Pd-CNTs Composites

From the XRD pattern presented in figure 4.8, the results confirmed the face-centered cubic (FCC) structure of palladium nanoparticles impregnated on the surface of the CNTs. No extra peaks were observed near the reflection angles of both PdNPs and CNTs, indicating a highly crystalline nature of the prepared adsorbent. This observed phenomenon in the XRD patterns of Pd-CNTs composite matches with the SAED pattern depicted in plate X (c) (SAED pattern of Pd-CNTs). Also, Figure 4.9 revealed the XRD results of Pd-Ag-CNTs composites. It can be observed that all of the CNTs based nano-adsorbent showed characteristic diffraction peak at 2θ value of 26.13°which indicates that the materials are highly graphitic in nature. Apart from the intense peak of CNTs, the spectrum shows that palladium and silver were also present which further confirm the incorporation of PdNPs and AgNPs onto the CNTs.

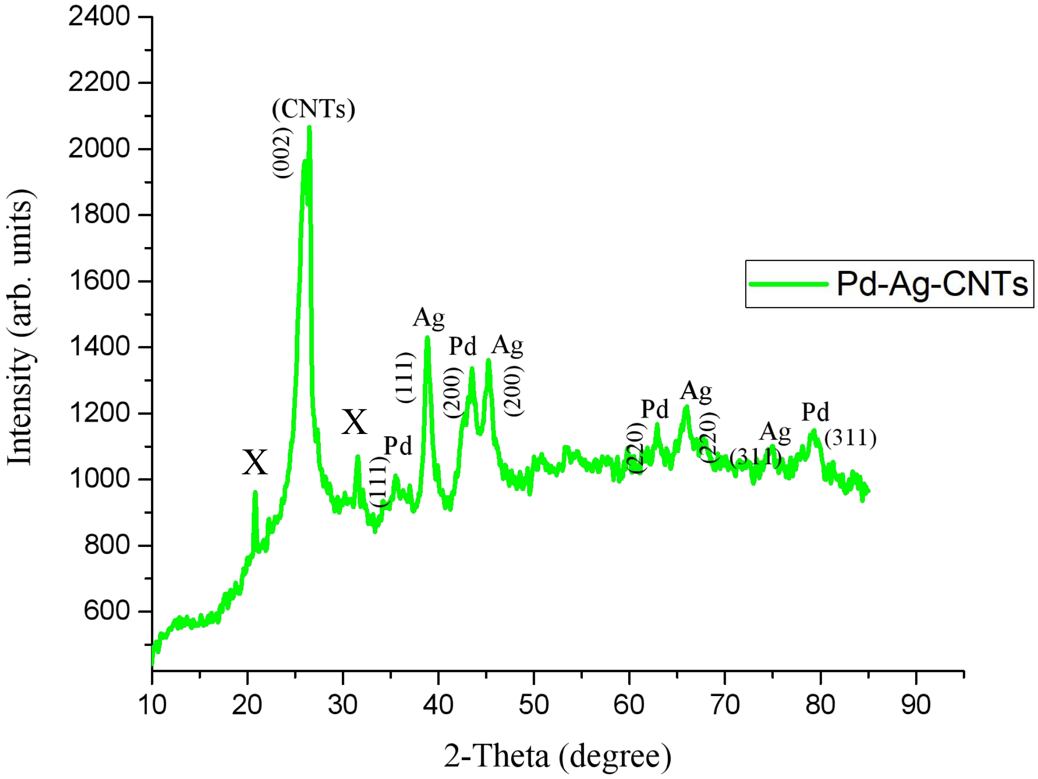

Figure 4.9: X-ray diffraction pattern of synthesized Pd-Ag-CNTs composites

Furthermore, some additional reflection angle at 2*θ* values of 21.6° and 32.1° which were indexed to (X) are also found in the diffraction pattern of Pd-Ag-CNTs composites. These diffraction angles probably belong to some of the secondary metabolites present in the plant extract employed in the biochemical syntheses of palladium and silver nanoparticles (Thangaswamy *et al.,* 2021). A further growth of the Pd (111), (200), (220) and (311) peaks on Ag-CNTs composites led to the suppression and shift of crystal plane of Ag (111), (200), (220) and (311) at 2*θ* value of 38.11, 44.29, 64.45 and 77.41°,while a significant increment was observed for the growth of (002) plane of CNTs. The shift of the crystal plane is ascribed to the difference in the ionic radii of C, Ag and Pd ion. The ionic radii of Pd and Ag ions are greater than the C ion (Pd: 1.40, Ag: 1.60, and C: 0.70). This implies the dopants (Pd and Ag nanoparticles) can be arranged as interstitial atoms inside the CNTs lattices. This suggests changes in the location of the lattice parameters, and thus, influences the difference in ionic radii of the involved elements (Chen *et al*., 2021). This could be the reason for the variations of the lattice planes. It also suggests the existence of synergistic effect of both PdNPs and AgNPs impregnated on CNTs. However, the observed trend agree with the HRSEM image (Plate XI (d)) which shows that both Pd and Ag were deposited on the CNTs surfaces. According to Debye Scherrer equation, the crystallite sizes of the purified CNTs and impregnated nanocomposites (nano-adsorbents) were calculated from the XRD patterns and the results showed the average crystallite sizes of (Pd-Ag-CNTs > Pd-CNTs > Ag-CNTs > P-CNTs), which is among important criteria needed for effective adsorption (Table 4.5).

Table 4.4: Crystalline size of P-CNTs, Ag-CNTs, Pd-CNTs and Pd-Ag-CNTs Nanocomposites

Composite Samples	Variation of Crystalline size (nm)		
P-CNTs	17.84	15.68	5.48
Ag-CNTs	13.77	18.97	8.26
Pd-CNTs	21.64	18.90	15.67
Pd-Ag-CNTs	22.74	29.74	25.81

It was found that the crystallite size of the composites material increased as Pd and Ag nanoparticles were incorporated. The observed variation may be attributed to the deposition rate of Ag and Pd nanoparticles as well as homogeinity of the material. Pre-synthesis treatment during the formation of the crystals and thermal aging may also affect the structural, optical, electrical properties of the composite material (Chen *et al*., 2021). Thus this may be the reason for an increase in the crystallite size of CNTs after the Pd and Ag doping (Aliyu and Srivastava, 2021).

4.3.4.4 Brunauer-Emmett-Teller (BET) Analysis of Purified Carbon Nanotubes and Impregnated Nanocomposites

The BET analysis provides a better insight into the textural properties of the prepared adsorbent, especially the specific surface area, pore volume and pore size distribution of the purified carbon nanotubes and impregnated carbon nanocomposites. The samples were characterized using BET N_2 adsorption-desorption isotherm and the results are presented in Table 4.6.

Table 4.5: Brunauer-Emmett-Teller (BET) analysis of the functionalized carbon nanotubes

Nanocomposites	Specific Surface Area (m^2/g)	Total Surface Area (m^2)	Pore Volume (cc/g)	Pore Size (nm)
P-CNTs	227.63	27.32	0.0827	3.156
Pd-CNTs	356.3	42.756	0.1454	5.839
Ag-CNTs	352.5	42.3	0.1475	5.749
Pd-Ag-CNTs	392.5	47.1	0.1502	6.214

According to Table 4.6, it was found that the BET specific surface area of the adsorbents are in order of Pd-Ag-CNTs > Pd-CNTs >Ag-CNTs >P-CNTs. The results indicate that the incorporation of silver and palladium nanoparticles to the P-CNTs increased the specific surface area of the nano-adsorbents. The increased specific surface area is an evidence of more active site on the adsorbent surfaces, which is of advantage to the occurrence of the redox reaction, and then improvement on the adsorptive performance of the material (Bano *et al.*, 2020).

The DR pore size distributions revealed in Table 4.6 indicate that the Pd/Ag doped CNTs nanocomposites is highly mesoporous compared to other composites. The pore size distribution varies as the metallic nanoparticles are incorporated. The impregnation of the binary Pd and Ag nanoparticles increased the specific surface area of the composite for about 42.01 % (from 227.63 to 392.5 m^2/g). Noteworthy is the fact that pore size of Pd-CNTs is more than the corresponding Ag/CNTs.So, it is reasonable that the presence of AgNPs in the CNTs based nanocomposites led to the moderate change in the pore size of the Pd-Ag-CNTs composites.

In summary, the pore size of the three nano-adsorbent, along with comparison with purified-CNTs are provided and the results are in the range of 3.156 to 6.214 nm which falls within 2-50 nm range classified by International Union of Pure and Applied Chemistry (IUPAC). Based on the IUPAC classification, material with pore size less than 2 nm are micro-porous, material within 2-50 nm are mesoporous, while greater than 50 nm are said to be macroporous in nature (Fletcher, 2008, Moosavi *et al.*, 2020). Thus, the pore size of the prepared nano-adsorbent in this study revealed that they are mesoporous in nature.

The observation made from this study conform to what was highlighted in the XRD results (see Table 4.5), in which the crystallite size of Pd-Ag-CNTs nano-composite is greater than the corresponding Pd/CNTs and Ag/CNTs nanocomposites. The slight variation may be attributed to the ionic radius of the metals, in which Pd is smaller in relation to Ag metals, which is linked to the free movement of PdNPs within the layer of CNTs wall. Thus, allowing the proper formation of a porous structured carbon skeleton with significant amount of Pd content. The increase in the pore size of the nanocomposites facilitates the transport of charge during charge and discharge, which enhances the performance efficiency of the adsorbent materials (Li *et al*., 2016).

4.4 Treatment of Industrial Animal Feed Processing Wastewater

4.4.1 Physicochemical analysis of industrial animal feed processing wastewater

Temperature is one of the essential indicator parameters of water quality in respect to existence and control of behavioral characteristics of aquatic organism (Liu *et al*., 2018). Temperature has direct effect on other wastewater indicator parameters such as pH and its variation in water bodies can directly affect the metabolic rate of organisms (Halilu *et al*., 2018). Thus, the result obtained in the present study revealed that the temperature of the raw industrial animal feed processing wastewater was 28.20 °C. After treatment with the nano-adsorbent, the temperature of the treated wastewater varies between minimum of 29.40 °C and maximum of 29.90 °C for Ag-CNTs and Pd-Ag-CNTs nano-adsorbent respectively. Temperature increase in aquatic environment may become a barrier to migration of fishes and other aquatic lives. As a consequence, this may seriously affect the reproduction of new breeds. Also, increase in water temperature can led to increase in solubility of metals and thus, toxicity of certain compounds. Temperature is also linked to the dissolved oxygen concentration. That is, the warmer the water, the less oxygen that it can hold (Stillman, 2019). Therefore, increase in temperature influence the rate of microbial activity.

Table 4.6: Physicochemical characterization of animal feed processing industry wastewater (Before and After Adsorption study) and WHO guideline limits

Physico-chemical parameters	Raw sample	Treatment using P-CNTs	Treatment using Ag-CNTs	Treatment using Pd-CNTs	Treatment using Pd-Ag-CNTs	Standard Limit	
						WHO, 2017 USEPA, 2018	NIS, 2015
Temperature (^{o}C)	28.20±1.38	29.20±1.62	29.40±1.57	29.50±1.23	29.90±1.86	Ambient	Ambient
pH	6.28±0.98	7.94±1.02	7.80±0.79	7.60±0.81	7.88±0.77	5.5-8.5	6.5-8.5
Turbidity (NTU)	244±24.69	12.00±2.54	4.80±0.57	6.28±0.72	4.15±0.49	5	5
Conductivity (µS/cm)	684±31.21	410.00±27.76	325±19.87	328±26.90	320±22.92	1000	1000
TDS (mg/L)	456±18.25	272.83±11.83	217±8.19	219±9.99	213±6.32	600	500
TSS (mg/L)	160±15.13	4.00±0.26	0.78±0.03	1.80±0.08	0.66±0.01	0.75	0.75
DO (mg/L)	3.78±1.39	4.95±1.22	4.90±1.10	5.20±1.48	5.40±1.32	5-6	Min.4
COD (mg/L)	450±29.16	60.00±2.67	35.60±2.00	35.00±2.11	34.40±2.08	40	-
BOD (mg/L)	90±13.34	15.40±1.01	8.30±0.76	7.10±0.60	6.70±0.89	10/5-7	6

Keys: TDS = Total dissolve solids, TSS = Total suspended solids, COD = Chemical Oxygen Demand and BOD = Biochemical oxygen demand pH measurements is a simple parameter which have direct influence on the level of metal ion in the water as well as other indicator of water quality. The pH of a water body is very important since quite number of chemical reactions in aquatic habitat are measured by any change in its value (Fakayode, 2005). In the present study, the results presented in Table 4.7 indicates that the pH value is 6.28±0.98, while the pH level varied between 7.60±0.81 and 7.94±1.02 in the treated wastewater. The results shows that the pH value increased and the suitable pH was obtained using Pd-CNTs nano-adsorbent. The pH level recorded against the raw wastewater sample maybe due to the type/sources of the constituent materials utilized during production of feed. This may subsequently leach to the water bodies during cleaning and washing of the equipment. According to Lokhande *et al*. (2011), any substance or solution that is highly acidic or alkaline would affect the solubility, mobility and metal toxicity in the water and consequently kill marine lives living within the environment. Waters with pH value range of 6.5-9.0 are exceptional and preferable for most aquatic creatures, while the range of water desirable for human tolerable levels by (WHO) and (NIS) standards is 6.5 to 8.5 (WHO, 2017; NIS, 2015). In the raw wastewater, it can be observed that the pH value was slightly lower than the permissible limit, while the treated wastewater fall within the range of WHO and NIS standard limits. Therefore, it can be concluded that the treated water in this study can be reuse for irrigation purposes.

Turbidity is an important property which measure the transparency and/or cloudiness of a liquid and its contributed usually by suspended solids and colloidal materials (such as clay, silt, microbes, rock fragments) in water. The turbidity of wastewater before the application of the nano-adsorbents was 244±24.69 NTU. After treatment with the nanoadsorbent, the turbidity significantly reduced to the range of values between

4.15±0.49 and 12.00±2.54 NTU. The results indicates that the maximum turbidity value obtained after treatment with P-CNTs and Ag-CNTs adsorbents is slightly higher than the permissible limits, while treatment with other nano-adsorbents (Pd-Ag-CNTs and Pd-CNTs) revealed that the turbidity values falls within standard limits (5 NTU) set by WHO and USEPA (2018). Since turbidity measures the cloudiness caused by the presence of suspended solids, it appears that the greater the level of total suspended solids in water, the cloudier the water and consequently, the higher the measured turbidity. Also, conductivity is commonly used to determine the concentration of dissolved ions generally known as total dissolved solids which is also an indicator of water quality (Khan *et al*., 2013). An increase in conductivity of water gives information on the total dissolved solids which can be used to determine physiological effects on plants and animals in water.

From Table 4.7, the conductivity values for the raw wastewater was 684±31.21uS/cm, which was reduced to 320±22.92, 325±19.87,328±26.90 and 410.00±27.76 µS/cm, after treatment with Pd-Ag-CNTs, Ag/CNTs, Pd-CNTs and P-CNTs, correspondingly. In both cases (the raw and treated wastewater), the conductivity values falls within the permissible limit of 1000 µS/cm set by WHO. The wastewater obtained from the animal feed processing industry shows TDS values of 456±18.25 mg/L,but reduced to the concentration level of 213±6.32 to 272.83±11.83 mg/L after treatment with adsorbent materials. The treated wastewater exhibit different removal efficiency with percentage values presented in the following order 53.29 % (Pd-Ag-CNTs) > 52.41 % (Ag-CNTs) 51.97 % > (Pd-CNTs) > 40.45 % (P-CNTs). Based on the results obtained before and after treatment of the wastewater, the TDS concentration values all lies below the WHO/USEPA and NIS standard limits. According to Lokhande *et al*. (2011), water can be classified on the basis of concentration of TDS, as desirable for drinking at concentration up to 500 mg/L. With respect to this classification, it can be deduced that the treated wastewater with each of nano-adsorbent can be considered safe for irrigation purposes and other aquatic animal can still survive in the treated wastewater, since water with TDS value within the range of 2000-3600 mg/L favours aquatic animals (NIS, 2015). TDS gives information on the level of both organic and inorganic dissolved compounds which may increase the turbidity of water (Khan *et al*., 2013). Salt like chloride, sulphate, carbonate, bicarbonate, phosphate, and nitrate of sodium, magnesium, potassium, calcium, manganese and iron are found dissolved in water bodies. They are known to increase the density of water and affects the osmoregulation of freshwater in aquatic organisms, reduces the availability and utility of oxygen, water for drinking, irrigation and other industrial purposes (Boyd and Tucker, 2019).

In the present investigation, the total suspended solids of the raw animal feed processing industry wastewater is 160±15.13 mg/L. After treatment with the adsorbents, the concentration reduced to 0.66±0.01 mg/L, 0.78±0.03 mg/L, 1.80±0.88 mg/L and 4.00±0.26 mg/L for Pd-Ag-CNTs, Ag-CNTs, Pd-CNTs and P-CNTs respectively. The suspended solid did not necessarily mean that matters floats and remain on water layer, but they are under suspension and thus remain in water (Halilu *et al*., 2018). It can be noticed that Pd-Ag-CNTs and Ag-CNTs treated wastewater maybe suitable for aquatic life or irrigation purpose when discharged into the river since the nano-adsorbents had approximately 100 % removal efficiency of TSS.

Dissolved oxygen is also an important water quality parameter used in determining the contamination levels of industrial wastewater. In the present investigation, it was found that the DO of industrial animal feed processing wastewater prior to treatment was

3.78±1.39 mg/L, and after treatment, the values varied between 4.90±1.10 to 5.40±1.32 mg/L, with Pd-CNTs nanoadsorbent being the highest and Ag-CNTs representing the lowest value. The result indicates that DO value of the raw samples do not fall within the acceptable limit of 5-6 mg/L (WHO, 2017; USEPA, 2018) or minimum value of 4 mg/L (NIS, 2015), but after treatment with the nanoadsorbents, the value increase to the level within the standard limits set by WHO/USEPA and NIS. In addition to this, the level of DO in water is inversely proportional to the amount of BOD. That is, the low DO is the same as high BOD. Biochemical oxygen demand is a measure of pollution effect and its regarded as one of the most common measures of organic pollutant in wastewater. The result indicates that the BOD value was 99±13.34 mg/L before treatment. Thereafter, the BOD of the treated wastewater reduced to low values of 15.40±1.01 mg/L, 7.10±0.60 mg/L, 8.30±0.76 mg/L and 6.70±0.89 mg/L for P-CNTs, Pd-CNTs, Ag-CNTs and Pd-Ag-CNTs respectively. It is important to note that the adsorbents P-CNTS, Pd-CNTs and Ag-CNTs were able to reduce approximately 84.44%, 92.82 % and 91.61 % of BOD from the wastewater. While Pd-Ag-CNTs nanoadsorbent (removed 93.23 % of the BOD) which fall within the permissible limit of 5-7 mg/L reported by USEPA (2018) and safe limit of 10 mg/l set by WHO (2017). In summary, high BOD value observed in the raw samples is an indication of polluted water while low BOD contents noticed after the treatment indicates that the water is of good quality. This suggests that there is abundance of free oxygen in the treated wastewater since BOD directly affects the amount of dissolved oxygen (DO) in water.

COD is similar in function to BOD, in that both measure the relative oxygen depletion effect of wastewater. The COD test is used to quantify the amount of organic matter (pollutants) in a wastewater (Lokhade *et al*., 2011). In COD determination, the level of oxygen demand is valuable in classifying the contamination level and existence of biologically resistant substances. It is a very important parameter for Wastewater as well as control of waste treatment. From the results presented in Table 4.7, the COD value in the wastewater collected is 450±29.16 mg/L, which is more than 10 folds of the safe discharge limits recommended by WHO and NIS standards. After the treatment process with the nano-adsorbents, the COD level reduced to 60.00±2.67 mg/L, 35.00±2.11 mg/L, 35.60±2.00 mg/L, and 34.40±2.08 mg/L with corresponding percentage removal efficiency of 86.66%, 92.20 %, 92.08 % and 92.35 % respectively, hereby meeting up with the standard permissible limit of 40 mg/L as stated by USEPA (2018).

4.4.2 Heavy metal analysis of industrial animal feed processing wastewater

On the basis of removal of selected heavy metals, Pd/Ag/CNTs nanoadsobent was chosen regarding the results obtained from the physicochemical analysis of the raw and treated animal feed processing industry wastewater.

Table 4.7: Mean concentration of selected heavy metals of industrial animal feed processing wastewater (Before and After Adsorption Study) and standard limit

Heavy metals	**Raw sample**	**Treatment using Pd-Ag-CNTs**	**Standard Limit**	
			WHO (2017)/ USEPA (2018)	NIS (2015)
Copper (mg/L)	1.143±0.27	0.253±0.12	1.00	1.00
Iron (mg/L)	0.979±0.36	0.114±0.06	0.5	0.3
Manganese (mg/L)	0.747±0.28	0.167±0.09	1.0	-
Nickel (mg/L)	0.611±0.19	0.001±0.001	0.02	-

The results of selected heavy metal ions analyzed from the raw and treated animal feed processing industry wastewater are presented in Table 4.8, with WHO, EPA and NIS guideline limits. This indicates that copper concentration was above the standard limits. Copper "being among the heavy metals" used as a growth promoter in feed formulations, it is highly required in functioning of young pigs. Regions where farm animals are fed with feeds and forages that are deficient in copper will suffer from anemia. This deficiency can be corrected by adding suitable mineral suppliments into feeds which are needed for the formation of haemoglobin. The presence of Cu in the wastewater samples could be as a results of different processes involved in the manufacturing process. It was noticed that concentration of copper before the treatment of the raw wastewater was 1.143 mg/L, and the concentration reduced to 0.253 mg/L after treatment with the nanoadsorbent. This result indicates that 77.86 % removal efficiency was achieved for Pd-Ag-CNTs nano-adsorbent. Although humans can handle proportionally large amounts of copper, but its acute exposure can cause different health problems like gastro-intestinal effects such as diarrhoea, nausea, vascular injury, vomiting and anemia among others. As a consequence, these problems can results to life threatening diseases. It is worthy to note that the post-treated result of copper shows its safe for reuse due to the fact that it falls below the permissible limit of 1 mg/L (see Table 8).

Iron is an essential element required for the growth of animals (Llorens *et al.*, 2019). It is used as a food supplement in manufacturing animal feeds and may improve physiological effect such as blood parameters, organ weight and nutritional status. Iron can be found in water bodies through washing of the equipments, but its presence in excessive amount in wastewater can leads to build up in plant species when used for irrigation purposes. This can be detrimental to plant growth and even the food chain. According to USEPA (2018), Fe in water is safe to ingest at concentration range between 0.4-1 mg/kg of body weight per day. From the results presented in Table 4.8, it can be observed that Fe content before treatment was 0.979 mg/l, while at post treatment with the developed Pd/Ag/CNTs adsorbents, the level of Fe concentration reduced to 0.114 mg/L, with percentage removal efficiency of 88.36 %. This results indicates that the developed adsorbents was able to reduced Fe concentration levels to values within the standard limit of 0.5 mg/L set by WHO (2017)/EPA (2018).

EFSA issued a report on the use of manganese-based additives in feeding stuffs (EFSA, 2013). Following the re-evaluation of EFSA report, a list of authorizations of manganese compounds (such as manganous chloride tetrahydrate; manganous oxide, manganous sulphate, monohydrate; manganese chelate of amino acids hydrate and manganese chelate of glycine, hydrate) in feeds additive have been reported in literature (EFSA, 2021). Manganese, serve as a nutrient in humans and animals and play a vital role in bone mineralization, regulation of protein and energy metabolism (EFSA, 2020). However, it is toxic at high exposure levels and according to Agency for Toxic Substances and Disease Registry (ATSDR, 2012), the amount of Mn recommended as daily intake in drinking water should not exceed 5 mg/day (Ogu and Akinnibosun, 2020). This is because its exposure is associated with health problems such as intellectual quotient scores in school-aged children and high incidence of hyperactive behaviours (Coetzee *et al*., 2016). Table 4.8 shows that the concentration of Mn is 0.747 mg/L for raw wastewater and after treatment, the concentration reduced to 0.167 mg/L which translated to approximately 77.64 % removal efficiency using Pd-Ag-CNTs nano-adsorbent.

Certain feed materials contain metallic nickel since it is used as a catalyst in their production (EFSA, 2019). Despite their small amount in feeds, their role in normal metabolism is highly valued. Deficiency or excess of nickel can result in immune system disorders and impairement of overall health status and decreases in production performance (Ahlström *et al*., 2019). Moreover, different forms of Ni occur naturally in the environment, and its widely applied in chemical and food-processing industry as catalyst and pigment. Although, animal requirements for Ni have not been clearly defined and are estimated to range between 50-100 μg Ni/Kg feed to prevent clinical symptoms of deficiency (Živkov Baloš *et al*., 2017). Exposure of nickel and nickel related compounds can cause respiratory tract cancer if the dosage exceeds the allowable concentration of 1 μg of Ni/L (Morris, 2020). In the present study, the Ni content of the animal feed processing industry wastewater is 0.611 mg/L and after treatment with the adsorbent material, the values was 0.001 mg/L for the prepared nano-adsorbents. It was noticed that the nano-adsorbent (Pd-Ag-CNTs) removed approximately 99.84 % of Ni from the wastewater samples, hence meeting up with the maximum required limit of 0.02 mg/L as stated by USEPA (2018). Overall, the removal efficiency obtained from the physicochemical results informed the choice of Pd-Ag-CNTs for the batch adsorption studies of selected heavy metal ion.

4.4.3 Batch adsorption of heavy metals in animal feed processing industry wastewater

Studies on the effect of different parameters on adsorption efficiency of the prepared nanoadsorbent for the removal of Cu, Fe, Mn and Ni from raw industrial animal feed processing wastewater was investigated. The following parameters such as the contact time of interaction with the sorbent, the mass of the adsorbent (dosage) and the temperature were investigated and the results obtained with respect to each adsorption parameters are presented as follow:

- **Effect of contact time**

The effect of contact time on adsorption of Cu, Fe, Mn and Ni from industrial animal feed processing wastewater is shown in Figure 4.10 using Pd-Ag-CNTs nanoadsorbent.

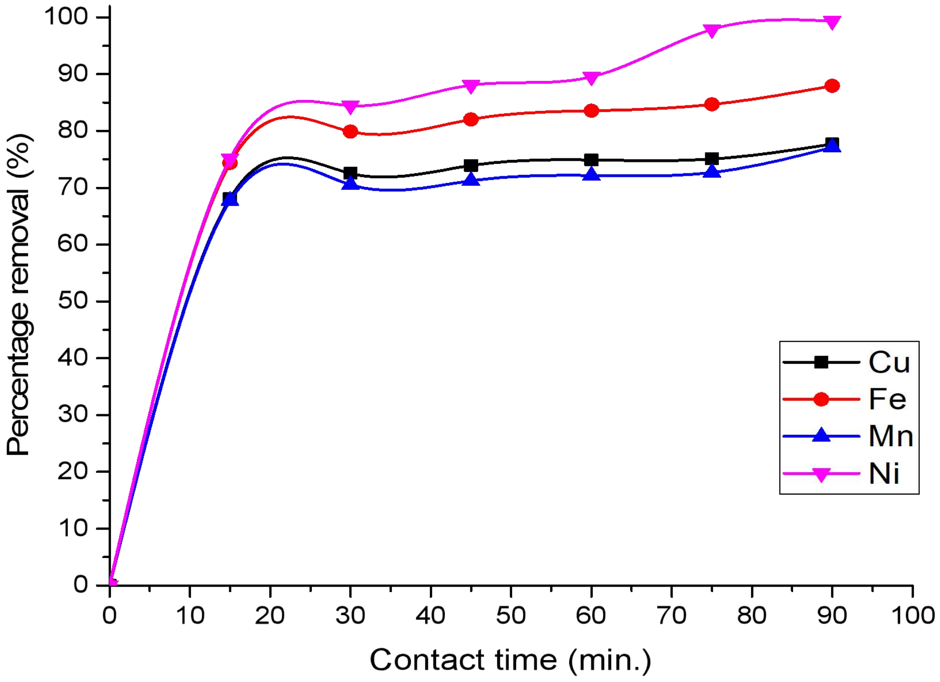

Figure 4.10: Percentage removal of metal ion adsorption on Pd-Ag-CNTs nanocomposites [Dosage (10 mg/50 cm^3), Stirring Speed (200 rpm), and temperature (30 °C)]

As illustrated in Figure 4.10, the time of contact between the selected metal ion and nano-adsorbents was investigated in the range of 15-90 min. and it was observed that as interaction time increases, removal efficiency also increases. Worthy of note is the fact that the increase in removal efficiency of Fe and Ni ion was very quick within the first 30 min. Thereafter, there was no significant effect in the percentage removal efficiency of both metal ions. On the other hand, slower adsorption process was observed for Cu and Mn ion, which signifies a smaller uptake of metal ion as compared to the former ions. Therefore, the optimum time to attain the maximum removal of metal ion was 30 min. This suggests that the adsorbed molecules diffused rapidly onto the pores of the nano-adsorbents (Pd-Ag-CNTs) due to strong interaction and competition among the selected metal ions (Ebadollahzadeh and Zabihi, 2020). Further, the increase in the removal efficiency of the selected metal ion reduced until it reach the equilibrium stage (90 min). Here, it implies that the adsorbent-adsorbate system has reached the equilibrium and additional increase in time of interaction rarely influences the percentage removal efficiency of the selected metal ion. It can be deduced that the removal rate would remain unchanged after the equilibrium time of interaction and this may be linked to the repulsive forces between the nano-adsorbents and the selected metal ions (Zhao *et al.*, 2018). Thus, this study suggests the occurrence of double phase sorption mechanism (fast and slow adsorption rate). This was found similar to the report of Liu *et al.* (2017) who observed that adsorption mechanism involve external and internal diffusion process.

As observed in this present study, the respective value of 77.69 (for Cu), 87.95 (Fe), 77.12 (Mn) and 99.35 (for Ni) are the maximum percentage removal efficiency noticed when the equilibrium sorption data was considered. With respect to the selected metals, the ionic radius decreases in the order of 137 Å (Mn) > 128Å (Cu) >126Å(Fe) >125Å (Ni) in the analyzed wastewater. The smaller the size of ionic radius, the faster the removal of the metal ion from the wastewater (Bohli *et al.*, 2013). Thus, the metal with smaller atomic radius will promptly reach the surface binding site faster compared to those of larger atomic radius. In general, the percentage removal of metals is found to be in the order Ni>Fe>Cu>Mn in the analyzed wastewater. Hence, it is important to mention that the maximum percentage removal of metals differs significantly and was based on specific interaction between adsorbent-adsorbate species. Nevertheless, Ni ion adsorbed better when compared to adsorption of other studied metal ion. Further, noteworthy is the fact that 100 % removal efficiency was never achieved using the test nanoadsorbent. This is so because of the presence of other radical scavengers in the wastewater which also compete for the adsorption sites or due to the blocking of adsorbent pores by suspended solids in the wastewater. The effect of varying the contact time was also investigated and it was observed that the selected metals adsorbed better at different time of contact. The reason for this observation might be linked with the large surface area of Pd-Ag-CNTs, which was available throughout the adsorption process.

- Effect of Adsorbent Dosage

To evaluate the effect of concentration on the adsorption efficiency of the nano-adsorbent for removal of metal ions, the study was carried out by varying the mass of adsorbents from 10 mg to 60 mg in 50 cm^3 of wastewater sample.

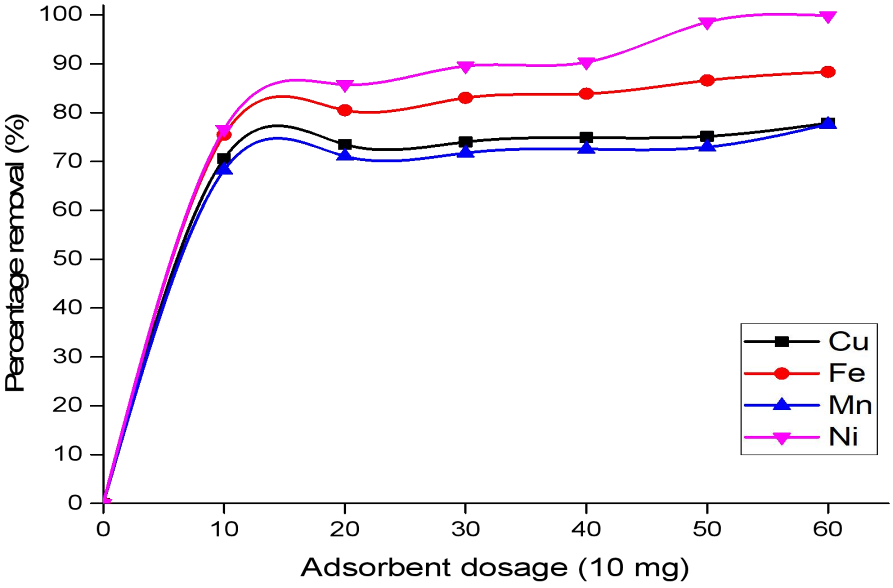

Figure 4.11: Effect of adsorbent dosage on heavy metals adsorption onto Pd-Ag-CNTs nanocomposites (Time of Contact (90 min.), stirring speed (200 rpm), and temperature (30 °C)]

The figure indicates that the percentage removal increases as the adsorbent dosage increases from 10 to 60 mg per 50 cm^3 of the wastewater irrespective of the metal ions. The observed increment may be connected to the increase in the required number of active sites as a function of dosage. This is in accordance with the work of Almomani, (2020) who reported an increased removal efficiency of heavy metals from 18.6 % to 92.0% as the adsorbents increased from 5 to 25 g/L at 20 °C. The present study implies that, there exist a linear relationship between the mass of an adsorbent and the concentration of metal ion. Further, it can be deduced that availability of binding site in the nanoadsorbent enhances the percentage removal of Ni and Fe (metals) while in the case of Cu and Mn, a considerable increment was rarely noticed in the removal efficiency. This is due to the fact that there was fast removal rate of the former which led to competition for binding sites, and thus trigger the partial blockage of the pores around the nanoadsorbent surface. Nevertheless, it was observed that maximum percentage removal of Cu, Fe, Mn and Ni by Pd-Ag-CNTs were 77.87 %, 88.36 %, 77.64 and 99.84 %, respectively.

- Effect of Temperature on Adsorption Capacity

Figure 4.12 illustrates the effects of temperature on the adsorption capacity and percentage removal of heavy metals from industrial animal feed processing wastewater. The experimental results revealed that maximum removal was attained at temperature of 80 °C for all the metals.

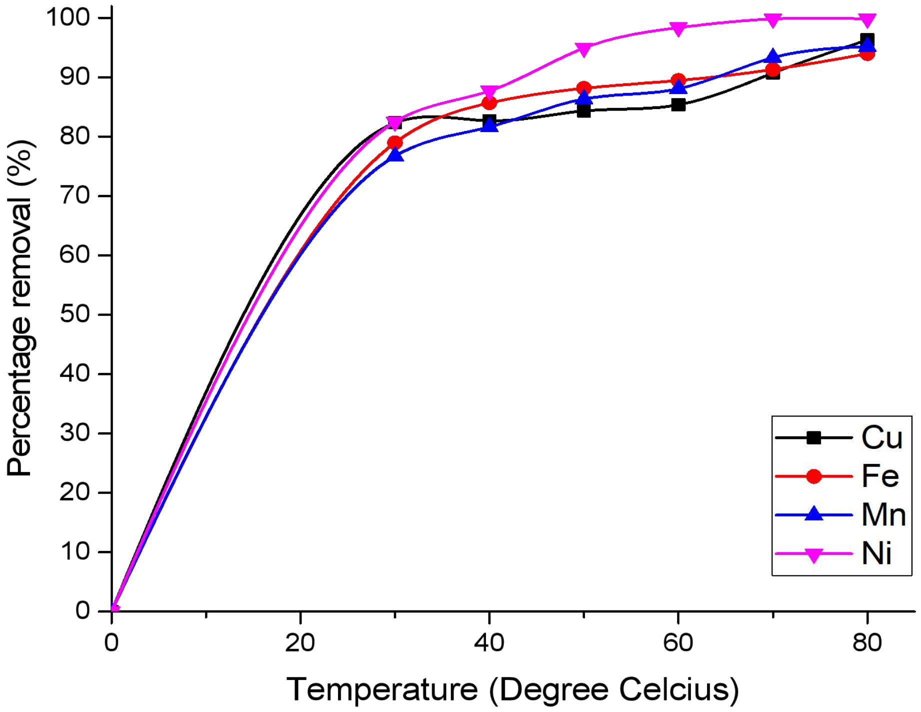

Figure 4.12: Effect of temperature on metal Ion adsorption onto Pd-Ag-CNTs nanocomposites [Adsorbent dosage (10 mg/50 cm^3), Stirring speed (200 rpm), and time of contact (60 min.)]

It can be noticed that increasing the solution temperature from 30 °C to 80 °C resulted to increase in percentage removal efficiency of all metals, with the exception of nickel ion with the adsorption rate level off at temperature of 70 °C and 80 °C. The possible reason for such behavior may be ascribed to the acid modification of the CNTs surface and impregnation of metallic nanoparticles. Acid modification was responsible for the formation of temperature dependent surface sites which influenced the sorption capacity of the adsorbent material under the influence of variation of temperature (Patra *et al.*, 2020).

An increase in temperature caused increased in the mobility of adsorbate species, hence increased removal efficiency of the metal ions (Fosso-kankeu *et al.*, 2017). This implies that the solution temperature is directly proportional to the percentage metals adsorbed, indicating that the adsorption process is endothermic in nature (Yagub *et al.*, 2014). This prediction was affirmed by determining the thermodynamic parameters like enthalpy change, entropy change and Gibbs free energy, which also provide supplementary information as regards the adsorption mechanism. However, the present study showed that the investigated metal ions (Cu, Fe, Mn and Ni) are adsorbed on the prepared Pd-Ag-CNTs nano-adsorbent with maximum removal efficiency in the order of 99.84 (Ni) > 88.36 (Fe) > 77.87 (Cu) > 77.64 (Mn).

4.4.4 Adsorption isotherm models

The adsorption isotherm models are used to examine the mechanism of adsorption, nature of the adsorbent surface, affinity and favourability of the adsorbate to the adsorbent surface (Lima *et al.*, 2015). It also reveals the extent to which the adsorbate captured by the adsorbent surface (Q_e) and the amount of adsorbate left in the liquid phase (C_e) (Kasperiski *et al.*, 2018, Lima *et al.*, 2015). In this study, six isotherm models namely; Langmuir, Freundlich, Dubinin Radushkevich (D-R), Temkin, Halsey and Flory Huggins (F-H) models were applied to explore the behavior of metal ions adsorption on the prepared nano-adsorbents. The data obtained were used to establish which model best fitted the adsorption process.

It is evident that Langmuir isotherm model describes adsorption mechanism with monolayer adsorption and identify the distribution of metal ions between homogenous surface active site and liquid phase, with no interaction of the adsorbed molecules with the neighboring adsorption site (Yusuff *et al.*, 2019). Based on the estimation of maximum adsorption capacity (Q_m) of the nano-adsorbents, it is important to note that the equilibrium monolayer capacity (Q_e) reach the highest peak (Plateau region) (Dechnik *et al.*, 2016). In view of this, the Langmuir isotherm parameters of the non-linear curve fitting are presented in Table 4.9, where Q_e, represent the monolayer sorption capacity, and b_L and Q_m are Langmuir constant related to the energy of sorption and maximum adsorption capacity (mg/g). R_L denotes variation of separation factors (L/mg) whether the adsorption is irreversible (R_L= 0), favourable ($0<R_L<1$) or linear or unfavourable (R_L=1 or R_L>1) (Abdel-Ghani and El-Chaghaby, 2014).

For the nano-adsorbent (Pd-Ag-CNTs), the maximum adsorption capacity of Cu, Fe, Mn and Ni were determined as 0.8175, 4.003, 1.0570 and 1000 mg/g. It was observed that the adsorption capacity of the prepared adsorbents was greater for Ni, followed by Fe and Mn. This is corroborated by the observation made from the effect of contact time and it is the same reason advanced earlier (as in heavy metals with smaller ionic radius diffuse faster than the corresponding metals with larger ionic radius). However, different behavioural pattern was observed for adsorption of Cu onto Pd-Ag-CNTs nano-adsorbent, which recorded adsorption capacity value of less than unity. This suggest that there is low affinity between the Cu ion and Pd-Ag-CNTs adsorbent. And to a greater extent, an increase in adsorptioan density of a solute on any adsorbent would reduce the tendency of adsorbent to adsorb (Tran *et al.*, 2019). This may be due to increasing competition among solute ions or molecules and a decrease in the number of vacant sites available for further adsorption (Li *et al*., 2020).

The energy of adsorption which is related to the heat of sorption (L/mg) by the nano-adsorbent was represented in Table 4.9. The estimated heat of adsorption (b_L) of Pd-Ag-CNTs for Ni was -1036.3 L/mg, which was greater than Cu (-2.7685 L/mg), Fe (-2.9868 L/mg) and Mn (-3.5541 L/mg). This implies that the heat of adsorption is less favourable for Cu, Fe and Mn in industrial animal feed processing wastewater. The observed trend in the adsorption behavioural pattern matches with the order of ionic radius of metals. This implies that preferential sorption behavior could be explained in term of ionic radius of metals. Also, it can be deduced that high concentration of Cu, Fe and Mn after treatment process is as a result of increase heat of adsorption (b_L) (Sharma *et al*., 2019). In addition, an important feature of Langmuir isotherm is the dimensionless separation factors, R_L which is indicative of the isotherm shape that envisages whether an adsorption process is favourable, unfavourable or linear and/or irreversible (Abdel-Ghani and El-Chaghaby, 2014; Ibisi and Asoluka, 2018). The results of separation factor (R_L) of metal ions adsorption by the tested adsorbent are shown in Table 4.9. The result showed that R_L values of all the analyzed metals is less than zero with the exception of Ni which is greater than 0 but less than unity. This suggests that the adsorption of Ni metal by nanoadsorbents is more favourable than other metal ion analyzed. Hence, the adsorption of Cu, Fe and Mn onto Pd-Ag-CNTs nano-adsorbent can be concluded to be unfavourable for Langmuir isotherm model. This study asserted the favourability of selected metal ion adsorption on the nano-adsorbent and signifies that Ni presented the highest Q_{mmc} value by Pd-Ag-CNTs nano-adsorbent. The regression correlation co-efficient (R^2) values from Table 4.9 indicates R^2 values between 0.4649 -0.9691. This implies that the adsorption data of all ions onto the nano-adsorbents does not agree well with Langmuir models, therefore indicating that the adsorption phenomenon cannot be best described by this model.

The Freundlich adsorption isotherm is an indicator of the level of heterogeneity of the nano-adsorbent surface. It explains the interaction between an adsorbed molecules (sorbate) on a non-uniform surface (heterogenous surface), and the Freundich constant K_F and n_F were calculated from the intercept and slope of the plot of lnq_e Vs lnC_e which indicate adsorption capacity and the adsorption intensity (Abdel-Ghani *et al.,* 2009). Also in Table 4.9, the highest maximum sorption capacity (K_F) of Pd-Ag-CNTs for the analysed metals was recorded for Cu (3501.064 mg/g). While the K_F values of the test adsorbent on Fe, Mn and Ni were in the order of 1269.989 mg/g (Mn) > 78.886 mg/g (Fe)>2.1459 mg/g (Ni). The Freundlich constant (K_F) indicates the adsorption capacity of the nano-adsorbent at equilibrium level in a solution and higher K_F value suggests a higher adsorption capacity. Additionally, the n_F values (adsorption intensity) which is an indication of the degree of non-linearity between solution concentration and adsorption process predicts the favourability of metal ions on nano-adsorbents. That is, the n_F value suggests adsorption intensity is a physical process if ($n > 1$), and chemical process ($n < 1$) or linear ($n = 1$). The calculated result of n_F values are thus presented in Table 4.9, and it can be observed that n_F values of Pd-Ag-CNTs for Ni is greater than the corresponding Cu, Fe and Mn ions (n_F values of Ni was found greater than unity). This implies a favourable sorption of Ni by Pd-Ag-CNTs when compared to other metals. Therefore, this study suggest that the adsorption phenomenon is a chemical process except for Ni adsorption on the prepared nano-adsorbent which showed n_F values greater than unity (physical process). This implies the adsorption isotherm is characterized by a convex Freundlich isotherm (Shen *et al.*, 2018). Also, it can be inferred that Freundlich adsorption isotherm is independent of the size (atomic or ionic) of each metal ion. Based on the regression correlation co-efficient (R^2) values, it was observed that R^2 values for the adsorption of all metals using Freundlich model is lower than Langmuir Model except for nickel and copper. In most cases, determination of best fitting relationship and validating the best isotherm model have always been through the use of linear correlation coefficient (R^2) values. But, because of the inherent bias from this transformation, sum of square error (SSE) and non-linear-chi square test (χ^2) were employed. This model have been introduced to further justify the suitability of the best isotherm model. Coupled with the highest correlation coefficient (R^2) values, there must be closeness between the data of the q_{cal} and q_{exp} alongside a low value of statistical validity models. That is, lower value suggest which model best fitted the adsorption processes. In line with this, the Flory-Huggins isotherm model has the highest coefficient of determination (R^2) which signifies the good fit of the models for all the analyzed metals. This assertion was justified with lower SSE and χ^2 values obtained when compared with other isotherm models. Thus indicating the closeness of the model experimental results to the calculated result obtained.

Table 4.8a: Isotherm constants for the adsorption of metal ions on Pd-Ag-CNTs nanocomposites

Isotherm models with Equations	Parameters (units)	Metal ion			
		Cu	Fe	Mn	Ni
Langmuir	q_{max} (mg/g)	0.8175	4.0032	1.057	1000
$\frac{C_e}{q_e} = \frac{1}{K_L q_{max}} + \frac{C_e}{q_{max}}$	K_L (L/mg)	-2.7685	-2.9868	-3.5541	1036.3
	Q_{mmc} (mg/g)	-0.2953	-1.3403	-0.2974	0.965
$R_L = \frac{1}{1 + K_L C_o}$	R_L	-0.462	-0.5197	-0.6043	0.0016
	R^2	0.8805	0.9691	0.7599	0.4649
	SSE	0.1038	0.0271	0.4946	0.8877
	χ^2	0.0917	0.0229	0.2830	0.9671
Freundliuch	K_F (mg/g)	3501.064	78.886	1269.989	2.1459
$Logq_e = LogK_f + {}^{1}/_{n} LogC_e$	$1/n_F$	6.3506	2.2316	4.5777	0.2367
	n_F	0.1575	0.4481	0.2185	4.2248
	R^2	0.9672	0.9502	0.7167	0.9111
	SSE	0.0500	0.0173	0.1044	0.1182
	χ^2	0.1285	0.1086	0.0417	0.2256
Dubini-Radushkevich	q_m (mg/g)	581.3773	2.8718	94.9927	1.3484
$\ln q_e = lnq_m - K_{(D-R)}\epsilon^2$	K_{D-R}(mol^{-2}KJ^{-2})	5x10^{-7}	1x10^{-7}	3x10^{-7}	5x10^{-9}
$\epsilon = RT\ln(1 + 1/{}^{1}/_{C_e})$	E (KJmol^{-1})	-1000	-2236.07	-1290.99	-10000
$E = \frac{1}{\sqrt{2K_{(D-R)}}}$	R^2	0.8456	0.9194	0.6844	0.4982
	SSE	0.8849	1.9515	0.8675	0.8183
	χ^2	0.9218	0.1086	0.0417	0.2256
Temkin	A	11.85	3.8741	5.2086	0.2406
$q_e = AlnK_T + A\ln C_e$	b_T (Jmol^{-1})	191.5377	585.8708	435.7643	9433.591

Table 4.8b: Isotherm constants for the adsorption of metal ions on Pd-Ag-CNTs nanocomposites

Isotherm models with Equations	Parameters (units)	Metal ion			
		Cu	Fe	Mn	Ni
$A = \frac{RT}{b}$	K_T ((Lmg^{-1})	3.9499	9.3455	5.9865	2810
	R^2	0.7817	0.8434	0.6026	0.4491
	SSE	1.6848	0.9793	1.1957	1.2478
	χ^2	1.4928	0.9984	1.0897	1.0026
Flory-Huggins	Ln$_{KFH}$	-0.6709	-0.5773	-1.0592	-0.3991
$ln\frac{\theta}{C_o} = lnK_{FH} + nln\,(1-\theta)$	K_{FH} (Lmol^{-1})	0.5112	0.5614	0.3467	0.6709
	n_{FH}	-0.3014	-0.2141	-0.4841	-0.0715
$\theta = (1 - C_e/C_o)$	ΔG° (KJmol^{-1})	-1522.97	-1310.36	-2404.31	-905.926
$\Delta G^{\circ} = RTlnK_{FH}$	R^2	0.9947	0.9787	0.9924	0.7098
	SSE	2.07 x 10^{-5}	0.0004	0.0001	0.0368
	χ^2	0.0131	0.0058	0.0023	0.0277
Halsey	K_H	0.2766	0.1412	0.2099	0.0397
$q_e = \frac{1}{n_H}ln\frac{K_H}{C_e}$	1/n_{H}\``	-6.3506	-2.2316	-4.5777	-0.2367
$q_e = \frac{1}{n_H}lnK_H - \frac{1}{n_H}lnC_e$	n_H	-0.1575	-0.4481	-0.2185	-4.2248
	R^2	0.8672	0.9502	0.7167	0.6111
	SSE	1.6848	0.9793	1.2183	1.3070
	χ^2	0.0258	0.6914	1.2102	1.7182

Therefore, indicating that the isotherm data of analysed metals by Pd-Ag-CNTs nano-adsorbents does not fitted well to Freundlich model. Nevertheless, the equilibrium sorption data for Ni metal using Pd-Ag-CNTs fitted Freundlich much better than Langmuir isotherm model.

The D-R model was used to determine the extent of adsorption with Gaussian energy distribution on heterogeneous surfaces. The semi-empirical model which is based on the estimates of saturation theoretical capacity or sorption affinity and mean free energy of adsorption ($K_{D\text{-}R}$) are determined by plotting lnq_e against lnq_m . The experimental results are presented in Table 4.9 where a maximum saturation capacity (q_m) for Pd-Ag-CNTs adsorbent was 581.3773 mg/g (Cu). The least q_m for the tested nano-adsorbent was recorded to be 1.3484 mg/g (Ni), which was found lesser than 94.9927 mg/g (Mn) and 2.8718 mg/g (Ni). This results further affirmed that the test nano-adsorbent had greater affinity for metal ions with high adsorption capacity. The mean free energy (E) as represented in Table 4.9 was calculated from the experimental data to distinguish the types of adsorption process. It can be seen that a lower ($E_{D\text{-}R}$) value were obtained from D-R adsorption isotherm model, indicating physical nature of sorption of metal ion onto the tested nano-adsorbents. Small regression co-efficient (R^2) value for D-R isotherm model were also presented in Table 4.9. This suggests that the adsorption data were poorly fitted. However, it can be observed that the regression correlation co-efficient (R^2) for Temkin model is relatively small when compared to that obtained using D-R isotherm model.

The Temkin model describes interaction of solute molecule from aqueous phase with a non-uniform phase (heterogenous surface). It is based upon the assumption that heat of adsorption of all molecules in the layer decreases on covering of solid surface. The Temkin isotherm constant (K_T) denotes the maximum binding energy. Temkin parameters are presented in Table 4.9 indicates that Ni had the highest K_T values (2810 dm^3/g). This signifies a higher binding probability onto Pd-Ag-CNTs nanoadsorbents. Other K_T values recorded for Pd-Ag-CNTs were estimated to be 3.9499 dm^3/g, 5.9865

dm^3/g and 9.3455 dm^3/g for Cu, Mn and Fe respectively. The estimated values suggest a lower binding energy by the tested nano-adsorbent. The variation in this results could be attributed to different behavior of metal ions and their ionic radii towards the prepared nano-adsorbent. Further, the heat of adsorption (b_T) for metal ions on the test nano-adsorbent were calculated from the plot of q_e against lnC_e, and the parameters are also represented in Table 4.9. According to the result, it can be inferred that the sorption energy (b_T) is endothermic in nature. The observed level of b_T in this study shows that there is a high level of interaction between the nano-adsorbents and the adsorbed molecules. Thus, indicating that the adsorption of metal ions on Pd-Ag-CNTs is physical adsorption (An evidence of ion exchange mechanism during adsorption process). As revealed in the Table 4.9, the (R^2) values for Temkin model were found to be in the range of 0.4491 to 0.8434, indicating a relatively small adsorption potential for the metal ions on the nano-adsorbent when compared to other isotherm models.

The Florry-Huggin isotherm model was used to determine the degree of coverage of adsorbate onto the adsorbent. The Florry-Huggins adsorption equilibrium constant (K_{FH}) reveals the spontaneity of an adsorption process and the values were presented in Table 4.9. It was observed that Pd-Ag-CNTs adsorbed Ni better with maximum Gibb's free energy (K_{FH}) of 0.6709 dm^3/mol and the least K_{FH} value was observed for Mn (0.3467 dm^3/mol). The results of n_{F-H}, which is an indication of the amount of metal ions adsorbed by the nano-adsorbent were also presented in Table 4.9. Based on the calculated results, the values ranged from -0.4841 to -0.0715. However, the fitting of experimental data to F-H isotherm model attests to high degree of surface coverage of metal ions by the nanoadsorbents. The (R^2) value estimated from Flory Huggin's isotherm model were also displayed in Table 4.9 and suggests that the experimental data best fitted Flory-Huggin's models and also affirmed the sustainability of the tested nano-adsornbent for the removal of metal ions from the industrial animal feed processing wastewater.

Halsey isotherm parameters for the metal ions are shown in Table 4.9 where K_H and n_H values were obtained from the plot of lnq_e vs lnC_eas represented in Appendix L (I-IV). The value of K_H which is an indication of equilibrium binding constant reveals that Pd-Ag-CNTs nano-adsorbent had the highest K_H for Cu (0.2766) and least K_H for Ni (0.0397). In addition, the n_H value of the tested adsorbent ranged between -0.4481 to -0.1575. The magnitude of Halsey exponent (n_H) indicates that adsorption phenomenon is good. Nonetheless, Halsey correlation coefficient (R^2) is obtained from the plots and it was noticed that Halsey model is best fitted only for the removal of Fe metal by Pd-Ag-CNTs nano-adsorbents. Surprisingly, the R^2 value of Halsey and Freundlich isotherm model was found to be the same. This could be attributed to the heterogeneous distribution of surface active sites and multiple adsorption layer on the nano-adsorbents (Bozorgi *et al.*, 2018). By comparing the six (6) isotherm models, it can be concluded that the equilibrium best fit the Florry-Huggins model due to high correlation co-efficient (R^2) followed by Freundlich, Langmuir, Halsey, Dubinin-Raduskevich and Temkin model in descending order. The experimental data estimated from the isotherm models demonstrate that the used nanoadsorbent possess higher affinity towards the selected metal ions.

Table 4.10 showed the percentage removal efficiency of various adsorbents and present study, and it was observed that several studies have reported similar removal efficiencies with satisfactory results. However, the present study implies that Pd/Ag/CNTs has great capability for adsorption of all the selected metals particularly Ni metal ion. The affinity of metal ions for specific adsorbents depends on several operational conditions such as the nature of adsorbent, ionic properties, and adsorption mechanism. Conversely, it appeared that the current study reveal higher percentage removal efficiency compared to other studies irrespective of the adsorbent type or nature of the treateed wastewater. The higher affinity of Ni (II) to Pd/Ag/CNTs nanoadsorbents may be attributed to higher electronegativity value, the values of which are 1.91 for Ni (II), 1.90 for Cu, 1.83 for Fe and 1.55 for Mn (II). This justify the observed trends in the removal efficiency of the selected metal ions in the present study.

Table 4.9: Removal efficiency of various adsorbents and present study

S/N	Adsorbents	Experimental Condition	Metal Analysed	Wastewater	Percentage removal (%)	Reference
1.	Fe_3O_3/Cyclodetrin polymer	Temperature = 25 ; pH = 5.5; Initial Concentration = 300 mg/ml	Ni^{2+}	Simulated	7.3	Badruddoza *et al*., 2013
2.	Biomass	Dosage = 0.1 g; Temperature = 30 °C; Contact time = 120 min; pH = 2-5 (Cu), 2-7 (Mn)	Cu (II), Mn	Simulated	57.45 (Cu) 66.41 (Mn)	Meitei and Prasad, 2014
3.	Oxidized MWCNTs	pH = 5; Temperature = 298K	Cu (II), Ni (II)	Simulated	-	Lasheen *et al*., 2015
4.	Tartaric acid modified MWCNTs	pH = 5.5; Temperature = 298	Cu (II)	Simulated	-	Zhao *et al*., 2015
5.	GO/MWCNTs/Fe_3O_4	pH =7.0; Contact time = 24 h; Dosage = 25 mg; Temperature = 25 °C	Cu (II)	Simulated	20.90	Long *et al*., 2017
6.	Super paramagnetic Fe_2O_3 NP	pH = 6; dosage = 0.05 g; Temperature = 25 °C	Ni (II)	Simulated	69	Nithya *et al*., 2018
7.	Fe_3O_4/TiO_2/CN	Contact time = 60 min; pH = 7; Temperature = 25 °C; Dosage = 45 mg	Ni (II)	Simulated	75	Mousavi *et al*., 2019
8.	PHB-CNTs	Contact time = 70 min pH = 5.63-5.65 dosage = 20 mg	Cu, Ni, Fe	Electroplating Wastewater	15.92 (Fe) 77.95 (Ni) 83.08 (Cu)	Bankole *et al*., 2019a
9	P-CNTs	Contact time = 70 min pH = 5.63-5.65 dosage = 20 mg	Ni, Fe, Cu Mn	Industrial animal feed wastewater	70 (Ni), 66 (Fe), 65 (Cu) 60 (Mn)	Bankole *et al*., 2019b
10.	Microwave-functionalized rice husk cellulose	Dosage = 4 g/l; Contact time = 60 min; pH = 5.5; Temperature = 20 °C	Ni (II)	Electroplating Wastewater	96.38	Qu *et al*., 2020
11.	Pd-Ag-CNTs	Contact time = 60 min Dosage = 10 mg Temperature = 25 °C	Cu, Fe, Mn, Ni	Animal Feed Processsing Industry Wastewater	77.86 (Cu) 88.36 (Fe) 77.64 (Mn) 99.84 (Ni)	This study

Also, the observed trend for adsorption of metal ions on Pd-Ag-CNTs can be linked to the ionic radii in such a way that, smaller ionic radius of the associated metals correspond to higher sorption level of the selected metal ions (Park *et al.*, 2019). Similarly, Bankole and co-workers found the affinity order of the selected metal ions towards the PHB-CNTs at pH range of 5.63-5.65 as Ni > Cu > Fe, which agrees with the above mentioned trends. The general observation implies that Pd-Ag-CNTs nanoadsorbent is effective enough for the treatment of industrial animal feed processing wastewater.

4.4.5 Adsorption kinetic study

The kinetics model provides useful information regarding the mechanism of an adsorption of metal ion onto the nano-adsorbents, which in turn govern the rate determining step of the adsorption process to attain equilibrium (Singh *et al.*, 2021). In this study, the adsorptoion kinetics of metal ions onto the nano-adsorbents were examined using pseudo-first order, pseudo-second order and intra-particle diffusion models. The experimental data of adsorption kinetics and non-linear curve fitting parameters are presented in Table 4.10 and Appendix N, P and Q.

Table 4.10 revealed the values of the rate constants and other parameters as estimated from the plot of lnC_T against time (t), $^{t}/_{q_t}$ against t, and q_e against $t^{1/2}$, respectively. The best fitted curve was decided based on the highest correlation coefficient. The (R^2) values of the experimental data using pseudo-first order kinetics was far from unity based on the test adsorbent, thereby indicating poor adsorption kinetics in relation to other models. This implies that the adsorption kinetics did not follow pseudo-first order kinetic model. According to Table 4.10, the (R^2) value were observed to be highest for pseudo-second order kinetics when compared to other models studied. Also, the adsorption capacity (Q_{cal}) values from pseudo-second order kinetics were match closest to those obtained from the experimental adsorption equilibrium capacity (Q_{exp}).

This suggest that pseudo-second order kinetic model can suitably describe the adsorption kinetic of metal ion on the nano-adsorbents since most of the data points were perfectly fitted. The observed results may be connected to the fact that the prepared nano-adsorbent has large specific surface area (392.5 m^2/g) with increased surface active site, which invariably explain the high adsorption rate of metal ions by the adsorbent. The correlation coefficient (R^2) in Table 4.10 further confirmed that the adsorption of metal ions from wastewater followed pseudo-second order kinetics better than other kinetic models. For all the analyzed metal ions, it was observed that the calculated (R^2) values for pseudo-second order kinetics were found very close to unity. Whereas, the obtained R^2 values for pseudo-first order and intra-particle diffusion model were far from pseudo-second order R^2 value.

On the contratry, diffusion rate of metal ions onto the nano-adsorbents were determined using intra-particle diffusion model. The q_t, which indicates the amount of metal ions adsorbed at time t (mg/mg) and K_{int}, which is the intra-particle diffusion rate constant (mg/mg/min) are presented in Table 4.11.

Table 4.10: Kinetic model parameters for the adsorption of selected metal ion by Pd-Ag-CNTs nanocomposites

Kinetic models with Equations	**Parameters (units)**	**Metal ion**			
		Cu	Fe	Mn	Ni
	$q_{exp.}$ (mg/g)	2.96	2.87	1.92	2.0233
Pseudo-first-order	$Q_{cal.}$(mg/g)	2.5979	2.4123	1.6598	1.5001
$\boldsymbol{Ln\,(C_t) = Ln\,(C_e) - Kt}$	K_1(/min)	-0.0015	-0.002	-0.0014	-0.0035
	R^2	0.8700	0.9212	0.8916	0.9346
	SSE	0.0013	0.00317	0.0010	0.0049
	χ^2	0.00018	0.0014	0.0008	0.0015
Pseudo-second-order	$q_{cal.}$ (mg/g)	3.012	2.9499	1.9372	2.1716
$\boldsymbol{\frac{t}{q_t} = \frac{1}{K_2 {q_e}^2} + \frac{1}{q_e} t}$	K_2(min^{-1})	0.1163	0.0839	6.5369	17.5288
	R^2	0.9991	0.9987	0.9965	0.9948
	SSE	0.3788	0.5891	3.7156	4.4007
	χ^2	0.2970	0.5607	3.2585	2.4147
Intra-particle diffusion	$K_{int.}$ (mg/g.min$^{-1/2}$)	0.0565	0.0715	0.0341	0.0859
$\boldsymbol{q_t = K_t t^{1/2}b + C}$	R^2	0.9272	0.9661	0.8595	0.964
	C	2.4134	2.1783	1.5518	1.2132
	SSE	0.0054	0.0131	0.0041	0.0060
	χ^2	0.0029	0.0039	0.0023	0.0082

The regression analysis of the experimental data on a plots of q_t against $t^{1/2}$ should have pass through the origin. However, the plots gave a straight line that did not pass through the origin with intra-particle diffusion rate constant (K_{int}) within the range of 0.0341-0.0859 mg/g/min, (R^2) value between 0.8595 and 0.9661, and intercept value varying between 1.2132-2.4134 mg/g. Therefore, this results suggests a degree of boundary layer control, and implies that the adsorption of metal ion on the nano-adsorbents are (multi-step kinetic adsorption) (Almomani *et al.*, 2020). Based on the regression (R^2) and intercept (c) values obtained, it can be concluded that the intra-particle diffusion model could not be the rate determining step. Hence, the experimental data exhibited a higher correlation coefficient values with pseudo-second-order (R^2= 0.9991 (Cu); 0.9987 (Fe); 0.9965 (Mn) and 0.9948 (Ni)) than with first-order (R^2= 0.8700 (Cu); 0.9212 (Fe); 0.8916 (Mn); 0.9346 (Ni)) and intraparticle diffusion model (R^2 = 0.9272 (Cu); 0.9661 (Fe); 0.8595 (Mn) and 0.9640 (Ni)). Thus, indicating that the kinetic determining step of adsorption of all metal ions onto Pd/Ag/CNTs nanoadsorbent is based on chemical adsorption process (rather than physical adsorption) via the exchange of valence electrons or electron sharing between the adsorbent surface and the adsorbate molecules. Among the three kinetic models applied, the best fitting one is determined based on the use of SSE and χ^2 values to further explain the error deviation between the experimental and predicted equilibrium adsorption kinetic data, after linear analysis. As indicated in Table 4.11, it appeared that pseudo-first order kinetic model were the most suitable models to satisfactorily describe the adsorption phenomenon since the magnitude of SSE and χ^2 values determines the best fitted kinetic model. Indeed smaller values were found when modeling the kinetic data using pseudo-first order model.

4.4.6 Adsorption thermodynamics study

The estimation of thermodynamic parameters is very essential in determining the spontaneity and heat changes involved during temperature-dependent transfer of molecules (sorption) from solutions onto the solid phase (adsorbent) material. The results of thermodynamic studies of the present survey are presented in Table 4.11. Therein, impact of temperature on the adsorption of selected metal ions (Cu, Fe, Mn and

Ni) by Pd-Ag-CNTs was examined at 30-80 ℃, and the value of ΔG° were found within the ranges of 52178.17-56784.12 KJ/mol (Cu), 44018.8-47984.32 (Fe), 59138.66-64299.16 (Mn), 192357-208475.4 (Ni). However, the ΔG° positive values indicates that the adsorption process is non-spontaneous. The enthalpy and entropy values for the tested adsorbents were found to be 24266.07 and -92.12 (Cu), 19987.69 and -79.31 (Fe), 27866.03 and -103.21 (Mn) and 94679.83 and -322.37 (Ni), respectively.

Table 4.11: Constants of Thermodynamics Model Through Adsorption of Selected Metal Ions (Cu, Fe, Mn and Ni) by Pd-Ag-CNTs

Metals	Temperature (°C)	ΔG° (KJ/mol)	ΔH° (KJ/mol)	ΔS° (KJ/mol/K)	K_c
Cu	303	52178.17	24266.07	-92.12	1.00 x 10-9
	313	53099.36			1.40 x 10-9
	323	54020.55			1.80 x 10-9
	333	54941.74			2.41 x 10-9
	343	55862.93			3.11 x 10-9
	353	56784.12			3.96 x 10-9
Fe	303	44018.80	19987.69	-79.31	2.60 x 10-8
	313	44811.90			3.30 x 10-8
	323	45605.00			4.20 x 10-8
	333	46398.11			5.27 x 10-8
	343	47191.21			6.50 x 10-8
	353	47984.32			7.93 x 10-8
Mn	303	59138.66	27866.03	-103.21	6.40 x 10-11
	313	60170.76			9.10 x 10-11
	323	61202.86			1.30 x 10-10
	333	62234.96			1.73 x 10-10
	343	63267.06			2.32 x 10-10
	353	64299.16			3.06 x 10-10
Ni	303	192357.0	94679.83	-322.37	6.90 x 10-34
	313	195581.0			2.30 x 10-33
	323	198804.0			7.10 x 10-33
	333	202028.1			2.04 x 10-32
	343	205251.7			5.52 x 10-32
	353	208475.4			1.41 x 10-31

In general, it was observed that ΔG° value increased with increase in temperature of adsorption, suggesting that there is increase in feasibility of adsorption of metal ion onto

Pd-Ag-CNTs nano-adsorbent at higher temperature (adsorption is more favourable at higher temperature). Also, ΔH° values were found positive and this further confirmed that the adsorption of selected heavy metals was endothermic in nature. The necessity of large heats to remove metals from the liquid solution made the adsorption mechanism more of endothermic process (Al-Sou'od, 2012; Boulaiche *et al.*, 2019). It is possible that increasing temperature could have enhanced both the surface and pore diffusion of the studied adsorbents because temperature plays an important role in the transformation of surface complexation structures (Al-Essa and Khalili, 2018). Besides, negative values of ΔS° is indicative of decreased degree of randomness at adsorbent-adsorbate interface. This justify the fact that the adsorption process involve an associative mechanism resulting to orderliness by way of forming a coordination complex between the ions and the nano-adsorbents. This can be related to the water holding capacity of the nano-adsorbent. In addition, there is a general increase in the rate of adsorption (K_c) as the temperature increases from 30-80 °C. This increment could be attributed to the strong electrostatic forces between the surface sites of the adsorbent and the adsorbed molecules (Razmi *et al.*, 2019; Bankole *et al.*, 2019b).

The comparison of the prepared Pd/Ag/CNTs nanoadsorbent with other nano based material is presented in Table 4.13. Many researchers have reported the adsorption capacity of the studied metal ions for several adsorbents. However, little or no literature provides sorption capacities of the selected metal ions onto Pd-Ag-CNTs nanoadsorbents. Hence, direct comparison of the literature data with the present study may lead to significant dissimilarities because adsorbents from literature data are made of distinct structural properties (that is, different surface area, functional group and different experimental factors such as pH, temperature and concentrations among others)

(Sargazi *et al*., 2019). For instance, sorption capacity of Cu and Ni onto nanokaolinite is 125 mg/g (Cu^{2+}) and 111 (Ni^{2+}) (Alasadi *et al*., 2019). A comparable value is observed for the same metal ions adsorbed on Pd-Ag-CNTs nanoadsorbent. The adsorption capacities are 1000 mg/g, 4.00 mg/g, 1.06 mg/g and 0.8175 mg/g. Herein, it was noticed that the adsorption capacity of Ni ion is greater than others in multiple folds. The low adsorption capacities of others metal ions may be connected to their higher concentration before treatment. This may be the reason for their low removal from industrial animal feed processing wastewater compared to the former (Ni ion). Overall, the novelty and relevance of Pd/Ag/CNTs nanoadsorbents in treatment of animal feed processing industry wastewater is explored and it was noticed that the removal efficiency of Pd/Ag/CNTs surpassed those other reported literature. Thus, indicating the efficacy of the test adsorbent in removal of water quality parameters and sequestration of selected metal ions as presented in Table 4.10.

Table 4.12a: Comparison of maximum adsorption capacity of Pd-Ag-CNTs with other adsorbents reported in literature.

S/N	Adsorbents	Waste water	Experimental condition	Metal ion	Maximum adsorption capacity (q_{max}) (mg/g)	Isotherm Model	Kinetic Model	Thermodynamic	Reference
1.	Biomass	Simulated Waste water	Dosage = 0.1 g; pH = 2-5 (Cu), 2-7 (Mn), Contact time = 120 min, Temperature = 30 °C.	Cu, Mn	52.6 (Cu), 35.7 (Mn)	Freundlich; Langmuir	Pseudo-first-order; Pseudo-second order	Spontaneous and feasible Decrease randomness exothermic	Meitei and Prasad, 2014
2.	Polyaniline nanocomposite	SWastewater	pH = 10; dosage = 10 g/l; contact time = 30 min	Mn	50.251	Freundlich; Langmuir	Pseudo-second order	-	Hallajiqomi and Eisazadeh *et al.*, 2017
3.	Metakaolin based geopolymer	Real waste water	pH = 2-7; dosage = 10-125 mg Temperature = 30 ; Contact time = 60 min. Initial concentration = 25 mg/l	Mn	72.34	Langmuir Freundlich Dubinin-Radushkevich	Pseudo-first-order model; Pseudo-second-order model Intra-particles diffusion	Endothermic Spontaneous Increased randomness	Kara *et al.*, 2018
4.	Metakaolin/CNTs	Natural ground water	Contact time = 120 min; Dosage = 20 mg; pH = 6	Fe, Mn	53.76 (Fe) 51.2 (Mn)	Langmuir Freundlich Temkin	Pseudo-second order model Intra-particle diffusion Elovich- kinetic model	Endothermic Increased randomness Spontaneous	Shaban *et al.*, 2017

Table 4.12b: Comparison of maximum adsorption capacity of Pd-Ag-CNTs with other adsorbents reported in literature.

S/N	Adsorbents	Waste water	Experimental condition	Metal ion	Maximum adsorption capacity (q_{max}) (mg/g)	Isotherm Model	Kinetic Model	Thermodynamic	Reference
5.	Kaolinite/Starch	Natural ground water	Contact time = 120 min; Dosage = 20 mg; pH = 6	Fe, Mn	46.80 (Fe) 34.26 (Mn)	Langmuir Freundlich Temkin	Pseudo-second (Fe) Elovich (Mn) Intra-particle diffusion	Exothermic Decreased randomness Non-spontaneous	Shaban *et al.*, 2017
6.	Nanokaolinite	Simulated waste water	Temperature = 30 Contact times = 120; pH = 5.5-6	Cu, Ni	125 (Cu) 111 (Ni)	Langmuir Freundlich	Pseudo-first-order; Pseudo-second order	Endothermic Spontaneous Increased randomness	Alasadi *et al.*, 2019
7.	$Fe_3O_4/TiO_2/CN$	Simulated waste water	Contact time = 60 pH = 7 Temperature = 25 Dosage = 45	Ni	75.76	Langmuir Freundlich	Pseudo-first-order; Pseudo-second order	Endothermic Increased Randomness Spontaneous	Mousavi *et al.*, 2019
8.	Flower Globular Magnesium Hydroxide (FGMH)	Simulated waste water	Dosage = 30 mg; Contact time = 50 min; pH = 6.07-7.71; Temperature = 25 °C	Ni	287.11	Langmuir Freundlich	Pseudo-first-order; Pseudo-second order Intraparticle diffusion model	-	Jiang *et al.*, 2019
9.	Super paramagnetic Fe_2O_3 NP	Simulated waste water	pH = 6; dosage = 0.05 g; Temperature = 25 °C	Ni	227.20	Langmuir Freundlich	-	-	Nithya *et al.*, 2018

Table 4.12c: Comparison of maximum adsorption capacity of Pd-Ag-CNTs with other adsorbents reported in literature.

S/N	Adsorbents	Waste water	Experimental condition	Metal ion	Maximum adsorption capacity (q_{max}) (mg/g)	Isotherm Model	Kinetic Model	Thermodynamic	Reference
10.	P-CNTs	Industrial waste watwater	Contact time = 70 min pH = 5.63-5.65 dosage = 20 mg	Cu, Ni, Fe	312.50 (Fe) 10.09 (Ni) 21.65 (Cu)	Langmuir Freundlich Dubinin-Radushkevich Temkin	Pseudo-first-order; Pseudo-second order Elovich Fractional Power Kinetic Model	Spontaneous Endothermic Increase Randomness B	Bankole *et al*., 2019b
11.	PHB-CNTs	Industrial waste water	Contact time = 70 min pH = 5.63-5.65 dosage = 20 mg	Cu, Ni, Fe	19.61 (Cu) 10.16 (Ni) 227.27 (Fe)	Langmuir Freundlich D-R Temkin	Pseudo-first-order; Pseudo-second order Elovich Fractional Power	Spontaneous Endothermic Increase Randomness	Bankole *et al*., 2019a
12.	Pd-Ag-CNTs	Animal Feed Processing Industry waste water	Contact time = 70 min pH = 5.63-5.65 dosage = 20 mg	Cu, Fe, Mn Ni	0.82 (Cu) 4.00 (Fe) 1.06 (Mn) 1000 (Ni)	Langmuir Freundlich D-R Temkin Florry-Huggins Halsey	Pseudo-first-order; Pseudo-second order Intra-particle diffusion model	Non-spontaneous Endothermic Decreased degree of randomness	This study

CHAPTER FIVE

5.0 CONCLUSION AND RECOMMENDATIONS

5.1 CONCLUSION

This study was based on the synthesis, and characterization of palladium-silver carbon nanotubes composites to improve adsorption of heavy metal ions and water indicator parameters from industrial animal feed processing wastewater. Carbon nanotubes was synthesized via a chemical catalytic vapour deposition on the prepared bi-metallic (Fe-Ni supported on kaolin) catalyst. Surface oxidation and purification of carbon nanotubes occurred in the presence of HNO_3 and H_2SO_4 followed by calcination in the furnace. Different concentrations of synthesized PdNPs and AgNPs were used individually and in combination for the modification of carbon nanotubes. The developed CNTs-based nanocomposites (Pd-CNTs, Ag-CNTs, Pd-Ag-CNTs) were successfully characterized and used as nano-adsorbent for the treatment of industrial animal feed processing wastewater. The influence of variables such as solution pH, adsorbent dosage and temperature effect were investigated. Further, the adsorption system mechanism was explained through investigation of isotherm model, kinetic model and thermodynamics. Based on the obtained results, the following conclusions were drawn:

i. The phytochemical results indicated that the plant extracts are very rich in secondary metabolites such as phenols, tannins, and flavonoids.

ii. A rapid synthesis of stabilized nano Ag and Pd were successfully obtained through the use of *Agerantum conyzoides* extracts as confirmed by various analytical results.

iii. For the produced carbon nanotubes, the optimum catalyst yield of 86.54 % was obtained at stirring speed of 2000 rpm, 10 g of mass of support, a pre-calcination time of 12 h and pre-calcination temperature of 120 °C.

iv. The optimum condition to the prepared high quality CNTs were temperature of (700 °C), reaction time (90 minute), flow rate of nitrogen gas (350 cm^3/min) and flow rate of acetylene (100 cm^3/min).

v. The composite (Pd-Ag-CNTs) was used as a metallic matrix nano-adsorbent and the result showed that the prepared nano-adsorbents was effective for treatment of industrial animal feed processing wastewater. The adsorption of metal ion onto Pd-Ag-CNTs nano-adsorbent was found to be least dependent on adsorbent dosage, although all process variables (solution pH, adsorbent weight and temperature) greatly influence the removal efficiency. For removal of Cu, Fe, Ni and Mn from industrial animal feed processing wastewater, the maximum percentage removal was found to be 77.87, 88.36, 77.64 and 99.84 % at optimum conditions of 90 min contact time, 60 mg of adsorbent dosage and 80 °C of solution temperature.

vi. The experimental equilibrium sorption data for the selected metal ions revealed that Flory-Huggins isotherm model best fitted, followedby Freundlich>Langmuir> Halsey >Dubinin-Raduskevich>Temkin model.

vii. The kinetic adsorption data of the analysed metal ions by Pd-Ag-CNTs was satisfactorily described for all studied models, however pseudo-second-order model was the most appropriate to describe the adsorption of metal ion among the three kinetic models. The order of kinetic models are pseudo-second order > pseudo-first-order > intra-particle diffusion rate model.

viii. The thermodynamic data indicated that the adsorption process is non-spontaneous and there is increase in the feasibility of adsorption of metal ion onto Pd-Ag-CNTs nano-adsorbents at higher temperature. The positive value of standard entropy change indicates a decrease in degree of randomness at adsorbent-adsorbate interface.

ix. It can be deduced that the modification of CNTs with Pd° and Ag° to give Pd-Ag-CNTs significantly improved the adsorption efficiency and it is reasonable enough to conclude that the investigated nanoadsorbent exhibited superior properties as an adsorbent to remove metal ions from industrial animal feed processing wastewater.

5.2 Recommendations

Futher studies should be carried out in the following area:

i. Pd-Ag-CNTs nanocomposite sshould be considered for column adsorption study.

ii. It should be recommended that the used nanoadsorbent is characterized with HRSEM and FTIR after adsorption study to help ascertain the mechanism of adsorption between the adsorbate-adsorbent interface

5.3 Contribution to knowledge

i. The study demonstrated for the first time the multi-step mechanistics pathway for incorporation of palladium and silver nanoparticles onto multi-walled carbon nanotubes using ultrasonic – assisted wet impregnations method.

ii. The synergistic effect of Pd and Ag on MWCNTs was charasterised and investigated as nanoadsorbent for the treatment of industrial animal feeds processing wastewater.

iii. The study showed that the prepared and characterized palladium/silver/carbon nanotubes composite is highly effective for the emoval of pollutant indicators and heavy metal ions from industrial animal feeds processing wastewaters

REFERENCES

Abazari, R., Mahjoub, A. R. & Shariati, J. (2019). Synthesis of a nanostructured pillar MOF with high adsorption capacity towards antibiotics pollutants from aqueous solution. *Journal of Hazardous Materials*, 366, 439-451.

Abbas, C., Binder, T. P., Beery, K. E., Cecava, M. J., Doane, P. H., Holzgraefe, D. P. & Solheim, L. P. (2009). Process for the production of animal feed and ethanol and novel animal feed. U.S. Patent No. 7,494,675. *Washington, DC: U.S. Patent and Trademark Office*.

Abdallh, M. N., Abdelhalim, W. S. & Abdelhalim, H. S. (2016). Industrial Wastewater Treatment of Food Industry using Best Techniques. *International Journal of Engineering and Science Invention*, 5(8), 15-28.

Abdel-Ghani, N. T. & El-Chaghaby, G. A., (2014). Biosorption for metal ions removal from aqueous solutions: A Review of Recent Studies. *International Journal of Latest Research in Science and Technology*. 3, 24-42.

Abdel-Ghani, N.T., Hegazy, A. K. & El-Chaghaby, G. (2009). Typha domingensis leaf powder for decontamination of aluminium, iron, zinc and lead: Biosorption kinetics and equilibrium modeling. *International Journal of Environmental Science and Technology*, 6, 243-248.

Abdelghany, T. M., Al-Rajhi, A. M., Al Abboud, M. A., Alawlaqi, M. M., Magdah, A. G., Helmy, E. A. & Mabrouk, A. S. (2018). Recent advances in green synthesis of silver nanoparticles and their applications: about future directions: A review. *BioNanoScience*, 8(1), 5-16.

Aboelfetoh, E. F., Elabedien, M. E. Z. & Ebeid, E. Z. M. (2021). Effective treatment of industrial wastewater applying SBA-15 mesoporous silica modified with graphene oxide and hematite nanoparticles. *Journal of Environmental Chemical Engineering*, 9(1), 104817.

Adeleye, A. S., Conway, J. R., Garner, K., Huang, Y., Su, Y. & Keller, A. A. (2016). Engineered Nanomaterials for Water Treatment and Remediation: Costs, Benefits, and Applicability.*Chemical Engineering Journal*, 286, 640-662.

Adetunji, C. O., Olaniyi, O. O. & Ogunkunle, A. T. J. (2013). Bacterial activity of crude extracts of Vernonia amygdalina on clinical isolates. *Journal of Microbiology and Antimicrobials*, 5(6), 60-64.

Adeyemo, A. A., Adeoye, I. O. & Bello, O. S. (2017). Adsorption of dyes using different types of clay: a review. *Applied Water Science*, 7(2), 543-568.

Agboola, O., Popoola, P., Sadiku, R., Sanni, S. E., Fayomi, S. O. & Fatoba, O. S. (2020). Nanotechnology in Wastewater and the Capacity of Nanotechnology for Sustainability. *In Environmental Nanotechnology,* 3, 1-45.

Ahlström, M. G., Thyssen, J. P., Wennervaldt, M., Menné, T. & Johansen, J. D. (2019). Nickel allergy and allergic contact dermatitis: A clinical review of immunology, epidemiology, exposure, and treatment. *Contact dermatitis*, 81(4), 227-241.

Ahmed, B., Hashmi, A., Khan, M. S. & Musarrat, J. (2018). ROS mediated destruction of cell membrane, growth and biofilms of human bacterial pathogens by stable metallic AgNPs functionalized from bell pepper extract and quercetin. *Advanced Powder Technology*, 29(7), 1601-1616.

Ahmed, I. & Jhung, S. H. (2017). Applications of metal-organic frameworks in adsorption/separation processes via hydrogen bonding interactions. *Chemical Engineering Journal*, 310, 197-215.

Ahsani, M., Hazrati, H., Javadi, M., Ulbricht, M. & Yegani, R. (2020). Preparation of antibiofouling nanocomposite PVDF/Ag-SiO2 membrane and long-term performance evaluation in the MBR system fed by real pharmaceutical wastewater. *Separation and Purification Technology*, 249, 116938.

Ajitha, B., Reddy, Y. A. K. & Reddy, P. S. (2015). Green synthesis and characterization of silver nanoparticles using Lantana camara leaf extract. *Materials Science and Engineering*: C, 49, 373-381.

Akpor, O. B. & Muchie, B. (2019).Environmental and public health implications of wastewater quality. *African Journal of Biotechnology*, 10(13), 2379-2387.

Al Badaii, F., Shuhaimi-othman, M. & Gasim, M. B. (2013). Water Quality Assessment of the Semenyith River, Selanger, Malaysia. *Journal of Chemistry*. 871056, 1-10. doi:10.1155/2013/871056.

Alasadi, A., Khaili, F. & Awwad, A. (2019). Adsorption of Cu (II), Ni (II) and Zn (II) ions by nano kaolinite: Thermodynamics and kinetics studies. *Chemistry International*, 5(4), 258-26.

Al-Essa, K. & Khalili, F. (2018). Heavy metals adsorption from aqueous solutions onto unmodified and modified Jordanian kaolinite clay: Batch and olumn techniques. *American Journal of Applied Chemistry*, 6 (1), 25-34.

Al-Ghouti, M. A. & Da'ana, D. A. (2020). Guidelines for the use and interpretation of adsorption isotherm models: A review. *Journal of Hazardous Materials*, *393*, 122383.

Ali, I., Alothman, Z. A. & Al-Warthan, A. (2016). Sorption, kinetics and thermodynamics studies of atrazine herbicide removal from water using iron nano-composite material.*International Journal of Environmental Science and Technology*, 13(2), 733-742.

Ali, S. G., Ansari, M. A., Jamal, Q. M. S., Khan, H. M., Jalal, M., Ahmad, H. & Mahdi, A. A. (2017). Antiquorum sensing activity of silver nanoparticles in *P. aeruginosa*: an in silico study. *In Silico Pharmacology*, 5(1), 12.

Aliyu, A., & Srivastava, C. (2021). Correlation between growth texture, crystallite size, lattice strain and corrosion behavior of copper-carbon nanotube composite coatings. *Surface and Coatings Technology*, *405*, 126596.

Aliyu, A., Abdulkareem, A. S., Kovo, A. S., Abubakare, O. K., Tijani, J. O. & Kariim, I. (2017). Synthesize Multi-Walled Carbon Nanotubes via Catalytic Chemical Vapour Deposition Method on Fe-Ni Bimetallic Catalyst Supported on Kaolin. *Carbon Letter*, 21, 33-50.

Almomani, F., Bhosale, R., Khraisheh, M. & Almomani, T. (2020). Heavy metal ions removal from industrial wastewater using magnetic nanoparticles (MNP).*Applied Surface Science*, 506, 144924.

Al-Saidi, H. M., Abdel-Fadeel, M. A., El-Sonbati, A. Z. & El-Bindary, A. A. (2016). Multi-walled carbon nanotubes as an adsorbent material for the solid phase extraction of bismuth from aqueous media: kinetic and thermodynamic studies and analytical applications. *Journal of Molecular Liquids*, 216, 693-698.

Al-Sou'od, K. (2012). Adsorption isotherm studies of chromium (VI) from aqueous solutions using Jordanian pottery materials. *APCBEE Procedia,* 1, 116–125

Ambroz, F., Macdonald, T. J., Martis, V. & Parkin, I. P. (2018). Evaluation of the BET Theory for the Characterization of Meso and Microporous MOFs. *Small Methods*, 2(11), 1800173.

American Public Health Association (APHA)/American Water Works Association/Water Environment Federation.(2017). Standard Methods for the Examination of Water and Wastewater, *Twenty-third edition Washington*, U.S.A.

Amin, M. & Chetpattananondh, P. (2019). Biochar from extracted marine Chlorella sp. residue for high efficiency adsorption with ultrasonication to remove Cr (VI), Zn (II) and Ni (II). *Bioresource Technology*, 289, 121578.

Amin, M. T., Alazba, A. A. & Manzoor, U. (2014). A Review: Removal of pollutants from Water/Wastewater using Different Types of Nanomaterials. *Advances in Materials Sciences and Engineering*, ID: 825910, 24. Doi: 10.1155/2014/825910.

Amin, M., Anwar, F., Janjua, M. R. S. A., Iqbal, M. A. & Rashid, U. (2012). Green synthesis of silver nanoparticles through reduction with Solanum xanthocarpum L. berry extract: characterization, antimicrobial and urease inhibitory activities against Helicobacter pylori. *International Journal of Molecular Sciences*, 13(8), 9923-9941.

Ammendola, P., Raganati, F. & Chirone, R. (2017). CO_2 adsorption on a fine activated carbon in a sound assisted fluidized bed: Thermodynamics and kinetics. *Chemical Engineering Journal*, 322, 302-313.

Anandalakshmi, K., Venugobal, J. & Ramasamy, V. (2016). Characterization of silver nanoparticles by green synthesis method using *Pedalium murex* leaf extract and their antibacterial activity. *Applied Nanoscience*, 6(3), 399-408.

Anderson, G. J., & Frazer, D. M. (2017). Current understanding of iron homeostasis. *The American journal of clinical nutrition*, 106(supplementary), 1559S-1566S.

Angin, D. (2014). Utilization of activated carbon produced from fruit juice industry solid waste for the adsorption of Yellow 18 from aqueous solutions. *Bioresource Technology*, 168, 259-266.

Aniyikaiye, T. E., Oluseyi, T., Odiyo, J. O. & Edokpayi, J. N. (2019).Physico-chemical analysis of wastewater discharge from selected paint industries in Lagos, Nigeria. *International Journal of Environmental Research and Public Health*, 16(7), 1235.

Ankanna, S. T. N. V. K. V. P., Prasad, T. N. V. K. V., Elumalai, E. K. & Savithramma, N. (2010). Production of biogenic silver nanoparticles using Boswellia ovalifoliolata stem bark. *Digest Journal of Nanomaterials and Biostructures*, 5(2), 369-372

Ansari, M. A. & Alzohairy, M. A. (2018). One-pot facile green synthesis of silver nanoparticles using seed extract of Phoenix dactylifera and their bactericidal potential against MRSA. *Evidence-Based Complementary and Alternative Medicine*, 2, 1-9.

Arias, L. R. & Yang, L. (2009). Inactivation of bacterial pathogens by carbon nanotubes in suspensions. *Langmuir*, 25(5), 3003-3012.

Aroca, R. (2006). Surface-enhanced vibrational spectroscopy. John Wiley & Sons.

Arsiya, F., Sayadi, M. H. & Sobhani, S. (2017). Green synthesis of palladium nanoparticles using *Chlorella vulgaris*. *Materials Letters*, 186, 113-115.

ATSDR (2012). Manganese. https://www. atsdr.cdc. gov/substances/ toxsubstance. asp?To-xid =23. Accessed 19 Apr 2019

Association of Official Analytical Chemists (AOAC) (1984). Official Methods of Analysis of the Association of Official Analytical Chemists, 14th edition, AOAC, Arlington, VA.

Association of Official Analytical Chemists (2017). Official Methods of Analysis of the Association of Official Analytical Chemists, 14th edition, AOAC, Arlington, VA.

Atieh, M. A. (2011). Removal of chromium (VI) from polluted water using carbon nanotubes supported with activated carbon. *Procedia Environmental Sciences*, *4*, 281-293.

Ayawei, N., Ebelegi, A. N. & Wankasi, D. (2017). Modelling and interpretation of adsorption isotherms. *Journal of Chemistry*, 1, 16-28.

Ayawei, N., Ekubo, A. T., Wankasi, D. & Dikio, E. D. (2015). Adsorption of congo red by Ni/Al-CO3: equilibrium, thermodynamic and kinetic studies. *Oriental Journal of Chemistry*, 31(3), 1307.

Aziz, N., Mindaryani, A., Taftazani, A. & Biyantoro, D. (2018). Effect of temperature to adsorption capacity and coefficient distribution on rare earth elements adsorption (Y, Gd, DY) using SIR. In IOP Conference Series: *Materials Science and Engineering*, 349(1), 012041.

Babaei, A. A., Azari, A., Kalantary, R. R. & Kakavandi, B. (2015). Nitrate Removal from Aqueous Solution using CNTs magnetized by Zero-valent iron. *Water Science and Technology*, 1988, 72-11.

Badruddoza, A. Z. M., Shawon, Z. B. Z., Tay, W. J. D., Hidajat, K. & Uddin, M. S. (2013). Fe_3O_4/cyclodextrin polymer nanocomposites for selective heavy metals removal from industrial wastewater. *Carbohydrate Polymers*, *91*(1), 322-332.

Bai, C., Wang, L. & Zhu, Z. (2020). Adsorption of Cr (III) and Pb (II) by graphene oxide/alginate hydrogel membrane: Characterization, adsorption kinetics, isotherm and thermodynamics studies. *International Journal of Biological Macromolecules*, 147, 898-910.

Banerjee, S. & Chattopadhyaya, M. C. (2017).Adsorption characteristics for the removal of a toxic dye, tartrazine from aqueous solutions by a low cost agricultural by-product. *Arabian Journal of Chemistry*, 10, S1629-S1638.

Bankar, A., Joshi, B., Kumar, A. R. & Zinjarde, S. (2010) Banana peel extract mediated novel route for the synthesis of silver nanoparticles. *Colloids and Surfaces A: Physicochemical and Engineering Aspects*, 368(1–3): 58–63.

Bankole, M. T., Abdulkareem, A. S., Mohammed, I. A., Ochigbo, S. S., Tijani, J. O., Abubakre, O. K. & Roos, W. D. (2019a). Selected heavy metals removal from electroplating wastewater by purified and polyhydroxylbutyrate functionalized carbon nanotubes adsorbents. *Scientific Reports*, 9(1), 1-19.

Bankole, M. T., Usman, N. A., Tijani, J. O., Adegboye I. K. & Abdulkareem, A. S. (2019b). Treatment of industrial animal feed processing wastewater using functionalized nano-adsorbent. *Journal of Chemical Society of Nigeria*, 44(6), 1-9.

Bankole, M. T., Mohammed, I. A., Abdulkareem, A. S., Tijani, J. O., Ochigbo, S. S., Abubakre, O. K. & Roos, W. S (2018). Optimization of Supported Bimetallic (Fe-Co/$CaCO_3$) Catalyst synthesis Parameters for Carbon Nanotubes Growth Using Factorial Experimental Design, *Journal of Alloys and Compounds*, 749, 85-102.

Bano, Z., Saeed, R. Y., Zhu, S., Xia, M., Mao, S., Lei, W., & Wang, F. (2020). Mesoporous CuS nanospheres decorated rGO aerogel for high photocatalytic activity towards Cr (VI) and organic pollutants. *Chemosphere*, 246, 125846.

Bardestani, R., Patience, G. S. & Kaliaguine, S. (2019). Experimental methods in chemical engineering: specific surface area and pore size distribution measurements-BET, BJH, and DFT. *The Canadian Journal of Chemical Engineering*, *97*(11), 2781-2791.

Behera, T., Swain, P., Rangacharulu, P. V. & Samanta, M. (2014). Nano-Fe as feed additive improves the hematological and immunological parameters of fish, Labeo rohita H. *Applied Nanoscience*, *4*(6), 687-694.

Bernal, V., Giraldo, L. & Moreno-Piraján, J. C. (2018). Physicochemical properties of activated carbon: their effect on the adsorption of pharmaceutical compounds and adsorbate–adsorbent interactions. *Journal of Carbon Research*, 4(4), 62.

Bhatnagar, A. & Minocha, A. K. (2014). Conventional and non-Conventional Adsorbents for Removal of Pollutants from Water.*Indian Journal of Chemical Technology*, 13, 203-217.

Bhattacharya, S., Sacha, I., Mukhopadyay, A., Chattopadhyay, D., Ghozu, U. & Chatterjee, D. (2013). Role of Nanotechnology in water Treatment and Purification: Potential Application and Implications. *International Journal of Chemical Science and Technology*, 3(3), 59-64.

Bhosale, A. & Bhanage, M. B. (2015). Silver nanoparticles: Synthesis, characterization and their application as a sustainable catalyst for organic transformations. *Current Organic Chemistry*, 19(8), 708-727.

Blair, R. (2018). *Nutrition and feeding of organic poultry. CABI.*

Bohli, T., Villaescusa, I. & Ouederni, A. (2013). Comparative study of bivalent cationic metals adsorption Pb (II), Cd (II), Ni (II) and Cu (II) on olive stones chemically activated carbon. *Journal of Chemical Enginering and Process Technology*, 4(4), 1-7.

Bora, T. & Dutta, J. (2014). Applications of Nanotechnology in Wastewater Treatment-A Review. *Journal of Nanoscience and Nanotechnology*, 14, 613-626.

Borase, H. P., Salunke, B. K., Salunkhe, R. B., Patil, C. D., Hallsworth, J. E., Kim, B. S. & Patil, S. V. (2014). Plant extract: a promising biomatrix for ecofriendly, controlled synthesis of silver nanoparticles. *Applied Biochemistry and Biotechnology*, 173(1), 1-29.

Borrego, B., Lorenzo, G., Mota-Morales, J. D., Almanza-Reyes, H., Mateos, F., López-Gil, E., de la Losa, N., Burmistrov, V.A., Pestryakov, A.N., Brun, A. & Bogdanchikova, N. (2016). Potential application of silver nanoparticles to control the infectivity of Rift Valley fever virus in vitro and in vivo. *Nanomedicine: Nanotechnology, Biology and Medicine*, 12(5), 1185-1192.

Bouberka, Z., Kacha, S., Kameche, M., Elmaleh, S. & Derriche, Z. (2005). Sorption study of an acid dye from an aqueous solutions using modified clays. *Journal of Hazardous Materials*, 119 (1-3), 117-124.

Boulaiche, W., Hamdi, B., & Trari, M. (2019). Removal of heavy metals by chitin: equilibrium, kinetic and thermodynamic studies. *Applied Water Science*, 9(2), 39.

Boyd, C. E. & Tucker, C. S. (2019). Water quality. *Aquaculture: Farming Aquatic Animals and Plants; John Wiley & Sons: Chichester, West Sussex, UK*, 63-92.

Bozorgi, M., Abbasizadeh, S., Samani, F. & Mousavi, S. E. (2018). Performance of synthesized cast and electrospun PVA/chitosan/ZnO-NH 2 nano-adsorbents in single and simultaneous adsorption of cadmium and nickel ions from wastewater. *Environmental Science and Pollution Research*, *25*(18), 17457-17472.

Brokesh, A. M. & Gaharwar, A. K. (2020). Inorganic biomaterials for regenerative medicine. *ACS Applied Materials and Interfaces*, *12*(5), 5319-5344.

Brown, B., Parker, C. B., Stoner, B. R. & Glass, J. T. (2011). Growth of vertically aligned bamboo-like carbon nanotubes from ammonia/methane precursors using a platinum catalyst.*Carbon*, 49(1), 266-274.

Butt, B. Z. (2020). Nanotechnology and Waste Water Treatment. In *Nanoagronomy* (Page 153-177). *Springer*, Cham. 17(1): 345-56

Byon, H. R., Lim, H. S., Song, H. J. & Choi, H. C. (2007). A synthesis of high purity single-walled carbon nanotubes from small diameters of cobalt nanoparticles by using oxygen-assisted chemical vapor deposition process.*Bulletin of the Korean Chemical Society*, 28(11), 2056-2060.

Carter, C. B. & Williams, D. B. (Eds.). (2016). *Transmission electron microscopy: Diffraction, imaging, and spectrometry*. *Springer, 3, 1-7*

Castle, A. B., Gracia-Espino, E., Nieto-Delgado, C., Terrones, H., Terrones, M. & Hussain, S. (2011). Hydroxyl-functionalized and N-doped multiwalled carbon nanotubes decorated with silver nanoparticles preserve cellular function.*ACS nano*, 5(4), 2458-2466.

Çelik, Y., Çelik, A., Flahaut, E. & Suvaci, E. (2016). Anisotropic mechanical and functional properties of graphene-based alumina.*Unpublished*

Chang, C. C., Yang, M. H., Wen, H. M. & Chern, J. C. (2002). Estimation of total flavonoid content in propolis by two complementary colorimetric methods. *Journal of Food and Drug Analysis*, *10*(3), 2-13.

Chen, B. H., Wang, B. W., Gao, P. Z., Zhang, P. & Chen, H. H. (2021). Effects of raw particle size and annealing on microstructure, electrical and mechanical behaviors of ZnO-based varistors. *Journal of Alloys and Compounds*, *872*, 159638.

Chen, C. M., Dai, Y. M., Huang, J. G. & Jehng, J. M. (2006). Intermetallic catalyst for carbon nanotubes (CNTs) growth by thermal chemical vapor deposition method.*Carbon*, 44(9) 1808-1820

Chen, C., Hu, J., Shao, D., Li, J. & Wang, X. (2009). Adsorption behavior of multiwall carbon nanotube/iron oxide magnetic composites for Ni (II) and Sr (II).*Journal of Hazardous Materials*, 164(2-3), 923-928.

Chen, T., Foo, C. & Tsang, S. C. E. (2021). Interstitial and substitutional light elements in transition metals for heterogeneous catalysis. *Chemical Science*, *12*(2), 517-532.

Cheng, N., Wang, B., Wu, P., Lee, X., Xing, Y., Chen, M. & Gao, B. (2021). Adsorption of emerging contaminants from water and wastewater by modified biochar: A review. *Environment. 19(1), 11-18*

Cho, H. H., Wepasnick, K., Smith, B. A., Bangash, F. K., Fairbrother, D. H. & Ball, W. P. (2010). Sorption of aqueous Zn [II] and Cd [II] by multiwall carbon nanotubes: the relative roles of oxygen-containing functional groups and graphenic carbon. *Langmuir*, 26(2), 967-981.

Coetzee, D. J., McGovern, P. M., Rao, R., Harnack, L. J., Georgieff, M. K. & Stepanov, I. (2016). Measuring the impact of manganese exposure on children's neurodevelopment: advances and research gaps in biomarker-based approaches.*Environmental Health*, 15(1), 1-20.

Condon, J. B. (2019). Surface Area and Porosity Determinations by Physisorption: Measurement, Classical Theories and Quantum Theory. *Elsevier*., 1, 8-9

Črešnar, K. P., Zemljič, L. F., Papadopoulos, L., Terzopoulou, Z., Zamboulis, A., Klonos, P. A., Bikiaris, D.N., Kyritsis, A. & Pissis, P. (2021). Effects of Ag, ZnO and TiO2 nanoparticles at low contents on the crystallization, semicrystalline morphology, interfacial phenomena and segmental dynamics of PLA. *Materials Today Communications*, *27*, 102192.

Crini, G., Lichtfouse, E., Wilson, L. D. & Morin-Crini, N. (2018). Adsorption-oriented processes using conventional and non-conventional adsorbents for wastewater treatment. In Green adsorbents for pollutant removal, Springer, 23-71.

Crini, G., Lichtfouse, E., Wilson, L. D. & Morin-Crini, N. (2019). Conventional and non-conventional adsorbents for wastewater treatment. *Environmental Chemistry Letters*, *17*(1), 195-213.

Cunningham, J., Al-Sayyed, G. & Srijaranai, S. (2018). Adsorption of model pollutants onto TiO_2 particles in relation to photoremediation of contaminated water. In *Aquatic and Surface Photochemistry* (Page 317-348). CRC Press.

Dą'browski, A. (2001). Adsorption from theory to practice. *Advances in Colloid and Interface Science*, 93(1-3), 135-224.

Dadi, D., Stellmacher, T., Senbeta, F., Van passel, S. & Azadi, H. (2016). Environmental and Health Impacts of Effluents from Textile Industries in Ethiopia: The case of Gelan and Dukem, *Oromia Regional State,* 1, 1-26.

Daoush, W. M. & Hong, S. H. (2013).Synthesis of Multi-Walled Carbon Nanotubes/Silver Nanoparticle Powders by Chemiacal Reduction in Aqueous Solution.*Journal of Experimental Nanoscience*, 8(5), 578-587.

Dechnik, J., Janiak, C. & De, S. (2016). Aluminium fumarate metal-organic framework: a super adsorbent for fluoride from water. *Journal of Hazardous Materials*, 303, 10-20.

Deshmukh, S. P., Patil, S. M., Mullani, S. B. & Delekar, S. D. (2019). Silver nanoparticles as an effective disinfectant: A review. *Materials Science and Engineering*: C, 97, 954-965.

Dinh, N. X., Chi, D. T., Lan, N. T., Lan, H., Tuan, H. V., Quy, N. V., Phan, V. N., Huy, T. Q. & Le, A. (2015). Water-Dispersible Silver Nanoparticles-Decorated Carbon Nanomaterials. *Applied Physics A*, 119, 85-95.

Dirisu, C. G., Mafiana, M. O., Dirisu, G. B. & Amodu, R. (2016).Level of pH in drinking water of an oil and gas producing community and perceived biological and health implications. *European Journal of Basic and Applied Sciences*, 3(3), 12-18.

Divya, K., Kurian, L. C., Vijayan, S. & Manakulam Shaikmoideen, J. (2016). Green synthesis of silver nanoparticles by Escherichia coli: Analysis of antibacterial activity. *Journal of Water and Environmental Nanotechnology*, 1(1), 63-74.

Eatemadi, A., Daraee, H., Karimkhanloo, H., Kouhi, M., Zarghami, N., Akbarzadeh, A. & Joo, S. W. (2014). Carbon nanotubes: properties, synthesis, purification, and medical applications. *Nanoscale Research Letters*, 9(1), 1-13.

Ebadollahzadeh, H. & Zabihi, M. (2020). Competitive adsorption of methylene blue and Pb (II) ions on the nano-magnetic activated carbon and alumina. *Materials Chemistry and Physics*, *248*, 122893.

Ebrahimi, P., Changizi, R., Ghobadi, S., Shohreh, P. & Vatandoust, S. (2020). Effect of Nano-Fe as Feed Supplement on Growth Performance, Survival Rate, Blood Parameters and Immune Functions of the Stellate Sturgeon (Acipenser stellatus). *Russian Journal of Marine Biology*, *46*(6), 493-500.

EFSA Panel on Additives and Products or Substances used in Animal Feed (FEEDAP). (2013). Scientific Opinion on the safety and efficacy of manganese compounds (E5) as feed additives for all species: manganese chelate of amino acids, hydrate, based on a dossier submitted by Zinpro Animal Nutrition Inc. *EFSA Journal*, *11*(8), 3324.

EFSA Panel on Additives and Products or Substances used in Animal Feed (FEEDAP), Bampidis, V., Azimonti, G., Bastos, M. D. L., Christensen, H., Dusemund, B., Durjava, M.F., Kouba, M., López-Alonso, M., López Puente, S. & López-Gálvez, G. (2021). Safety and efficacy of a feed additive consisting of manganese chelate of ethylenediamine for all animal species (Zinpro Animal Nutrition (Europe), Inc.). *EFSA Journal*, *19*(3), e06468.

EFSA Panel on Additives and Products or Substances used in Animal Feed (FEEDAP), Bampidis, V., Azimonti, G., Bastos, M. D. L., Christensen, H., Dusemund, B., Durjava, M.F., Kouba, M., & Ramos, F. (2020). Safety and efficacy of

Manganese chelates of lysine and glutamic acid as feed additive for all animal species. *EFSA Journal*, *18*(2), e06001.

El-Kady, A. A., & Abdel-Wahhab, M. A. (2018). Occurrence of trace metals in foodstuffs and their health impact. *Trends in Food Science & Technology*, *75*, 36-45.

Elmorsi, T. M. (2011). Equilibrium isotherms and kinetic studies of removal of methylene blue dye by adsorption onto miswak leaves as a natural adsorbent. *Journal of Environmental Protection*, 2(06), 817.

El-Sayed, G. O., Yehia, M. M. & Asaad, A. A. (2014). Assessment of activated carbon prepared from corncob by chemical activation with phosphoric acid. *Water Resources and Industry*, 7, 66-75.

Elsupikhe, R. F., Shameli, K., Ahmad, M. B., Ibrahim, N. A. & Zainudin, N. (2015). Green sonochemical synthesis of silver nanoparticles at varying concentrations of κ-carrageenan. *Nanoscale Research Letters*, 10(1), 1-8.

Emam-Ismail, M., El-Hagary, M., Shaaban, E. R., Moustafa, S. H. & Gad, G. M. A. (2019). Spectroscopic ellipsometry and morphological characterizations of nanocrystalline Hg1-xMnxO oxide diluted magnetic semiconductor thin films. *Ceramics International*, 45(7), 8380-8387.

Emodi, E. E. (2015). Empirical Analysis of the Effects of Household Solid Waste Disposal on the Residential Environmental Quality of Enugu Nigeria.*Sacha Journal of Environmental Studies*. 1, 7484.

Environmental Protection Agency (EPA). (2007). Monitoring and Assessing water quality, Volunteer Stream Monitoring Methods Manual, Chapter 5 section 2 Dissolved Oxygen and Biochemical Oxygen Demand. www.epa.gov.

EPA (2013). Energy efficiency in water and wastewater facilities: A guide to developing and implementing greenhouse gas reduction programs. *US Environmental Protection Agency Office of Water, Washington, D.C., USA.*

EPA. (1997). United States Environmental Protection Agency. Volunteers Stream Monitoring: A Methods Manual.

European Food Safety Authority (EFSA), Arcella, D., Gergelova, P., Innocenti, M. L., López-Gálvez, G. & Steinkellner, H. (2019). Occurrence data of nickel in feed and animal exposure assessment. *EFSA Journal*, *17*(6), e05754.

European Food Safety Authority (EFSA). (2004). "Opinion of the Scientific Panel on additives and products or substances used in animal feed (FEEDAP) on the re-evaluation of coccidiostat Sacox® 120 microGranulate in accordance with article 9G of Council Directive 70/524/EEC." *EFSA Journal,* 2(7): 76.

Fakayode, S. O. (2005). Impact assessment of industrial effluent on water quality of the receiving Alaro River in Ibadan, Nigeria. *African Journal of Environmental Assessment and Management*, 10, 1-13.

Fan, H., Ma, Y., Wan, J., Wang, Y., Li, Z. & Chen, Y. (2020).Adsorption properties and mechanisms of novel biomaterials from banyan aerial roots via simple modification for ciprofloxacin removal. *Science of The Total Environment*, 708, 134630.

Ferreira, A. M., Roque, É. B., Fonseca, F. V. D. & Borges, C. P. (2015). High flux microfiltration membranes with silver nanoparticles for water disinfection. *Desalination and Water Treatment*, 56(13), 3590-3598.

Fissan, H., Ristig, S., Kaminski, H., Asbach, C. & Epple, M. (2014). Comparison of different characterization methods for nanoparticle dispersions before and after aerosolization. *Analytical Methods*, 6(18), 7324-7334.

Fletcher, A. J. (2008). Porosity and sorption behaviour.Adsorption.

Fosso-kankeu, E., Mittal H., Waanders, F. & Sinha, S. (2017).Thermodynamic properties and adsorption behaviour of hydrogel nanocomposites for cadmium removal from mine effluents, *Journal of Industrial and Engineering Chemistry*. 48 (2017) 151–161.

Francis, S., Joseph, S., Koshy, E. P. & Mathew, B. (2017). Green synthesis and characterization of gold and silver nanoparticles using *Mussaenda glabrata* leaf extract and their environmental applications to dye degradation. *Environmental Science and Pollution Research*, 24 (21), 17347-17357.

Geerdink, R. B., van den Hurk, R. S. & Epema, O. J. (2017). Chemical oxygen demand: Historical perspectives and future challenges. *Analytica Chimica Acta*, *961*, 1-11.

Geethalakshmi, R. & Sarada, D. V. L. (2012). Gold and silver nanoparticles from Trianthema decandra: synthesis, characterization, and antimicrobial properties. *International Journal of Nanomedicine*, 7, 5375.

Genchi, G., Carocci, A., Lauria, G., Sinicropi, M. S. & Catalano, A. (2020). Nickel: Human health and environmental toxicology. *International Journal of Environmental Research and Public Health*, *17*(3), 679.

Gharibzahedi, S. M. T. & Jafari, S. M. (2017). The importance of minerals in human nutrition: Bioavailability, food fortification, processing effects and nanoencapsulation. *Trends in Food Science and Technology*, *62*, 119-132.

Giardino, C., Bresciani, M., Braga, F., Cazzaniga, I., De Keukelaere, L., Knaeps, E. & Brando, V. E. (2017). Bio-optical modeling of total suspended solids. In Bio-optical Modeling and Remote Sensing of Inland Waters. *Elsevier*, 1, 129-156.

Gopinath, S. M., Rak esh, C. K., Murthy, T. N. & Dayananda, K. S. (2012). Preliminary phytochemical evaluation of leaf extracts of *Gymnema sylvestre*, *Phyllanthus* *amarus*, *Phyllanthus reticulatus* of Siddarabetta, Tumkur district, Karnataka. *International Journal of Pharmacognosy and Phytochemical Research*, 4(3), 109-111

Granbohm, H., Kulmala, K., Iyer, A., Ge, Y. & Hannula, S. P. (2017). Preparation and photocatalytic activity of quaternary GO/TiO_2/Ag/AgCl nanocomposites. *Water, Air & Soil Pollution*, *228*(4), 127.

Gul, H. & Nasreen, S. (2018). Heavy Metal Uptake From Contaminated Water Using Carbon Nanotubes: A Review. *Environmental Contaminants Reviews (ECR)*, 1(2), 4-8.

Gupta, A. & Balomajumder, C. (2015). Simultaneous adsorption of Cr (VI) and phenol onto tea waste biomass from binary mixture: multicomponent adsorption, thermodynamic and kinetic study. *Journal of Environmental Chemical Engineering*, 3(2), 785-796.

Gupta, V., Moradi, O., Tyagi, I., Agarwal, S., Sadegh, H., Shahryari-Ghoshekandi, R., Makhlouf, A., Goodarzi, M., Garshasbi, A. (2016). Study on the removal of heavy metal ions from industry waste by carbon nanotubes: effect of the surface modification: a review. *Critical Review on Environmental Science and Technology*. 46(2), 93–118.

Gurunathan, S. & Kim, J. H. (2016).Synthesis, toxicity, biocompatibility, and biomedical applications of graphene and graphene-related materials.*International Journal of Nanomedicine*, 11, 1927.

Gurunathan, S., Han, J. W., Kwon, D. N. & Kim, J. H. (2014).Enhanced antibacterial and anti-biofilm activities of silver nanoparticles against Gram-negative and Gram-positive bacteria. *Nanoscale Research Letters*, 9(1), 1-17.

Gusain, R., Kumar, N., & Ray, S. S. (2020). Recent advances in carbon nanomaterial-based adsorbents for water purification. *Co-ordination Chemistry Reviews*, *405*, 213111.

Hagarová, I. & Nemček, L. (2021). Application of Metallic Nanoparticles and Their Hybrids as Innovative Sorbents for Separation and Pre-concentration of Trace Elements by Dispersive Micro-Solid Phase Extraction: A Minireview. *Frontiers in Chemistry*, *9*, 302.

Haldorai, Y., Kharismadewi, D., Tuma, D. & Shim, J. J. (2015).Properties of chitosan/magnetite nanoparticles composites for efficient dye adsorption and antibacterial agent.*Korean Journal of Chemical Engineering*, 32(8), 1688-1693.

Halilu, T., Chalie, A. & Yilma, D. (2018). Analysis of the level of some selected physicochemical parameters present in wastewater effluent discharged from Wolkite University, Gurage Zone, Ethiopia. *Journal of Analytical and Bioanalytical Techniques*, 9(5), 413.

Hallajiqomi, M. & Eisazadeh, H. (2017). Adsorption of manganese ion using polyaniline and it's nanocomposite: Kinetics and isotherm studies. *Journal of Industrial and Engineering Chemistry*, *55*, 191-197.

Hassan, Y. I., Lahaye, L., Gong, M. M., Peng, J., Gong, J., Liu, S., Gay, C.G. & Yang, C. (2018). Innovative drugs, chemicals, and enzymes within the animal production chain. *Veterinary Research*, *49*(1), 1-17.

Hennebel, T., Van Nevel, S., Verschuere, S., De Corte, S., De Gusseme, B., Cuvelier, C. & Verstraete, W. (2011). Palladium nanoparticles produced by fermentatively cultivated bacteria as catalyst for diatrizoate removal with biogenic hydrogen. *Applied Microbiology and Biotechnology*, 91(5), 1435-1445.

Herrera-Ramirez, J. M., Perez-Bustamante, R. & Aguilar-Elguezabal, A. (2019).An overview of the synthesis, characterization, and applications of carbon nanotubes.*Carbon-Based Nanofillers and Their Rubber Nanocomposites*, 47-75.

Herrero-Latorre, C., Barciela-García, J., García-Martín, S. & Pena-Crecente, R. M. (2018). Graphene and carbon nanotubes as solid phase extraction sorbents for the speciation of chromium: A review. *Analytica Chimica Acta*, 1002, 1-17.

Hu, Y., Cheng, H. & Tao, S. (2017). Environmental and human health challenges of industrial livestock and poultry farming in China and their mitigation. *Environment International*, *107*, 111-130.

Hu, Z., Tong, G., Lin, D., Chen, C., Guo, H., Xu, J. & Zhou, L. (2016). Graphene-reinforced metal matrix nanocomposites–a review. *Materials Science and Technology*, 32(9), 930-953.

Huang, X., Chang, X., He, Q., Cui, Y., Zhai, Y. & Jiang, N. (2008). Tris (2-aminoethyl) amine functionalized silica gel for solid-phase extraction and preconcentration of Cr (III), Cd (II) and Pb (II) from waters. *Journal of Hazardous Materials*, 157(1), 154-160.

Huang, X., Yang, J., Hou, B., Wang, J., Tian, B., Bi, J., Wang, N. & Li, X. (2019). Nanomaterials for the Removal of Heavy Metals from Wastewater. *Nanomaterial*, 9, 424.

Hussain, J., Husain, I., Arif, M. & Gupta, N. (2017).Studies on heavy metal contamination in Godavari river basin. *Applied Water Science*, 7(8), 4539-4548.

Ibisi, N. E. & Asoluka, C. A. (2018). Use of agro-waste (Musa paradisiaca peels) as a sustainable biosorbent for toxic metal ions removal from contaminated water. *Chemistry International*, *4*(1), 52.

Iftekhar, S., Ramasamy, D. L., Srivastava, V., Asif, M. B. & Sillanpää, M. (2018). Understanding the factors affecting the adsorption of Lanthanum using different adsorbents: A critical review. *Chemosphere*, 204, 413-430.

Iijima, S. (1991). Helical microtubules of graphitic carbon. *Nature*, 354 (6348), 56–58.

Inyinbor, A. A., Adebesin, B. O., Oluyori, A. P., Adelani,-Akande, T. A., Dada, A. O. & Oreofe, T. A. (2018). Water Pollution: Effects, Prevention, and Climatic Impact, Water Challenges of an Urbanizing World, Matjaz Glavan, *Intechopen*, 3, 1-6.

Ipek, I., Kabay, N. & Yüksel, M. (2017). Separation of bisphenol A and phenol from water by polymer adsorbents: Equilibrium and kinetics studies. *Journal of Water Process Engineering*, 16, 206-211.

Islam, M. S., Akter, N., Rahman, M. M., Shi, C., Islam, M. T., Zeng, H. & Azam, M. S. (2018). Mussel-inspired immobilization of silver nanoparticles toward antimicrobial cellulose paper. *ACS Sustainable Chemistry & Engineering*, 6(7), 9178-9188.

Jatoi, A. W., Ogasawara, H., Kim, I. S. & Ni, Q. Q. (2020).Cellulose acetate/multi-wall carbon nanotube/Ag nanofiber composite for antibacterial applications.*Materials Science and Engineering*: C, 110, 110679.

Jebril, S., Jenana, R. K. B. & Dridi, C. (2020). Green synthesis of silver nanoparticles using Melia azedarach leaf extract and their antifungal activities: In vitro and in vivo. *Materials Chemistry and Physics*, *248*, 122898.

Ji, Y., Wen, Y., Zhang, S., Zhang, J. & Cai, G. (2019). A Simple Low Cost Method to Prepare Lignocellulose Composites for Efficient Removal of Cd (II) from Wastewater. *Polymers*, 11(711).

Jiang, D., Yang, Y., Huang, C., Huang, M., Chen, J., Rao, T. & Ran, X. (2019). Removal of the heavy metal ion nickel (II) via an adsorption method using flower globular magnesium hydroxide. *Journal of Hazardous Materials*, *373*, 131-140.

John, T., Gladytz, A., Kubeil, C., Martin, L. L., Risselada, H. J. & Abel, B. (2018). Impact of nanoparticles on amyloid peptide and protein aggregation: a review with a focus on gold nanoparticles. *Nanoscale*, 10(45), 20894-20913.

Johnson, J. A., Makis, J. J., Marvin, K. A., Rodenbusch, S. E. & Stevenson, K. J. (2013). Size-dependent hydrogenation of p-nitrophenol with Pd nanoparticles synthesized with poly (amido) amine dendrimer templates. *The Journal of Physical Chemistry C*, 117(44), 22644-22651.

Jung, J. H., Oh, H. C., Noh, H. S., Ji, J. H. & Kim, S. S. (2006). Metal nanoparticle generation using a small ceramic heater with a local heating area. *Journal of Aerosol Science*, 37(12), 1662-1670.

Kadam, J., Madiwale, S., Bashte, B., Dindorkar, S., Dhawal, P. & More, P. (2020). Green mediated synthesis of palladium nanoparticles using aqueous extract of Gymnema sylvestre for catalytic reduction of Cr (VI). *SN Applied Sciences*, 2(11), 1-13.

Kalhapure, R. S., Sonawane, S. J., Sikwal, D. R., Jadhav, M., Rambharose, S., Mocktar, C. & Govender, T. (2015). Solid lipid nanoparticles of clotrimazole silver complex: an efficient nano antibacterial against *Staphylococcus aureus* and MRSA. *Colloids and Surfaces B: Biointerfaces*, 136, 651-658.

Kambale, E. K., Nkanga, C. I., Mutonkole, B. P. I., Bapolisi, A. M., Tassa, D. O., Liesse, J. M. I., Krause, R.W. & Memvanga, P. B. (2020). Green synthesis of antimicrobial silver nanoparticles using aqueous leaf extracts from three Congolese plant species (Brillantaisia patula, Crossopteryx febrifuga and Senna siamea). *Heliyon*, *6*(8), e04493.

Kandah, M. I. & Meunier, J. L. (2007). Removal of nickel ions from water by multi-walled carbon nanotubes. *Journal of Hazardous Materials*, 146(1-2), 283-288.

Kang, S., Mauter, M. S. & Elimelech, M. (2008). Physicochemical determinants of multiwalled carbon nanotube bacterial cytotoxicity. *Environmental Science & Technology*, 42(19), 7528-7534.

Kara, I., Tunc, D., Sayin, F. & Akar, S. T. (2018). Study on the performance of metakaolin based geopolymer for Mn (II) and Co (II) removal. *Applied Clay Science*, *161*, 184-193.

Karunadasa, H. I. & Solis-Ibarra, D. (2019). U.S. Patent No. 10, 272, 384. Washington, DC: U.S. Patent and Trademark Office.

Kasperiski, F. M., Lima, E. C., Umpierres, C. S., dos Reis, G. S., Thue, P. S., Lima, D. R., Dias, S. L., Saucier, C. & da Costa, J. B. (2018). Production of porous activated carbons from Caesalpinia ferrea seed pod wastes: highly efficient removal of captopril from aqueous solutions. *Journal of Cleaner Production*, 197, 919-929.

Kaviya, S., Santhanalakshmi, J. & Viswanathan, B. (2011). Green synthesis of silver nanoparticles using *Polyalthia longifolia* leaf extract along with D-sorbitol: study of antibacterial activity. *Journal of Nanotechnology*, 1, 7-15.

Kennedy, B., Peura, S., Hammar, U., Vicenzi, S., Hedman, A., Almqvist, C., Andolf, E., Pershagen, G., Dicksved, J., Bertilsson, S. & Fall, T. (2010). Oral microbiota development in early childhood. *Scientific Reports*, 9(1), 1-14.

Khan, N., Hussain, S. T., Saboor, A., Jamila, N. & Kim, K. S. (2013). Physicochemical investigation of the drinking water sources from Mardan, Khyber Pakhtunkhwa, Pakistan. *International Journal of Physical Sciences*, 8(33), 1661-1671.

Khan, W. S., Hamadneh, N. N. & Khan, W. A. (2016). Polymer nanocomposites–synthesis techniques, classification and properties. *Science and applications of Tailored Nanostructures*, 50, 137-145.

Khatami, M., Mehnipor, R., Poor, M. H. S. & Jouzani, G. S. (2016). Facile biosynthesis of silver nanoparticles using Descurainia sophia and evaluation of their antibacterial and antifungal properties. *Journal of Cluster Science*, 27(5), 1601-1612.

Kolawole, A. O., Olaleye, M. T. & Ajele, J. O. (2007). Antioxidant properties and Glutathione S-transferases inhibitory activity of *Alchornea cordifolia* leaf extract in Acetaminophen toxicity. *Iranian Journal of Pharmacology and Therapeutics*, 6(1), 63-70.

Krishnaraj, C., Jagan, E. G., Ramachandran, R., Abirami, S. M., Mohan, N. & Kalaichelvan, P. T. (2012).Effect of biologically synthesized silver nanoparticles on *Bacopa monnieri* (Linn.) Wettest plant growth metabolism. *Process Biochemistry*, 47(4), 651-658.

Krishnaveni, M., Asiri, A. M. & Anandan, S. (2020). Ultrasound-assisted synthesis of unzipped multiwalled carbon nanotubes/titanium dioxide nanocomposite as a promising next-generation energy storage material. *Ultrasonics Sonochemistry*, 66, 105105.

Kruis, F. E., Fissan, H. & Rellinghaus, B. (2000). Sintering and evaporation characteristics of gas-phase synthesis of size-selected PbS nanoparticles. *Materials Science and Engineering: B*, 69, 329-334.

Kumar, A., Jigyasu, D. K., Subrahmanyam, G., Mondal, R., Shabnam, A. A., Cabral-Pinto, M. M. S., Malyan, S.K., Chaturvedi, A.K., Gupta, D.K., Fagodiya, R. K. & Bhatia, A. (2021). Nickel in terrestrial biota: Comprehensive review on contamination, toxicity, tolerance and its remediation approaches. *Chemosphere*, 129996.

Kyaw, S. T., Maung, M. M. & Aung, M. K. T. (2018). X-ray diffraction characterization for optimal crystallite aggregates of phyto-synthesized silver nanoparticles (agnps) by *Ocimum sanctum* l. Leaf extract. *Journal of Chemistry*, 2, 7-15

Largitte, L. & Pasquier, R. (2016). A review of the kinetics adsorption models and their application to the adsorption of lead by an activated carbon. *Chemical Engineering Research and Design*, 109, 495-504.

Larrude, D. G., Marcelo, E. H. M. & Freire Jr, F. L. (2014). A Wet Chemical Route for the Decoration of CNT with Silver naoparticle.*Carbon,* 654068, 1-7.

Lasheen, M. R., El-Sherif, I. Y., Sabry, D. Y., El-Wakeel, S. T. & El-Shahat, M. F. (2015). Removal of heavy metals from aqueous solution by multiwalled carbon nanotubes: equilibrium, isotherms, and kinetics. *Desalination and Water Treatment*, *53*(13), 3521-3530.

Lee, S. J., Jeong, J. R., Shin, S. C., Kim, J. C. & Kim, J. D. (2004). Synthesis and characterization of superparamagnetic maghemite nanoparticles prepared by coprecipitation technique. *Journal of Magnetism and Magnetic Materials*, 282, 147-150.

Le-Minh, N., Sivret, E. C., Shammay, A. & Stuetz, R. M. (2018). Factors affecting the adsorption of gaseous environmental odors by activated carbon: A critical review. *Critical Reviews in Environmental Science and Technology*, 48(4), 341-375.

Lens, P. N. L., Visser, A., Janssen, A. J. H., Pol, L. H. & Lettinga, G. (1998). Biotechnological treatment of sulfate-rich wastewaters. *Critical Reviews in Environmental Science and Technology*, 28(1), 41-88.

Li, L., Gao, P., Gai, S., He, F., Chen, Y., Zhang, M. & Yang, P. (2016). Ultra small and highly dispersed Fe3O4 nanoparticles anchored on reduced graphene for supercapacitor application. *Electrochimica Acta*, 190, 566-573.

Li, X. & Lenhart, J. J. (2012). Aggregation and dissolution of silver nanoparticles in natural surface water. *Environmental Science & Technology*, 46(10), 5378-5386.

Li, Y. H., (2008). Carbon nanotubes-the promising adsorbent in wastewater treatment. *Journal of Physics: Conference Series*, 61, 140

Li, Y. H., Ding, J., Luan, Z., Di, Z., Zhu, Y., Xu, C., Wu, D. & Wei, B. (2003). Competitive adsorption of Pb2+, Cu2+ and Cd2+ ions from aqueous solutions by multiwalled carbon nanotubes. *Carbon*, 41(14), 2787-2792.

Li, Y., Wang, Z., Xie, X., Zhu, J., Li, R. & Qin, T. (2017). Removal of Norfloxacin from aqueous solution by clay-biochar composite prepared from potato stem and natural attapulgite. Colloids and Surfaces A: *Physicochemical and Engineering Aspects*, 514, 126-136.

Li, Y., Zimmerman, A. R., He, F., Chen, J., Han, L., Chen, H., Hu, X. & Gao, B. (2020). Solvent-free synthesis of magnetic biochar and activated carbon through ball-mill extrusion with Fe3O4 nanoparticles for enhancing adsorption of methylene blue. *Science of The Total Environment*, *722*, 137972.

Li, Z. & Yang, P. (2018). Review on Physicochemical, Chemical and Biological Processes for Pharmaceutical Wastewater.*Earth and Environmental Science*, 113, 012185.doi: 10.1088/1755/-1315/113/1/012185.

Lima, É. C., Adebayo, M. A. & Machado, F. M. (2015).Kinetic and equilibrium models of adsorption.In Carbon nanomaterials as adsorbents for environmental and biological applications. *Springer*, Cham.33-69

Lin, K., Wu, C. & Chang, J. (2014). Advances in synthesis of calcium phosphate crystals with controlled size and shape. *Acta Biomaterialia*, 10(10), 4071-4102.

Lingamdinne, L. P., Koduru, J. R. & Karri, R. R. (2019). A comprehensive review of applications of magnetic graphene oxide based nanocomposites for sustainable water purification. *Journal of Environmental Management*, 231, 622-634.

Liu, J., Fu, J., Ni, T. & Yang, Y. (2019). Fracture toughness improvement of multi-wall carbon nanotubes/graphene sheets reinforced cement paste. *Construction and Building Materials*, 200, 530-538.

Liu, X., Hu, X., Ao, X., Wu, X. & Ouyang, S. (2018). Community characteristics of aquatic organisms and management implications after construction of Shihutang Dam in the Gangjiang River, China. *Lake and Reservoir Management*, *34*(1), 42-57.

Liu, X., Lu, S., Liu, Y., Meng, W. & Zheng, B. (2017). Adsorption of sulfamethoxazole (SMZ) and ciprofloxacin (CIP) by humic acid (HA): characteristics and mechanism. *Royal Society of Chemistry A Advances*, *7*(80), 50449-50458.

Liu, Y. & Liu, Y. J. (2008). Biosorption isotherms, kinetics and thermodynamics. *Separation and Purification Technology*, *61*(3), 229-242.

Liu, Y., Hou, D. & Wang, G. (2004). A simple wet chemical synthesis and characterization of hydroxyapatite nanorods. *Materials Chemistry and Physics*, 86(1), 69-73.

Llorens, J. V., Soriano, S., Calap-Quintana, P., Gonzalez-Cabo, P. & Moltó, M. D. (2019). The role of iron in Friedreich’s ataxia: insights from studies in human tissues and cellular and animal models. *Frontiers in Neuroscience*, *13*, 75.

Lokhande, R. S., Singare, P. U. & Pimple, D. S. (2011). Study on physico-chemical parameters of waste water effluents from Taloja industrial area of Mumbai, India. *International Journal of Ecosystem, 1(1), 1-9.*

Lombard, W. A. (2020). The role of input costs in determining feed prices. *Stockfarm*, 10(4), 9-11.

Long, S., Zhao, L., Shi, T., Li, J., Yang, J., Liu, H., Mao, G., Qiao, Z. & Yang, Y. (2018). Pollution control and cost analysis of wastewater treatment at industrial parks in Taihu and Haihe water basins, China. *Journal of Cleaner Production*, 172, 2435-2442.

Long, Z., Zhan, Y., Li, F., Wan, X., He, Y., Hou, C. & Hu, H. (2017). Hydrothermal synthesis of graphene oxide/multiwalled carbon nanotube/Fe 3 O 4 ternary nanocomposite for removal of Cu (II) and methylene blue. *Journal of Nanoparticle Research*, *19*(9), 1-16.

Lu, D., Liu, Q., Zhang, T., Cai, Y., Yin, Y. & Jiang, G. (2016). Stable silver isotope fractionation in the natural transformation process of silver nanoparticles. *Nature Nanotechnology*, 11(8), 682-686.

Madian, M., Ummethala, R., Naga, A. O. A. E., Ismail, N., Rümmeli, M. H., Eychmüller, A. & Giebeler, L. (2017). Ternary CNTs/TiO2/CoO nanotube composites: improved anode materials for high performance lithium ion batteries. *Materials*, 10(6), 678.

Madima, N., Mishra, S. B., Inamuddin, I. & Mishra, A. K. (2020). Carbon-based nanomaterials for remediation of organic and inorganic pollutants from wastewater:A review. *Environmental Chemistry Letters*, 1-23.

Madrakian, T., Afkhami, A., Ahmadi, M. & Bagheri, H. (2011).Removal of some cationic dyes from aqueous solutions using magnetic-modified multi-walled carbon nanotubes. *Journal of Hazardous Materials*, 196, 109-114.

Maggini, S., Pierre, A. & Calder, P. C. (2018). Immune function and micronutrient requirements change over the life course. *Nutrients*, *10*(10), 1531.

Malaki, M., Xu, W., Kasar, A. K., Menezes, P. L., Dieringa, H., Varma, R. S. & Gupta, M. (2019). Advanced metal matrix nanocomposites. *Metals*, *9*(3), 330.

Malik, A. & Khan, S. (2014). Environmental Deterioration and Human Health. *Natural and Anthropogenic Determinants*, 421(2), 45.

Mallakpour, S. (2018). Ultrasonic-assisted fabrication of starch/MWCNT-glucose nanocomposites for drug delivery. *Ultrasonics Sonochemistry*, 40, 402-409.

Mananghaya, M. R., Santos, G. N. & Yu, D. (2019). Solubility of aminotriethylene glycol functionalized single wall carbon nanotubes: A density functional based tight binding molecular dynamics study. *Journal of Computational Chemistry*, *40*(8), 952-958.

Mehmood, M. A., Qadri, H., Bhat, R. A., Rashid, A., Ganie, S. A. & Dar, G. H. (2019). Heavy metal contamination in two commercial fish species of a trans-Himalayan freshwater ecosystem. *Environmental Monitoring and Assessment*, *191*(2), 104.

Meitei, M. D. & Prasad, M. N. V. (2014). Adsorption of Cu (II), Mn (II) and Zn (II) by Spirodela polyrhiza (L.) Schleiden: equilibrium, kinetic and thermodynamic studies. *Ecological Engineering*, *71*, 308-317.

Michiels, J. A., Kevers, C., Pincemail, J., Defraigne, J. O. & Dommes, J. (2012). Extraction conditions can greatly influence antioxidant capacity assays in plant food matrices. *Food Chemistry*, 130(4), 986-993.

Minnesota Pollution Control Agency (MPCA). (2009). Low Dissolved Oxygen in Water: Causes, Impact on Aquatic Life - An Overview. *Water Quality/Impaired Water*, 3-24.

Mishra, A. K. (2014). Nanocomposites in wastewater treatment.CRC press.

Mishra, S., Bharagava, R. N., More, N., Yadav, A., Zainith, S., Mani, S. & Chowdhary, P. (2019). Heavy metal contamination: an alarming threat to environment and human health. In *Environmental biotechnology: For sustainable future* (Page, 103-125). *Springer,* Singapore.

Mittal, A. K., Chisti, Y. & Banerjee, U. C. (2012). Synthesis of metallic nanoparticles using plant extracts. *Biotechnology Advances*, 31(2), 346-356.

Moghadam, A. D., Omrani, E., Menezes, P. L. & Rohatgi, P. K. (2015). Mechanical and tribological properties of self-lubricating metal matrix nanocomposites reinforced by carbon nanotubes (CNTs) and graphene–a review. *Composites Part B: Engineering*, 77, 402-420.

Mohamad, A. A., Ali, S. I. & El-Baz, F. K. (2013).Antioxidant and antibacterial activities of crude extracts and essential oils of *Syzygium cumini* leaves.*Plos one*, 8(4), e60269.

Mohamed, R. M. & Shawky, A. (2018). CNT supported Mn-doped ZnO nanoparticles: simple synthesis and improved photocatalytic activity for degradation of malachite green dye under visible light. *Applied Nanoscience*, 8(5), 1179-1188.

Mohan, A. C. & Renjanadevi, B. (2016).Preparation of zinc oxide nanoparticles and its characterization using scanning electron microscopy (SEM) and X-ray diffraction (XRD).*Procedia Technology*, 24, 761-766.

Mohd Zainol, M. K., Abdul-Hamid, A., Abu Bakar, F. & Pak Dek, S. (2009). Effect of different drying methods on the degradation of selected flavonoids in *Centella asiatica.International Food Research Journal*, 16(4), 531-537.

Mojica, M., Alonso, J. A. & Méndez, F. (2013).Synthesis of fullerenes.*Journal of Physical Organic Chemistry*, 26(7), 526-539.

Moosavi, A., Amooey, A. A. & Marzbali, M. H. (2020). Extraordinary adsorption of acidic fuchsine and malachite green onto cheap nano-adsorbent derived from eggshell. *Chinese Journal of Chemical Engineering*, 28(6), 1591-1602.

Morris, J. W. (2020). Nickel Speciation, Microbial Community Structure, and Chemical Attributes in the Rhizosphere of Nickel Hyperaccumulating and Non-accumulating Plants Growing in Serpentine Soils.*Separation and Purification Technology, 10-24*

Mousavi, S. V., Bozorgian, A., Mokhtari, N., Gabris, M. A., Nodeh, H. R. & Ibrahim, W. A. W. (2019). A novel cyanopropylsilane-functionalized titanium oxide magnetic nanoparticle for the adsorption of nickel and lead ions from industrial wastewater: Equilibrium, kinetic and thermodynamic studies. *Microchemical Journal*, *145*, 914-920.

Nagar, N. & Devra, V. (2018). Green synthesis and characterization of copper nanoparticles using *Azadirachta indica* leaves. *Materials Chemistry and Physics*, 213, 44-51.

Naithani, V., Nair, S. & Kakkar, P. (2006). Decline in antioxidant capacity of Indian herbal teas during storage and its relation to phenolic content. *Food Research International*, 39(2), 176-181.

National Population Inventory (NPI) (2019). National Pollutant Inventory, Australian Government Department of Environment and Energy, Canberra, Australia http://www.npi.gov.au/ (accessed 23/07/2019).

Natsuki, J., Natsuki, T. & Hashimoto, Y. (2015). A review of silver nanoparticles: synthesis methods, properties and applications. *International Journal of Material Sciences and Applications*, 4(5), 325-332.

Naushad, M., Alqadami, A. A., AlOthman, Z. A., Alsohaimi, I. H., Algamdi, M. S. & Aldawsari, A. M. (2019).Adsorption kinetics, isotherm and reusability studies for the removal of cationic dye from aqueous medium using arginine modified activated carbon.*Journal of Molecular Liquids*, 293, 111442.

Navaladian, S., Viswanathan, B., Varadarajan, T. K. & Viswanath, R. P. (2009). A rapid synthesis of oriented palladium nanoparticles by UV irradiation. *Nanoscale research letters*, *4*(2), 181-186.

Nguyen, T. K. O., Le, Q. T., Kanabkaew, T., Chitaporpan, S. & Le, T. N. H. (2020).Introduction to Environmental Management and Services.*TORUS 3-Toward an open Resource Using Services: Cloud Computing for Environmental Data*, 1-16

Nidheesh, P. V. & Gandhimathi, R. (2014). Effect of solution pH on the performance of three electrolytic advanced oxidation processes for the treatment of textile wastewater and sludge characteristics. *RSC Advances*, 4(53), 27946-27954.

Nigeria Industrial Standar (NIS). (2015). Nigeria Standard for Drinking Water Quality, NIS-554-2015, 16-17.

Nithya, K., Sathish, A., Kumar, P. S. & Ramachandran, T. (2018). Fast kinetics and high adsorption capacity of green extract capped superparamagnetic iron oxide nanoparticles for the adsorption of Ni (II) ions. *Journal of Industrial and Engineering Chemistry*, *59*, 230-241.

Niwa, T., Hatamoto, M., Yamashita, T., Noguchi, H., Takase, O., Kekre, K. A., Ang, W.S., Tao, G., Seah, H. & Yamaguchi, T. (2016). Demonstration of a full-scale plant using an UASB followed by a ceramic MBR for the reclamation of industrial wastewater.*Bioresource Technology*, 218, 1-8.

Ogu, G. I. & Akinnibosun, F. I. (2020). Health risks associated with heavy metals in commercial chicken meat via consumption within southern nigeria. *African Journal of Health, Safety and Environment*, *1*(1), 22-37.

Oloyede, O. I. (2005). Chemical profile of unripe pulp of Carica papaya. *Pakistan Journal of Nutrition*, 4(6), 379-381.

Olukosi, O. A., van Kuijk, S. & Han, Y. (2018). Copper and zinc sources and levels of zinc inclusion influence growth performance, tissue trace mineral content, and carcass yield of broiler chickens. *Poultry Science*, *97*(11), 3891-3898.

Osabohien, R., Adeleye, N. & DE Alwis, T. (2020).Agro-financing and food production in Nigeria. *Heliyon*, *6*(5), e04001.

Ouyang, M., Huang, J. L., & Lieber, C. M. (2002). Fundamental electronic properties and applications of single-walled carbon nanotubes. *Accounts of Chemical Research*, *35*(12), 1018-1025.

Ovais, M., Khalil, A. T., Islam, N. U., Ahmad, I., Ayaz, M., Saravanan, M. & Mukherjee, S. (2018). Role of plant phytochemicals and microbial enzymes in biosynthesis of metallic nanoparticles. *Applied Microbiology and Biotechnology*, *102*(16), 6799-6814.

Owlad, M., Kheireddine, Aroua, M., Daud, W. A. W. & Baroutians, S. (2009). Removal of Hexavalent Chromium-Contaminated Water and Wastewater: A Review. *Water, Air and Soil Pollution*, 200: 59-77.

Pallauf, J., Kauer, C., Most, E., Habicht, S. D., & Moch, J. (2012). Impact of dietary manganese concentration on status criteria to determine manganese requirement in piglets. *Journal of Animal Physiology and Animal Nutrition*, *96*(6), 993-1002.

Pandey, J. K., Swarnkar, R. K., Soumya, K. K., Dwivedi, P., Singh, M. K., Sundaram, S. & Gopal, R. (2014). Silver nanoparticles synthesized by pulsed laser ablation: as a potent antibacterial agent for human enteropathogenic gram-positive and gram-negative bacterial strains. *Applied Biochemistry and Biotechnology*, 174(3), 1021-1031.

Panigrahi, S., Kundu, S., Basu, S., Praharaj, S., Jana, S., Pande, S., Ghosh, S. K. & Pal, T. (2006). Cysteine functionalized copper organosol: synthesis, characterization and catalytic application. *Nanotechnology*, 17(21), 5461.

Park, C. M., Wang, D., Han, J., Heo, J. & Su, C. (2019). Evaluation of the colloidal stability and adsorption performance of reduced graphene oxide–elemental silver/magnetite nanohybrids for selected toxic heavy metals in aqueous solutions. *Applied Surface Science*, *471*, 8-17.

Patel, H. (2019). Fixed-bed column adsorption study: A comprehensive review. *Applied Water Science*, 9(3), 1-17.

Pathak, C. S., Mishra, D. D., Agarwala, V. & Mandal, M. K. (2013). Optical properties of ZnS nanoparticles prepared by high energy ball milling. *Materials Science in Semiconductor Processing*, *16*(2), 525-529.

Patra, C., Shahnaz, T., Subbiah, S. & Narayanasamy, S. (2020). Comparative assessment of raw and acid-activated preparations of novel Pongamia pinnata shells for adsorption of hexavalent chromium from simulated wastewater. *Environmental Science and Pollution Research*, 1-16.

Peng, S., He, J., Hu, J., Huang, X. & Jiang, P. (2015). Influence of functionalized MgO nanoparticles on electrical properties of polyethylene nanocomposites. *IEEE Transactions on Dielectrics and Electrical Insulation*, 22(3), 1512-1519.

Peng, X., Li, Y., Luan, Z., Di, Z., Wang, H., Tian, B. & Jia, Z. (2003).Adsorption of 1, 2-dichlorobenzene from water to carbon nanotubes.*Chemical Physics Letters*, 376(1-2), 154-158.

Pérez-López, B. & Merkoçi, A. (2012).Carbon nanotubes and graphene in analytical sciences. Microchimica Acta, 179(1-2), 1-16.

Petla, R. K., Vivekanandhan, S., Misra, M., Mohanty, A. K. & Satyanarayana, N. (2011). Soybean (Glycine max) leaf extract based green synthesis of palladium nanoparticles.

Poddar, M. K., Arjmand, M., Sundararaj, U. & Moholkar, V. S. (2018). Ultrasound-assisted synthesis and characterization of magnetite nanoparticles and poly (methyl methacrylate)/magnetite nanocomposites. *Ultrasonics Sonochemistry*, 43, 38-51.

Prasek, J., Drbohlavova, J., Chomoucka, J., Hubalek, J., Jasek, O., Adam, V. & Kizek, R. (2011). Methods for carbon nanotubes synthesis. *Journal of Materials Chemistry*, 21(40), 15872-15884.

Puett, C., Inscoe, C., Lu, J., Lee, Y. & Zhou, O. (2019). Generating synthetic mammograms for stationary 3D mammography. In Medical Imaging 2019: Physics of Medical Imaging 10948, 1094807). *International Society for Optics and Photonics*.

Qiu, L., Scheider, K., Radwan, S. A., Larkin, L. S., Saltonstall, C. B., Feng, Y., Zhang, X. & Norris, P. M. (2017). Thermal transport barrier in carbon nanotube array nano-thermal interface materials. *Carbon*, 120, 128-136.

Qu, J., Tian, X., Jiang, Z., Cao, B., Akindolie, M. S., Hu, Q. Feng, C., Feng, Y., Meng, X. & Zhang, Y. (2020). Multi-component adsorption of Pb (II), Cd (II) and Ni (II) onto microwave-functionalized cellulose: Kinetics, isotherms, thermodynamics, mechanisms and application for electroplating wastewater purification. *Journal of Hazardous Materials*, 387, 121718.

Rahman, G., Najaf, Z., Mehmood, A., Bilal, S., Mian, S. A. & Ali, G. (2019). An overview of the recent progress in the synthesis and applications of carbon nanotubes. *Journal of Carbon Research*, 5(1), 3.

Rajaura, R. S., Singhal, I., Sharma, K. N. & Srivastava, S. (2019). Efficient chemical vapour deposition and arc discharge system for production of carbon nano-tubes on a gram scale. *Review of Scientific Instruments*, 90(12), 123903.

Rao, Y., Han, F., Chen, Q., Wang, D., Xue, D., Wang, H. & Pu, S. (2019). Efficient degradation of diclofenac by LaFeO3-Catalyzed peroxymonosulfate oxidation, kinetics and toxicity assessment. *Chemosphere*, 218, 299-307.

Rashed, M. N. (2013). Adsorption Techniques for the Removal of Organic Pollutants from Water and Wastewater. *Intech Open Science*, 7(1); 167-194. doi:10.5772/54048.

Rashmi, M. A., Verghese, A., Shivashankar, S., Chakravarthy, A. K., Sumathi, M. & Kandakoor, S. (2017). Does change in tannin content in mango (Mangifera indica) fruits influence the extent of fruit fly (Bactrocera dorsalis Hendel) herbivory. *Journal of Entomology and Zoology Studies*, *5*(4), 381-385.

Rastkari, N., Ahmadkhaniha, R. & Yunesian, M. (2009).Single-walled carbon nanotubes as an effective adsorbent in solid-phase microextraction of low level methyl tert-butyl ether, ethyl tert-butyl ether and methyl tert-amyl ether from human urine. *Journal of Chromatography B*, 877(14-15), 1568-1574.

Rathouse, A. K. & Dhatwalia, V. k. (2016). Toxicity and Waste Management using Bioremediation, *IGI Global*, Hershey, *Intech Open Science*, 2, 1-13

Ravelo-Pérez, L. M., Herrera-Herrera, A. V., Hernández-Borges, J. & Rodríguez-Delgado, M. Á. (2010). Carbon nanotubes: solid-phase extraction. *Journal of Chromatography A*, 1217(16), 2618-2641.

Ray, P. Z. & Shipley, H. J. (2015). Inorganic nano-adsorbents for the removal of heavy metals and arsenic: A review. *RSC Advances*, 5(38), 29885-29907.

Razmi, F. A., Ngadi, N., Wong, S., Inuwa, I. M. & Opotu, L. A. (2019). Kinetics, thermodynamics, isotherm and regeneration analysis of chitosan modified pandan adsorbent. *Journal of Cleaner Production*, *231*, 98-109.

Rodriguez-Sanchez, L., Blanco, M. C. & Lopez-Quintela, M. A. (2000).Electrochemical synthesis of silver nanoparticles. *The Journal of Physical Chemistry B*, 104(41), 9683-9688.

Romero, V., Costas-Mora, I., Lavilla, I. & Bendicho, C. (2016).Graphene membranes as novel preconcentration platforms for chromium speciation by total reflection X-ray fluorescence. *RSC Advances*, 6(1), 669-676.

Sadegh, H., Ghoshekandi, R. S., Masjedi, A., Mahmoodi, Z. & Kazemi, M. (2016). A review on Carbon nanotubes adsorbents for the removal of pollutants from aqueous solutions. *International Journal of Nano Dimensions*. 7(2), 109.

Sadegh, H., Shahryari-Ghoshekandi, R., Tyagi, I., Agarwal, S. & Gupta, V.K. (2015). Kinetic and thermodynamic studies for alizarin removal from liquid phase using poly-2-hydroxyethyl methacrylate (PHEMA). *Journal of Molecular Liquids*, 207, 21–27

Saeidi, N. & Parvini, M. (2016). Accuracy of Dubinin-Astakhov and Dubinin-Radushkevich adsorption isotherm models in evaluating micropore volume of bentonite. *Periodica Polytechnica Chemical Engineering*, 60(2), 123-129.

Sahebian, S., Zebarjad, S.M., Vahdati Khaki, J. & Lazzeri, A. (2016). The Decoration of Multi-Walled Carbon Nanotubes with Nickel Oxide Nanoparticles using Chemical Method. *International Nanotechnology letter,* 6, 183-190.

Salam, H. A., Sivaraj, R. & Venckatesh, R. (2014). Green synthesis and characterization of zinc oxide nanoparticles from Ocimum basilicum L. var. purpurascens Benth.-Lamiaceae leaf extract. *Materials letters*, 131, 16-18.

Saminathan, K. (2015). Biosynthesis of silver nanoparticles using soil Actinomycetes Streptomyces sp. *International Journal of Current Microbiology and Applied Sciences*, 4(3), 1073-1083.

Sandoval, D. R., Yan, W., Michelsen, M. L. & Stenby, E. H. (2018). Influence of adsorption and capillary pressure on phase equilibria inside shale reservoirs. *Energy & Fuels*, 32(3), 2819-2833.

Sargazi, G., Afzali, D. & Mostafavi, A. (2019). A novel microwave assisted reverse micelle fabrication route for Th (IV)-MOFs as highly efficient adsorbent nanostructures with controllable structural properties to CO and CH4 adsorption: Design, and a systematic study. *Applied Organometallic Chemistry*, *33*(4), e4816.

Shaban, M., Hassouna, M. E., Nasief, F. M. & AbuKhadra, M. R. (2017). Adsorption properties of kaolinite-based nanocomposites for Fe and Mn pollutants from aqueous solutions and raw ground water: kinetics and equilibrium studies. *Environmental Science and Pollution Research*, *24*(29), 22954-22966.

Shahbeig, H., Bagheri, N., Ghorbanian, S. A., Hallajisani, A. & Poorkarimi, S. (2013). A new adsorption isotherm model of aqueous solutions on granular activated carbon. *World Journal of Modelling and Simulation*, 9(4), 243-254.

Shameli, K., Ahmad, M. B., Yunus, W. M. Z. W., Rustaiyan, A., Ibrahim, N. A., Zargar, M. & Abdollahi, Y. (2010).Green synthesis of silver/montmorillonite/chitosan bionanocomposites using the UV irradiation method and evaluation of antibacterial activity. *International Journal of Nanomedicine*, 5, 875.

Sharma, M., Singh, J., Hazra, S. & Basu, S. (2019). Adsorption of heavy metal ions by mesoporous ZnO and TiO_2/ZnO monoliths: adsorption and kinetic studies. *Microchemical Journal*, *145*, 105-112.

Sharma, R. K., Patel, S. & Pargaien, K. C. (2012). Synthesis, characterization and properties of Mn-doped ZnO nanocrystals. *Advances in Natural Sciences: Nanoscience and Nanotechnology*, 3(3), 035005.

Sharma, S. K. & Sanghi, R. (2012).Advances in Water Treatment and Pollution Prevention.*Springer*, *Dordrenht,* 3(1): 6-13

Shen, J., Wang, X., Zhang, L., Yang, Z., Yang, W., Tian, Z. & Tao, T. (2018). Size-selective adsorption of methyl orange using a novel nano-composite by encapsulating HKUST-1 in hyper-crosslinked polystyrene networks. *Journal of Cleaner Production*, 184, 949-958.

Shen, W., Li, X., Lu, X., Guo, W., Zhou, S. & Wan, Y. (2018). Experimental study and isotherm models of water vapor adsorption in shale rocks. *Journal of Natural Gas Science and Engineering*, *52*, 484-491.

Shin, H. S., Choi, H. C., Jung, Y., Kim, S. B., Song, H. J. & Shin, H. J. (2004). Chemical and size effects of nanocomposites of silver and polyvinyl pyrrolidone determined by X-ray photoemission spectroscopy. *Chemical Physics Letters*, 383(3-4), 418-422.

Silva, A. M., Lima, R. M. & Leão, V. A. (2012). Mine water treatment with limestone for sulfate removal. *Journal of Hazardous Materials*, 221, 45-55.

Singh, N. B. & Onuegbu, C. U. (2020). Nano-Minerals as Livestock Feed Additives. In *21st Century Nanoscience-A Handbook* (pp. 20-1). CRC Press.

Singh, S., Kapoor, D., Khasnabis, S., Singh, J. & Ramamurthy, P. C. (2021). Mechanism and kinetics of adsorption and removal of heavy metals from wastewater using nanomaterials. *Environmental Chemistry Letters*, 1-31.

Singh, V., Shrivastava, A. & Wahi, N. (2015). Biosynthesis of silver nanoparticles by plants crude extracts and their characterization using UV, XRD, TEM and EDX. *African Journal of Biotechnology*, 14(33), 2554-2567.

Song, Y., Kong, A., Ji, Y., He, B., Wang, H. & Li, J. (2019). Adsorption for copper (II) ion with chitosan-SP/PET composite adsorbent enhanced by electric field. *Adsorption Science & Technology*, 37(3-4), 274-287.

Srivastava, P., Yadav, A. K. & Mishra, B. K. (2015). The effects of microbial fuel cell integration into constructed wetland on the performance of constructed wetland. *Bioresource Technology*, 195, 223-230.

Stensberg, M. C., Wei, Q., Mc Lamore, E. S., Porterfield, D. M., Wei, A. & Sepulveda, M. S. (2011). Toxicological Studies on Silver Nanoparticles: Challenges and Opportunities in Assessment, Monitoring and Imaging. *Nanomedicine*, 6(5), 879-898.

Stillman, J. H. (2019). Heat waves, the new normal: summertime temperature extremes will impact animals, ecosystems, and human communities. *Physiology*, 34 (2), 86-100.

Sunar, N. M., Hamdan, R., Khalid, A., Hafizah, N., Zaidi, E., Azhar, A. T. S. & Muhamad, M. S. (2018). In-situ water quality assessment at recretional lake by using grab sampling technique. *Unpublished.*

Suryawanshi, P. L., Gumfekar, S. P., Bhanvase, B. A., Sonawane, S. H. & Pimplapure, M. S. (2018). A review on microreactors: Reactor fabrication, design, and cutting-edge applications. *Chemical Engineering Science*, 189, 431-448.

Swedish, E. P. A. (2006). Statute book of the Swedish EPA. General advice about small-scale household wastewater treatment facilities. Naturvårdsverkets författningssamling. Naturvårdsverkets allmänna råd om små avloppsanordningar för hushållsspillvatten.) NFS, 7.

Szabó, A., Perri, C., Csató, A., Giordano, G., Vuono, D. & Nagy, J. B. (2010).Synthesis methods of carbon nanotubes and related materials. *Materials*, 3(5), 3092-3140.

Taleshi, F. (2012). Evaluation of new processes to achieve a high yield of carbon nanotubes by CVD method. *International Nano Letters*, 2(1), 23.

Taman, R. I., Ossman, M. E., Mansoor, M. S. & Frag, H. A. (2015). Metal Oxide Nanoparticles as an Adsorbent for Removal of Cd (II) ions from Aqueous Solution. *Journal of Advanced Chemical Engineering*, 5, 3-8

Tandon, S. & Sai, N. (2020). Recycling of agriculture waste into efficient adsorbent. In Environmental Concerns and Sustainable Development. *Springer, Singapore*. 365-379

Tepeli, Y. & Anik, U. (2016). Preparation, characterization and electrochemical application of graphene-metallic nanocomposites. *Electroanalysis*, 28(12), 3048-3054.

Thangaswamy, S. J. K., Mir, M. A. & Muthu, A. (2021). Green synthesis of mono and bimetallic alloy nanoparticles of gold and silver using aqueous extract of Chlorella acidophile for potential applications in sensors. *Preparative Biochemistry & Biotechnology*, 1-10.

Thomas, M. R. (2017). "High-Fat and High-Protein Animal Feed Supplement and Process of Manufacture."*U.S. Patent Application No*. 15/607,288.

Tian, Y. & Wu, J. (2018). A comprehensive analysis of the BET area for nanoporous materials. *AIChE Journal*, *64*(1), 286-293.

Tien, D. C., Liao, C. Y., Huang, J. C., Tseng, K. H., Lung, J. K., Tsung, T. T., Kao, W. S. Tsai, T. H., Cheng, T. W. & Yu, B. S. (2008). Novel Technique for Preparing a Nano-Silver Water Suspension by the Arc-Discharge Method. *Review on Advance Material Science*, 18, 750–756

Torab-Mostaedi, M., Asadollahzadeh, M., Hemmati, A. & Khosravi, A. (2015). Biosorption of lanthanum and cerium from aqueous solutions by grapefruit peel: equilibrium, kinetic and thermodynamic studies. *Research on Chemical Intermediates*, *41*(2), 559-573.

Tran, H. N., Nguyen, D. T., Le, G. T., Tomul, F., Lima, E. C., Woo, S. H., Sarmah, A.K., Nguyen, H.Q., Nguyen, P.T., Nguyen, D. D. & Chao, H. P. (2019). Adsorption mechanism of hexavalent chromium onto layered double hydroxides-based adsorbents: A systematic in-depth review. *Journal of Hazardous Materials*, *373*, 258-270.

Turunc, E., Binzet, R., Gumus, I., Binzet, G. & Arslan, H. (2017). Green synthesis of silver and palladium nanoparticles using Lithodora hispidula (Sm.)

Griseb.(Boraginaceae) and application to the electrocatalytic reduction of hydrogen peroxide. *Materials Chemistry and Physics*, 202, 310-319.

U.S. Environmental Protection Agency. (2018). 2018 edition of the drinking water standards and health advisories tables (EPA 822-F-18-001). Retrieved from https://www.epa.gov /sites /production/files/ 2018-03/documents/dwtable2018.pdf

Uddin, M. K. (2017). A review on the adsorption of heavy metals by clay minerals, with special focus on the past decade. *Chemical Engineering Journal*, 308, 438-462.

Uma, K., Chong, S., Mohan, S. C., Jothivenkatachalam, K., Yang, T. C. K. & Lin, J. H. (2020). Multi-functional RGO-supported α-Fe_2O_3 nanocomposites for high-performance pseudocapacitors and visible light–driven photocatalytic applications. *Ionics*, 1-10.

Upadhyayula, V. K., Deng, S., Mitchell, M. C. & Smith, G. B. (2009). Application of carbon nanotube technology for removal of contaminants in drinking water: A review. *Science of the Total Environment*, 408(1), 1-13.

Vecitis, C. D., Zodrow, K. R., Kang, S. & Elimelech, M. (2010).Electronic-structure-dependent bacterial cytotoxicity of single-walled carbon nanotubes. *ACS nano*, 4(9), 5471-5479

Vijayakumar, M., Priya, K., Nancy, F. T., Noorlidah, A. & Ahmed, A. B. A. (2013). Biosynthesis, characterisation and anti-bacterial effect of plant-mediated silver nanoparticles using Artemisia nilagirica. *Industrial Crops and Products*, 41, 235-240.

Wang, J. & Guo, X. (2020). Adsorption isotherm models: Classification, physical meaning, application and solving method. *Chemosphere*, 127279.

Weber Jr, W. J. & Morris, J. C. (1963). Kinetics of adsorption on carbon from solution. *Journal of the sanitary engineering division*, 89(2), 31-59.

Wei, Y., Jiao, Y., An, D., Li, D., Li, W. & Wei, Q. (2019). Review of dissolved oxygen detection technology: From laboratory analysis to online intelligent detection. *Sensors*, *19*(18), 3995.

Wilkinson, J. M. & Lee, M. R. F. (2018). Use of human-edible animal feeds by ruminant livestock. *Animal*, *12*(8), 1735-1743.

Wolska, K. I. & Grudniak, A. M. (2020). Synergistic Activity of Nanoparticles and Other Antimicrobials Against Pathogenic Bacteria. In *Microbial Nanotechnology* (Page 241-255). CRC Press.

Wong, S., Ngadi, N., Inuwa, I. M. & Hassan, O. (2018). Recent advances in applications of activated carbon from biowaste for wastewater treatment: a short review. *Journal of Cleaner Prbroduction*, 175, 361-375.

World Health Organization (WHO).(2017). Guidelines for Drinking water Quality. *Fourth Edition. Incorporating First Addendum.* ISBN: 978-924-1549950.

Xie, J., Lai, L., Lin, L., Wu, D., Zhang, Z. & Kong, H. (2015). Phosphate removal from water by a novel zeolite/lanthanum hydroxide hybrid material prepared from coal fly ash. *Journal of Environmental Science and Health*, Part A, 50(12), 1298-1305.

Xu, Y., Yan, M. & Liu, Z. (2017). Synthesis & Characterization of Carbon Nanotubes Doped Carbon Aerogels. *IOP Conference Series Materials Science and Engineering*, 275, 012006.doi: 10.1088/1757-899x/275/1/012006.

Yagub, M.T.., Sen, T.K., Afroze, S. & Ang, H.M. (2014). Dye and its removal from aqueous solution by adsorption: a review, *Advance Colloid Interface Science*. 209 (2014) 172–184.

Yang, C. M., Park, J. S., An, K. H., Lim, S. C., Seo, K., Kim, B., Park, K.A., Han, S., Park, C.Y. & Lee, Y. H. (2005).Selective removal of metallic single-walled carbon nanotubes with small diameters by using nitric and sulfuric acids. *The Journal of Physical Chemistry B*, 109(41), 19242-19248.

Yang, F. & Massey, I. Y. (2019). Exposure routes and health effects of heavy metals on children. *Biometals*, *32*(4), 563-573.

Yang, G., Zhou, Y., Pan, H. B., Zhu, C., Fu, S., Wai, C. M., Du, D., Zhu, J. J. & Lin, Y. (2016). Ultrasonic-assisted synthesis of Pd–Pt/carbon nanotubes nanocomposites for enhanced electro-oxidation of ethanol and methanol in alkaline medium. *Ultrasonics Sonochemistry*, 28, 192-198.

Yin, Y., Rioux, R. M., Erdonmez, C. K., Hughes, S., Somorjai, G. A. & Alivisatos, A. P. (2004). Formation of hollow nanocrystals through the nanoscale Kirkendall effect. *Science*, 304(5671), 711-714.

Yu, F., Wu, Y. & Ma, J. (2012). Influence of the pore structure and surface chemistry on adsorption of ethylbenzene and xylene isomers by KOH-activated multi-walled carbon nanotubes. *Journal of Hazardous Materials*, 237, 102-109.

Yu, Y., Qiao, N., Wang, D., Zhu, Q., Fu, F., Cao, R., Wang, R., Liu, W. & Xu, B. (2019). Fluffy honeycomb-like activated carbon from popcorn with high surface area and well-developed porosity for ultra-high efficiency adsorption of organic dyes. *Bioresource Technology*, *285*, 121340.

Yuan, K., Song, H. & Li, S. (2018). Application of Bioaugmentation Technology in Cold-Rolling Emulsion Wastewater Treatment and Analysis of Microbial Community.*Materials Science and Engineering*.392, 052029. doi:10.1088/1757-899x/392/5/052029.

Yusuff, A. S., Popoola, L. T. & Babatunde, E. O. (2019). Adsorption of cadmium ion from aqueous solutions by copper-based metal organic framework: equilibrium modeling and kinetic studies. *Applied Water Science*, *9*(4), 1-11.

Zafisah, N. S., Ang, W. L., Johnson, D. J., Mohammad, A. W. & Hilal, N. (2018). Effect of different filter aids used in cake filtration process on the removal of suspended solids in anaerobically digested palm oil mill effluent (POME). *Desalination and Water Treatment*, 110, 362-370.

Zare, K., Gupta, V. K., Moradi, O., Makhlouf, A. S. H., Sillanpää, M., Nadagouda, M. N., Sadegh, H., Shahryari-Ghoshekandi, R., Pal, A., Wang, Z. J. & Kazemi, M. (2015). A comparative study on the basis of adsorption capacity between CNTs and activated carbon as adsorbents for removal of noxious synthetic dyes: a review. *Journal of Nanostructure in Chemistry*, 5(2), 227-236.

Zero Discharge of Hazardous Chemical (ZDHC). (2016). Wastewater Guidelines. Retrieved fromhttp://www.roadmaptozero.com/fileadmin/pdf/file_2016/ZDHC_wastewater_guideline

Zhang, H., Omer, A. M., Hu, Z., Yang, L. Y., Ji, C. & Ouyang, X. K. (2019). Fabrication of magnetic bentonite/carboxymethyl chitosan/sodium alginate hydrogel beads for Cu (II) adsorption. *International Journal of Biological Macromolecules*, *135*, 490-500.

Zhang, H., Wang, J., Zhou, B., Zhou, Y., Dai, Z., Zhou, Q., Christie, P. & Luo, Y. (2018). Enhanced adsorption of oxytetracycline to weathered microplastic polystyrene: Kinetics, isotherms and influencing factors. *Environmental Pollution*, 243, 1550-1557.

Zhang, K., Wang, X., Guo, X., He, T. & Feng, Y. (2014). Preparation of highly visible light active Fe–N co-doped mesoporous TiO 2 photocatalyst by fast sol–gel method. *Journal of Nanoparticle Research*, *16*(2), 1-9.

Zhang, X. F., Liu, Z. G., Shen, W. & Gurunathan, S. (2016). Silver nanoparticles: Synthesis, characterization, properties, applications, and therapeutic approaches. *International Journal of Molecular Sciences*, 17(9), 1534.

Zhao, G., Huang, X., Tang, Z., Huang, Q., Niu, F. & Wang, X. (2018). Polymer-based nanocomposites for heavy metal ions removal from aqueous solution: a review. *Polymer Chemistry*, *9*(26), 3562-3582.

Zhao, X. H., Jiao, F. P., Yu, J. G., Xi, Y., Jiang, X. Y. & Chen, X. Q. (2015). Removal of Cu (II) from aqueous solutions by tartaric acid modified multi-walled carbon nanotubes. *Colloids and Surfaces A: Physicochemical and Engineering Aspects*, *476*, 35-41.

Zhao, X., Zhu, H., Zhang, B., Chen, J., Ao, Q. & Wang, X. (2015). XRD, SEM, and XPS analysis of soybean protein powders obtained through extraction involving reverse micelles. *Journal of the American Oil Chemists' Society*, 92(7), 975-983.

Zhou, J., Wang, P., Wang, C., Goh, Y. T., Fang, Z., Messersmith, P. B. & Duan, H. (2015). Versatile core–shell nanoparticle/metal–organic framework nanohybrids: Exploiting mussel-inspired polydopamine for tailored structural integration. *ACS nano*, 9(7), 6951-6960.

Zhu, M., Wang, J., Outlaw, R. A., Hou, K., Manos, D. M. & Holloway, B. C. (2007). Synthesis of carbon nanosheets and carbon nanotubes by radio frequency plasma enhanced chemical vapor deposition. *Diamond and Related Materials*, 16(2), 196-201.

Zhu, X., Hou, D., Tao, H. & Li, M. (2020). Simply synthesized N-doped carbon supporting Fe_3O_4 nanocomposite for high performance supercapacitor. *Journal of Alloys and Compounds*, 821, 153580.

Zielińska, A., Skwarek, E., Zaleska, A., Gazda, M. & Hupka, J. (2009). Preparation of silver nanoparticles with controlled particle size. *Procedia Chemistry*, 1(2), 1560-1566.

Zinicovscaia, I. (2016). Conventional Methods of Wastewater Treatment. *Cyanobacteria for Bioremediation of Wastewater*, 3, 17-25.

Živkov Baloš, M., Ljubojević, D., & Jakšić, S. (2017). The role and importance of vanadium, chromium and nickel in poultry diet. *World's Poultry Science Journal*, *73*(1), 5-16.

Zohra, T., Ovais, M., Khalil, A. T., Qasim, M., Ayaz, M. & Shinwari, Z. K. (2019). Extraction optimization, total phenolic, flavonoid contents, HPLC-DAD analysis and diverse pharmacological evaluations of *Dysphania ambrosioides* (L.) Mosyakin & Clemants. *Natural Product Research*, 33(1), 136-142.

Zou, K., Zhang, H. & Duan, X. (2007). Studies on the formation of 5-aminosalicylate intercalated Zn–Al layered double hydroxides as a function of Zn/Al molar ratios and synthesis routes. *Chemical Engineering Science*, 62(7), 2022-2031.

Zuykov, M., Pellettier, E. & Demers, S. (2011). Colloidal Complexed Silver and Silver Nanoparticles in Extrapallial Fluid of *Mytilus edulis*. *Marine Environmental Resources*, 17, 17-21.

APPENDICES

Appendix A: Percentage Removal of Selected Heavy Metal Ions onto Pd-Ag-CNTs with Respect to Contact Time

Time (min)	Cu	Fe	Mn	Ni
10	68.15398	74.36159	67.73762	75.12275
20	72.52843	79.87743	70.54886	84.45172
30	73.92826	82.02247	71.21821	88.05237
40	74.89064	83.55465	72.15529	89.52537
50	75.06562	84.67824	72.69076	97.87234
60	77.69029	87.94688	77.10843	99.34534

Appendix B: Percentage Removal of Selected Heavy Metal Ions onto Pd-Ag-CNTs with Respect to Adsorbent Dosage

Adsorbent dosage	Cu	Fe	Mn	Ni
10	70.60367	75.48519	68.27309	76.59574
20	73.49081	80.4903	71.08434	85.76105
30	74.01575	83.04392	71.75368	89.52537
40	74.89064	83.86108	72.55689	90.3437
50	75.15311	86.619	72.9585	98.527
60	77.86527	88.35546	77.64391	99.83633

Appendix C: Percentage Removal of Selected Heavy Metal Ions onto Pd-Ag-CNTs with Respect to Effect of Temperature

Temperature	Cu	Fe	Mn	Ni
303	82.32721	78.95812	76.70683	82.48773
313	82.67717	85.69969	81.65997	87.72504
323	84.33946	88.15117	86.34538	94.92635
333	85.38933	89.47906	88.08568	98.36334
343	90.72616	91.31767	93.30656	99.83633
353	96.32546	93.97344	95.18072	99.83633

Appendix D: Experimental Batch Adsorption Data of Cu using Pd-Ag-CNTs

M (g)	Ce (mg/L)	q (mg)	Q (mg/g)
10	0.336	0.04035	4.035
20	0.303	0.042	2.1
30	0.297	0.0423	1.41
40	0.287	0.0428	1.07
50	0.284	0.04295	0.859
60	0.253	0.0445	0.741667

Appendix E: Experimental Batch Adsorption Data of Fe using Pd-Ag-CNTs

M (g)	Ce (mg/L)	q (mg)	Q (mg/g)
10	0.24	0.03695	3.695
20	0.191	0.0394	1.97
30	0.166	0.04065	1.355
40	0.158	0.04105	1.02625
50	0.131	0.0424	0.848
60	0.114	0.04325	0.720833

Appendix F: Experimental Batch Adsorption Data of Mn using Pd-Ag-CNTs

M (g)	Ce (mg/L)	q (mg)	Q (mg/g)
10	0.237	0.0255	2.55
20	0.216	0.02655	1.3275
30	0.211	0.0268	0.893333
40	0.205	0.0271	0.6775
50	0.202	0.02725	0.545
60	0.167	0.029	0.483333

Appendix G: Experimental Batch Adsorption Data of Ni using Pd-Ag-CNTs

M (g)	Ce (mg/L)	q (mg)	Q (mg/g)
10	0.143	0.0234	2.34
20	0.087	0.0262	1.31
30	0.064	0.02735	0.911667
40	0.059	0.0276	0.69
50	0.009	0.0301	0.602
60	0.001	0.0305	0.508333

Appendix H (I-IV): Linear Plots of Langmuir Isotherm Model

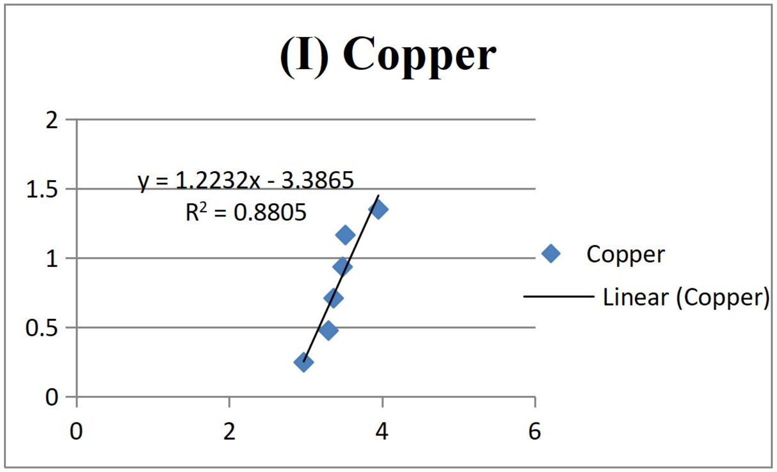

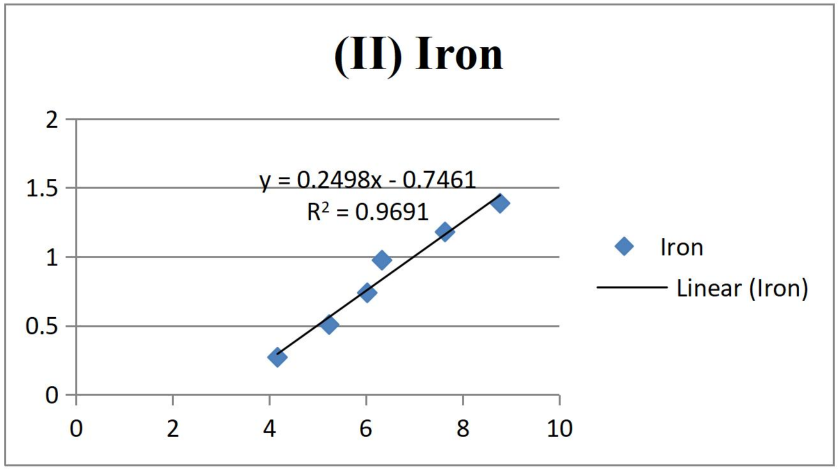

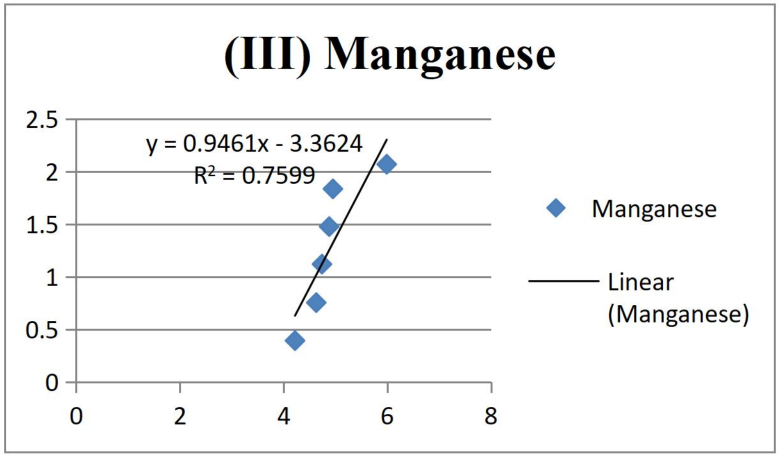

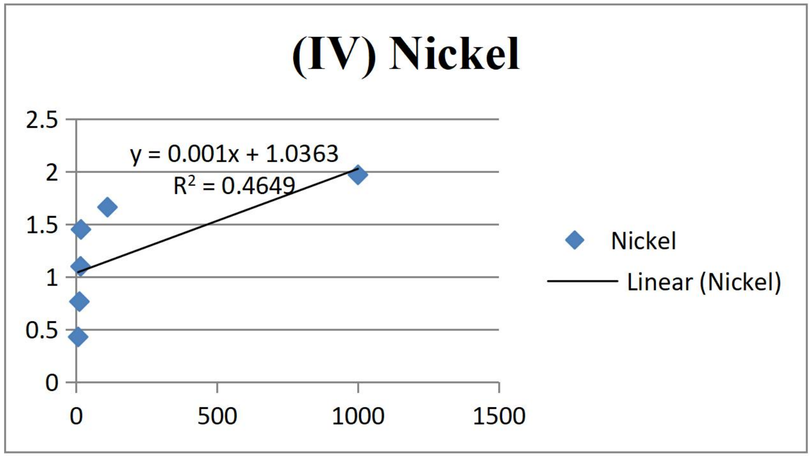

Appendix I (I-IV): Linear Plot of Freundlich Isotherm Model

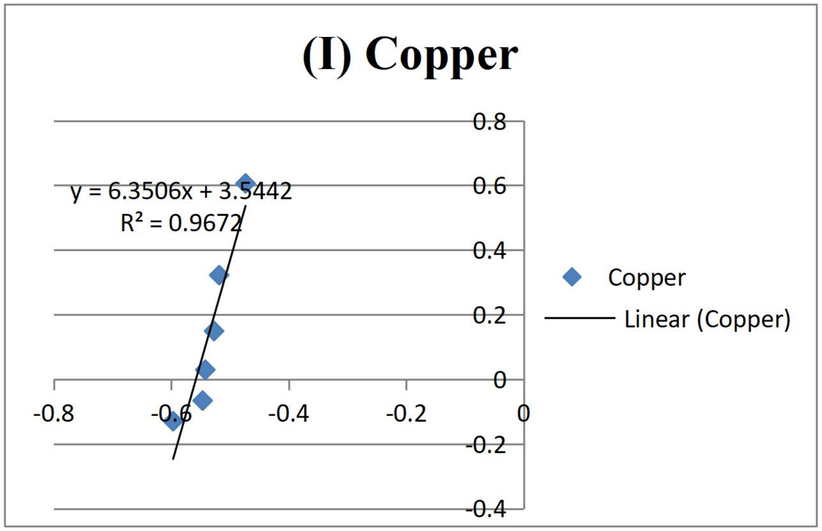

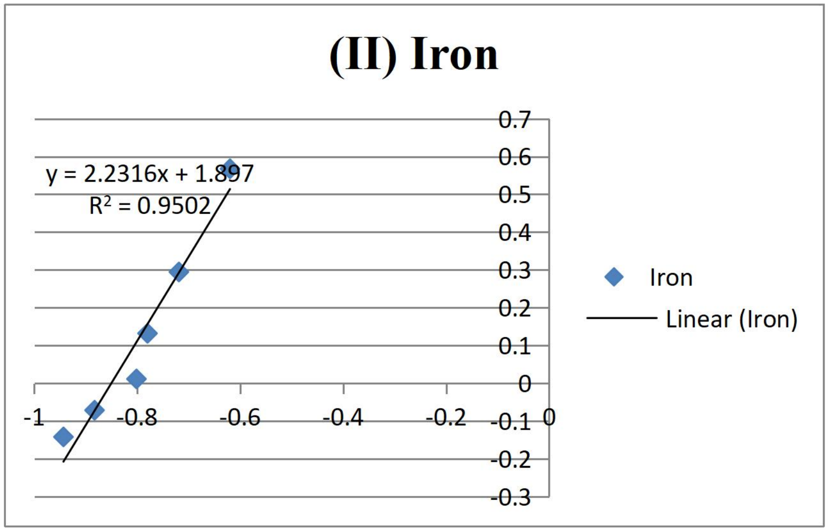

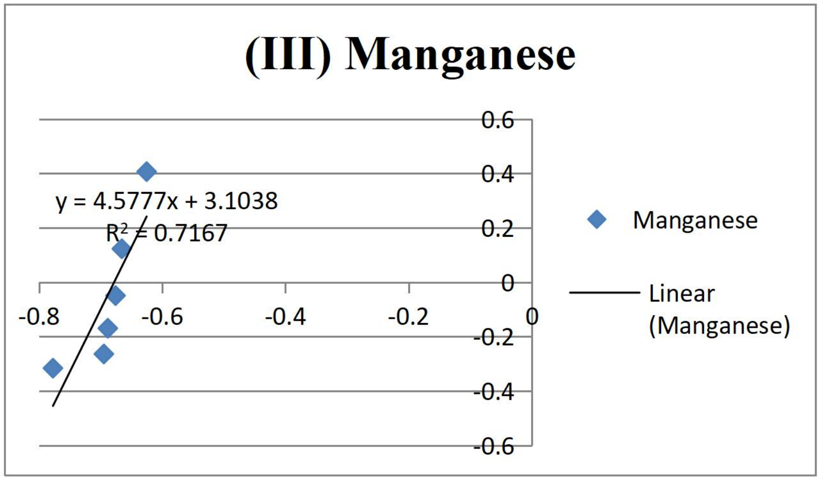

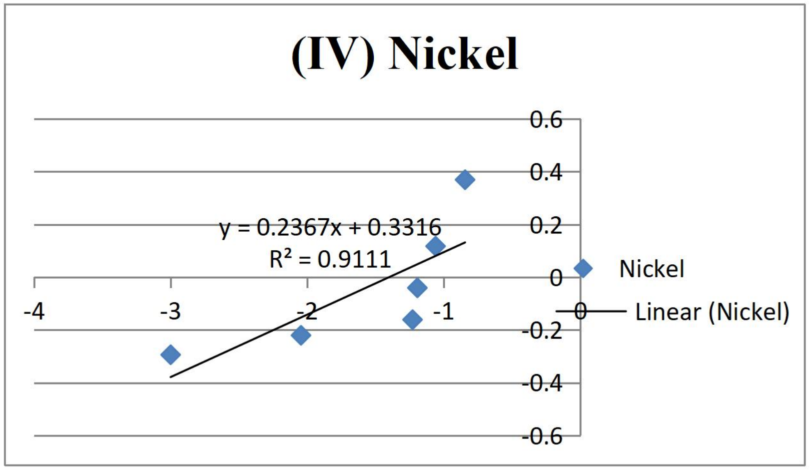

Appendix J (I-IV): Linear Plot of Freundlich Isotherm Model

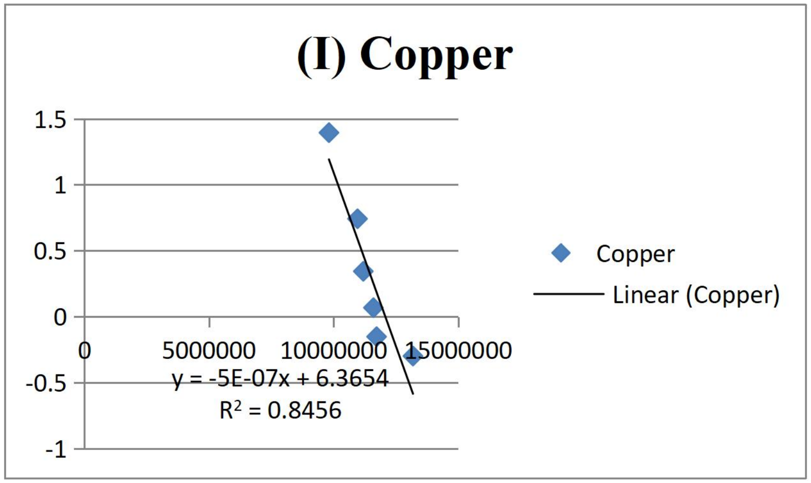

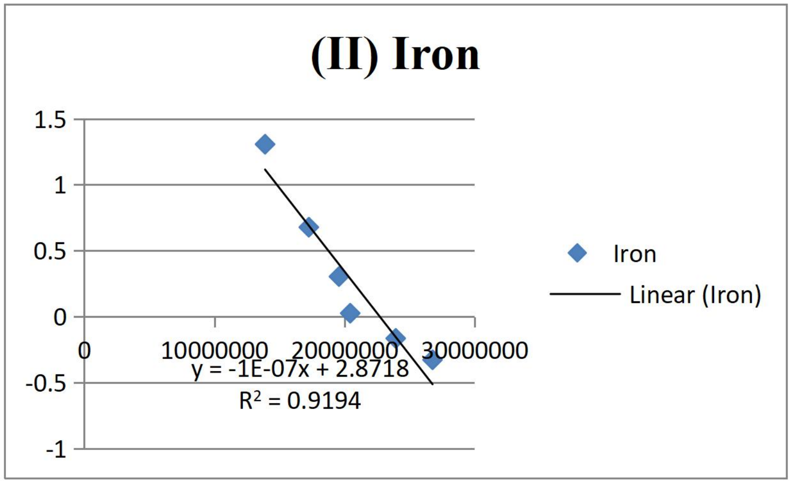

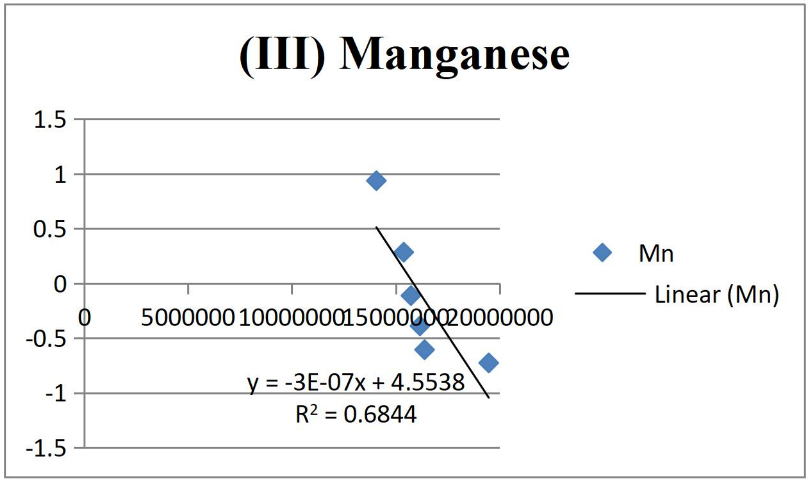

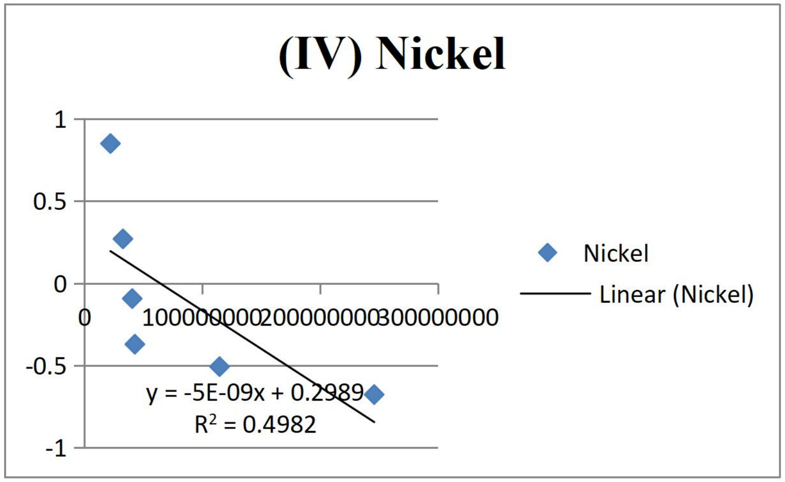

Appendix K (I-IV): Linear Plot of Temkin Isotherm Model

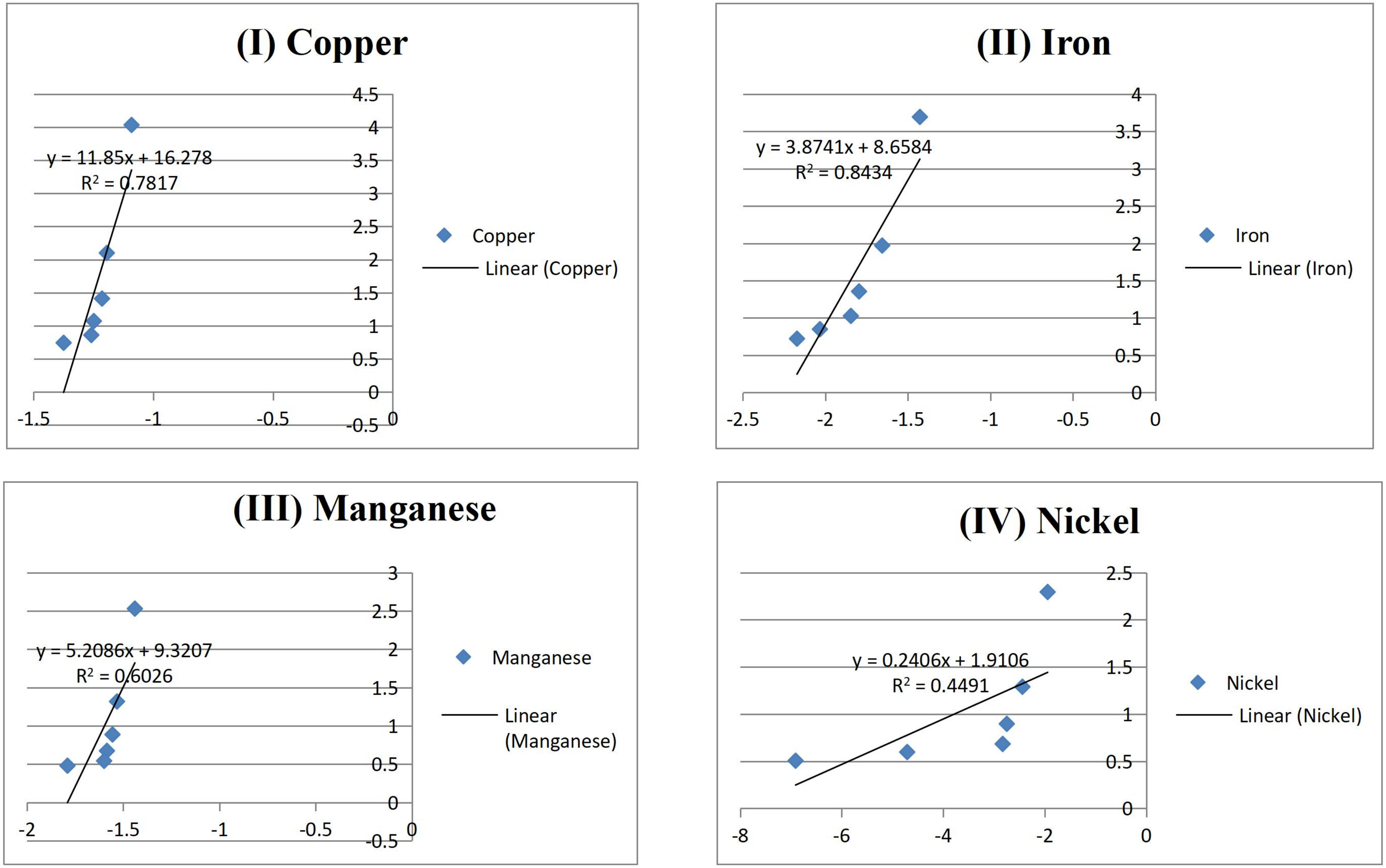

Appendix L (I-IV): Linear Plots of Halsey Isotherm Model

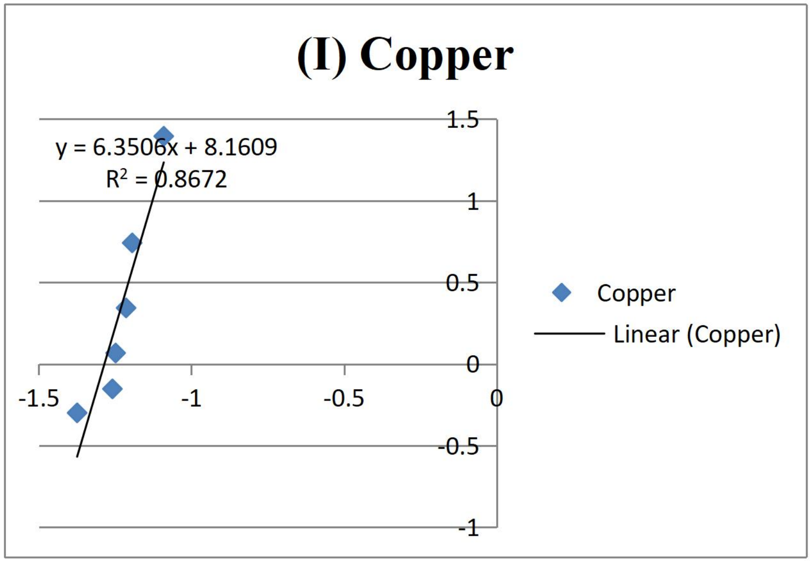
(I) Copper

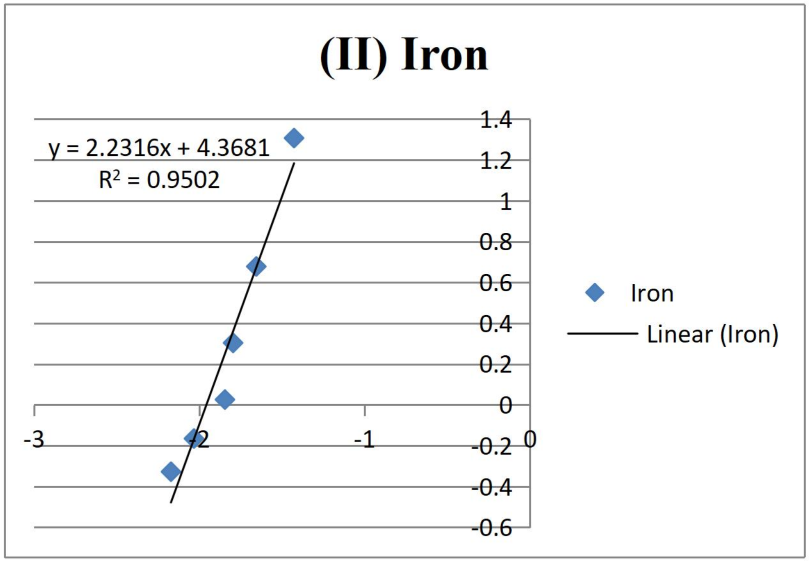
(II) Iron

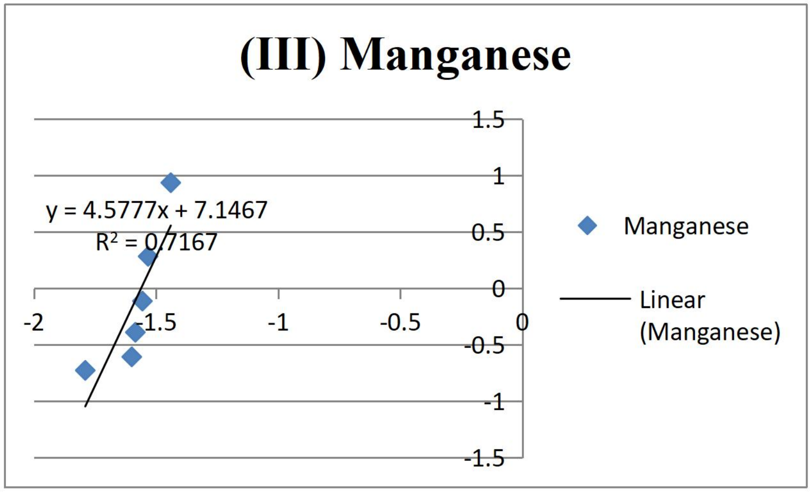
(III) Manganese

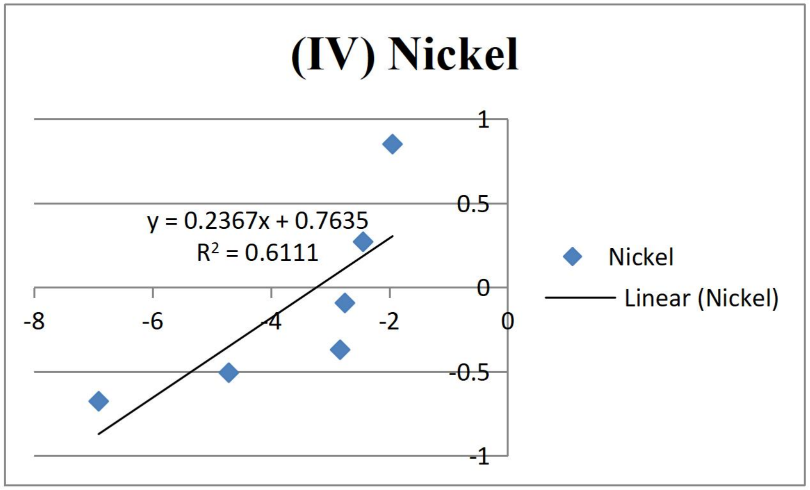
(IV) Nickel

Appendix M (I-IV): Linear Plots of Florry-Huggin's Isotherm Model

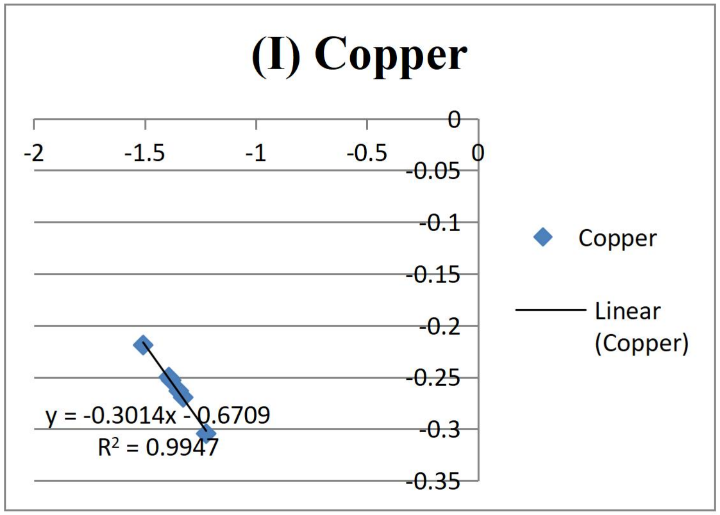
(I) Copper

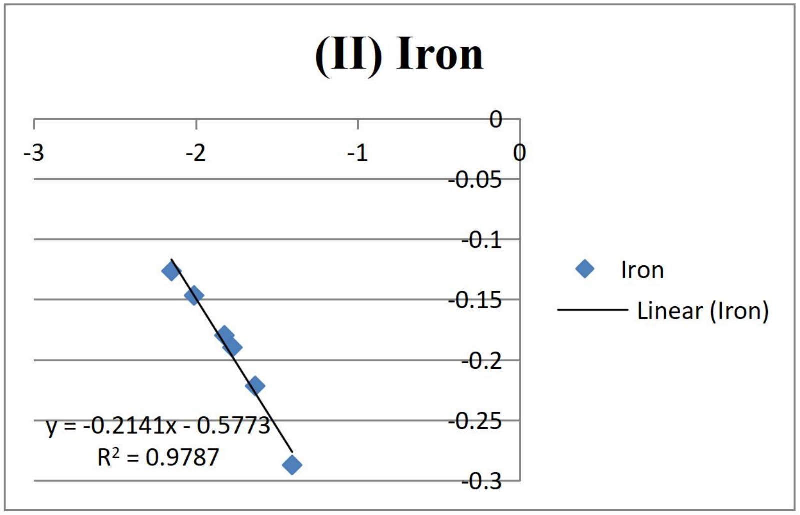
(II) Iron

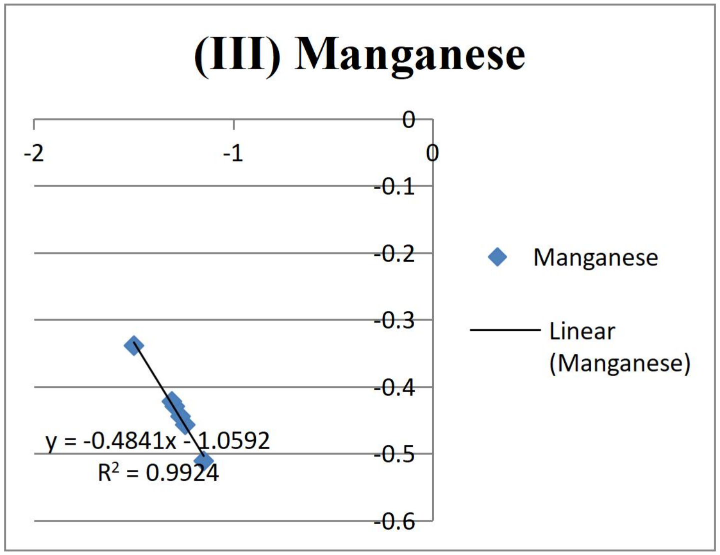
(III) Manganese

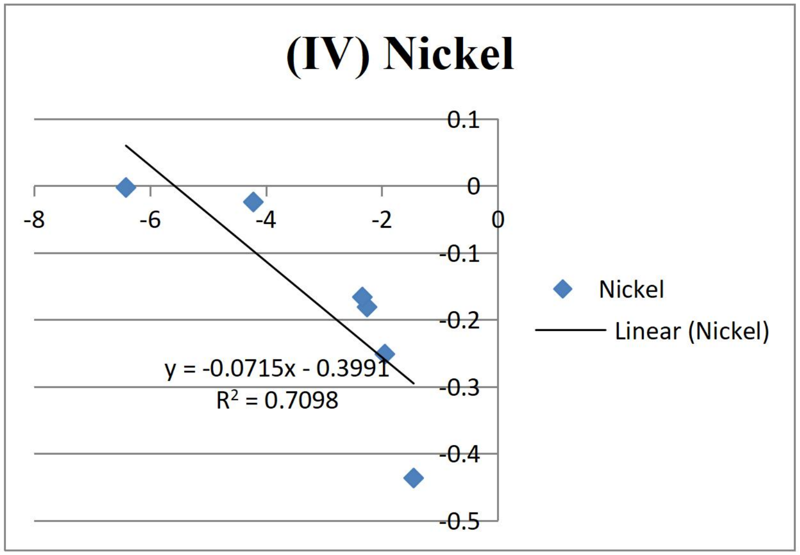
(IV) Nickel

Appendix N (I-IV): Linear Plots of Pseudo-First-Order Kinetic Model

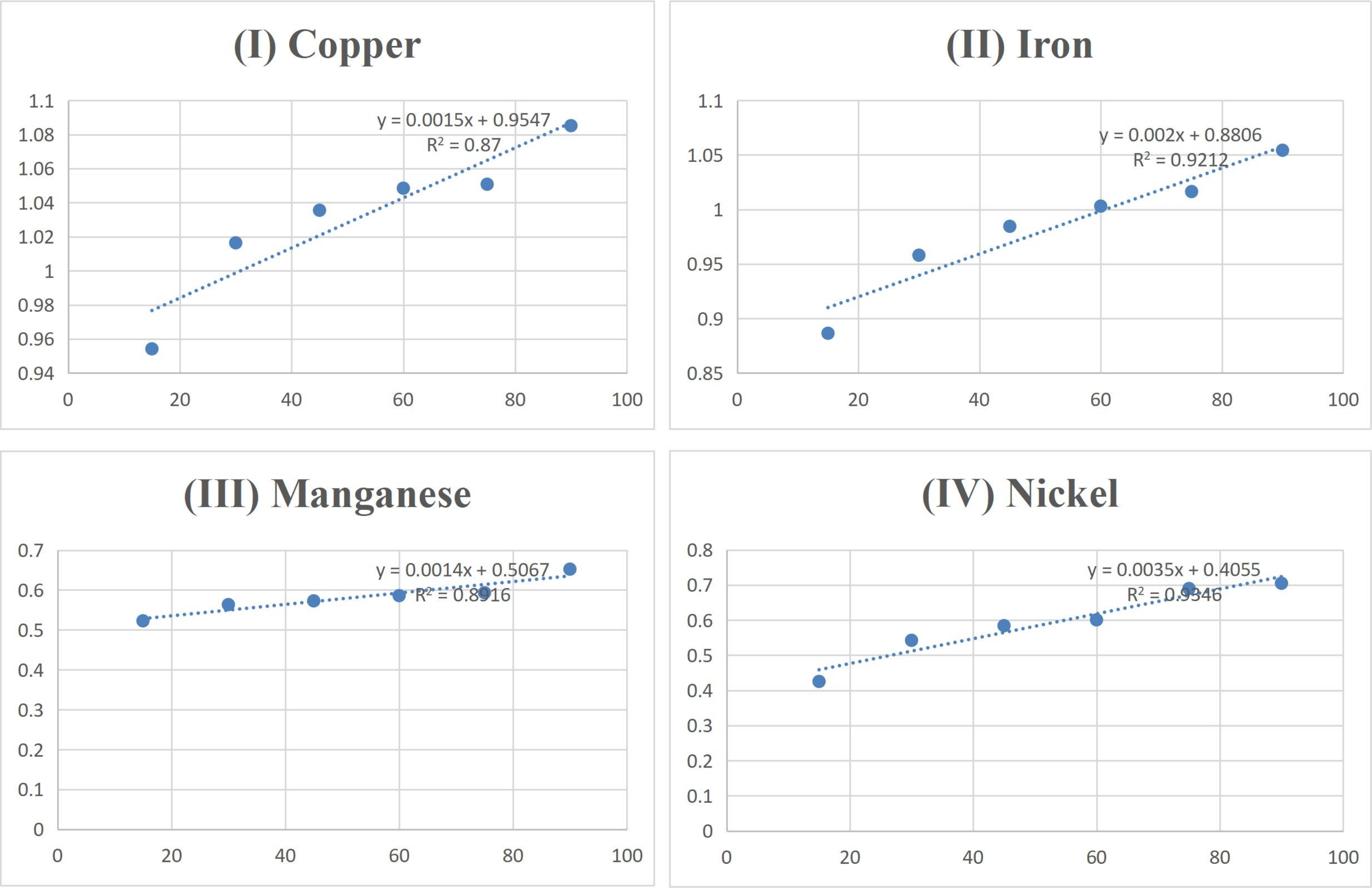

Appendix O (I-IV): Linear Plots of Pseudo-Second-Order Kinetic Model

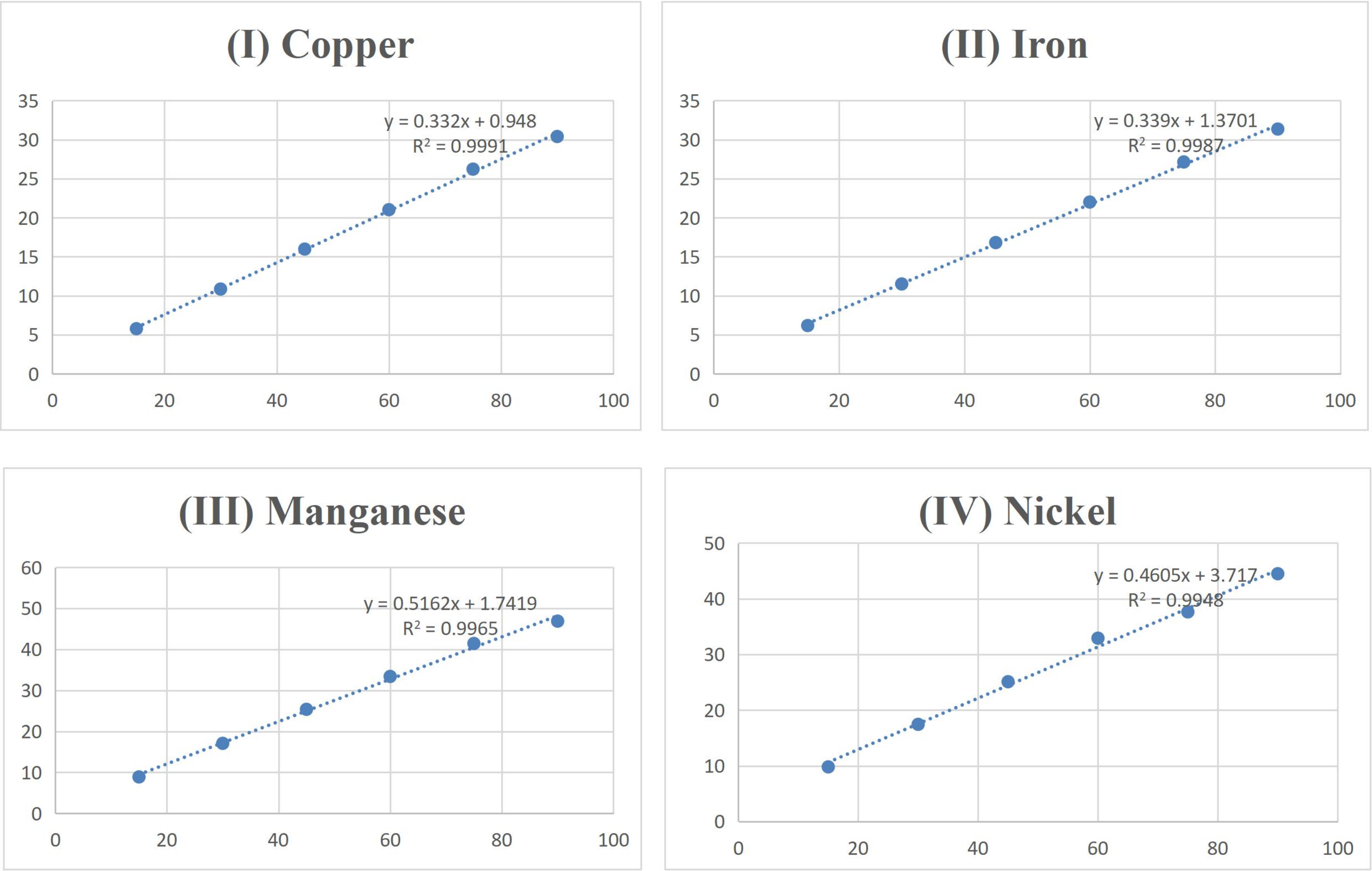

Appendix P (I-IV): Linear Plots of Intraparticles Diffusion Model

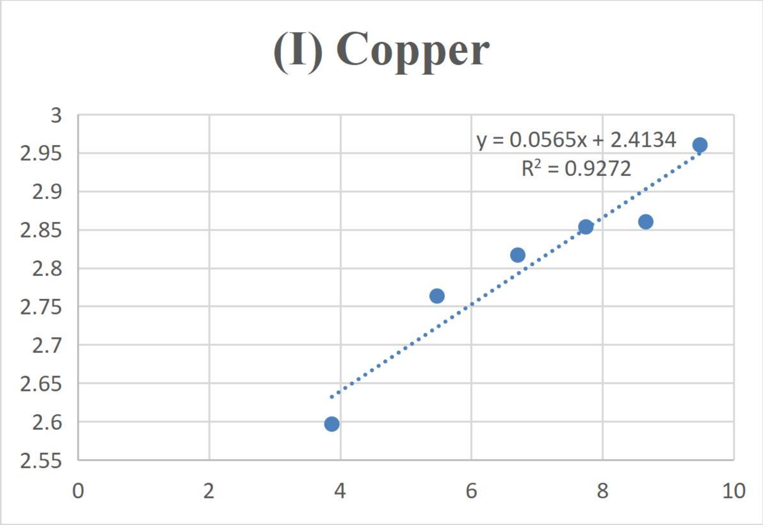

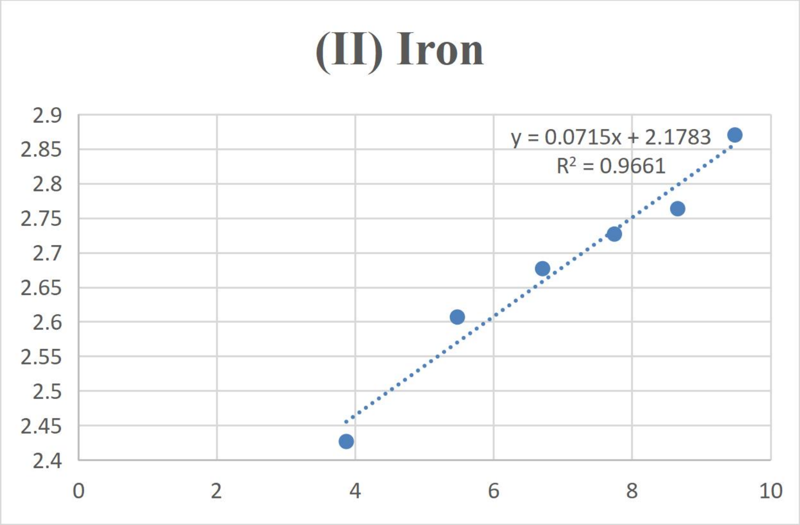

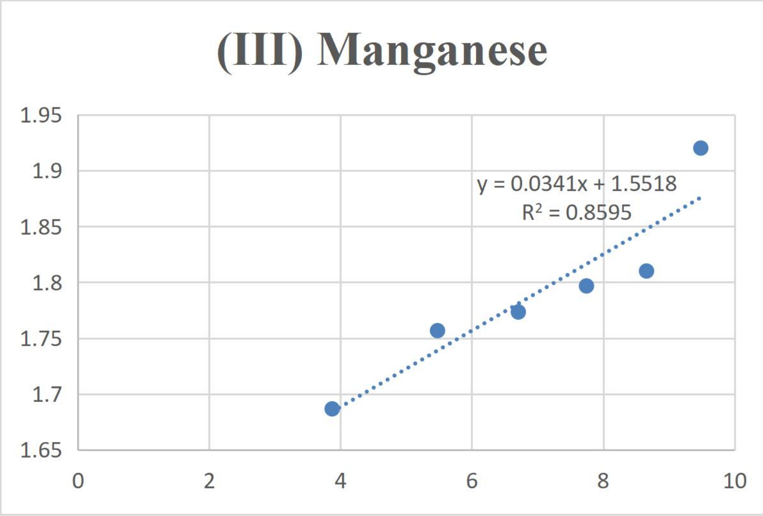

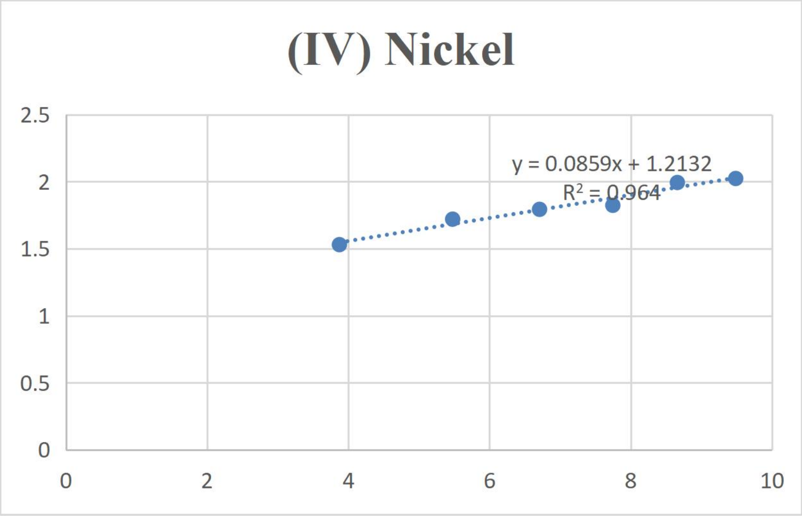

Appendix Q: Linear Plots of Thermodynamics